Mathematical Modelling of Transporter Kinetics

Thomas R. B. Grandjean

A thesis submitted in partial fulfilment of the requirement for the degree of Doctor of Philosophy in Engineering

University of Warwick, School of Engineering

September 2013

Contents

List of Figures

List of Tables

Acknowledgements

There are many people who have been instrumental in supporting me to undertake the research included in my thesis. To begin with I would like to thank my academic and industrial supervisors Dr Mike Chappell and Dr James Yates respectively. Their guidance and support and been invaluable throughout my studies. I would also like to thank the UK MRC Capacity Building Initiative and AstraZeneca for funding my research. I am also grateful to all the scientists at AstraZeneca who have looked after me during my visits, especially Dr Charlie O'Donnell, Dr Simone Stahl, and Alex Lench for collecting the experimental data.

I would like to thank everyone at the School of Engineering at University of Warwick. In particular I would like to thank Dr Neil Evans and Prof Keith Godfrey for their help. I would also like to thank my family, in particular mum and dad for always encouraging me to apply myself, my friends Mark Maidment and Dave Nicholls for their advice, and everyone in the Judo Club at the University of Warwick for making my time here so enjoyable.

And last but not least, I would like to thank Squidger; you're the best.

Thomas Grandjean. Coventry, September 2013

Declaration

This thesis, and the material presented therein, is my own work. It has not been submitted for a degree at any other university.

The following articles have been published, or are in the progress of submission as a result of the work contained within this thesis:

Grandjean, T. R., Chappell, M. J., Yates, J. T., Jones, K., Wood, G., & Coleman, T. (2011). Compartmental modelling of the pharmacokinetics of a breast cancer resistance protein. *Computer methods and programs in biomedicine*, 104(2), 81-92.

Grandjean, T. R., Chappell, M. J., Yates, J. W., & Evans, N. D. (2013). Structural identifiability analyses of candidate models for *in vitro* Pitavastatin hepatic uptake. *Computer methods and programs in biomedicine*. In Press, Corrected Proof, Available online 17 July 2013

Grandjean, T. R., Chappell, M. J., Lench, A. M., Yates, J. T., O'Donnell, C. J. (2013) Experimental and Mathematical Analysis of *in vitro* Hepatic Uptake, submitted to *Drug Metabolism and Disposition*

Grandjean, T. R., Chappell, M. J., Yates, J. T., & Evans, N. D. (2012, August). Structural Identifiability and Indistinguishability Analyses of *in vitro* Pitavastatin Hepatic Uptake. In *Biological and Medical Systems* (Vol. 8, No. 1, pp. 361-366).

Grandjean, T. R., Chappell, M., Yates, J., Jones, K., Coleman, T., & Wood, G. (2009, August). Compartmental Modelling of the Pharmacokinetics of a Breast Cancer Resistance Protein. In *Modeling and Control in Biomedical Systems* (Vol. 7, No. 1, pp. 115-120).

Grandjean, T. R., Yates, J. T., Chappell, M. J. (2010) Compartmental Modelling of the Pharmacokinetics of an Efflux Transporter, 8th Central European Symposium on Pharmaceutical Technology, *Scientia Pharmaceutica* POT12

Grandjean, T. R., Lench, A., Yates, J. T., Chappell, M. J., O'Donnell, C. J. (2010) Experimental and Mathematical Analysis of Hepatic Uptake, 8th Central European Symposium on Pharmaceutical Technology, *Scientia Pharmaceutica* PPAT07

Grandjean, T. R., Experimental and Mathematical Analysis of Pitavastatin Hepatic Uptake Across Species, Drug Metabolism Discussion Group (DMDG) open Meeting; September 14-16, 2011; Cambridge, England.

Grandjean, T. R., Yates, J. T., Chappell, M. J., Compartmental modelling of *in vivo* drug interaction in hepatic uptake, PKUK Conference 2012: Programme and Abstract Book. *PKUK Conference 2012*, Dorking, UK. 7-9 November 2012.

Grandjean, T. R., Lench, A., Yates, J. T., Chappell, M. J., O'Donnell, C. J. Experimental and Mathematical Analysis of Pitavastatin Hepatic Uptake Across Species, PKUK Conference 2011: Programme and Abstract Book. *PKUK Conference 2011*, Durham, UK. 9-11 November 2011.

Grandjean, T. R., Yates, J. T., Chappell, M. J. Compartmental Modelling of the Pharmacokinetics of an Efflux Transporter, presented at *Pharmacokinetics UK (PKUK)*; November 3-5, 2010; Bristol, England.

Grandjean, T. R., Lench, A., Yates, J. T., Chappell, M. J., O'Donnell, C. J. Experimental and Mathematical Analysis of Hepatic Uptake, presented at *Pharmacokinetics UK (PKUK)*; November 3-5, 2010; Bristol, England.

Abstract

Membrane transport proteins have recently been discovered to be ubiquitously expressed in the human body and of paramount importance in cellular uptake. Since all pharmaceutical compounds must pass through numerous cell membranes to travel and be absorbed by their target cells in order to achieve their desired therapeutic effects, transporters have attracted a lot of attention as a research field. As an emerging focus area, the precise mechanism of action of many of these transporters remains to be fully elucidated. In order to gain a detailed insight into these processes it is proposed to carry out mechanistic modelling of the pharmacokinetics of transporters. This thesis details the models developed to further our understanding of carrier mediated transport.

The current knowledge on cellular uptake and efflux are discussed and mathematical models are developed for two prominent transporters. Structural identifiability and indistinguishability analyses are performed on all the models developed using a variety of methods to investigate the applicability of each method. Model fits gave very good agreement with *in vitro* data provided by AstraZeneca across a variety of experimental scenarios and different species. Mechanistic models for *in vivo* applications are also developed and found to characterise hepatic uptake in rat accurately. Recommendations for further work to fully validate the models developed so that they can perform robust, predictive simulations are proposed.

The research in this thesis demonstrates that mechanistic modelling of complex biological processes allows for greater understanding of such systems.

Chapter 1

Thesis Introduction

In recent decades more emphasis has been placed on the role of mathematical modelling in medicine and biology since it offers a quantitative approach to support new drug development, assist decision-making in pharmacology, and improve clinical trial design. Modelling and simulation have also been shown to improve the fundamental knowledge of the mechanisms in cells and organisms, many of which are still not fully understood. The exposure (pharmacokinetics - PK) and effect (pharmacodynamics - PD) of therapeutic drugs can be determined by mathematically modelling drug absorption and tissue uptake. This may be achieved by compartmental modelling that involves dividing the biological system into a finite number of compartments that interact by material or information flowing from one compartment to another. This type of mathematical modelling is used in biology, complex systems theory, engineering, epidemiology, information science, pharmacology, physics, social science, and systems biology. In recent years this research field has moved away from non-compartmental methods, such as estimating the area under the curve (AUC) of a plasma concentration-time plot to quantify the exposure to a drug, because physiologically based pharmacokinetic (PBPK) modelling has been shown to have a superior predictive ability and strength in data integration as well as enabling mechanistic insights into the complex and often non-linear physiological processes. Traditionally, compartmental modelling has been

implemented at the macroscopic scale, but in recent years these techniques have also been use to investigate cellular level interactions and mechanisms.

In order to achieve their desired therapeutic effects drugs need to travel to and be absorbed by target cells. Throughout this process and subsequent metabolism the pharmaceutical agent must pass through numerous cell membranes. Carrier-mediated uptake via specific carrier proteins or transporters has been proposed as the process that is responsible for the transport of molecules and particles across cell membranes. Membrane transporter proteins are a key determinant of the trans-membrane passage of drugs and therefore have attracted much attention. Breast Cancer Resistance Protein (BCRP) and Organic Anion Transporting Polypeptide (OATP) are two prominent transporters that were selected for investigation in this thesis. Breast cancer is the most common cancer among women by a large margin and ranks second overall to lung cancer worldwide. An estimated 1.38 million new breast cancer cases were diagnosed in 2008 (Ferlay *et al.* 2010). Developing a compartmental model to predict the uptake of an anti-cancer substrate into target cells has far reaching implications in cancer research. It provides a platform for optimising maximum possible substrate binding and is therefore an invaluable tool into effectively targeting the areas desired. It also provides a fundamental understanding of the drug's pharmacokinetics, crucial for development of new treatments. OATP also has implications for oncology; however the main focus in this thesis is modelling its role in hepatic uptake of statins, which are used to treat hypercholesterolaemia. High cholesterol is often associated with coronary disease, since it can cause atherosclerosis. Coronary heart disease remains the UK's single biggest killer, with an estimated 74,000 deaths in 2011 (British Heart Foundation).

Despite their clinical significance the exact mechanisms of actions of these transporters remains a challenge for the research field. OATP and BCRP have been modelled extensively and their physiological and chemical structures are fairly well understood. However, no mechanistic models are available in the literature for BCRP binding kinetics and the mathematical model developed in this thesis is completely novel for this transporter. Conversely, a handful of *in vitro* mechanistic models have been developed for OATP but these have only been applied to rat data and have several limitations. The models developed in this thesis not only offer advantages in terms of the number of species evaluated (rat, dog, and human), but allow for statistical comparison as to which fits describe the data more accurately and are implemented using a numerical integrator that is able to cope with stiff systems. The OATP systems were found to be highly stiff in Chapter 4, with a stiffness ratio of up to 10^{11}.

No mechanistic models for *in vivo* hepatic uptake have previously been published and therefore the model developed in this thesis is entirely novel. Measuring endogenous substances such as bile acid is an experimentally convenient way to explore the impact of transporter mediated drug-drug interactions *in vivo*, however this has not been modelled mechanistically previously.

1.1 Aims and Objectives

The aim of this thesis is to use compartmental modelling analysis to develop novel models to describe the mechanisms of two prominent transporters. The intention here is to elucidate the processes inherent in transporter action. Therefore the objectives of this thesis are to:

- Investigate the existing knowledge of membrane transporter proteins and their mechanism of action
- Examine the current techniques for biomedical systems modelling
- Develop a mechanistic model to describe *in vitro* BCRP competitive binding
- Develop a mechanistic model to describe *in vitro* OATP hepatic uptake in rat
- Investigate this model's potential for scaling across species (dog and human)
- Develop a mechanistic model to describe *in vivo* OATP competitive binding in rat
- Explore current methods for performing structural identifiablity and indistinguishability analyses and their applicability to the non-linear models developed

1.2 Thesis Outline

In this thesis the investigation will concentrate on developing mathematical models based on mass balance principles to describe transporter action. The relevant background literature is discussed in Chapter 2, which has been divided into four sections concerning mathematical modelling in pharmacology, compartmental modelling, structural identifiability and indistinguishability analyses, and transporters in pharmacokinetics and pharmacodynamics. In line with most pharmaceutical applications attention is focused on non-linear systems. The different mechanisms of influx and efflux into cells are described in detail as they provide the foundation for the model development.

The models developed using compartmental modelling methods to describe the pharmacokinetics of Hoechst 33342 following administration into a culture medium

containing a population of transfected cells (HEK293 hBCRP) are detailed in Chapter 3. The intention here was to derive a compartmental model to characterise substrate binding to DNA and in addition account for the effect of transportation of the substrate out of the cell. Two models are developed: a four compartment model was developed to mathematically describe the saturable binding of Hoechst 33342 to BCRP, and a seven compartment model derived to account for competitive binding in the presence of a potent inhibitor, Fumitremorgin C. Steady state analyses and structural identifiability analyses are performed on both models. The parameterised mathematical models are subsequently used to estimate any unknown rate constants and parameters from *in vitro* data provided by AstraZeneca in order to obtain information on the relative binding affinities to the BCRP transporter.

Chapter 4 details six candidate models derived to describe *in vitro* hepatic uptake in three species, namely rat, dog, and human. The structural identifiabiabilty and indistinguishability of the non-linear compartmental models are investigated in detail and the applicability of current methods to perform the analyses is discussed. Two models are selected, one for rat and human and one for dog, since they reproduce experimental data provided by AstraZeneca the most accurately. Simultaneous fits of numerous different concentrations are directly compared to the existing modelling approaches currently utilised to establish which models are the most suitable. The robustness of the proposed models is evaluated with sensitivity analyses and stiffness factors of the models are considered.

The *in vivo* data models developed in Chapter 5 build on the *in vitro* data modelling of the two previous chapters. Two compartmental models proposed incorporate the competitive binding elements of the BRCP model from Chapter 3 and the OATP uptake mechanism from Chapter 4 to describe how oral doses of Cyclosporine A

(CsA) effect endogenous bile acid levels in rat. The structural identifiabiabilty of the models is explored using a variety of methods and the applicability of current methods to perform the analyses is considered once more. Simultaneous fits for three different initial concentrations of CsA and one control group with no CsA administered are subsequently performed to estimate any unknown rate constants and parameters from *in vitro* data provided by AstraZeneca.

The overall project conclusions and recommended future work are discussed in Chapter 6.

1.3 References

Ferlay, J., Shin, H. R., Bray, F., Forman, D., Mathers, C., & Parkin, D. M. (2010). Estimates of worldwide burden of cancer in 2008: GLOBOCAN 2008. *International journal of cancer*, *127*(12), 2893-2917.

British Heart Foundation website: http://www.bhf.org.uk/heart-health/conditions/cardiovascular-disease.aspx last accessed 26/09/2013

Chapter 2

Literature Review

Mathematical modelling now plays an increasingly crucial role in medicine and biology and has become a universally researched topic area (see for example: Doucet 1992, Carson & Cobelli 2001, Ottersen 2000, Hoppensteadt 2002). Wide ranging applications, such as epidemiological research, planning and evaluation of preventive and control programmes, clinical trials, measurement of health, cost-benefit analysis, diagnosis of patients, and in maximising the effectiveness of operations aimed at attaining specified goals within existing resources (Verma *et al.* 1981) have proved the usefulness of modelling over many decades. Mathematical modelling is particularly important in new drug development, which occurs once a compound has been identified as a potential drug, in order to establish its suitability as a medication (Sheiner & Steimer 2000). Mathematical models are used to determine the appropriate formulation and dosing from a combination of *in vitro* and *in vivo* studies, as well as clinical trials. A phenomenally expensive and time-consuming process, normally this tends to be limited to larger pharmaceutical companies because of the amount of capital required for such research and development (R&D). A large proportion of the R&D budget is spent on investigating the pharmacokinetics and pharmacodynamics of new and existing drugs. The word pharmacokinetics comes from the Ancient Greek words for "drug"; *pharmakon*, and "to do with motion"; *kinetikos*. It is the study of how living organisms affect specific pharmaceutical agents after administration. It is often split into four main categories: absorption (the process of entering the blood stream), distribution (dispersion into

tissues), metabolisation (transformation of the compound into mebolites), and excretion (removal of the drug from the body). The word pharmacodynamics also finds its root in *pharmakon*, however it is combined with the Ancient Greek word for "power"; *dynamikos*. It is the other main branch of pharmacology, which is concerned with the study of pharmaceutical agents' physiological and biochemical effects on living organisms. Pharmacodynamics involves investigating the often non-linear mechanism of drug action and the resulting relationship between drug concentration and effect. In laymen's terms, pharmacodynamics may simply be described as what the drug does to the body, whereas pharmacokinetics is what the body does to the drug (Burton 2006).

This literature review is split into four main sections. First, the topic of mathematical modelling in pharmacology is introduced and the most influential literature assessed. A physiologically insightful and mechanistic type of modelling, namely compartmental modelling is presented in the second section. The relevant literature, both championing and critiquing the methodology is appraised. Thirdly, the important theoretical topics of structural identifiability and indistinguishability analyses, and their applications to biomedical systems modelling are reviewed. The focus is on non-linear systems, in line with most pharmaceutical applications and the models described in the following chapters of this thesis. Transporters are integral membrane transport proteins that are involved in the movement of ions, small molecules, and macromolecules, such as another protein across biological membranes. They play a crucial role in facilitating or preventing drug movement around the body (Ho & Kim 2005). The fourth section details the importance of transporters in pharmacokinetics and pharmacodynamics, and how most cellular uptake is governed by these proteins. The literature on two prominent transporters is

evaluated, justifying the author's reasons to model their mechanisms in this thesis. Finally conclusions are drawn with regard to the compartmental modelling of transporter action.

2.1 Mathematical Modelling in Pharmacology

Systems biology is an emerging field of study at the forefront of biomedical and biological scientific research. Although biology based, it is an inter-disciplinary approach that focuses on the complex interactions and mechanisms within biological systems. The overarching aims of systems biology are to model and discover emergent properties of cells, tissues, and organisms functioning as a holistic system. These typically involve developing mathematical models of metabolic networks and cell signalling networks. In fact, systems biology may be considered as the application of dynamic systems theory to molecular biology (Klipp *et al.* 2008).

However mathematical modelling and biology were not always so intricately interlinked. Particularly in clinical pharmacology, where historically drug development has been based on a relatively improvisatory trial and error process (Holford *et al.* 2000). Although there were some models published in the literature before, the seminal manuscript Sheiner *et al.* 1979 published in the 'Journal of Clinical Pharmacology and Therapeutics', in which Lewis B. Sheiner (1940-2004) and his colleagues simultaneously modelled the pharmacokinetics and pharmacodynamics of the neuromuscular blocking agent, D-tubocurarine, has been cited over a thousand times. Through his scientific writings, teaching programmes, and collaboration with scientists around the world, Sheiner championed model-based drug development, that is to say applying statistical models of drug efficacy and

safety to preclinical and available clinical data. This paradigm, presented in the influential manuscript by Sheiner 1997, offered a quantitative approach to improving clinical pharmacology and drug development decision-making. For example, in Miller *et al.* 2005, pharmacokinetic and pharmacodynamic (PK/PD) modelling was used to predict potency, simulate various clinical trial scenarios, and confirm evidence of efficacy across studied doses. Three case studies are described where PK/PD modelling helped decision making and dose selection, design a Phase 2 study (drug testing on patients to assess efficacy and safety) with a number of important learning experiences as well as extensive financial savings, and eliminated the need for some additional clinical trials, thus supporting the approval of the compound.

Sheiner's philosophy on clinical pharmacology, the "Learn and confirm" paradigm, has become the catchphrase for new drug development. It can be speculated that his work made regulatory bodies come to realise that proof of efficacy is only one step in a long process from drug discovery to manufacture. This is reflected in the guidelines that the Food and Drug Administration (FDA) issued in 1999: "Guidance for Industry: Population Pharmacokinetics", and in 2004: "Innovation or Stagnation: Challenge and Opportunity on the Critical Path to New Medical Products", the latter which cites Sheiner. In these papers, the FDA outlines the mechanisms and philosophy of pharmacokinetic and pharmacodynamic (PK/PD) modelling, and its important role in the efficient development of safe and effective drugs. This highlights the importance of integrating PK/PD modelling in drug development and its potential impact on decision making and financial savings.

Newly discovered compounds are analysed for suitability through efficacy studies, toxicology studies, and absorption, distribution, metabolism and excretion (ADME) studies to optimise the balance of properties necessary to convert leads into effective

medicines. These types of studies are widely used in drug discovery; however, as mentioned previously, such drug development was generally based on a relatively improvisatory trial and error process. Before long, advances in combinatorial and library chemistry generated many more molecules of interest that could feasibly be screened through these traditional methods (Selick *et al.* 2002). The sheer number of molecules and studies made it impractical both time-wise and financially. Furthermore, even though increasing numbers of compounds were screened, fewer suitable molecules were delivered and eventually became considered as suitable medicines. Drug selection became widely viewed as the bottleneck in the drug discovery and development process (Grass & Sinko 2002). Due to the incessant rising cost and reduced productivity of drug development (Kuhlman 1999 and Paul *et al.* 2010), interest in the use of alternative methods to stimulate clinical pharmacology continued to grow. Whereas, originally PK/PD modelling was predominantly only performed in patient studies using the population approach (Ette & Ludden 1995, Sheiner & Wakefield 1999, and Williams & Ette 2000), predictive models were now required in order to achieve an efficient selection process and support critical financial decisions. PK/PD modelling therefore evolved from a discipline primarily applied to therapeutic drug monitoring to one that plays a vital role in new drug development (Williams & Ette 2000 and Selick *et al.* 2002). Combined with pharmaceutical companies' increased use of biomarkers and clinical trial simulations, PK/PD modelling and simulation has had an even bigger impact on drug development over the last decade.

Modelling and simulation may assist in Phase I (drug testing on healthy volunteers for dose--ranging) of drug development by predicting the outcomes of certain assays. Subsequently, the experimental outcomes can be compared to the simulated

predictions and confirm or refute the proposed assumptions. Furthermore modelling is particularly useful for censoring because of assay limitation, characterisation of non-linearity, estimating exposure-response relationships, combined analyses, sparse sampling studies, special population studies, integrating PK/PD knowledge for decision making, simulation of Phase II trials, predicting multiple dose profiles from single doses, bridging studies and formulation development (Aarons *et al*. 2001). PK/PD modelling and simulation can also be used as a quantitative tool to help provide answers on efficacy and safety of new drugs, faster and at a lower cost. The value of modelling becomes greater as more data are accumulated through a development programme, especially if data for related drugs are available and shared via publications. Modelling and simulation now plays a crucial role in reshaping early trials by more effective extraction of information from studies, better integration of knowledge across studies and more precise predictions of trial outcomes, thereby allowing more informed decision making. PK/PD modelling is now used from the preclinical phase through all clinical phases of new drug development, as it leads to fewer failed compounds, fewer study failures, and smaller numbers of studies needed for registration.

Modelling and simulation are essential in systems biology and provide new approaches to investigate experimental data, ultimately improving understanding of the mechanisms in cells and organisms (Mendes *et al.* 2005, Kell 2006). Furthermore, the models and simulations offer systematic strategies for fundamental issues in biology and medicine (Carson & Cobelli 2001). PK/PD modelling offers a coherent framework to support drug development and investigate the effects of potential new drugs on biochemical mechanisms and pathways (Aksenov *et al.* 2005). PK/PD models, normally consisting of sets of differential equations, are

commonly utilised to describe the inter- and intra-cellular mechanisms and dynamic interactions (Wolkenhauer *et al.* 2008). One such dynamic model frequently implemented in pharmaceutical research is compartmental analysis.

2.2 Compartmental Modelling

Compartmental modelling, or multi-compartment modelling and flow modelling, is a type of mathematical modelling in which the system is divided into a finite number of homogenous and well mixed pools called compartments (Anderson 1983; Godfrey 1983). The compartments interact by material flowing from one compartment to another. The material or information may be fluids, money, energy, or resources (Walter & Contreras 1999). There may be input and output flows into and from one or more compartments, to and from outside the network, namely inflows and outflows, respectively.

Mass conservation holds for all transfers in and out of compartments and therefore ordinary differential equations are used to describe the rate of change of material from each compartment (Jacquez & Simon 1993). The main assumption is that the concentration of substance in each compartment is uniformly equal and well distributed. Therefore a compartmental model is a lumped parameter system model. Such models may be linear or non-linear, however the amount or quantity of material in each compartment must be greater than or equal to zero, thus compartmental systems are a special subset of non-negative systems.

The most general form of compartmental equations for a linear or non-linear system of n compartments is given by:

$$\frac{dx_i}{dt} = f_{i0} + \sum_{\substack{j=1 \\ j \neq i}}^{n} f_{ij} - \sum_{\substack{j=1 \\ j \neq i}}^{n} f_{ji} - f_{0i} \text{ for } i = 1, 2, \ldots, n \quad (2.1)$$

where x_i is the concentration or quantity of material in compartment i, f_{ij} is the flow rate to compartment i from compartment j, and the subscript 0 denotes the environment. In linear, or time-invariant, compartmental models the flow rates (f_{ij}) are directly proportional to the quantity and concentration of material in the donor compartment (x_j). The system equations therefore become:

$$\frac{dx_i}{dt} = \sum_{\substack{j=1 \\ j \neq i}}^{n} k_{ij} x_j - \sum_{\substack{j=1 \\ j \neq i}}^{n} k_{ji} x_i - k_{0i} x_i + u_i(t) \text{ for } i = 1, 2, \ldots, n \quad (2.2)$$

where the input flow rate f_{i0} has been written as $u_i(t)$, which is the input or control function, and is given by:

$$f_{ij} = k_{ij} x_j \quad (i \neq j). \quad (2.3)$$

An example of a two-compartment model for oral drug administration is given in *Figure* 2.1. In this example, the first compartment, q_1, represents the quantity of drug in the gut while the second, q_2, represents the quantity of drug in the plasma. The dose, d_1, is taken orally and can be modelled as an initial condition. The drug is absorbed into the blood stream via the rate constant, k_a, and then eliminated via the rate constant, k_e, shown as $k_{absorption}$ and $k_{elimination}$ in *Figure* 2.1, respectively.

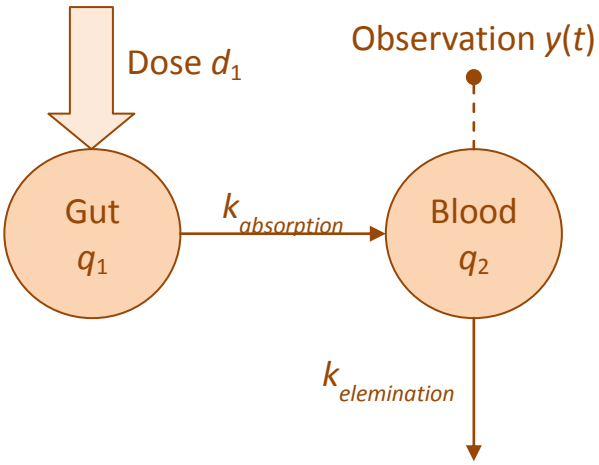

Figure 2.1: First order oral absorption model

The resulting differential equations are given by:

$$\frac{dq_1}{dt} = -k_a q_1, \tag{2.4}$$

$$\frac{dq_2}{dt} = k_a q_1 - k_e q_2, \tag{2.5}$$

with initial conditions

$$q_1(0) = d_1, \tag{2.6}$$

$$q_2(0) = 0. \tag{2.7}$$

The observation, *y*, is normally a concentration measurement from a blood sample and is therefore given by:

$$y = \frac{q_2}{v_2}, \tag{2.8}$$

where v_2 is the volume of distribution, *i.e.* the volume of plasma within which the drug is mixed.

In pharmacokinetic modelling, the compartments were originally exclusively macroscopic, representing different parts of the body, such as organs and the systemic blood stream. In fact, Jacquez 1996 defines compartmental systems as being comprised of *macroscopic* subunits. However, compartmental modelling is now also applied at the microscopic scale, right down to the cellular level, where each compartment may represent a different part of the cell, such as the apical and basolateral membranes (see Gonzalez-Alvarez *et al.* 2005 and Kalvass & Pollack 2007 for example). In fact, mathematical models of biological systems are now part of the standard procedure implemented to investigate complex dynamic, non-linear interaction mechanisms in cellular processes (Hengl *et al.* 2007).

Compartmental models are considered relatively easy to develop, use, and are intuitively clear. They provide a uniform theory and systematic methods for developing dynamic models of systems and experiments in many areas of biomedicine, ranging from analysing the electrical behaviour of a dendrite (Lindsay *et al.* 2007) to measuring amyloid deposition to improve Alzheimer's disease diagnosis (Price *et al.* 2005). They are applied in diverse areas of biology such as carcinogenesis, channel and receptor kinetics, ecosystem modelling, epidemiology, genetics, intermediary metabolism, mutation rate and evolution, and pharmacokinetics (Jacquez 1996). The application of compartmental modelling has grown into other fields, such as ecology, engineering, physics, and even hydrochemistry, where compartmental analysis has used estimate aquifer parameters in non-steady flow (Adar & Sorek 1989). Furthermore, compartmental models are

also extensively applied to a wide ranging form of competition models, input-output analysis, and networks.

In physiology it is common for modellers to distinguish between process models, which describe systems and processes, and data models. Process driven models attempt to describe the inherent mechanisms at work in the system, whereas data driven models are selected to fit one or more particular data sets without reference to the processes at work. The widely used statistical linear and polynomial regression models are examples of data driven models. Naturally, it is possible to apply modelling that is a combination of data driven and process driven models. Due to the compartments having a physiological representation, compartmental models are intrinsically process driven. However, compartmental models may be used to fit experimental data for which there is no physiological interpretation for the compartments used or for the processes involved in the interaction between the compartments. Evidently such models are much less useful than the former as they do not provide any physiological insight. Human physiology concerns itself with studying function and thus mechanistic models, which describe the processes and interactions, are more practical to enhance our understanding. Furthermore, the large majority of human physiological characteristics are closely homologous to the corresponding aspects of animal physiology. Therefore a compartmental model developed from animal experimentation may be readily applicable in humans. Perhaps it may require some parameter scaling and minor modifications. At worst, it will offer some understanding for the physiological processes present and provide a solid foundation to model development, whereas a data driven model is very unlikely to share the same model interchange ability and applicability across species. Besides the advantage of inter-species transpositions, compartmental models also facilitate

extrapolation from one mode of administration to another (*e.g.* intravenous to oral). As a result, modellers prefer using process driven models and the application of compartmental modelling for estimating physiological parameters from experimental data has increased in popularity (Ahearn *et al.* 2005).

Physiologically based pharmacokinetic (PBPK) models and techniques aim to predict the ADME of natural or synthetic chemical substances in animal species. They tend to be compartmental, as the motivation is usually to produce a mechanistic model by mathematically describing the anatomical, physiological, physical, and chemical interactions and phenomena occurring in ADME processes. The compartments generally correspond to predefined organs and tissues and the interconnections representing blood and lymph flows.

Compartmental modelling has its roots in biomedical systems modelling, growing out of attempts to understand epidemiology. Mathematical modelling of the outbreak and spread of disease in populations had been studied for many years and in 1927, a simple deterministic compartmental model was formulated; the mass action susceptible-infected-recovered model of Kermark & Mckendrick 1927. Their model has stood the test of time and been successful in predicting the behaviour of numerous epidemic outbreaks (Brauer & Castillo-Châvez 2012) and to this date it remains the gold standard for predicting infectious disease and intervention effectiveness (Miller 2012).

Almost independently, compartmental modelling also emerged from efforts to employ radiolabelled compounds for analysing experiments on distribution and metabolism. The utilisation of radiolabelled compounds as tracers dates back to the early 1920's. Our understanding of metabolism grew from the work that followed

and mathematical analyses to quantify the distribution did not take long to appear. Useful parameters such as metabolic clearance rates and mean transit times may be estimated from tracer experiments. While some of these parameters can be obtained without postulating models to describe the distribution and metabolic rate of compounds, mechanistic models to describe the kinetic behaviour of the circulating tracers are desirable. Their purpose is to obtain important physiological and biochemical information. Although the term had yet to be coined, Artom *et al.* 1938 published a linear three compartmental model for radiolabelled rat phospholipids in blood, liver, and skeleton. Kinetic theory was eventually developed and compartmental modelling has been applied to pharmacokinetics since the 1960's (Jacquez 1996).

While compartmental modelling is widely regarded as offering the best approximation to the actual interactions between the body and a drug, alternative methods are implemented in pharmaceutical discovery and development. Non-compartmental modelling is centred on estimating the area under the curve (AUC) of a plasma concentration-time plot to quantify the exposure to a drug. Further estimation of global pharmacokinetic metrics are then induced from plasma concentration-time plot, such as *clearance*, the volume of plasma cleared of the drug per unit time, which is the ratio of the amount of drug administered over the AUC; the *apparent volume of distribution* V_d, the volume in which a drug appears to be distributed, which is ratio of the amount of drug administered over the plasma concentration; the *elimination half-life* $t_{1/2}$, the time required for amount of drug to reach half of its original value; the *elimination rate constant* k_e, the rate at which a drug is removed from the systemic blood stream, which is the ratio of $\ln(2)$ over

elimination half-life or the ratio of clearance over the apparent volume of distribution; and the *absorption rate* k_a, the rate at which a drug is absorbed into the systemic blood stream, which is normally estimated from linear regression and curve stripping. Wise 1985 suggests alternative power functions of the form At^{-a} or $At^{-a}e^{-bt}$ to describe the concentration-time plots. Although these non-compartmental approaches are highly dependent on the plasma sampling schedule, they produce sufficiently accurate results usually deemed adequate for bioequivalence studies. Furthermore non-compartmental modelling is also generally more versatile, that is to say it is not necessary to assume any specific homogenous pools or to conceptualise the interactions and mechanism occurring. The main advantage of non-compartmental approaches over compartmental analysis is that it is not required to develop and validate an appropriate physiological model that describes the inherent mechanism in action. On the other hand, the main disadvantage of non-compartmental modelling is the vastly inferior predictive ability, the lack of data integration, and absence of mechanistic insight (Rowland *et al.* 2011).

There is abundant literature on compartmental modelling, both supporting and criticising the approach. Gurpide & Mann 1970 warned against the temptation of constructing models comprised of as many compartments as exponential terms that have been identified in the experimental data time series. Here the danger is misapplying compartmental analysis, which is a pitfall for all modelling approaches. Non-compartmental techniques can just as easily be inappropriately applied as compartmental analysis. Furthermore, regardless of the modelling approach used, compartmental or non-compartmental, one may also easily misinterpret the analysis or the results. However DiStefano 1982 shows that non-compartmental analysis always underestimates the volume of distribution and the transit time under certain

conditions; that is if any pools that synthesise or metabolise substances are not directly measured then the results are assured to be erroneous.

Critiques of compartmental modelling include that it is not always clear which is the better model when more than one model of equivalent complexity is consistent with the collected data (Zieler 1981). A phenomenon named 'vanishing exponentials' (Wagner 1976), where one or two relatively unimportant exponential terms appear to disappear when fitting to data, is said to exacerbate the model selection ambiguity issue. Lastly, there is some criticism of the very assumptions behind compartmental modelling; i.e. that a small number of homogenous well mixed compartments is unrealistic and difficult to justify physiologically (Gillespie 1991). However, in glucose insulin kinetics, traditional non-compartmental analysis is revealed to contain structural errors that obstruct physiological insight (Cobelli *et al*. 1984). It is clear that compartmental modelling alone cannot solve and explain the complex biological and chemical reactions and interactions inside the human body, however, applied appropriately it is a very powerful tool to elucidate and quantify the mechanisms present. Although more demanding in terms of mathematical analysis, computational power required, and physiological representation, compartmental modelling is more functional and makes superior use of the data collected. The mechanistic nature of using compartmental modelling to study the pharmacokinetics of compounds may also lead to recommendations on how to improve experimental design, for example Clausen *et al.* 2006 used a simple compartmental model to propose insulin preparation enhancements.

Compartmental analysis continues to dominate pharmacokinetic modelling. It has been applied to numerous compounds and substances, such as topotecan (Cheung *et al.* 2008), lipoproteins (Barrett *et al.* 1998), remifentanil (Egan *et al.* 2004), tissue-

type plasminogen activator (Godfrey *et al.* 1998), nuclear proteins (Carrero *et al.* 2003), and morphine both in plasma and cerebrospinal fluid (Meineke *et al.* 2002; Groenendaal *et al*. 2007). The glucose minimal model, a compartmental model, remains the gold standard for glucose-insulin interactions in diabetes treatment (Man *et al.* 2002). The intestine has been modelled as simultaneous and consecutive intestinal transit flows for the oral absorption of atenolol (Yu & Amidon 1999), and iron (Sarria *et al.* 2004). Compartmental analysis has been applied to *in vivo* scenarios, to describe chylomicron and plasma free fatty acids in rat (Hultin *et al.* 1996) and tryptophan decarboxylase in living brain from positron emission tomograms (Cumming & Gjedde 1998). Compartmental models have been used to demonstrate that urea-nitrogen production is modulated by protein intake in man (Fouillet *et al*. 2008), to quantify the kinetic parameters alpha-linolenic acid conversion (Goyens *et al.* 2005), and model cell proliferation by anti-cancer agents (Ali *et al*. 2007). It has also recently been applied to model the immune system against melanoma cells (Pennisi *et al.* 2011) and model tumour growth and cytotoxic effects of taxotere in xenografts (Evans *et al.* 2013).

The theory and application of compartmental modelling may be split into three parts. The first is developing a plausible model of the mechanisms and processes at work in a specific biological system. Dependent on how much is known and established already on the biology and physiology in the field from which the problem arises, this may require considerable background research. It is important that the accumulated knowledge and theories justify the compartmental model. The structure and transfer processes in the model should have physiological meaning in terms of the known or suspected processes and structure of the real life system. Once a particular compartmental model has been formulated to describe the system being

studied, the second part is to develop the analytical theory. The mathematics for linear compartmental models is well defined, comparatively complete and relatively straight-forward; however it is inherently more complicated for non-linear models. A non-linear system is one whose output is not directly proportional to its input, or one that does not satisfy the superposition principle, whereas a linear system fulfills these conditions (Walker *et al.* 2008). The third and final part is often the most difficult, least understood, and most widely incorrectly implemented. Given one or more plausible models describing a system, structural identifiability and indistinguishability, sometimes described as the *inverse problem*, asks "do the data uniquely determine the unknown parameters and which of the models best describes the physiological mechanisms?". This normally puts restrictions on the model structure and experiment design, which has implications on how the data and which data should be collected. The concepts and theory for structural identifiability and indistinguishability are more complex and more subtle than the analytical theory of the forward problem; i.e. describing how a compartmental system behaves for given initial values, inflows, and outflows.

2.3 Structural Identifiability and Indistinguishability

Structural identifiability arises from the inverse problem of inferring from the known, or assumed, properties of a biomedical or biological system a suitable model structure and estimates for the corresponding rate constants and other parameters (Walter & Prozanto 1997). Under an assumption of the availability of perfect noise-free data, structural identifiability analysis considers the uniqueness of the unknown

model parameters from the input-output structure and initial conditions corresponding to proposed experiments to collect data for parameter estimation (Bellman & Åström 1970, Godfrey & DiStefano 1987). This is a fundamental, but often overlooked, theoretical prerequisite to experiment design, system identification and parameter estimation, since numerical estimates for unidentifiable parameters are effectively physiologically meaningless. To reiterate, compartmental models are process driven models, that is to say the compartments and model parameters have biological meaning (*Section* 2.2). If parameter estimates are to be used to inform about intervention or inhibition strategies, or other critical decisions, then it is essential that the parameters be uniquely identifiable. Such analysis is highly relevant to large-scale, highly complex systems, which are typical in chemical kinetics and systems biology. It is important to note that an *a priori* structurally identifiable model does not necessarily guarantee *a posteriori* numerical parameter identifiability (Carson & Cobelli 2001), for example see Grandjean *et al.* 2011, however it should greatly increase the confidence in the parameter estimation process for the given system observation(s).

Structural identifiability is often an issue when applying compartmental models to biological systems, as frequently it is not possible to observe every individual compartment, i.e. measure the concentration in each compartment. In the pharmaceutical experiments performed in drug research and development, biologists are generally restricted to measuring a small part of the system. For example they may be able to measure the concentration of a drug in the systemic circulation by taking blood samples; however they may not be able to directly observe the concentration in organs such as the brain and the liver. In order to infer the concentrations in the unobserved compartments, it is essential for the model to be

structurally identifiable. In other words the observations of the system need to uniquely determine the model parameters.

Observation and measurement errors are not included in the *a priori* theoretical analysis. Structural identifiability is concerned with establishing whether or not there is enough information in the observations to uniquely determine the unknown parameters. Structural identifiability assumes continuous, noise-free data, therefore it is not necessary to physically perform the experiments; the results can be established from the model of the experiment. In fact, the analysis should always be performed before the experiments as the results can impact on the experimental design and may render some experiments futile. The issue of trying to estimate parameter values in the presence of real, often discontinuous, and noisy data is a non-structural quantitative problem. It only necessitates a very small amount of *a posteriori* kinetic data to solve the problem (Cobelli & Distefano 1980). The *a posteriori* numerical identifiability analyses are based on local sensitivities of the unknown parameters, the Fisher Information Matrix, the covariance matrix, or the Hessian of the least square function (Srinath & Gunawan 2010). Recent publications on this topic (Bandara *et al.* 2009, Kreutz & Trimmer 2009, He *et al.* 2010) recommend using model based experimental design to iteratively improve the accuracy of the parameter estimates. Other authors (*Raul et al.* 2009) have proposed a method based on exploiting the profile likelihood that derives confidence intervals and can be used for experimental planning and model reduction. Nevertheless, it is a separate technical problem that the modeller needs to address and it should not detract from the prerequisite of satisfying *a priori* structural identifiability. Whilst some authors refer to parameter estimation from experimental data as identifiability, i.e. numerical or practical identifiability, this *a posteriori* parameter identification should not be

confused with structural identifiability. In this thesis the author will use structural identifiability and numerical identifiability to distinguish between the two.

Another structural identifiability issue that may occur in pharmacology is bioavailability in oral compartmental models. Bioavailability is the fraction of an orally administered dose that reaches the systemic circulation unchanged (Shah *et al.* 1992). When drugs are administered orally, not all the drug reaches the systemic blood stream due to incomplete absorption and first-pass metabolism. This is where a drug is absorbed by the digestive system and enters the hepatic portal system after a drug is swallowed. It is mediated through the portal vein into the liver before it can reach the rest of the body. The liver metabolises many drugs before they can emerge into the rest of the circulatory system and as a result only a reduced amount of the initial dose reaches the blood stream. Bioavailability and other observation gains can cause structural identifiability problems, however the issue can be circumvented as bioavailability can be estimated from non-compartmental methods using separate experiments to compare intravenous administration blood concentrations with oral blood concentration data (Amidon *et al.* 1995).

Structural identifiability is an essential pre-requisite in process driven models, as the resulting data are to be used to obtain parameter values that have a physiological meaning. Consequently, structural identifiability is often believed to not be as critical for data driven models, which are selected to fit one or more particular data sets without reference to the processes at work. However, parameter fitting software packages generally struggle when attempting to estimate non-identifiable parameters (Chis *et al.* 2011). Numerical optimisation algorithms may oscillate between numerous possible solutions, considerably reducing the confidence in the accuracy of the parameter values. There are many examples in the literature, where parameter

estimation has been difficult, and in some cases impossible, largely because the models are structurally unidentifiable (Lipniacki *et al.* 2004, Brown *et al.* 2004, Achard & De Schutter 2006, Piazza *et al.* 2008, Gutenkunst *et al.* 2007). These publications detail how the respective authors were unable to obtain unique and meaningful estimates for the unknown parameters since broad ranges of parameter values result in similar model predictions.

Despite the implications, structural identifiability analysis is often ignored in biomedical systems modelling. The vast majority of modelling studies are implemented without any consideration of structural identifiability, even though they do not offer any physiological insight and may cause numerical identification issues during parameter estimation, perhaps because it significantly reduces the complexity of the mathematical modelling. Regardless of the motivations, structural identifiability and indistinguishability is necessary for all models, whether they are data or process driven.

Still under an assumption of the availability of perfect, noise-free data, structural indistinguishability analysis considers the uniqueness of the postulated model's input-output structures corresponding to proposed experiments to collect data for parameter estimation (Evans *et al.* 2004). That is to say, it is possible to discriminate between the candidate models of the biological system. In order to infer the inherent mechanism, it is crucial to be able to distinguish between two or more plausible models that have different pathways or biological mechanisms. Indistinguishable models have mathematically equivalent input-output structures, therefore rendering the experiments to establish which model is superior completely futile (Kholodenko *et al.* 2005). Structural indistinguishability is therefore a critical prerequisite to experiment design, in order to differentiate between plausible model mechanisms.

In pharmacokinetic modelling, it is important to characterise the biological mechanisms present, but there may be a number of models depicting different processes that describe the experimental data accurately. The models could be represented by similar mathematical equations (see Érdi & Tóth 1989 and Espenson 1995); however without formal mathematical analyses of the model's input/output structure, postulated mechanisms are only rejected if they are inconsistent with the available experimental data. As with structural identifiability analyses, although the problem has been described in the literature for over three decades (Cobelli & Salvan 1977 and Franco *et al.* 1986), structural indistinguishability is routinely overlooked in biomedical systems modelling.

2.3.1 Mathematical Formulation and Definitions

Since both structural identifiability and indistinguishability are formal *a priori* methods, it is essentially less complicated to define them formally than informally. In order to describe indistinguishability formally, the following pair of autonomous non-linear systems with the same input vector $\boldsymbol{u}(t)$ are considered:

$$\Sigma(\boldsymbol{p})\begin{cases}\dot{\boldsymbol{q}}(t,\boldsymbol{p}) = \boldsymbol{F}(\boldsymbol{q}(t,\boldsymbol{p}),\boldsymbol{u}(t),\boldsymbol{p}),\ \boldsymbol{q}(0,\boldsymbol{p}) = \boldsymbol{q}_0(\boldsymbol{p}),\\ \boldsymbol{y}(t,\boldsymbol{p}) = \boldsymbol{h}(\boldsymbol{q}(t,\boldsymbol{p}),\boldsymbol{p}),\end{cases} \tag{2.9}$$

$$\tilde{\Sigma}(\tilde{\boldsymbol{p}})\begin{cases}\dot{\tilde{\boldsymbol{q}}}(t,\tilde{\boldsymbol{p}}) = \tilde{\boldsymbol{F}}(\tilde{\boldsymbol{q}}(t,\tilde{\boldsymbol{p}}),\boldsymbol{u}(t),\tilde{\boldsymbol{p}}),\ \tilde{\boldsymbol{q}}(0,\tilde{\boldsymbol{p}}) = \tilde{\boldsymbol{q}}_0(\tilde{\boldsymbol{p}}),\\ \tilde{\boldsymbol{y}}(t,\tilde{\boldsymbol{p}}) = \tilde{\boldsymbol{h}}(\tilde{\boldsymbol{q}}(t,\tilde{\boldsymbol{p}}),\boldsymbol{p}),\end{cases} \tag{2.10}$$

where the vectors $\boldsymbol{p}$ and $\tilde{\boldsymbol{p}}$ are constant (time-independent) parameter vectors, i.e. $\boldsymbol{p} = (p_1, p_2, \ldots, p_r)^T$ and $\tilde{\boldsymbol{p}} = (\tilde{p}_1, \tilde{p}_2, \ldots, \tilde{p}_{\tilde{r}})^T$; the vectors $\boldsymbol{q}(t,\boldsymbol{p})$ and $\tilde{\boldsymbol{q}}(t,\tilde{\boldsymbol{p}})$ are the l - dimensional state variable vectors, i.e. $\boldsymbol{q} = (q_1, q_2, \ldots, q_l)^T$ and $\tilde{\boldsymbol{q}} = (\tilde{q}_1, \tilde{q}_2, \ldots, \tilde{q}_l)^T$, such that the vectors $\boldsymbol{q}_0(\boldsymbol{p})$ and $\tilde{\boldsymbol{q}}_0(\tilde{\boldsymbol{p}})$ are the initial condition vectors, which may

be functions of the unknown parameters $\boldsymbol{p}$ and $\tilde{\boldsymbol{p}}$, respectively, in which case the parameter dependent initial conditions $\boldsymbol{q}_0(\boldsymbol{p})$ and $\tilde{\boldsymbol{q}}_0(\tilde{\boldsymbol{p}})$ are well defined for a given $\boldsymbol{p}$ and $\tilde{\boldsymbol{p}}$, respectively; and the vectors $\boldsymbol{y}(t, \boldsymbol{p})$ and $\tilde{\boldsymbol{y}}(t, \tilde{\boldsymbol{p}})$ are the n-dimensional output vectors, i.e. $\boldsymbol{y} = (y_1, y_2, \ldots, y_n)^T$ and $\tilde{\boldsymbol{y}} = (\tilde{y}_1, \tilde{y}_2, \ldots, \tilde{y}_n)^T$. In biomedical systems modelling, the input is generally the dose of drug administered whereas the output normally represents the measurement(s) or observation(s) of the given system experiment.

The vector of system equation(s) of model (2.9), $\boldsymbol{F}$, and the corresponding vector of observation function(s), $\boldsymbol{h}$, are generally non-linear functions of the system state vector, $\boldsymbol{q}(t, \boldsymbol{p})$; input vector, $\boldsymbol{u}(t)$; and parameter vector, $\boldsymbol{p}$. Similarly for the system equation(s) vector of model (2.10), $\tilde{\boldsymbol{F}}$, and the corresponding observation function(s) vector $\tilde{\boldsymbol{h}}$, which are both normally non-linear functions of the system state vector, $\tilde{\boldsymbol{q}}(t, \tilde{\boldsymbol{p}})$; input vector, $\boldsymbol{u}(t)$; and parameter vector, $\tilde{\boldsymbol{p}}$. All these functions, namely $\boldsymbol{F}$, $\tilde{\boldsymbol{F}}$, $\boldsymbol{h}$, and $\tilde{\boldsymbol{h}}$, are assumed to be rational polynomial functions, i.e. algebraic fractions where both the numerator and the denominator are polynomials, and therefore all four are analytical functions. Likewise, the initial conditions $\boldsymbol{q}_0(\cdot)$ and $\tilde{\boldsymbol{q}}_0(\cdot)$ assumed to be analytic functions in $\boldsymbol{p}$ and $\tilde{\boldsymbol{p}}$, respectively. It also assumed that $\boldsymbol{u}(\cdot) \in \Upsilon[0, \tau]$, where Υ is the set of admissible inputs for the models (2.9) and (2.10) on the time interval $[0, \tau]$, where $\tau > 0$. It is possible for this set to be empty, that is to say there are no inflows.

Both models $\Sigma(\boldsymbol{p})$ and $\tilde{\Sigma}(\tilde{\boldsymbol{p}})$ contain the same number of state variables (m) and the same number of output variables (n), however the algebraic forms of the system equation(s), $\boldsymbol{F}$ and $\tilde{\boldsymbol{F}}$, are not necessarily identical. The number of parameters in

model $\Sigma(\boldsymbol{p})$, r, is not necessarily equal to the number of parameters in model $\tilde{\Sigma}(\tilde{\boldsymbol{p}})$, $\tilde{r}$.

The parameter vector $\boldsymbol{p}$ is in an open subset of $\mathbb{R}^s$, which denotes the set of admissible parameter vectors for the model (2.9) for s a positive integer: $\boldsymbol{p} \in \Omega$. Likewise the parameter vector $\tilde{\boldsymbol{p}}$ is in an open subset $\mathbb{R}^{\tilde{s}}$, which denotes the set of admissible parameter vectors for the model (2.10) for $\tilde{s}$ a positive integer: $\tilde{\boldsymbol{p}} \in \tilde{\Omega}$. Given a particular, constant, and feasible parameter vector $\boldsymbol{p} \in \Omega$, the resulting output vector $\boldsymbol{y}(t, \boldsymbol{p})$ will depend on the input vector $\boldsymbol{u}(t)$. Similarly for the model $\tilde{\Sigma}(\tilde{\boldsymbol{p}})$; given a particular, constant, and feasible parameter vector $\tilde{\boldsymbol{p}} \in \tilde{\Omega}$, the resulting output vector $\tilde{\boldsymbol{y}}(t, \tilde{\boldsymbol{p}})$ will be affected by changes in the input vector $\boldsymbol{u}(t)$. This relationship between the output vectors and the input vector is referred to as the input/output behaviour. The two systems $\Sigma(\boldsymbol{p})$ and $\tilde{\Sigma}(\tilde{\boldsymbol{p}})$, are defined as *input/output indistinguishable*, written $\Sigma(\boldsymbol{p}) \sim \tilde{\Sigma}(\tilde{\boldsymbol{p}})$, if $\boldsymbol{y}(t, \boldsymbol{p}) = \tilde{\boldsymbol{y}}(t, \tilde{\boldsymbol{p}})$ for all input $\boldsymbol{u} \in \Upsilon[0, \tau]$ and for all $t \in [0, \tau)$. Given a generic $\boldsymbol{p} \in \Omega$, that is for all $\boldsymbol{p} \in \Omega$ except possibly for some vectors that are elements in a subset of a closed set of Lebesgue measure zero where the rational functions are not defined, the models Σ and $\tilde{\Sigma}$ are defined as *structurally indistinguishable*, written $\Sigma \sim \tilde{\Sigma}$, if there exist a $\tilde{\boldsymbol{p}} \in \tilde{\Omega}$ such that $\Sigma(\boldsymbol{p}) \sim \tilde{\Sigma}(\tilde{\boldsymbol{p}})$ and vice versa, *i.e.* given a generic $\tilde{\boldsymbol{p}} \in \tilde{\Omega}$ there exists a $\boldsymbol{p} \in \Omega$ such that $\Sigma(\boldsymbol{p}) \sim \tilde{\Sigma}(\tilde{\boldsymbol{p}})$.

Structural identifiability is a special case of indistinguishabilty; given a generic $\boldsymbol{p} \in \Omega$ the model $\Sigma(\boldsymbol{p})$ is defined as *globally structurally identifiable* if the equation $\boldsymbol{y}(t, \boldsymbol{p}) = \boldsymbol{y}(t, \tilde{\boldsymbol{p}})$ for all input $\boldsymbol{u} \in \Upsilon[0, \tau]$ and for all $t \in [0, \tau)$ implies that $\boldsymbol{p} = \tilde{\boldsymbol{p}}$.

It also very useful to determine whether individual parameters are identifiable; for a given output and well defined initial conditions, an *unidentifiable* parameter can take an (uncountably) infinite set of values, whereas a *non-uniquely (locally) identifiable* parameter can take any of a distinct (countable) set of values. A parameter is *globally identifiable* if for a given output and well defined initial conditions, it can only take one value.

If all of the unknown parameters are globally identifiable, the system model is structurally globally identifiable (SGI). In the case that all parameters are locally identifiable and at least one is non-uniquely identifiable then the model is structurally locally identifiable (SLI). In the case where at least one parameter is unidentifiable then the model is structurally unidentifiable (SU).

Numerous techniques for performing a structural identifiability analysis on linear parametric models exist and this is a well-understood topic (Godfrey & DiStefano 1987 and Walter 1987). Similarly for structural indistinguishability analysis (Godfrey & Chapman 1990), as structural identifiability is a special case of structural indistinguishability the same methods can generally be used with minor modifications. The Laplace transform approach, or transfer function approach, is normally the method selected to analyse linear models, see Jacquez & Greif 1985 for a thorough discussion of this method. However, when modelling biological and biochemical systems, non-linear interactions are ubiquitous. In pharmacology, doubling the dose of a drug very rarely doubles the effect, as many of the cellular uptake mechanisms are saturable and concentration dependent. One of the best known models for enzyme kinetics incorporates Michaelis-Menten kinetics, named after German biochemist Leonor Michaelis and Canadian physician Maud Menten (see Johnson & Goody 2011 for an English translation of the original publication in

German - Michaelis & Menten 1913). Biochemical reactions involving a single substrate are often assumed to follow Michaelis-Menten kinetics, without regard to the model's underlying assumptions (Gunawardena 2012). Furthermore most drugs do not satisfy the superposition principle, that it to say when administering two different substances together, their resulting effect is not the simple addition of their individual effects. The resultant action may be synergistic, when the drug's effect is amplified; antagonistic, when the drug's effect is diminished; or even a new effect may be created that neither substances produces on its own. Although these interactions are typically drug-drug related, there also exist interactions with foods, plants, and herbs. Consequently, most biological systems and mechanisms are governed by non-linear differential equations. The Laplace transform approach is not applicable to non-linear systems and analysis techniques for non-linear ordinary differential equations (ODE) models is an area that is still under development (Miao *et al.* 2011). Assessing *a priori* structural identifiability and indistinguishability of non-linear dynamic systems is particularly challenging (Murray Smith 1998, Audoly *et al.* 2001). There are a number of techniques available for non-linear systems, including:

- Taylor series approach or power series expansion (Pohjanpalo 1978)
- similarity transformation based approaches (Tunali & Tarn 1987; Vajda *et al.* 1989)
- Volterra and Generating Power Series Approaches (Lecourtier *et al.* 1987)
- identifiability tests derived from differential algebra techniques (Fliess & Glad 1993, Ljung & Glad 1994, Saccomani *et al.,* 2003)
- identifiability tableaus (Balsa-Canto *et al.* 2010)
- direct test (Denis-Vidal *et al.* 2001, Walter *et al.* 2004)

- approach based on the implicit function theorem (Xia & Moog 2003)
- identifiability test for reaction networks (Cracim & Pantea 2008, Davidescu & Jorgensen 2008, Szederkényi 2009)
- recently formulated algebraic input/output relationship approach (Evans *et al.* 2012)
- minimal output sets (Anguelova *et al*. 2012)

However, many of these approaches rapidly become mathematically intractable with increasing model size and complexity (Margaria *et al.*, 2001; White *et al.*, 2001). Significant computational problems can also arise even for relatively simple models (Jiménez-Hornero *et al*. 2008 and Meshkat *et al*. 2009). There is no 'one size fits all' technique that is amenable to every model; all the methods have greatly varying levels of success, depending on the model to which they are applied. Furthermore it is virtually impossible to predict, which methods are guaranteed to work for a specific model structure. Selecting an appropriate approach is problematic and they are often difficult to implement. Nevertheless, a structural identifiability analysis has been successfully applied to a large-scale non-linear mathematical model (43 state variables and 81 parameters) of a highly complex biomedical system (Cheung *et al*. 2008).

There are very few reviews on the different methods for performing structural identifiability and indistinguishability analyses on non-linear systems in the literature. Cobelli & Distefano 1980 only review very few basic techniques but exemplify the pitfalls on non-identifiability with some in depth examination of several physiological system models. Raue *et al.* 2011 includes a review of some applicable methods for structural identifiability analysis of biological system models and reinforces the importance of the *a priori* analysis. Chis *et al.* 2011 is the most

comprehensive review, as it includes the broadest range of methods and applies them to six models of widely varying complexity; however the authors are heavily biased in favour of their own method (identifiability tableaus) even though it fails to produce conclusive results in all but the simplest cases and some results contradict the other methods.

2.3.2 Methods

The non-linear approaches for structural identifiability implemented in the subsequent chapters are described below. Six different methods and tests were applied to all the models developed in order to establish whether each model was structurally identifiable and in order to investigate the suitability of each method for the candidate models proposed.

2.3.2.1 A Similarity Transformation Approach for Uncontrolled Systems (STAUS)

Given a linear model structure, this approach generates all the linear models that have the same input/output behaviour. It has also been successfully applied to non-linear models by mapping the state equations to a linear set (Evans *et al.* 2005). Given a non-linear mathematical model of the following general form:

$$\dot{\boldsymbol{x}}(t, \boldsymbol{p}) = \boldsymbol{f}(\boldsymbol{x}(t, \boldsymbol{p}), \boldsymbol{p}) \tag{2.11}$$

$$\boldsymbol{x}(0, \boldsymbol{p}) = \boldsymbol{x}_0(\boldsymbol{p}) \tag{2.12}$$

$$\boldsymbol{y}(t, \boldsymbol{p}) = \boldsymbol{h}(\boldsymbol{x}(t, \boldsymbol{p}), \boldsymbol{p}) \tag{2.13}$$

where $\boldsymbol{p}$ is the r dimensional vector of unknown parameters. The n dimensional vector $\boldsymbol{x}(t, \boldsymbol{p})$ is the state vector, such that $x_0(\boldsymbol{p})$ is the initial state and $\boldsymbol{y}(t, \boldsymbol{p})$ is

the observation vector. For an autonomous system with no input, this approach initially entails establishing an Observability Rank Criterion (ORC). This is performed by defining a function $\boldsymbol{H}$ given by

$$\boldsymbol{H}(x, \boldsymbol{p}) = (\mu_1(x, \boldsymbol{p}), \ldots, \mu_n(t, \boldsymbol{p}))^{\mathrm{T}} \tag{2.14}$$

where $\mu_1(\boldsymbol{x}, \boldsymbol{p})$ is the observation function $\boldsymbol{h}$, and $\mu_n(\boldsymbol{x}, \boldsymbol{p})$ is the *Lie derivative* of the previous term, given by

$$\mu_n(x, \boldsymbol{p}) = L_f \mu_{n-1}(x) = \frac{\partial \mu_{n-1}}{\partial \boldsymbol{x}}(x) \cdot f(x) \tag{2.15}$$

where $\boldsymbol{h}$ is the observation from (2.13) and $\boldsymbol{f}$ the vector of the system coordinate functions given by (2.11). If the Jacobian matrix with respect to $\boldsymbol{x}$, evaluated at $\boldsymbol{x}_0(\boldsymbol{p})$, of the resultant function $\boldsymbol{H}(\cdot, \boldsymbol{p})$ is non-singular, then the system (2.11) - (2.13) is said to satisfy the ORC and it is possible to construct a smooth mapping from the state corresponding to a parameter vector $\tilde{\boldsymbol{p}}$, indistinguishable from $\boldsymbol{p}$, to the state corresponding to $\boldsymbol{p}$. For a particular $\boldsymbol{p}$, let $\boldsymbol{H}_p$ denote the vector field $\boldsymbol{H}(\cdot, \boldsymbol{p})$. According to Theorem 4 from Evans *et al.* 2005, a smooth map λ is calculated using

$$\boldsymbol{H}_{\boldsymbol{p}}(\boldsymbol{\lambda}(x)) = \boldsymbol{H}_{\tilde{\boldsymbol{p}}}(x) \tag{2.16}$$

Equations can then be derived from the initial conditions $\boldsymbol{x}_0$, the model structure $\boldsymbol{f}$ and the observation function $\boldsymbol{h}$ by using:

$$\boldsymbol{\lambda}(\boldsymbol{x}_0(\tilde{\boldsymbol{p}})) = \boldsymbol{x}_0(\boldsymbol{p}) \tag{2.17}$$

$$\boldsymbol{f}(\boldsymbol{\lambda}(\boldsymbol{x}(t, \tilde{\boldsymbol{p}})), \boldsymbol{p}) = \frac{\partial \boldsymbol{\lambda}}{\partial \boldsymbol{x}}(\boldsymbol{x}(t, \tilde{\boldsymbol{p}}))\, \boldsymbol{f}(\boldsymbol{x}(t, \tilde{\boldsymbol{p}}), \tilde{\boldsymbol{p}}) \tag{2.18}$$

$$\boldsymbol{h}(\boldsymbol{\lambda}(\boldsymbol{x}(t, \tilde{\boldsymbol{p}})), \boldsymbol{p}) = \boldsymbol{h}(\boldsymbol{x}(t, \tilde{\boldsymbol{p}}), \tilde{\boldsymbol{p}}) \tag{2.19}$$

The resulting system of equations are solved simultaneously for $\boldsymbol{p}$ and the model is structurally globally identifiable (SGI) if $\boldsymbol{p} = \tilde{\boldsymbol{p}}$ is the only solution, that is to say all the parameters are globally uniquely identifiable. A set of distinct solutions gives rise to a structurally locally identifiable (SLI) model. Otherwise the model is structurally unidentifiable (SU). The main limitation for applying this method is that it can be very memory intensive to solve (2.16) and thus compute a smooth map λ, particularly if the model equations contain complicated non-linear terms. In some cases, solving (2.16) yields more than one solution or solutions including square roots and other non integer powers, which mean that a smooth map λ cannot be computed and it is therefore not possible to apply the approach.

2.3.2.2 A Sufficient Condition for Unidentifiability

As a straightforward consequence of the similarity transformation approach for uncontrolled systems described above the approach gives rise to a sufficient condition for unidentifiability (Evans *et al.* 2005). In this instance, instead of calculating the smooth map λ from solving (2.16) using the observation vector field $\boldsymbol{H}$, the smooth map λ is assumed to be of the form

$$\lambda(\boldsymbol{x}) = (t_1 x_1, ..., t_n x_n)^{\mathrm{T}} \tag{2.20}$$

where $t_i (\neq 0) \in \mathbb{R}$ and n is the number of states. Again the identities (2.17) - (2.19) are used to generate the relevant equations which are solved for $\tilde{\boldsymbol{p}}$ and t_1, ..., t_n. If there are an (uncountable) infinite number of solutions, then the model is structurally unidentifiable (SU). The main limitation of this method is that it only assesses unidentifiability and cannot show that a model is identifiable.

2.3.2.3 Differential Algebra Approach Using Characteristic Sets (DAACS)

This approach consists of generating the input/output structure of the given model of the general form (2.11) - (2.13) solely in terms of the observation function $\boldsymbol{y}(t, \boldsymbol{p})$ and its derivatives using characteristic sets (Fliess & Glad 1993, Ljung & Glad 1994). Assuming the observation $\boldsymbol{y}(t, \boldsymbol{p}) = \boldsymbol{h}(\boldsymbol{x}(t, \boldsymbol{p}), \boldsymbol{p})$ is linear, this approach considers two parameter vectors $\boldsymbol{p}$ and $\tilde{\boldsymbol{p}}$, that produce the same output for all t, and thus produce the same derivatives of the observation for all t, i.e.

$$y^{(n)}(t, \boldsymbol{p}) = y^{(n)}(t, \tilde{\boldsymbol{p}}), \text{ for all } t. \tag{2.21}$$

If it is possible to generate and expression $g(y, \ldots, y^{(n-1)}, \boldsymbol{p})$ derived from the model equations $\boldsymbol{f}(\boldsymbol{x}(t, \boldsymbol{p}), \boldsymbol{p})$ purely in terms of the observation vector $\boldsymbol{y}(t, \boldsymbol{p})$ and its derivatives then the approach entails solving

$$g(y, \ldots, y^{(n-1)}, \boldsymbol{p}) = g(y, \ldots, y^{(n-1)}, \tilde{\boldsymbol{p}}) \tag{2.22}$$

for $\boldsymbol{p}$. This method requires the model to satisfy the ORC and is implemented using the Rosenfeld-Gröbner algorithm in Maple 2010, which calculates a characteristic set for the model with a particular ranking of variables, where one member of the characteristic set gives the input/output map $g(y, \ldots, y^{(n-1)}, \boldsymbol{p})$. A second input/output map is generated by substituting $\boldsymbol{p}$ for $\tilde{\boldsymbol{p}}$ in the original map. If equating the monomials of these two functions produces only one solution for the unknown parameters, then the system is SGI. The Rosenfeld-Gröbner algorithm in Maple 2010 can be very memory intensive, particularly if the model equations contain complicated non-linear terms.

2.3.2.4 Algebraic Input/Output Relationship Approach (Ai/oRA)

This is the most recent approach, developed by Evans *et al.* 2012. Given a model of the general form (2.11) - (2.13) that satisfies the ORC, this approach generates the corresponding input/output map for the system. This approach requires calculating the *Lie derivatives* of the observation function, defined in *Equation* (2.15). These are used as inputs into the Univariate Polynomial or Groebner Bases algorithms in Maple, producing the input/output relationship for the model. Again, a second input/output map is generated by substituting $\boldsymbol{p}$ for $\tilde{\boldsymbol{p}}$ in the original input/output relationship. If equating the monomials of these functions produces only one solution for the unknown parameters, then the system is SGI. The Univariate Polynomial algorithm in Maple 2010 is probably the most efficient algorithm out of all the approaches described, however it can still be very memory intensive, particularly if the model equations contain complicated non-linear terms.

2.3.2.5 Non-differential Input/Output Observable Normal Form Approach (NDi/oONF)

This approach also generates the input/output structure for the given model, solely in terms of *Lie derivatives* of the observation function, defined in *Equation* (2.15). This is achieved using a co-ordinate transformation into the Observable Normal Form. Given a model of the general form (2.11) - (2.13) which satisfies the ORC, the *Lie derivatives* are calculated and solved simultaneously as a system of equations to obtain expressions for all the states in term of these *Lie derivatives*. These are subsequently substituted into the derivative with respect to time of the highest *Lie derivative* to give an input/output map of the model. If equating the monomials of this function produces only one solution for the unknown parameters, then the system is SGI. Assuming the model is reduced to its minimal form; the number of

Lie derivatives required is one more than the number of state variables. Therefore this approach tends to be the least memory intensive to implement for systems with few states.

2.3.2.6 Taylor series expansion

This general method, introduced in Pohjanpalo 1978, is commonly used for systems with a single input and can be applied to both linear and non-linear systems. Given a mathematical model of the general form (2.9), the components of the observation vector $y_i(t, \boldsymbol{p})$ are expanded as a Taylor series around the known initial condition.

$$y_i(t, \boldsymbol{p}) = y_i(0, \boldsymbol{p}) + \dot{y}_i(0, \boldsymbol{p})t + \ddot{y}_i(0, \boldsymbol{p})\frac{t^2}{2!} + \ldots + y_i^{(k)}(0, \boldsymbol{p})\frac{t^k}{k!} + \ldots \qquad (2.23)$$

where

$$y_i^{(k)}(0, \boldsymbol{p}) = \left.\frac{d^k y_i}{dt^k}\right|_{t=0} \quad \text{for } k = 1, 2, \ldots \qquad (2.24)$$

The Taylor series coefficients $y_i^{(k)}(0, \boldsymbol{p})$ are measurable and unique for a particular output. Equating the Taylor series coefficients obtained from $\boldsymbol{y}(t, \boldsymbol{p})$ with those derived from $\boldsymbol{y}(t, \tilde{\boldsymbol{p}})$ produces a system of equations. If there is only one solution for the unknown parameters, then the model is SGI. The total number of unknown model parameters determines the minimum number of Taylor series coefficients required to establish structurally identifiability and this causes significant computational problems in models with numerous unknown model parameters.

2.3.2.7 Structural Indistinguishability

As described previously, structural identifiability is a special case of structural indistinguishability and therefore the same approaches can generally be implemented

with minor modifications. However it is not possible to use the STAUS technique to investigate structural indistinguishability of models that have different number of states. For DAACS, Ai/oRA, and NDi/oONF the input/output maps generated can be compared to investigate if they are structurally distinguishable. This is implemented by equating the monomials and solving for the unknown parameter vector $\boldsymbol{p}$. The Taylor series expansion as described above is also used to implement a structural indistinguishability analysis. In this approach, the corresponding coefficients of the Taylor series expansions around the initial condition of the observation function for each of the two candidate models, i.e. $y_1(t, \boldsymbol{p}_1)$ and $y_2(t, \boldsymbol{p}_2)$, are compared term by term to ascertain relationships between the parameter sets for the two different models. This process continues until either all parameters can be uniquely related between the two candidate models or a generic contradiction ensues (i.e. from established relationships for the parameters from the early coefficients, it is necessary for certain parameters in one or both models to be zero, which generically cannot be the case). In practice, it is not a pre-requisite to calculate as many Taylor series coefficients as there are unknown model parameters, as often distinguishability will be ascertained from the early coefficients of the Taylor series expansions.

2.4 Transporters in pharmacokinetics and pharmacodynamics

First and foremost, drugs need to travel to and be absorbed into the target cells in order for them to reach the biological receptors where they can be metabolised and eventually have the desired therapeutic effect. An administered drug needs to enter to systemic circulation in order to be distributed to various tissues in the body. The drug is subsequently eliminated from the body by metabolism, normally in the liver, and eventually excreted into bile or urine. During all these pharmacological processes, the drug molecule will have passed through numerous cell membranes. As such, one of the most important factors in establishing the pharmacokinetic properties of a new pharmaceutical compound is the permeability of biological membranes.

Even though it has generally been widely accepted that numerous medicinal molecules are transported across biological membranes via simple diffusion, it has recently been proposed that carrier mediated cellular uptake is responsible for most of the membrane drug transport in biological systems (Dobson & Kell 2008; Sugano *et al.* 2010). Carrier-mediated transport is the process of molecules and particles moving across membranes, such as cell membranes, the blood-brain barrier (BBB), and the gastrointestinal mucosa, via a specific carrier protein or transporter (Petzinger & Geyer 2006). This process differs from simple passive diffusion where particles move from a region of higher concentration to a region of lower concentration without a transporter. There are two forms of carrier-mediated transport; active transport and facilitated diffusion. Active transport is a non-linear

saturable process which requires energy and can move substances against its concentration gradient (Shugarts & Benet 2009), as opposed to passive transport (simple diffusion, facilitated diffusion, filtration, and osmosis) which does not require energy and can only move substances down its concentration gradient. There are two categories of active transport determined by the type of energy used. Primary active transport requires chemical energy, i.e. adenosine triphosphate (ATP), whereas secondary active transport involves using the potential energy stored in electrochemical gradients.

Primary active transport, often referred to as *ATP-powered pumps* or simply *pumps*, is a coupled chemical reaction. ATP hydrolysis of ATP into adenosine diphosphate (ADP), which can be further hydrolysed to give energy, and orthophosphate (P_i), an inorganic phosphate, is coupled to transporting ions or small molecules against a concentration or electrochemical gradient across a biological membrane. The combined reaction is energetically favourable (Lodish *et al.* 2000) and is illustrated in *Figure* 2.2. The mechanism is characterised by substances binding rapidly and reversibly to a transporter protein located on the biological membrane of epithelial cells and are translocated from the intracellular to the extracellular milieu, generally against a steep diffusion gradient. ATP-powered pumps include sodium pumps, proton pumps, and calcium pumps, which transport sodium, hydrogen, and calcium respectively. One the most interesting features of primary active transport is that the pumps are reversible and can function as ATP synthesisers, which is how mitochondria and chloroplasts store energy.

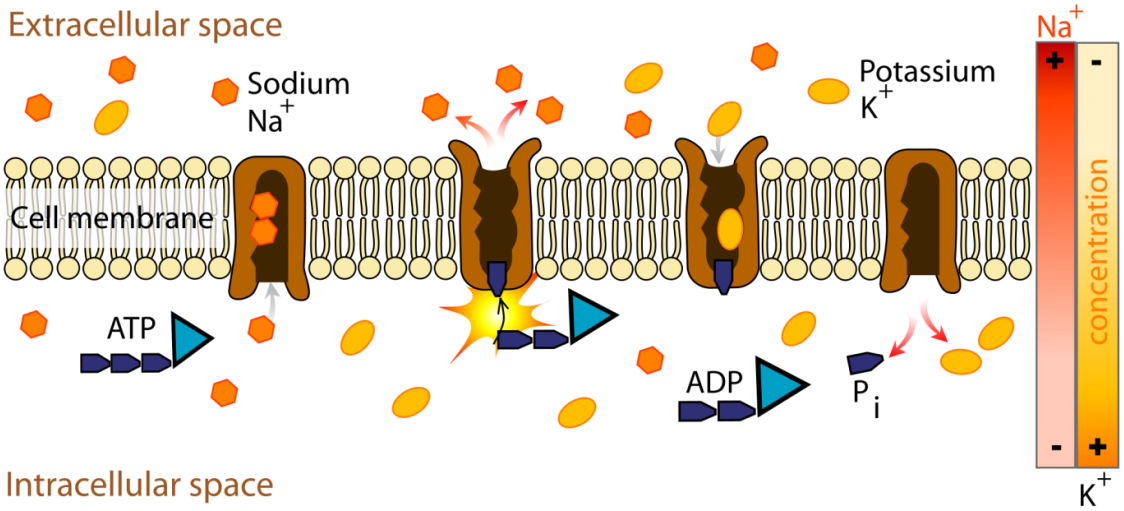

Figure 2.2: Example of primary active transport - the sodium-potassium pump (Na^+/K^+-ATPase), where the transporter uses ATP to simultaneously pump three sodium ions (Na^+) and two potassium ions (K^+) in and out of the cell, respectively (courtesy of Mariana Ruiz Villarreal).

In secondary active transport, sometimes called *co-transport* or *coupled transport*, a carrier protein couples the transport of a solute, usually an ion, in the direction of its electrochemical gradient to the transport of a second solute against its concentration gradient (Shechter 1986). The potential energy stored in the electrochemical ion gradient is used to transport the second solute (see *Figure* 2.3). The ion is generally referred to as the driving ion, as its movement is responsible for providing the energy required to drive the solute against its concentration gradient. The coupling between the driving ion and the solute is crucial to the process, as both must be bound to the transporter at the same time for the membrane translocation to occur. It is appropriate to call this process secondary active transporter since the electrochemical concentration gradient of the driving ion is maintained by primary active transport. The driving ion is generally sodium and its gradient is maintained by the sodium-potassium adenosine triphosphatase (Na^+/K^+-ATPase), which co-transports sodium out of the cell and potassium into the cell (see *Figure* 2.2). Secondary active

transport was first discovered by Robert K. Crane (Crane *et al.* 1961). He is accredited with being the first to formulate the concept of flux coupling in biology (Wright & Turk 2004; Boyd 2008). Secondary active carrier proteins, or cotransporters, are classified into two categories; symporters and antiporters, depending on the relative direction of movement of the driving ion and the cotransported molecule. Symporters cotransport both in the same direction, whilst antiporters translocate the cotransported molecule in the opposite direction to the driving ion. Examples of active transport include the re-absorption of glucose, amino acids, and salts by the proximal convoluted tubule of the nephron in the kidney.

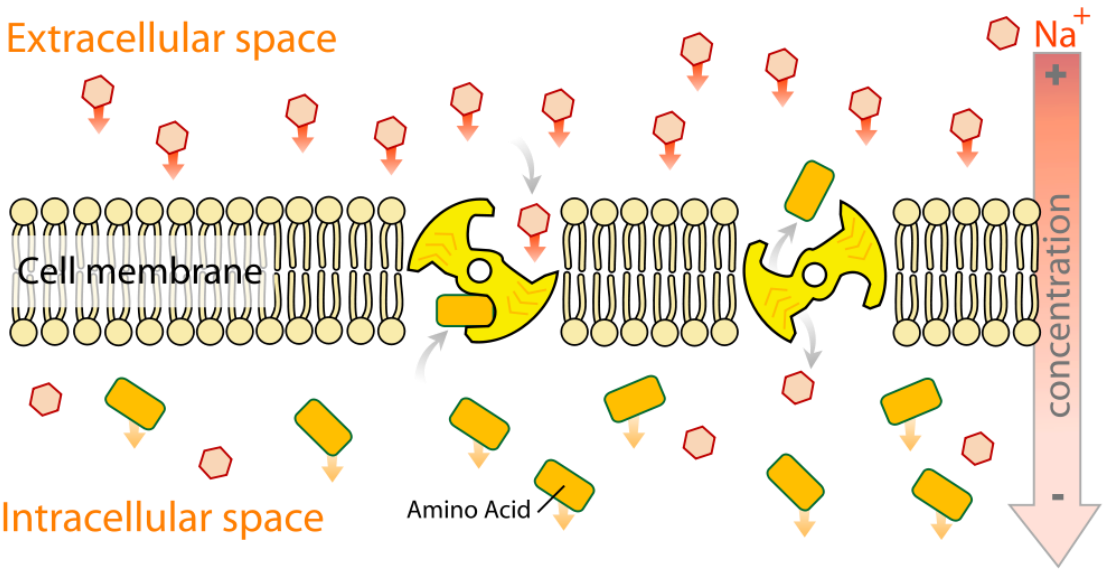

Figure 2.3: Example of secondary active transport - the energy stored in the sodium (Na+) concentration is utilised to efflux amino acids out of the cell. The sodium (Na+) concentration gradient is characteristically created and maintained by primary active transport; the diffusion of this driving ion (Na+) back across the biological membrane provides the energy for secondary active transport (courtesy of Mariana Ruiz Villarreal).

On the other hand facilitated diffusion is not energy dependent and cannot move substances against a concentration gradient. The main difference between facilitated

diffusion and simple diffusion is that the former occurs by means of a membrane protein located on the apical and basolateral membrane and as a result, it displays the properties of specificity, competition, and saturation. The membrane protein, or uniporter, can either be an ion channel or a carrier protein as shown in *Figure* 2.4. Channel proteins transport water and certain specific ions. Structurally, they are arranged in a protein lined passageway across the cell membrane's epithelium. Some channel proteins can be open or shut in response to specific signals, such as membrane potential difference, physical pressure, and ligand binding. Uniporter carrier proteins are a membrane transport protein to which solutes bind and are translocated in the decreasing direction of the solute concentration gradient. For example, cellular glucose absorption occurs by facilitated diffusion (Alberts 1998).

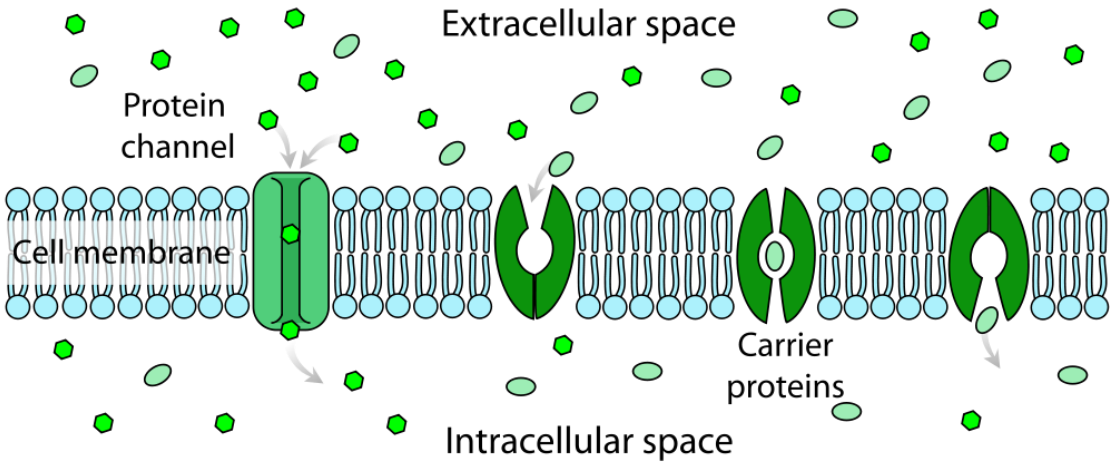

Figure 2.4: Diagram illustrating facilitated diffusion - membrane transport proteins assist the movement of molecules across the biological membrane. There are two mechanisms in actions, in the protein channel the molecules pass through the channel within the protein and in carrier proteins, the transporter modifies its shape in order to allow molecules to influx into the intracellular environment (courtesy of Mariana Ruiz Villarreal).

Inherently, all carrier mediated processes, both primary and secondary active transport and facilitated diffusion, are saturable due to the limited number of binding sites on the carrier protein and similar substances are able to compete for the transporter, which is when competitive inhibition occurs (Fromm & Kim 2011, Yoshida *et al.* 2013).

The rate of transport of the different types of active transport tends to differ significantly owing to the differences in their mechanism of operation. In channel proteins, multiple ions or water molecules can move simultaneously in a single file at a very fast rate (up to 10^8 per second), whereas in pumps and cotransporters move only approximately 10^2 - 10^4 molecules per second (Lodish *et al.* 2000). This is because each substrate molecule is required to bind to the transporter, which then must undergo a conformational change in order to translocate the substrate.

The carrier mediated process has been recognised for at least 25 years (Cabantchik & Ginsburg 1977, Crane 1977) and over the last two decades, a vast number of membrane transport proteins have been discovered. It has become increasingly apparent that transporters play a critical role in the ADME of a wide variety of drugs in clinical use (Mizuno *et al.* 2003). In fact it is now generally accepted that most drugs cannot cross the plasma membrane by simple diffusion and therefore most of the cellular uptake and excretion involves transporters (Sugano *et al.* 2010; Marin 2012). This is an intuitive result, as cells are likely to have evolved a high level of specificity for the substance transported to regulate their external membranes. This ensures only the right nutrients can influx and to efflux toxins. Even uptake of molecules, such as water and urea, which can diffuse across simple cell membranes (pure phospholipid bilayers) is commonly accelerated by membrane transport proteins (Lodish *et al.* 2000). Transporters are integral membrane proteins; that is to

say protein molecules that are permanently attached to and spread ubiquitously along the biological membrane across which they transport substances. Carrier proteins are widely distributed across the body, in all the extracellular membranes, and are responsible for transporting a wide range of substrates, such as acetyl coenzyme A, amino acids and oligopeptides, ammonium, bile salts, biogenic amines, carboxylate and other organic anions, choline, essential metals, fatty acids and lipids, glucose and other sugars, inorganic cations and anions, neurotransmitters, nucleosides, thyroid hormone, urea, and vitamins (He *et al.* 2009).

It is crucial to investigate the interactions between transporters and drugs in important organs such as the intestine, kidney, and liver. Understanding the mechanisms of transport is critical in determining the extent of ADME of a drug substrate in man. The pharmacokinetic profile of a particular compound in the body is determined by the cellular uptake and efflux across the phospholipid bilayer, which is impeded or expedited by the specific dispersion of transport proteins.

Since the increasing appreciation of the role that transport proteins play in ADME, an International transporter consortium (ITC), consisting of about 50 academic, industrial, and regulatory scientist was established in 2007 (International Transporter Consortium 2010). In their latest publication the ITC conclude that better *in silico* tools are required to improve mechanistic understanding and assessment of intracellular drug and metabolite concentrations, and that the development of mathematical models to inform clinical studies in order to fully address the impact of uptake and efflux transporters is a key area for academic research (Giacomini & Huang 2013). Robust mechanistic models of transporters will aid with dose selection, drug interaction prediction, and inter-subject variability in drug response.

There are over 400 membrane transporter proteins annotated in the human genome divided into two major categories: ATP binding cassette (ABC) and solute carrier (SLC) (DeGorter *et al.* 2012, Liu *et al.* 2012). The latter is the larger category; over 380 different SLC sequences have been identified which are grouped into 48 subcategories (Fredriksson *et al.* 2008). Less than half of these subcategories have been described in clinical pharmacology. The SLC membrane transport protein function by either facilitated diffusion (protein channel or uniporter) or secondary active transport (symporter or antiporter). Most facilitate cellular uptake, however, depending on the orientation of the driving ion and the coupled substrate concentration gradients across the biological membrane, certain SLC carriers exhibit efflux or bidirectional properties. The smaller ABC transporter category has seven subcategories for the 49 unique proteins obtained from the human genome (Dean & Allikmets 2001). The ABC transporters are ATP pumps using primary active transport and are therefore efflux transporters by definition. Irrespective of whether they are influx of efflux transporters, a distinction can be made between absorptive and secretory transporters, with the latter mediating drug excretion from the circulation into bile and the former being involved in transporting substrates into the systemic blood stream.

Out of the hundreds of unique protein isoforms, around twenty (PEPT1, PEPT2, OCT1, OCT2, OCTN1, OCTN2, OAT1, OAT2, OAT3, OAT4, MATE1, MATE2-K, OATP1A2, OATP1B1, OATP1B3, OATP2B1, OATP4C1, MDR1, MRP2, MRP3, MRP3, BCRP) are currently considered to be the transporters that exert the greatest impact on clinical pharmacology (Mizuno & Sugiyama 2002; Tsuji 2002; Ho & Kim 2005; Ito *et al.* 2005; Shitara *et al.* 2005; Endres *et al.* 2006; Zair *et al.* 2008). Investigating and modelling all of them would easily take at least one lifetime and is

evidently beyond the scope of this thesis. Consequently the author has focussed on two specific prominent transporters; one from the ATP binding cassette, breast cancer resistance protein (BCRP), and one from the SLC family, OATP1B1.

2.4.1 Breast Cancer Resistance Protein (BCRP)

Breast cancer resistance protein (BCRP), ABCG2 gene, is the only member of the ABCG subfamily that is involved in mediating drugs. It is sometimes referred to as Mitoxantrone Resistance-associated protein - MXR (Miyake *et al.* 1999) or Placenta specific ABC transporter - ABC-P (Allikmets *et al.* 1998); all appropriate names as it was discovered to significantly reduce efficacy of the antineoplastic agent mitoxantrone in breast cancer treatment (Ross *et al.* 1999), and heavily expressed in placenta.

It impedes the absorption and enhances the excretion of many endogenous and xenobiotic compounds, including various anticancer agents. The ABCG subfamily protein isoforms are structurally characterised by one transmembrane domain and one ATP-binding site. This configuration is about half the size of the minimal functional structure of an ABC transporter, which consists of two transmembrane regions, each comprised of two cytoplasmic ATP binding areas and six transmembrane helices (Locher 2009). As a result BRCP is considered a half transporter, which is believed to dimerise to form a functioning transporter. Dimerisation is a chemical reaction in which two monomers react to form a dimer, or molecule of two identical halves. There is some evidence to suggest that BCRP exists and functions as a homotetramer, i.e. a protein complex comprising of four identical subunits (Xu *et al.* 2004). BCRP was originally discovered in a multidrug-resistant breast cancer cell line and therefore most of the initial reported substrates

are anticancer agents. To date, a large number of functionally and structurally diverse hydrophobic drug substrates have been identified as BRCP substrates, such as abacavir, albendazole sulfoxide, camptothecin, cerivastatin, cimetidine, ciprofloxacin, dipyridamole, edaravone sulfate, erlotinib, flavopiridol, gefitinib, glibenclamide, imatinib, lamivudine, methotrexate, Mitoxantrone, nelfinavir, nitrofurantoin, norfloxacin, ofloxacin, olmesartan, oxfendazole, pitavastatin, rosuvastatin, SN-38, sulfasalazine, topotecan, zidovudine (Cusatis & Sparreboom 2008, Robey *et al.* 2009, Sarkadi *et al.* 2006, van Herwaarden & Schinkel 2006). The exact mechanism and clear structural relationship is yet to be fully elucidated (Russel 2010). BRCP is highly expressed in many tissues; predominantly in plasma membranes with important barrier functions, such as the canalicular membrane of brain (Hartz *et al.* 2010), intestine, kidney (Huls *et al.* 2009), liver, and placenta capillaries.

BCRP is expressed in the brush border membrane of the gut where in conjunction with ABCB1 and MRP2, it plays an important role as the human body's first line of defence against xenobiotics, impeding absorption into the systemic blood stream. It actively pumps a wide range of compounds and metabolites back into the gut lumen and thereby limits the oral bioavailability of a wide range of drug substrates (Russel 2010).

In the liver, BCRP plays a critical role in drug elimination, extracting drugs with high protein binding from the systemic blood stream. It is expressed in the canalicular membrane of hepatocytes, where alongside with MRP2, it is predominantly responsible for pumping conjugated and unconjugated anionic drugs into bile.

BCRP is also expressed in the kidney where it is involved in renal drug excretion (Maliepaard *et al.* 2001; Huls *et al.* 2008, Takashima *et al.* 2013). Alongside three other apical ABC transporters (MDR1/P-gp, MRP2, and MRP4) at the proximal tubule brush border membrane, BCRP is responsible for mediating the elimination of a wide variety of amphipathic drugs and metabolites from the systemic blood stream into urine.

It is also expressed in stem cells, where its function is believed to protect the cells against xenobiotics (Zhou *et al.* 2001), and has been found to have implications for the survival of stem cells and tumour cells under hypoxia (Krishnamurthy *et al.* 2004). It is of particular interest in oncology as it actively effluxes chemotherapeutics, such as mitoxantrone and topotecan, across the cell membrane, significantly impeding their efficacy by limiting the amount of therapeutic that can accumulate in the target region. Functioning as an obstacle to drug penetration, BCRP reduces the effectiveness of some drugs and as a consequence often increases drug resistance, which may aggravate and complicate the disease (Doyle & Ross 2003). Multidrug resistance of tumour cells is a common cause of treatment failure in cancer.

2.4.2 Organic Anion Transporting Polypeptide (OATP)

The SLCO gene subfamily of SLC is comprised of twelve organic anion transporting polypeptides (OATPs) that co-transport large and hydrophobic organic anions (Type II). OATPs mainly mediate a variety of amphipathic organic substances, such as thyroid hormones, toxins, steroid conjugates, bile salts, and a wide range of drugs (Hagenbuch & Gui 2008). There is some evidence to suggest that these transmembrane glycoproteins use secondary active transport and act as organic anion

antiporters, however, similarly to BCRP, the exact mechanism is yet to be fully elucidated (Mahagita *et al.* 2007, Russel 2010). Whilst some OATPs are expressed ubiquitously, OATP1B1 (one of the eleven human OATP isoforms) is exclusively found on the liver, expressed on brush border membranes. Other SLC influx transporters are expressed at the sinusoidal membrane of hepatocytes, such as OATP1B3, OATP2B1, OAT2, and OCT1, however OATP1B1 has been identified as particularly significant for mediating many clinically important compounds, such as angiotensin converting enzyme (ACE) inhibitors, glitazones, macrolide antibiotics, sartans, and statins. There is also evidence of some relevant drug-drug interactions being described with the immunosuppressant drug cyclosporine A for OATP1B1 mediated statin transport (Endres *et al.* 2006). Common variants of the OTAP1B1 gene, SCL01B1, have been highly correlated to an increased risk of simvastatin induced myopathy in a genome wide study (Link *et al.* 2008). Although these genotypes have been shown to be linked with elevated statin blood concentrations, there is still some debate in the literature as to whether simvastatin is in fact an OATP1B1 substrate (Choi *et al.* 2010; Romaine *et al.* 2009).

OATP1B1 is of central importance in hypercholesterolaemia, as it mediates so many statins, which lower cholesterol by inhibiting the HMG-CoA reductase enzyme in the liver. High cholesterol is often associated with cardiovascular disease, because atherosclerosis, or thickening of the artery walls as a result of the accumulation of fatty materials, is one of the major precursors to cardiovascular disease. Cardiovascular disease is the leading cause of deaths worldwide and statins have also been shown to beneficial with a decrease in mortality and further heart disease in those who are at high risk, in particular in patients with a history of cardiovascular disease. OATP1B3, a homolog of OATP1B1, exhibits comparable substrate

specificity; however its expression is more concentrated around the central vein hepatocyte basolateral membranes. Both these organic anion antiporters are critical determinants in hepatobiliary elimination, extracting drugs with a high protein binding from the systemic blood stream. As hepatic influx is generally the rate limiting factor in removing compounds from blood circulation and subsequently excreting them into bile, OATP1B1 and OATP1B3 are crucial factors in drug disposition and exposure. Their genetic variability and inhibition is of particular interest in clinical pharmacology as they are major contributors to patient inter-individual variability in hepatic elimination and drug-drug interactions (Noe *et al.* 2007, Kalliokoski & Niemi 2009). OATP1B1 substrates include a functionally and structurally diverse range of amphipathic drugs such as atorvastatin, atrasentan, benzylpenicillin, bosentan, caspofungin, cerivastatin, digoxin, enalapril, ezetimibe glucuronide, fexofenadine, fluvastatin, methotrexate, olmesartan, pitavastatin, pravastatin, rifampicin, rosuvastatin, simvastatin, SN-38, temocapril, troglitazone sulfate, and valsartan (Dobson & Kell 2008, Hu *et al.* 2008, Nies *et al.* 2008, Noe *et al.* 2007, Katz *et al.* 2006, Oswald *et al.* 2008, Abe *et al.* 2001, Maeda *et al.* 2006).

2.4.3 Previous kinetics modelling

There is a significant amount of drug release kinetic modelling in the literature, where a wide variety of different coatings, formulations, and drug manufacturing methods are investigated in order to establish the best way for oral administered drugs to dissolve in the body. Recently, Dash *et al.* 2010 and Siepmann & Peppas 2012 comprehensively reviewed the spectrum of mathematical models in this field. Specific matrix structure and topologies are modelled to investigate the mechanisms and numerically quantify the release rates. The motivation behind this modelling is

to control the drug delivery such that drug concentrations do not dangerously increase too rapidly and subsequently exceed their toxic threshold, or conversely that drug concentrations never reach or fall below their effective therapeutic level. However this modelling is limited to solid pharmaceutical dose dissolution and does not concern itself with the gut absorption rate or further transport kinetics and metabolisation of the compounds.

The chemical structure of transporters has also been modelled, including both OATP (see for example Chang *et al.* 2005, Meier-Abt *et al.* 2006) and BCRP (Ecker *et al.* 2008), however this pharmacophore modelling is only concerned with molecular structure of transporters and not their kinetics.

Although OATP1B1 and BCRP have been and continue to be comprehensively researched both *in vitro* and *in vivo*, using functional assays and human clinical studies (Maeda & Sugiyama 2008), the literature on modelling these transporters kinetics mathematically is surprisingly sparse. Perhaps because scientists have only begun studying the pharmacogenetics of transporters and this research field is still very novel (Nakamura *et al.* 2008).

In a recent review of the current knowledge of BCRP structure and function (Ni *et al.* 2010), very few equilibrium or kinetic binding studies for substrates or inhibitors of BCRP were found in the literature. Özvegy et al. 2001 demonstrated the ATPase activity of BCRP to exhibit classical Michaelis-Menten kinetics but did not quantify or model the rate constants. Clark *et al.* 2006 investigated the association and dissociation kinetics of the anthracycline antibiotic [^{3}H]-daunomycin using plasma membranes isolated from insect cells, which express BCRP. Non-compartmental analyses, namely non-linear regression using Michaelis-Menten type kinetics, were

used to ascertain a dissociation constant $K_d = 564 \pm 57\text{nM}$ with the following equation:

$$B = \frac{B_{\max}[L]}{K_d + [L]}, \tag{2.25}$$

where B is the specific bound [^{3}H]-daunomycin; $B_{\max}$ is the maximal binding capacity; K_d is the dissociation constant; and $[L]$ is the ligand concentration. The fraction of [^{3}H]-daunomycin bound as a function of added drug concentration was also fitted using the following general dose response equation:

$$B = B_{\min} + \frac{(B_{\max} - B_{\min})}{1 + 10^{\left[(\log \text{IC}_{50} - L)^n\right]}}, \tag{2.26}$$

where B is the maximal [^{3}H]-daunomycin binding, $B_{\max}$ is the maximal binding, $B_{\min}$ is the minimum binding, IC_{50} is the concentration of drug that leads to half-maximal binding, n is the Hill slope factor and L is the $\log_{10}$(ligand concentration). A Hill slope coefficient of 1.4 was obtained and used to suggest two symmetric drug binding sites. Similarly McDevitt *et al.* 2008 used non-linear least squares regression to fit the general dose response relationship, *Equation* (2.26), to [^{3}H]-daunomycin using plasma membranes isolated from insect cells. Likewise Pozza *et al.* 2006 performed a direct nucleotide binding study monitored by quenching of intrinsic fluorescence of purified BCRP using non-compartmental methods. These results also suggest that cooperative binding in BCRP, implicating two separate substrate or inhibitor binding sites: one with a high affinity and one with a low affinity, in agreement with other published experiment data and BCRP chemical structure modelling (Hazai & Bikádi 2008).

It is not uncommon for non-compartmental methods to be implemented to study efflux transporters; Ginsburg & Stein 1991 fitted antimalarial chloroquine uptake by erythrocytes to investigate the mechanism of a proton pump but could not distinguish between the postulated modes of drug resistance, which is the main disadvantage and limitation of non-compartmental analysis. Other ATP pumps binding kinetics have been described by compartmental modelling, such as Sachs & Welt 1967, which described the primary active transport of potassium in human red blood cells; however at this time, no compartmental models for BRCP binding kinetics could be found in the literature. Bruyère *et al.* 2010 recently studied the effect of variation in the expression of some transporters, namely ABCB1, BCRP, and CYP3A4, along the human small intestine. The authors used the variation in distribution to scale intestinal absorption in whole body PBPK compartmental models but did not specifically investigate the binding kinetics of either transporter.

Conversely, OATP uptake has previously been analysed using compartmental models; three models have been identified in the literature previously; Paine *et al.* 2008 put forward a linear three compartment model, whilst Poirier *et al.* 2008 proposed a non-linear mechanistic two compartment model, which Menochet *et al.* 2012 extended by adding an extra parameter to account for non-specific cellular binding.

Paine *et al.* 2008 evaluated the disposition of three compounds in suspended rat hepatocytes: atorvastatin, marketed as a calcium salt to lower cholesterol and prevent cardiovascular disease under the trade name Lipitor by Pfizer; cerivastatin, a synthetic statin marketed by Bayer A.G. under the brand names Baycol and Lipobay, voluntary withdrawn in 2001 due to reports of fatal rhabdomyolysis and its resultant renal failure; and indometacin or indomethacin, a non-steroidal anti-inflammatory

drug. Although the linear three compartment model proposed in Paine *et al.*, 2008 offers improvement in describing experimental data compared to the standard method, the main limitations of the model are that it is linear and no structural identifiability analysis was performed. An analysis of this model suggests that it is in fact unidentifiable and any numerical estimates obtained can therefore not be considered with confidence. Despite this, Paine *et al.*, 2008 estimates the concentration in non-observed compartments and constructs an analogous physiological model for *in vivo* pharmacokinetics predictions.

In contrast, although no structural identifiability analysis was performed by Poirier *et al.*, 2008, an analysis suggests it is globally structurally identifiable. Here a broader range of physicochemical compounds is evaluated, namely taurocholate, estrone-3-sulfate, cholecystokinin octapeptide (CCK-8), deltorphin II, fexofenadine napsagatran, pravastatin, pitavastatin, and fluvastatin. The two compartment model proposed to describe hepatic uptake differentiates between active and passive processes in Chinese hamster ovary control cells and artificial membranes (parallel artificial membrane permeability assay), allowing for bidirectional passive distribution and secondary active transport. The non-linear mechanistic model offers improvements over the conventional kinetic methods; however one main limitation is that it does not account for non-specific binding of Pitavastatin.

Menochet *et al.*, 2012 is the most comprehensive non-linear mechanistic model; essentially identical to the Poirier *et al.*, 2008 model besides an extra parameter to account for non-specific cellular binding. Uptake of Rosuvastatin, Pravastatin, Pitavastatin, Valsartan, Bosentan, Telmisartan, and Repaglinide is investigated in freshly isolated rat hepatocytes. The latter two compounds are described with a model extension to account for metabolism; a complete mechanistic model

describing bidirectional passive diffusion, secondary active transport, intracellular binding, and metabolism. Some consideration was also given to structural identifiability as the authors use Differential Algebra for Identifiability of Systems (DAISY) software (Bellu *et al.* 2007) to verify the identifiability of the unknown kinetic parameters. A similar model will provide the basis for the compartmental modelling undertaken in this research. One of the main contributions of the models developed is the use of different species (rat, dog , and human hepatocytes), whereas all the previously mechanistic modelling has been performed on artificial, hamster, and rat cells.

2.5 Conclusion

Mathematical modelling is utilised in clinical pharmacology to numerically quantify drug absorption and tissue uptake, in order to determine exposure (pharmacokinetics - PK) and effect (pharmacodynamics - PD) of therapeutic drugs. Physiologically based pharmacokinetic (PBPK) modelling is gradually replacing non-compartmental methods and other more empirical approaches in new drug development because of their superior predictive ability, strength in data integration, and mechanistic insights into the complex and often non-linear physiological processes present. Historically a common PBPK approach, namely compartmental modelling, has been implemented at the macroscopic scale, modelling whole organs simultaneously to investigate the distribution of a drug around the whole body. Recently, these techniques have been applied at the cellular level, to explore the microscopic biological interactions and mechanisms. Membrane transporter proteins have been identified as key determinants of the trans-membrane passage of drugs and as a result they are a major factor in the pharmacokinetic, safety, and efficacy profiles of pharmaceutical

compounds. Two prominent transporters, namely OATP1B1 and BCRP, have been selected to be modelled mechanistically using compartmental analysis as their functions have clinically significant consequences on drug therapy. Furthermore, although their physiological and chemical structures are fairly well understood and have been modelled extensively, their exact mechanisms of action remain biological enigmas and very few mechanistic models have previously been used to characterise their binding kinetics.

The main contributions are to improve knowledge of the carrier mediated process, particularly:

- developing a novel mechanistic model to describe *in vitro* BCRP competitive binding to further our understanding of primary active transport by ATP-powered pumps. No previous mechanistic models have been published in the literature.
- developing a mechanistic model to describe *in vitro* OATP hepatic uptake to further our understand of secondary active transport by solute carriers. Some mechanistic models are available in the literature but are have limited their application to artificial, hamster, and rat cells. The models developed in this research are applied to rat, dog, and human data to ascertain whether cross species scaling is suitable.
- developing a mechanistic model to describe *in vivo* OATP hepatic uptake in rat to investigate the applicability and suitability of *in vitro* data models to *in vivo* data. No previous mechanistic models have been published in the literature.

Another contribution includes reviewing the current methods for performing structural identifiability and indinstinguishability analyses and their applicability to the non-linear models developed.

2.6 References

Aarons, L., Karlsson, M.O., Mentré, F., Rombout, F., Steimer, J. L., van Peer, A. (2001). Role of modelling and simulation in Phase I drug development. *European Journal of Pharmaceutical Science*. 2001 May; 13(2):115-22.

Abe, T., Unno, M., Onogawa, T., Tokui, T., Kondo, T. N. , Nakagomi, R. (2001). LST-2, a human liver-specific organic anion transporter, determines methotrexate sensitivity in gastrointestinal cancers. *Gastroenterology* 120: 1689-1699.

Achard, P., & De Schutter, E. (2006). Complex parameter landscape for a complex neuron model. *PLoS Computational Biology*, *2*(7), e94.

Adar, E., & Sorek, S. (1989). Multi-compartment modelling for aquifer parameter estimation using natural tracers in non-steady flow. *Advances in water resources*, *12*(2), 84-89.

Ahearn, T. S., Staff, R. T., Redpath, T. W., & Semple, S. I. K. (2005). The use of the Levenberg-Marquardt curve-fitting algorithm in pharmacokinetic modelling of DCE-MRI data. *Physics in Medicine and Biology*, *50*(9), N85.

Alberts, B. (Ed.). (1998). *Essential cell biology: an introduction to the molecular biology of the cell* (Vol. 1). Taylor & Francis.

Ali, R., Evans, N.D., Campbell, L., Errington, R., Godfrey, K. R., Smith, P. and Chappell, M. J. (2007) 'Modelling the control of cell proliferation by an anti-cancer agent.', *Measurements & Control*, 40 12 - 15 (0148-0057).

Allikmets, R., Schriml, L. M., Hutchinson, A., Romano-Spica, V., & Dean, M. (1998). A human placenta-specific ATP-binding cassette gene (ABCP) on chromosome 4q22 that is involved in multidrug resistance. *Cancer Research*, 58(23), 5337-5339.

Amidon, G. L., Lennernäs, H., Shah, V. P., & Crison, J. R. (1995). A theoretical basis for a biopharmaceutic drug classification: the correlation of in vitro drug product dissolution and *in vivo* bioavailability. *Pharmaceutical research*, *12*(3), 413-420.

Anderson, D. H. (1983). *Compartmental modeling and tracer kinetics* (p. 302). New York:: Springer-Verlag.

Anguelova, M., Karlsson, J., and Jirstrand, M. (2012). Minimal output sets for identifiability. Mathematical Biosciences, 239(1), 139-153.

Audoly, S., Bellu, G., D'Angio, L., Saccomani, M. P., and Cobelli, C. (2001). Global identifiability of nonlinear models of biological systems. *Biomedical Engineering, IEEE Transactions on*, *48*(1), 55-65.

Balsa-Canto, E., Alonso, A. A., & Banga, J. R. (2010). An iterative identification procedure for dynamic modeling of biochemical networks. *BMC systems biology*, *4*(1), 11.

Bandara, S., Schlöder, J. P., Eils, R., Bock, H. G., & Meyer, T. (2009). Optimal experimental design for parameter estimation of a cell signaling model. *PLoS computational biology*, *5*(11), e1000558.

Barrett, P. H. R., Bell, B. M., Cobelli, C., Golde, H., Schumitzky, A., Vicini, P., and Foster, D. M. (1998). SAAM II: simulation, analysis, and modeling software for tracer and pharmacokinetic studies. *Metabolism*, *47*(4), 484-492.

Bellman R., Åström K. J. (1970). On structural identifiability, *Math. Biosci*. 7 329.

Bellu, G., Saccomani, M. P., Audoly, S., and D'Angiò, L. (2007). DAISY: A new software tool to test global identifiability of biological and physiological systems. *Computer methods and programs in biomedicine*, 88(1), 52-61.

Boyd, C. A. R. (2008). Facts, fantasies and fun in epithelial physiology. *Experimental Physiology*, *93*(3), 303-314.

Brauer, F., & Castillo-Châavez, C. (2012). *Mathematical models in population biology and epidemiology*. Springer.

Brown, K. S., Hill, C. C., Calero, G. A., Myers, C. R., Lee, K. H., Sethna, J. P., & Cerione, R. A. (2004). The statistical mechanics of complex signaling networks: nerve growth factor signaling. *Physical biology*, *1*(3), 184.

Bruyère, A., Declèves, X., Bouzom, F., Ball, K., Marques, C., Treton, X., & Mouly, S. (2010). Effect of variations in the amounts of P-glycoprotein (ABCB1), BCRP (ABCG2) and CYP3A4 along the human small intestine on PBPK models for predicting intestinal first pass. *Molecular pharmaceutics*, 7(5), 1596-1607.

Burton, M. E. (Ed.). (2006). *Applied pharmacokinetics and pharmacodynamics: principles of therapeutic drug monitoring*. Lippincott Williams & Wilkins.

Cabantchik, Z. I., & Ginsburg, H. A. G. A. I. (1977). Transport of uridine in human red blood cells. Demonstration of a simple carrier-mediated process. *J Gen Physiol*, *69*(1), 75-96.

Carrero, G., McDonald, D., Crawford, E., de Vries, G., & Hendzel, M. J. (2003). Using FRAP and mathematical modeling to determine the *in vivo* kinetics of nuclear proteins. *Methods*, *29*(1), 14-28.

Carson, E., & Cobelli, C. (2001). *Modelling methodology for physiology and medicine*. Academic Press. *Pages 77-105*

Chang, C., Pang, K. S., Swaan, P. W., & Ekins, S. (2005). Comparative pharmacophore modeling of organic anion transporting polypeptides: a meta-analysis of rat Oatp1a1 and human OATP1B1. *Journal of Pharmacology and Experimental Therapeutics*, 314(2), 533-541.

Cheung, S. Y., Evans, N. D., Chappell, M. J., Godfrey, K. R., Smith, P. J., & Errington, R. J. (2008). Exploration of the intercellular heterogeneity of topotecan uptake into human breast cancer cells through compartmental modelling. *Mathematical biosciences*, *213*(2), 119-134.

Chis, O. T., Banga, J. R., & Balsa-Canto, E. (2011). Structural identifiability of systems biology models: a critical comparison of methods. *PloS one*, *6*(11), e27755.

Choi, M. K., Shin, H. J., Choi, Y. L., Deng, J. W., Shin, J. G., & Song, I. S. (2011). Differential effect of genetic variants of Na+-taurocholate co-transporting polypeptide (NTCP) and organic anion-transporting polypeptide 1B1 (OATP1B1) on the uptake of HMG-CoA reductase inhibitors. *Xenobiotica*, *41*(1), 24-34.

Clark, R., Kerr, I. D., Callaghan, R. (2006). Multiple drug binding sites on the R482G isoform of the ABCG2 transporter. *Br J Pharmacol*.;149(5):506-515.

Clausen, W. H. O., De Gaetano, A., & Vølund, A. (2006). Within-patient variation of the pharmacokinetics of subcutaneously injected biphasic insulin aspart as assessed by compartmental modelling. *Diabetologia*, *49*(9), 2030-2038.

Cobelli, C., & Distefano, J. J. (1980). Parameter and structural identifiability concepts and ambiguities: a critical review and analysis. *American Journal of Physiology-Regulatory, Integrative and Comparative Physiology*, *239*(1), R7-R24.

Cobelli, C., Salvan, A., (1977). Parameter estimation in a biological two compartment model- ii: a computer experimental study of the influence of the initial estimate in the parameterspace, of some sampling protocols and of weighting factors. *Mathematical Biosciences 37* (3-4), 267 - 274.

Cobelli, C., Toffolo, G., & Ferrannini, E. (1984). A model of glucose kinetics and their control by insulin, compartmental and noncompartmental approaches. *Mathematical biosciences*, *72*(2), 291-315.

Craciun, G., & Pantea, C. (2008). Identifiability of chemical reaction networks. *Journal of Mathematical Chemistry*, *44*(1), 244-259.

Crane, R. K. (1977). The gradient hypothesis and other models of carrier-mediated active transport. In *Reviews of Physiology, Biochemistry and Pharmacology, Volume 78* (pp. 99-159). Springer Berlin Heidelberg.

Crane, R. K., Miller, D., & Bihler, I. (1961). The restrictions on possible mechanisms of intestinal active transport of sugars. *Membrane transport and metabolism*, *439*.

Cumming, P. & Gjedde, A. (1998). Compartmental analysis of dopa decarboxylation in living brain from dynamic positron emission tomograms. *Synapse*, *29*(1), 37-61.

Cusatis, G. & Sparreboom, A. (2008). Pharmacogenomic importance of ABCG2. *Pharmacogenomics* 9:1005-1009.

Dash, S., Murthy, P. N., Nath, L., & Chowdhury, P. (2010). Kinetic modeling on drug release from controlled drug delivery systems. *Acta Pol Pharm*, 67(3), 217-223.

Davidescu, F. P., & Jørgensen, S. B. (2008). Structural parameter identifiability analysis for dynamic reaction networks. *Chemical Engineering Science*, *63*(19), 4754-4762.

Dean, M. and Allikmets, R. (2001). Complete characterization of the human ABC gene family. *J Bioenerg Biomembr* 33:475-479.

DeGorter, M. K., Xia, C. Q., Yang, J.J., and Kim, R. B. (2012) Drug Transporters in Drug Efficacy and Toxicity. *Annual Review of Pharmacology and Toxicology*. Vol. 52: 249-273.

Denis-Vidal, L., Joly-Blanchard, G., & Noiret, C. (2001). Some effective approaches to check the identifiability of uncontrolled nonlinear systems. *Mathematics and computers in simulation*, *57*(1), 35-44.

DiStefano, J. J. (1982). Noncompartmental vs. compartmental analysis: some bases for choice. *American* Dobson PD and Kell DB (2008) Carrier-mediated cellular uptake of pharmaceutical drugs: an exception or the rule?. *Nat Rev Drug Discov* 7:205-220.

Doyle, L. A., & Ross, D. D. (2003). Multidrug resistance mediated by the breast cancer resistance protein BCRP (ABCG2). Oncogene, 22(47), 7340-7358.

Ecker, G. F., Stockner, T., Chiba, P. (2008). Computational models for prediction of intercations with ABC-transporters. *Drug Discovery Today*. 13 April 2008 (7-8): 311-7.

Egan, T. D., Kern, S. E., Muir, K. T., & White, J. (2004). Remifentanil by bolus injection: a safety, pharmacokinetic, pharmacodynamic, and age effect investigation in human volunteers†. *British journal of anaesthesia*, *92*(3), 335-343.

Endres, C. J., Hsiao, P., Chung, F. S., & Unadkat, J. D. (2006). The role of transporters in drug interactions. *European journal of pharmaceutical sciences*, *27*(5), 501-517.

Érdi, P., Tóth, J. (1989). *Mathematical Models of Chemical Reactions*. Princeton University Press.

Espenson, J. H., (1995). *Chemical Kinetics and Reaction Mechanisms*. McGraw-Hill, Singapore.

Ette, E. I., Ludden, T. M. (1995). Population Pharmacokinetic Modeling: The Importance of Informative Graphics. *Pharmaceutical Research*, December 1995, Volume 12, Issue 12, pp 1845-1855.

Evans, N. D., Chappell, M. J., Chapman, M. J., Godfrey, K. R. (2004). Structural indistinguishability between uncontrolled (autonomous) nonlinear analytic systems. *Automatica* 40,1947-1953.

Evans, N. D., Dimelow, R., & Yates, J. (2012, August). Modelling of Tumour Growth and Cytotoxic Effect of Taxotere in Xenografts. In *Biological and Medical Systems* (Vol. 8, No. 1, pp. 278-283).

Evans, N. D., Moyse, H. A. J., Lowe, D., Briggs, D., Higgins, R., Mitchell, D., & Chappell, M. J. (2012). Structural identifiability of surface binding reactions involving heterogeneous analyte: Application to surface plasmon resonance experiments. *Automatica*.

Evans, N.D., White, L.J., Chapman, M.J., Godfrey, K.R., and Chappell, M.J. (2005) 'The structural identifiability of the susceptible infected recovered model with seasonal forcing'. *Mathematical Biosciences* 194, 175-197.

Fliess, M., Glad, S.T. (1993). *An algebraic approach to linear and nonlinear control*. (pp. 223-267). Birkhäuser Boston.

Food and Drug Administration (2004). Innovation; Stagnation: Challenge and Opportunity on the Critical Path to New Medical Products. www.fda.gov/oc/initiatives/criticalpath/whitepaper.html

Foster, D. M., & Jacquez, J. A. (1976). An analysis of the adequacy of the asymmetric carrier model for sugar transport. *Biochimica et Biophysica Acta (BBA)-Biomembranes*, *436*(1), 210-221.

Fouillet, H., Juillet, B., Bos, C., Mariotti, F., Gaudichon, C., Benamouzig, R., & Tomé, D. (2008). Urea-nitrogen production and salvage are modulated by protein intake in fed humans: results of an oral stable-isotope-tracer protocol and compartmental modeling. *The American journal of clinical nutrition*, *87*(6), 1702-1714.

Franco, R., Gavaldà, M. T., Canela, E. I., (1986). A computer program for enzyme kineticsthat combines model discrimination, parameter refinement and sequential experimental design. *Biochem J* 238 (3), 855-862.

Fredriksson, R., Nordstrom, K. J., Stephansson, O., Hagglund, M. G. and Schioth, H. B. (2008) The solute carrier (SLC) complement of the human genome: phylogenetic classification reveals four major families. *FEBS Lett* 582:3811-3816.

Fromm, M. F., Kim, R. B. (2011). Drug Transporters. *Handbook of Experimetal Pharmacology*, Vol. 201. ISBN 978-3-642-14541-4.

Giacomini, K. M., Huang, S-M. (2013). Transporters in Drug Development and Clinical Pharmacology. *Clinical Pharmacology & Therapeutic*; 94 1, 3-9.

Gillespie, W. R. (1991). Noncompartmental versus compartmental modelling in clinical pharmacokinetics. *Clinical pharmacokinetics*, *20*(4), 253-262.

Ginsburg, H., & Stein, W. D. (1991). Kinetic modelling of chloroquine uptake by malaria-infected erythrocytes: assessment of the factors that may determine drug resistance. *Biochemical pharmacology*, 41(10), 1463-1470.

Godfrey. K. R. & DiStefano III, J. J. (1987). Identifiability of model parameters, in Identifiability of Parametric Models: E. Walter (Ed.) p1 (Chapter 1) *Identifiability of Parametric Models*, Pergamon, Oxford.

Godfrey, K. R., Chapman, M. J., 1990. Identifiability and indistinguishability of linear compartmental models. Math. Comput. Simulat. 32, 273-295. models. *Math. Comput. Simulat*. 32, 273-295.

Godfrey, K. R., Tanswell, P., Bates, R. A., Chappell, M. J., & Madden, F. N. (1998). Nonlinear pharmacokinetics of tissue-type plasminogen activator in three animal species: a comparison of mathematical models. *Biopharmaceutics & drug disposition*, *19*(2), 131-140.

Godfrey, K. (1983) *Compartmental Models and Their Application*, Academic Press.

Gonzalez-Alvarez, I., Fernandez-Teruel, C., Garrigues, T. M., Casabo, V. G., Ruiz-Garcia, A., & Bermejo, M. (2005). Kinetic modelling of passive transport and active efflux of a fluoroquinolone across Caco-2 cells using a compartmental approach in NONMEM. *Xenobiotica*, *35*(12), 1067-1088.

Goyens, P. L., Spilker, M. E., Zock, P. L., Katan, M. B., & Mensink, R. P. (2005). Compartmental modeling to quantify α-linolenic acid conversion after longer term intake of multiple tracer boluses. *Journal of lipid research*, *46*(7), 1474-1483.

Grandjean, T. R., Chappell, M. J., Yates, J. T., Jones, K., Wood, G., & Coleman, T. (2011). Compartmental modelling of the pharmacokinetics of a breast cancer resistance protein. *Computer methods and programs in biomedicine*, *104*(2), 81-92.

Grass, G. M., Sinko, P. J. (2002). Physiologically-based pharmacokinetic simulation modelling. *Adv Drug Deliv Rev*. 31 March 2002; 54 (3): 433-51.

Groenendaal, D., Freijer, J., Mik, D. D., Bouw, M. R., Danhof, M., & Lange, E. C. M. (2007). Population pharmacokinetic modelling of non-linear brain distribution of morphine: influence of active saturable influx and P-glycoprotein mediated efflux. *British journal of pharmacology*, *151*(5), 701-712.

Gunawardena, J. (2012). Some lessons about models from Michaelis and Menten. *Molecular biology of the cell*, *23*(4), 517.

Gurpide, E., & Mann, J. (1970). Interpretation of isotopic data obtained from blood-borne compounds. *Journal of Clinical Endocrinology & Metabolism*, *30*(6), 707-718.

Gutenkunst, R. N., Waterfall, J. J., Casey, F. P., Brown, K. S., Myers, C. R., & Sethna, J. P. (2007). Universally sloppy parameter sensitivities in systems biology models. *PLoS computational biology*, *3*(10), e189.

Hagenbuch, B., & Gui, C. (2008). Xenobiotic transporters of the human organic anion transporting polypeptides (OATP) family. *Xenobiotica*, *38*(7-8), 778-801.

Hartz, A. M., Mahringer, A., Miller, D. S., & Bauer, B. (2010). 17-β-Estradiol: a powerful modulator of blood-brain barrier BCRP activity. *Journal of Cerebral Blood Flow & Metabolism*, *30*(10), 1742-1755.

Hazai, E., & Bikádi, Z. (2008). Homology modeling of breast cancer resistance protein (ABCG2). Journal of structural biology, 162(1), 63-74.

He, F., Brown, M., & Yue, H. (2010). Maximin and Bayesian robust experimental design for measurement set selection in modelling biochemical regulatory systems. *International Journal of Robust and Nonlinear Control*, *20*(9), 1059-1078.

He, L., Vasiliou, K., & Nebert, D. W. (2009). Analysis and update of the human solute carrier (SLC) gene superfamily. *Hum Genomics*, *3*(2), 195-206.

Hengl, S., Kreutz, C., Timmer, J., & Maiwald, T. (2007). Data-based identifiability analysis of non-linear dynamical models. *Bioinformatics*, *23*(19), 2612-2618.

Ho, R. H., & Kim, R. B. (2005). Transporters and drug therapy: Implications for drug disposition and disease&ast. *Clinical Pharmacology & Therapeutics*, *78*(3), 260-277.

Holford, N. H. G., Kimko, H. C., Monteleone, J. P. R., and Peck, C. C. (2000). Simulation of Clinical Trials. *Annual Review of Pharmacology and Toxicology*, Vol. 40: 209 -234

Hu, S., Franke, R. M., Filipski, K. K., Hu, C., Orwick, S. J., de Bruijn, E. A., Burger, H., Baker, S. D., and Sparreboom, A. (2008) Interaction of imatinib with human organic ion carriers. *Clin Cancer Res* 14:3141-3148.

Huls, M., Brown, C. D. A., Windass, A. S., Sayer, R., van den Heuvel, J. J. M. W., Heemskerk, S., & Masereeuw, R. (2007). The breast cancer resistance protein transporter ABCG2 is expressed in the human kidney proximal tubule apical membrane. *Kidney international*, *73*(2), 220-225.

Hultin, M., Savonen, R., & Olivecrona, T. (1996). Chylomicron metabolism in rats: lipolysis, recirculation of triglyceride-derived fatty acids in plasma FFA, and fate of core lipids as analyzed by compartmental modelling. *Journal of lipid research*, *37*(5), 1022-1036.

International Transporter Consortium (2010) Membrane transporters in drug development. *Nat Rev Drug Discov*. 9 March 2010 (3): 215-236

Ito, K., Suzuki, H., Horie, T., & Sugiyama, Y. (2005). Apical/basolateral surface expression of drug transporters and its role in vectorial drug transport. *Pharmaceutical research*, *22*(10), 1559-1577.

Jacquez, J. A. (1996). *Compartmental analysis in biology and medicine*. Ann Arbor: University of Michigan Press.

Jacquez, J. A., & Simon, C. P. (1993). Qualitative theory of compartmental systems. *Siam Review*, *35*(1), 43-79.

Jacquez, J. and Greif, P. (1985). Numerical parameter identifiability and estimability: Integrating identifiability, estimability, and optimal sampling design. Math. Biosci., 77, 201-227.

Jiménez-Hornero, J. E., Santos-Dueñas, I. M., Garci A-Garci, A. I. (2008). Structural identifiability of a model for the acetic acid fermentation process, *Math. Biosci.* 216 p154-162 (Epub 2008 September 27).

Johnson, K. A., & Goody, R. S. (2011). The original Michaelis constant: translation of the 1913 Michaelis-Menten paper. *Biochemistry*, *50*(39), 8264-8269.

Kalliokoski, A., Niemi, M. (2009). Impact of OATP transporters on pharmacokinetics. *Br J Pharmacol*. 2009 October; 158(3): 693-705. Published online 2009 September 28. doi: 10.1111/j.1476-5381.2009.00430.x

Kalvass, J. C., & Pollack, G. M. (2007). Kinetic considerations for the quantitative assessment of efflux activity and inhibition: implications for understanding and predicting the effects of efflux inhibition. *Pharmaceutical research*, *24*(2), 265-276.

Katz, D. A., Carr, R., Grimm, D. R., Xiong, H., Holley-Shanks, R., and Mueller, T. (2006). Organic anion transporting polypeptide 1B1 activity classified by SLCO1B1 genotype influences atrasentan pharmacokipharmacokinetics. *Clin Pharmacol Ther* 79: 186-196.

Kell, D. B. (2006). Metabolomics, modelling and machine learning in systems biology-towards an understanding of the languages of cells. *Febs Journal*, 273(5), 873-894.

Kermark, M. D., & Mckendrick, A. G. (1927). Contributions to the mathematical theory of epidemics. Part I. In *Proc. R. Soc. A* (Vol. 115, No. 5, pp. 700-721).

Kholodenko, B. N., Bruggeman, F. J., & Sauro, H. M. (2005). Mechanistic and modular approaches to modeling and inference of cellular regulatory networks. In *Systems Biology* (pp. 143-159). Springer Berlin Heidelberg.

Klipp, E., Herwig, R., Kowald, A., Wierling, C., & Lehrach, H. (2008). *Systems biology in practice: concepts, implementation and application*. John Wiley & Sons.

Kreutz, C., & Timmer, J. (2009). Systems biology: experimental design. *FEBS Journal*, *276*(4), 923-942.

Krishnamurthy, P., Ross, D. D., Nakanishi, T., Bailey-Dell, K., Zhou, S., Mercer, K. E., ... & Schuetz, J. D. (2004). The stem cell marker Bcrp/ABCG2 enhances hypoxic cell survival through interactions with heme. *Journal of Biological Chemistry*, *279*(23), 24218-24225.

Kuhlmann, J. (1999). Alternative strategies in drug development: clinical pharmacological aspects. Int J Clin Pharmacol Ther, December 1999; 37 (12): 575-83.

Lecourtier, Y., Lamnabhi-Lagarrigue, F., & Walter, E. (1987). Volterra and generating power series approaches to identifiability testing. *Identifiability of parametric models*, *30*(1), 50.

Lindsay, A. E., Lindsay, K. A., & Rosenberg, J. R. (2007). New concepts in compartmental modelling. *Computing and Visualization in Science*, *10*(2), 79-98.

Link, E., Parish, S., Armitage, J., Bowman, L., Heath, S., Matsuda, F., & Collins, R. (2008). SLCO1B1 variants and statin-induced myopathy--a genomewide study. *The New England journal of medicine*, *359*(8), 789.

Lipniacki, T., Paszek, P., Brasier, A. R., Luxon, B., & Kimmel, M. (2004). Mathematical model of NF- κ B regulatory module. *Journal of theoretical biology*, *228*(2), 195-215.

Liu, J. J., Lu, L., McKeage, M. J. (2012). Membrane Transporters as Determinants of the Pharmacology of Platinum Anticancer Drugs. *Current Cancer Drug Targets*. Vol 12 (8): 862-86.

Ljung, L., Glad, T. (1994) On global identifiability for arbitrary model parametrizations, *Automatica* 30 p265-276.

Lodish, H., Berk, A., Zipursky, S. L. (2000). *Molecular Cell Biology*. 4th edition. New York: W. H. Freeman; 2000. Section 15.2, Overview of Membrane Transport Proteins.

Maeda, K., Ieiri, I., Yasuda, K., Fujino, A., Fujiwara, H., Otsubo, K. (2006). Effects of organic anion transporting polypeptide 1B1 haplotype onpharmacokinetics of pravastatin, valsartan, and temocapril. *ClinPharmacol Ther* 79: 427-439.

Maeda, K., & Sugiyama, Y. (2008). Impact of genetic polymorphisms of transporters on the pharmacokinetic, pharmacodynamic and toxicological properties of anionic drugs. *Drug metabolism and pharmacokinetics*, *23*(4), 223-235.

Mahagita, C., Grassl, S. M., Piyachaturawat, P., & Ballatori, N. (2007). Human organic anion transporter 1B1 and 1B3 function as bidirectional carriers and do not mediate GSH-bile acid cotransport. *American Journal of Physiology-Gastrointestinal and Liver Physiology*, 293(1), G271-G278.

Maliepaard, M., Scheffer, G. L., Faneyte, I. F., van Gastelen, M. A., Pijnenborg, A. C., Schinkel, A. H., & Schellens, J. H. (2001). Subcellular localization and distribution of the breast cancer resistance protein transporter in normal human tissues. *Cancer research*, *61*(8), 3458-3464.

Man, C.D, Caumo, A., & Cobelli, C. (2002). The oral glucose minimal model: estimation of insulin sensitivity from a meal test. *Biomedical Engineering, IEEE Transactions on*, *49*(5), 419-429.

Margaria, G., Riccomagno, E., Chappell, M. J., & Wynn, H. P. (2001). Differential algebra methods for the study of the structural identifiability of rational function state-space models in the biosciences. *Mathematical Biosciences*, *174*(1), 1-26.

Marin, J. J. (2012). Plasma Membrane Transporters in Modern Liver Pharmacology. *Scientifica*, *2012*.

McDevitt, C. A., Crowley, E., Hobbs, G., Starr, K. J., Kerr, I. D., Callaghan, R. (2008). Is ATP binding responsible for initiating drug translocation by the multidrug transporter ABCG2? *Febs J.*; 275(17): 4354-4362.

Meier-Abt, F., Mokrab, Y., & Mizuguchi, K. (2006). Organic anion transporting polypeptides of the OATP/SLCO superfamily: identification of new members in nonmammalian species, comparative modeling and a potential transport mode. *The Journal of membrane biology*, 208(3), 213-227.

Meineke, I., Freudanthaler, S., Hofmann, U., Schaeffeler, E., Mikus, G., Schwab, M., ... & Brockmöller, J. (2002). Pharmacokinetic modelling of morphine, morphine-3-glucuronide and morphine-6-glucuronide in plasma and cerebrospinal fluid of neurosurgical patients after short-term infusion of morphine. *British journal of clinical pharmacology*, *54*(6), 592.

Mendes, P., Camacho, D., & De La Fuente, A. (2005). Modelling and simulation for metabolomics data analysis. *Biochemical Society Transactions*, 33(6), 1427-1429.

Ménochet, K., Kenworthy, K., Houston, J. B., Galetin, A. (2012). Simultaneous assessment of uptake and metabolism in rat hepatocytes: a comprehensive mechanistic model. *J Pharmacol Exp Ther*. 341 (1):2-15.

Meshkat, N., Eisenberg, M., Distefano 3rd, J. J. (2009). An algorithm for finding globally identifiable parameter combinations of nonlinear ODE models using Gröbner Bases, *Math. Biosci.* 222 p61-72.

Miao, H., Xia, X., Perelson, A. S., & Wu, H. (2011). On identifiability of nonlinear ODE models and applications in viral dynamics. *SIAM review*, *53*(1), 3-39.

Michaelis, L., Menten, M. L. (1913). Die Kinetik der Invertinwirkung. *Biochem* Z 49: 333-369.

Miller, R., Ewy, W., Corrigan, B. W., Ouellet, D., Hermann, D., Kowalski, K. G., Lockwood, P, Koup, J. R., Donevan, S., El-Kattan, A., Li, C. S. W., Werth, J. L., Feltner, D. E., and Lalonde, R. L. (2005). How modelling and simulation have enhance decision making in new drug development, *Journal of Pharmacokinetics and Pharmacodynamics* Volume 32, Issue 2, pp 185-197

Miller, J. C., Slim, A. C., & Volz, E. M. (2012). Edge-based compartmental modelling for infectious disease spread. *Journal of The Royal Society Interface*, *9*(70), 890-906.

Miyake, K., Mickley, L., Litman, T., Zhan, Z., Robey, R., Cristensen, B., ... & Bates, S. E. (1999). Molecular Cloning of cDNAs Which Are Highly Overexpressed in Mitoxantrone-resistant Cells Demonstration of Homology to ABC Transport Genes. *Cancer Research*, 59(1), 8-13.

Mizuno, N., Niwa, T., Yotsumoto, Y., Yuichi, S. (2003). Impact of Drug Transporter Studies on Drug Discovery and Development. *Pharmacological Reviews*. Vol 55 (3) 425-461.

Mizuno, N., & Sugiyama, Y. (2002). Drug transporters: their role and importance in the selection and development of new drugs. *Drug metabolism and pharmacokinetics*, *17*(2), 93-108.

Murray Smith, D. J. (1998). Methods for the external validation of contiuous system simulation models: a review. *Mathematical and Computer Modelling of Dynamical Systems*, *4*(1), 5-31.

Nakamura, T., Yamamori, M., & Sakaeda, T. (2008). Pharmacogenetics of intestinal absorption. *Current drug delivery*, *5*(3), 153-169.

Němcová, J. (2010). Structural identifiability of polynomial and rational systems. *Mathematical biosciences*, 223(2), 83-96.

Ni, Z., Bikadi, Z., Rosenberg, M. F., & Mao, Q. (2010). Structure and function of the human breast cancer resistance protein (BCRP/ABCG2). *Current drug metabolism*, 11(7), 603.

Nies, A. T., Schwab, M. and Keppler, D. (2008). Interplay of conjugating enzymes with OATP uptake transporters and ABCC/MRP efflux pumps in the elimination of drugs. *Expert Opin Drug Metab Toxicol* 4:545-568.

Noe, J., Portmann, R., Brun, M. E. and Funk, C. (2007). Substrate-dependent drug-drug interactions between gemfibrozil, fluvastatin and other organic anion-transporting peptide (OATP) substrates on OATP1B1, OATP2B1, and OATP1B3. *Drug Metab Dispos* 35:1308-1314.

Oswald, S., Konig, J., Lutjohann, D., Giessmann, T., Kroemer, H. K., RimRimmbach,C. (2008). Disposition of ezetimibe is influenced bypolymorphisms of the hepatic uptake carrier OATP1B1. *PharmacogenetGenomics* 18: 559-568.

Özvegy, C., Litman, T., Szakács, G., Nagy, Z., Bates, S., Váradi, A., & Sarkadi, B. (2001). Functional characterization of the human multidrug transporter, ABCG2, expressed in insect cells. Biochemical and biophysical research communications, 285(1), 111-117.

Paine, S. W., Parker, A. J., Gardiner, P., Webborn, P. J., Riley, R. J. (2008). Prediction of thepharmacokinetics of atorvastatin, cerivastatin, and indomethacin using kinetic models applied to isolated rat hepatocytes. *Drug Metab Dispos* 36:1365-1374.

Paul, S. M., Mytelka, D. S., Dunwiddi , C. T., Persinger, C. C., Munos, B. H., Lindborg, S. R. & Schacht, A. L. (2010). How to improve R&D productivity: the

pharmaceutical industry's grand challenge. *Nature Reviews Drug Discovery* 9, 203-214 (March 2010) | doi:10.1038/nrd3078.

Pennisi, M., Bianca, C., Pappalardo, F., & Motta, S. (2011). Compartmental mathematical modeling of immune system—melanoma competition. In *Proceedings of the 10th International Conference on Mathematical Methods in Science and Engineering (CMMSE 2011)* (pp. 930-934).

Petzinger, E., Geyer, J. (2006). Drug transporters in pharmacokinetics. *Naunyn-Schmiedeberg's Arch Pharmacology* 372: 465-475.

Piazza, M., Feng, X. J., Rabinowitz, J. D., & Rabitz, H. (2008). Diverse metabolic model parameters generate similar methionine cycle dynamics. *Journal of theoretical biology*, *251*(4), 628-639.

Pohjanpalo, H. (1978). System identifiability based on the power series expansion of the solution. *Math. Biosci.* 41, 21-33.

Poirier, A., Lave, T., Portmann, R., Brun, M. E., Senner, F., Kansy, M., Grimm, H. P., Funk, C. (2008). Design, data analysis, and simulation of in vitro drug transport kinetic experiments using a mechanistic in vitro model. *Drug Metab Dispos* 36:2434-2444.

Poller, B., Drewe, J., Krähenbühl, S., Huwyler, J., & Gutmann, H. (2010). Regulation of BCRP (ABCG2) and P-glycoprotein (ABCB1) by cytokines in a model of the human blood-brain barrier. Cellular and molecular neurobiology, 30(1), 63-70.

Pozza, A., Perez-Victoria, J. M., Sardo, A., Ahmed-Belkacem, A., Di Pietro, A. (2006). Purification of breast cancer resistance protein ABCG2 and role of arginine-482. *Cell Mol Life Sci.*; 63(16): 1912-1922.

Price, J. C., Klunk, W. E., Lopresti, B. J., Lu, X., Hoge, J. A., Ziolko, S. K., ... & Mathis, C. A. (2005). Kinetic modeling of amyloid binding in humans using PET imaging and Pittsburgh Compound-B. *Journal of Cerebral Blood Flow & Metabolism*, *25*(11), 1528-1547.

Raue, A., Kreutz, C., Maiwald, T., Bachmann, J., Schilling, M., Klingmüller, U., & Timmer, J. (2009). Structural and practical identifiability analysis of partially

observed dynamical models by exploiting the profile likelihood. *Bioinformatics*, *25*(15), 1923-1929.

Raue, A., Kreutz, C., Maiwald, T., Klingmüller, U., & Timmer, J. (2011). Addressing parameter identifiability by model-based experimentation. *IET systems biology*, *5*(2), 120-130.

Robey, R.W., To, K.K., Polgar, O., Dohse, M., Fetsch, P., Dean, M. and Bates, S. E. (2009). ABCG2: a perspective. *Adv Drug Deliv Rev* 61:3-13.

Romaine, S. P. R., Bailey, K. M., Hall, A. S., & Balmforth, A. J. (2009). The influence of SLCO1B1 (OATP1B1) gene polymorphisms on response to statin therapy. *The pharmacogenomics journal*, *10*(1), 1-11.

Ross, D. D., Yang, W., Abruzzo, L. V., Dalton, W. S., Schneider, E., Lage, H., & Doyle, L. A. (1999). Atypical multidrug resistance: breast cancer resistance protein messenger RNA expression in mitoxantrone-selected cell lines. *Journal of the National Cancer Institute*, 91(5), 429-433.

Rowland, M., Peck, C., Tucker, G. (2011). Physiologically-based pharmacokinetics in drug development and regulatory science. *Annu Rev Pharmacol Toxicol*.; 51:45-73.

Russel, F. G. (2010). Transporters: importance in drug absorption, distribution, and removal. In *Enzyme-and Transporter-Based Drug-Drug Interactions* (pp. 27-49). Springer New York.

Saccomani, M. Audoly, S., & D'Angiò, L. (2003). Parameter identifiability of nonlinear systems: the role of initial conditions. *Automatica*, 39, 619-632.

Sachs, J. R., & Welt, L. G. (1967). The concentration dependence of active potassium transport in the human red blood cell. *Journal of Clinical Investigation*, 46(1), 65.

Sarkadi, B., Homolya, L., Szakacs, G. and Varadi, A. (2006). Human multidrug resistance ABCB and ABCG transporters: participation in a chemoimmunity defense system. *Physiol Rev* 86: 1179-1236.

Sarria, B., Dainty, J. R., Fox, T. E., & Fairweather-Tait, S. J. (2004). Estimation of iron absorption in humans using compartmental modelling. *European journal of clinical nutrition*, *59*(1), 142-144.

Selick, H. E., Beresford, A.P., Tarbit, M. H. (2002). The emerging importance of predictive ADME simulation in drug discovery. *Drug Discovery Today*. 15 January 2002; 7 (2): 109-16.

Shah, V. P., Midha, K. K., Dighe, S., McGilveray, I. J., Skelly, J. P., Yacobi, A., and Spector, S. (1992). Analytical methods validation: bioavailability, bioequivalence, and pharmacokinetic studies. *Journal of Pharmaceutical Sciences*, *81*(3), 309-312.

Shechter, E. (1986). Secondary active transport. *Biochimie*, *68*(3), 357.

Sheiner, L., Wakefield, J. (1999). Population modelling in drug development. *Stat Methods Med Res* 8: 183-193.

Sheiner, L. B. & Steimer, J. L. (2000). Pharmacokinetic/Pharmacodynamic Modeling in Drug Development. *Annual Review of Pharmacology and Toxicology* Vol. 40: 67-95 DOI: 10.1146/annurev.pharmtox.40.1.67.

Sheiner, L. B. (1997). Learning versus confirming in clinical drug development. *Clin. Pharmacol.Ther*. 61:275-291.

Sheiner, L. B., Stanski, D. R., Vozeh, S., Miller, R., and Ham, J. (1979). Simultaneous modeling of pharmacokinetics and pharmacodynamics: application to d-tubocurarine. *Clinical pharmacology and therapeutics*, *25*(3), 358-371.

Shitara, Y., Horie, T., & Sugiyama, Y. (2006). Transporters as a determinant of drug clearance and tissue distribution. *european journal of pharmaceutical sciences*, *27*(5), 425-446.

Shitara, Y., Sato, H., & Sugiyama, Y. (2005). Evaluation of drug-drug interaction in the hepatobiliary and renal transport of drugs. *Annu. Rev. Pharmacol. Toxicol.*, *45*, 689-723.

Shugarts, S., Benet, L. Z. (2009). The Role of transporters in the Pharmacokinetics of orally administered drugs. *Pharm Res*. September; 26(9): 2039-2054. Published online 2009 June 30. doi: 10.1007/s11095-009-9924-0.

Siepmann, J., & Peppas, N. A. (2012). Modeling of drug release from delivery systems based on hydroxypropyl methylcellulose (HPMC). *Advanced drug delivery reviews*.

Srinath, S., & Gunawan, R. (2010). Parameter identifiability of power-law biochemical system models. *Journal of biotechnology*, *149*(3), 132-140.

Sugano, K., Kansy, M., Artursson, P., Avdeef, A., Bendels, S., Di, L., and Senner, F. (2010). Coexistence of passive and carrier-mediated processes in drug transport. *Nature reviews Drug discovery*, *9*(8), 597-614.

Szederkényi, G. (2009). Comment on "identifiability of chemical reaction networks" by G. Craciun and C. Pantea. *Journal of mathematical chemistry*, *45*(4), 1172-1174.

Takashima, T., Wu, C., Takashima-Hirano, M., Katayama, Y., Wada, Y., Suzuki, M., and Watanabe, Y. (2013). Evaluation of Breast Cancer Resistance Protein Function in Hepatobiliary and Renal Excretion Using PET with 11C-SC-62807. *Journal of Nuclear Medicine*, *54*(2), 267-276.

Tsuji, A. (2002). Transporter-mediated drug interactions. *Drug metabolism and pharmacokinetics*, *17*(4), 253-274.

Tunali, E.T., Tarn, T.J. (1987). New results for identifiability of nonlinear systems, *IEEE Trans. Automat. Contr.* 32 146-154.

Vajda, S., Godfrey, K.R., Rabitz, H. (1989). Similarity transformation approach to identifiability analysis of nonlinear compartmental models. *Math. Biosci.* 93, 217-248.

van Herwaarden, A. E. & Schinkel, A. H. (2006). The function of breast cancer resistance protein in epithelial barriers, stem cells and milk secretion of drugs and xenotoxins. *Trends Pharmacol Sci* 27:10-16.

Verma, B. I., Ray, S. K., Srivastava, R. N. (1981). Mathematical models and their application in medicine and heath. *Heatlth Popul Perspect Issues*. Jan-Mar; 4 (1): 42-58.

Wagner, J. G. (1976). Linear pharmacokinetic models and vanishing exponential terms: Implications in pharmacokinetics. *Journal of Pharmacokinetics and Biopharmaceutics*, *4*(5), 395-425.

Walker, J., Halliday, D., Resnick, R., & Walker, J. (2008). *Fundamentals of physics*. New York: Wiley.

Walter, E. (1987). *Identifiability of Parametric Models*, Pergamon, Oxford.

Walter, E., & Pronzato, L. (1997). Identification of parametric models. *Communications and Control Engineering*.

Walter, E., Braems, I., Jaulin, L., & Kieffer, M. (2004). Guaranteed numerical computation as an alternative to computer algebra for testing models for identifiability. In *Numerical Software with Result Verification* (pp. 124-131). Springer Berlin Heidelberg.

Walter, G. G., & Contreras, M. (1999). Compartmental Modeling with Networks. Modeling and Simulation in Science, *Engineering and Technology*.

White, L. J., Evans, N. D., Lam, T. J. G. M., Schukken, Y. H., Medley, G. F., Godfrey, K. R., & Chappell, M. J. (2001). The structural identifiability and parameter estimation of a multispecies model for the transmission of mastitis in dairy cows. *Mathematical biosciences*, *174*(2), 77-90.

Williams, P. J., Ette, E. l. (2000). The role of population pharmacokinetics in drug development in light of the Food and Drug Administration's 'Guidance for Industry: population pharmacokinetics'. *Clinical Pharmacokinetics*, December 2000, Volume 39, Issue 6, pp 285-395.

Wise, M. E. (1985). Negative power functions of time in pharmacokinetics and their implications. *Journal of Pharmacokinetics and Biopharmaceutics* 13, 309-346.

Wright, E. M., & Turk, E. (2004). The sodium/glucose cotransport family SLC5. *Pflügers Archiv*, *447*(5), 510-518.

Xia, X., & Moog, C. H. (2003). Identifiability of nonlinear systems with application to HIV/AIDS models. *Automatic Control, IEEE Transactions on*, *48*(2), 330-336.

Xu, J., Liu, Y., Yang, Y., Bates, S., & Zhang, J. T. (2004). Characterization of oligomeric human half-ABC transporter ATP-binding cassette G2. *Journal of Biological Chemistry*, *279*(19), 19781-19789.

Yoshida, K., Maeda, K., Sugiyama, Y. (2013). Hepatic and Intestinal Drug Transporters: Prediction of Pharmacokinetic Effects Caused by Drug-Drug Interactions and Genetic Polymorphisms. *Annual Review of Pharmacology and Toxicology* Vol. 53: 581-612.

Yu, L. X., & Amidon, G. L. (1999). A compartmental absorption and transit model for estimating oral drug absorption. *International journal of pharmaceutics*, *186*(2), 119-125.

Zaïr, Z. M., Eloranta, J. J., Stieger, B., & Kullak-Ublick, G. A. (2008). Pharmacogenetics of OATP (SLC21/SLCO), OAT and OCT (SLC22) and PEPT (SLC15) transporters in the intestine, liver and kidney. *Pharmacogenomics*, *9*(5), 597-624.

Zhou, S., Schuetz, J. D., Bunting, K. D., Colapietro, A. M., Sampath, J., Morris, J. J., & Sorrentino, B. P. (2001). The ABC transporter Bcrp1/ABCG2 is expressed in a wide variety of stem cells and is a molecular determinant of the side-population phenotype. *Nature medicine*, *7*(9), 1028-1034.

Zierler, K. (1981). A critique of compartmental analysis. *Annual Review of Biophysics and Bioengineering*, *10*(1), 531-562.

Chapter 3

Breast Cancer Resistance Protein Pharmacokinetics

In this chapter the pharmacokinetics of Hoechst 33342 following administration into a culture medium containing a population of transfected cells (HEK293 hBCRP) is described mathematically using compartmental modelling methods (Grandjean *et al.* 2011).

The most effective treatment for the spread of malignant tumours is the use of chemotherapeutics, specific pharmaceutical agents or drugs that are selectively toxic and destructive to metastatic cells and cancerous tissues. However cancer cells develop mechanisms that allow them to simultaneously resist the action of different anti-cancer compounds. A biological characteristic, known as multidrug resistance, can reduce the exposure of the diseased tissue and so have significant consequences for efficacious chemotherapy. Understanding and describing the mechanisms behind drug resistance is predicted to improve treatment success in oncology (Gottesman *et al.* 2002).

During the last four decades of research into multidrug resistance, numerous mechanisms in which cancerous cells impede chemotherapy have been discovered, namely altered expression and mutation of the target cell, modifications in survival and apoptotic pathways, and amended uptake or efflux transporter action. In the latter, drugs are actively ejected from the intracellular medium by the increased

activity of efflux transporters such as ATP dependent pumps (see *Section* 2.4). The resultant reduced drug concentration in the target intracellular region is a major cause of multidrug resistance and treatment failure in chemotherapy (Fetsch *et al.* 2006). One such important mechanism is efflux transport by the breast cancer resistance protein - BCRP (Doyle *et al.* 1998), which has been shown in previous antigens studies to be primarily expressed in biological cell membranes (Rocchi *et al*. 2000, Scheffer et al. 2000).

It is therefore crucial for efficacious chemotherapy to know whether a novel drug is a substrate for BCRP. As described in *Section* 1.1, the aim of this chapter is to produce a mechanistic compartmental model based on mass balance principles, which describes the saturable binding of Hoechst 33342 to BCRP.

The most direct way to investigate efflux pumps is to employ an assay with a radioactive or fluorescent substrate used as a probe where functional activity is quantitatively assessed by measuring the reduced concentration in the presence of a competing substrate (Aschner *et al.* 2006). The latter will act as an inhibitor, resulting in greater uptake of the probe. Rabindran *et al.* 1998 report that Fumitremorgin C (FTC) is a potent BCRP inhibitor, which therefore directly competes with Hoechst 33342 for the limited number of binding sites on BCRP, which in turn will effectively reduce the ability of the efflux transporter to resist the action of the anti-cancer compound.

This chapter reports the modelling of the kinetics of an assay that uses transfected cells that express BCRP. The assay indirectly measures the binding potential of a drug or similar molecule to BCRP by observing the effects on the kinetics of Hoechst 33342 (Lalande *et al.* 1981), a BCRP substrate. When Hoechst 33342 binds

to DNA the resulting complex fluoresces (Latt & Stetten 1976; Arndt-Jovin & Jovin 1977; Lalande *et al.* 1981; Olive *et al.* 1985). This allows the relative levels of Hoechst 33342 bound to DNA to be measured under different experimental conditions. Mathematical modelling of *in vitro* pharmacokinetic assays has proven useful elsewhere (Paine *et al.* 2008; Baker & Parton 2007). With this experimental scenario it is challenging to measure the binding affinity of a drug for BCRP because the only known quantities in the system are the initial extracellular concentrations of Hoechst 33342 and the drug of interest, as well as a fluorescence time series. The concept is to use the parameterised mathematical model to estimate any unknown rate constants and parameters from *in vitro* data provided by AstraZeneca in order to obtain information on the relative binding affinities to the BCRP transporter. Although the combination of Hoechst 33342 and FTC to study BRCP has been investigated previously (Huls *et al.* 2009), as far as the author is aware, no mechanistic models have previously been published.

3.1 Mathematical Model

Hoechst 33342 has been shown to be a substrate for BCRP previously (Kim *et al.* 2002; Scharenberg *et al.* 2002), it is readily taken up into living cells, is non-toxic and binds specifically and quantitatively to DNA whereupon it fluoresces (Latt & Stetten 1976; Arndt-Jovin & Jovin 1977; Lalande *et al.* 1981; Olive *et al.* 1985). Hoechst 33342 (and an inhibitor of interest) can be added to the medium in which the cells sit at the beginning of the experiment. The marker compound enters live cells and binds to DNA in the nucleus, resulting in fluorescence.

This fluorescence may be measured and is used as a surrogate to measure binding to DNA. The marker compound is a substrate of BCRP and so may be also transported out of the cell actively. In the model, compartments are used to represent different parts of the cell. Based upon what is known about the system a seven-compartment model illustrated in *Figure* 3.1 was used initially to describe the flow of the substrate and inhibitor within and in/out of the cell.

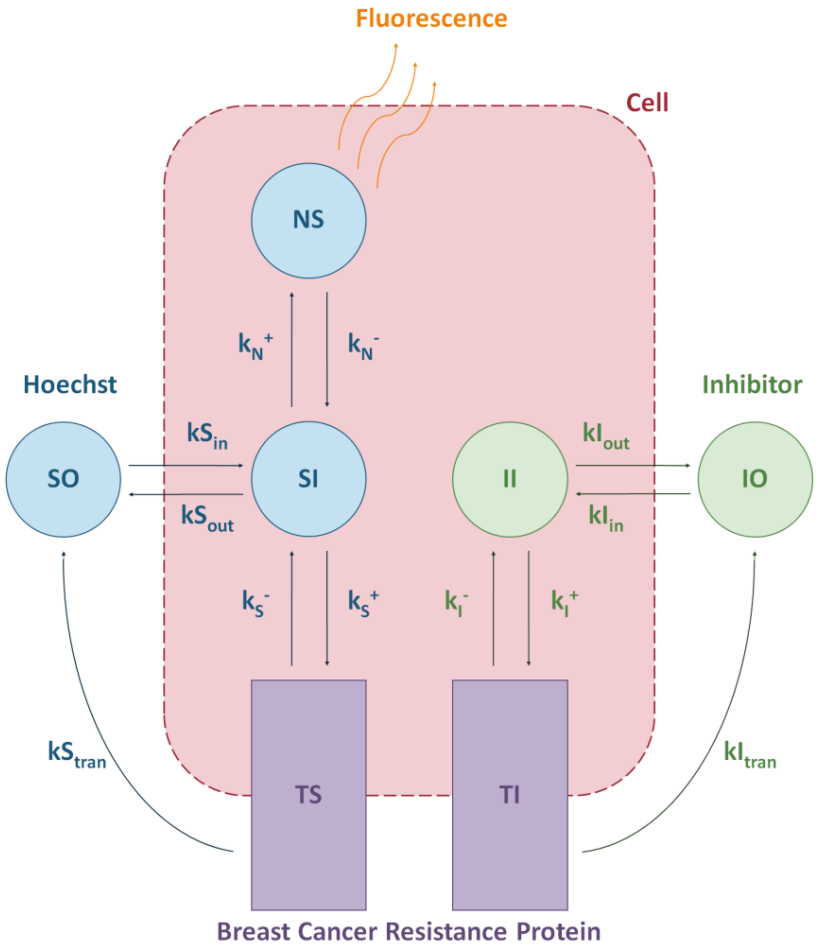

Figure 3.1: Mathematical model representation

Extracellular Hoechst 33342 (SO) diffuses into the cell (SI) and may then bind to DNA in the nucleus (NS) resulting in fluorescence. Hoechst 33342 is also transported out of the cell by a BCRP transporter (TS). Similarly extracellular

inhibitor FTC (IO) diffuses into the cell (II) and is also transported out by the BCRP transporter (TI).

Although the level of BCRP can conceptually be described by a single compartment, it is represented mathematically by two state variables (compartments) as there are two different complexes present; the substrate Hoechst 33342 and inhibitor FTC, which both compete for the same limited number of binding sites on BCRP transporter molecules.

The seven compartments used and the inter-compartmental rate transfers are summarised in *Table* 3.1.

Table 3.1: Description of the inter-compartmental rate transfer and compartments

Inter-compartmental rate transfers		**Compartments**	
kS_{in}	Marker compound cellular influx	*SO*	Extracellular quantity of marker compound
kS_{out}	Marker compound cellular efflux		
kI_{in}	Inhibitor cellular influx	*SI*	Intracellular quantity of marker compound
kI_{out}	Inhibitor cellular efflux		
k_N^+	Marker compound nuclear binding	*IO*	Extracellular quantity of inhibitor compound
k_N^-	Marker compound nuclear dissociation		
k_S^+	Marker compound transporter binding	*II*	Intracellular quantity of inhibitor compound
k_S^-	Marker compound transporter dissociation		
k_I^+	Inhibitor transporter binding	*TS*	Marker bound to transporter
k_I^-	Inhibitor transporter dissociation	*TI*	Inhibitor bound to transporter
kS_{tran}	Transporter flow back to marker compound	*NS*	Marker bound to the nucleus (DNA)
kI_{tran}	Transporter flow back to inhibitor		

3.1.1 System Equations

The system of ordinary differential equations (ODE) describing the model is derived using classical mass-balance principles, as per Jacquez 1996. The first order flow rates give rise to linear terms. *Equation* (3.1) shows the flows to and from the extracellular quantity of marker compound (SO), namely the reversible monomolecular substrate diffusion into the cell, kS_{out} and kS_{in}, and the transporter flow back to marker compound, kS_{tran}.

$$TS \xrightarrow{kS_{tran}} SO \underset{kS_{out}}{\overset{kS_{in}}{\rightleftharpoons}} SI \tag{3.1}$$

The law of mass action gives:

$$\frac{dSO}{dt} = kS_{out}SI - kS_{in}SO + kS_{tran}TS \tag{3.2}$$

whereas, the second order biological reactions give rise to non-linear terms. *Equation* (3.3) describes the flows to and from the quantity of marker bound to the BCRP transporter (TS), namely the non-linear reversible binding of the marker compound to the BCRP, with association and dissociation rate constants k_S^+ and k_S^-, and the transporter flow back to marker compound, kS_{tran}.

$$T + SI \underset{k_S^-}{\overset{k_S^+}{\rightleftharpoons}} TS \xrightarrow{kS_{tran}} SO \tag{3.3}$$

Where T is the quantity of transporter molecules with free binding sites. The law of mass action gives:

$$\frac{dTS}{dt} = k_S^+ SI\,T - \left(k_S^- + kS_{tran}\right)TS \tag{3.4}$$

The quantity of free transporter T can be eliminated given the relevant conservation law:

$$T + TS + TI = T_0 \tag{3.5}$$

where T_0 is the total number of transporter binding sites, *Equation* (3.4) therefore becomes:

$$\frac{dTS}{dt} = k_S^+ SI\left(T_0 - TS - TI\right) - \left(k_S^- + kS_{tran}\right)TS \tag{3.6}$$

The higher order biological reactions also give rise to nonlinear terms. *Equation* (3.7) describes the flows to and from the quantity of marker bound to the nucleus DNA (NS), namely the non-linear reversible binding of the marker compound to the DNA, with association and dissociation rate constants k_N^+ and k_N^-.

$$N + m\,SI \underset{k_N^-}{\overset{k_N^+}{\rightleftharpoons}} NS \tag{3.7}$$

where N is the quantity of DNA molecules with free binding sites and m is the order of the nucleus binding reaction, which represents the number of binding sites per molecule of DNA. The law of mass action gives:

$$\frac{dNS}{dt} = k_N^+ SI^m N - k_N^- NS \tag{3.8}$$

The quantity of free DNA molecules N can be eliminated given the relevant conservation law:

$$N + NS = N_0 \tag{3.9}$$

where N_0 is the total number of DNA binding sites. *Equation* (3.8) therefore becomes:

$$\frac{dNS}{dt} = k_N^+ SI^m \left(N_0 - NS\right) - k_N^- NS \tag{3.10}$$

The corresponding set of non-linear ODE characterising the proposed model is therefore given by the following:

$$\frac{dSO}{dt} = -kS_{in} SO + kS_{out} SI + kS_{tran} TS \tag{3.11}$$

$$\frac{dSI}{dt} = kS_{in} SO - kS_{out} SI - k_S^+ SI\left(T_0 - TS - TI\right) + k_S^- TS - k_N^+ SI^m \left(N_0 - NS\right) + k_N^- NS \tag{3.12}$$

$$\frac{dIO}{dt} = -kI_{in} IO + kI_{out} II + kI_{tran} TI \tag{3.13}$$

$$\frac{dII}{dt} = kI_{in} IO - kI_{out} II - k_I^+ II\left(T_0 - TI - TS\right) + k_I^- TI \tag{3.14}$$

$$\frac{dTS}{dt} = k_S^+ SI\left(T_0 - TS - TI\right) - \left(k_S^- + kS_{tran}\right) TS \tag{3.15}$$

$$\frac{dTI}{dt} = k_I^+ II\left(T_0 - TI - TS\right) - \left(k_I^- + kI_{tran}\right) TI \tag{3.16}$$

$$\frac{dNS}{dt} = k_N^+ SI^m \left(N_0 - NS\right) - k_N^- NS \tag{3.17}$$

There is also an eighth equation, the observation of the system in relative fluorescence units (RFU), given by

$$y = Fluorescence\,in\,RFU = NS \tag{3.18}$$

The inputs into the system are the extracellular quantity of marker compound and the extracellular quantity of inhibitor. However, instead of modelling them as inputs, they are included into the initial conditions, which are:

$$SO(0) = D_S \tag{3.19}$$

$$II(0) = D_{II} \tag{3.20}$$

$$IO(0) = D_{IO} \tag{3.21}$$

$$SI(0) = TS(0) = TI(0) = NS(0) = 0 \tag{3.22}$$

where D_S is the initial quantity of extracellular marker compound, D_{IO} is the initial quantity of extracellular inhibitor compound, and D_{II} is the initial quantity of intracellular inhibitor compound. The latter is non-zero because the inhibitor is added five minutes before the marker and has had time to diffuse into the cell (see *Section* 3.2 for more details). The measured outputs are in relative fluorescence units (RFU). Although the exact initial concentrations and volumes for both the marker and inhibitor compound are known, how both of these correlate to RFU is unknown. Furthermore, the split between the amount of inhibitor compounds inside and outside the cell is unknown. Therefore, in the model presented, all three initial conditions are considered to be unknown.

3.2 Experimental Data

Data were gathered at AstraZeneca (Alderley Park, UK). A multi-well plate provided 96 experiments with varying initial amounts of marker compound (ranging between

0.5 and 10 µmol) and inhibitor levels (ranging between 0 and 100 µmol) (see *Table* 3.2 for more details).

Table 3.2: Matrix showing the number of time series data for each experimental set up

		Hoechst Concentration [µM]					
		0.5	**1**	**2**	**5**	**10**	**Total**
Inhibitor Concentration [µM]	**0**	2	2	4	2	2	12
	0.1	2	2	4	2	2	12
	0.32	2	2	4	2	2	12
	1	2	2	4	2	2	12
	3.16	2	2	4	2	2	12
	10	2	2	4	2	2	12
	31.6	2	2	4	2	2	12
	100	2	2	4	2	2	12
	Total	16	16	32	16	16	96

Hoechst 33342 accumulation was measured using a POLARStarOptimas (BMG Labtech, Offenburg, Germany) fluorescence plate reader with excitation filter = 355 nm and emission filter = 460-10 nm, fluorescence was measured for 120-135 cycles, 1 cycle = 1 complete 96-well read, 30 s, Gain = 1200. Fluorescence data were captured by the Optima software for analysis.

The inhibitor was added at time t = 0 s to compartment IO and the compound marker was added five minutes later at time t = 300 s to compartment SO. The compound marker was added later to provide a measurement of the residual background noise fluorescence present during the experiments.

The average background RFU for the first five minutes was subtracted individually from each time series (to allow for potential inhibitor independence) and the data are time shifted to begin at time t = 300 s. A sample plot of the data is shown in *Figure* 3.2.

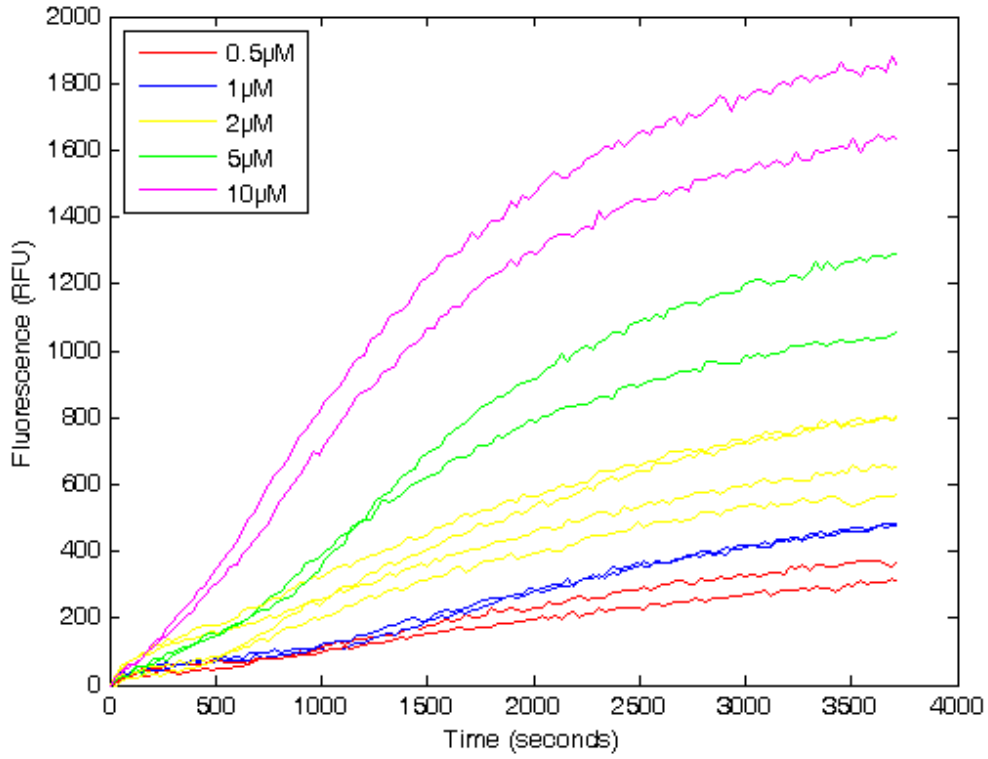

Figure 3.2: Sample data plot for different initial Hoechst concentrations with no inhibitor present

3.2.1 Reduced Model

The data provided leant themselves naturally to only modelling the marker compound without inhibitor as some control time series were collected with no inhibitor present. The inhibitor compartments and corresponding rate constants were therefore initially set to zero, reducing the system to a four-compartment system with ten parameters, illustrated in *Figure* 3.3.

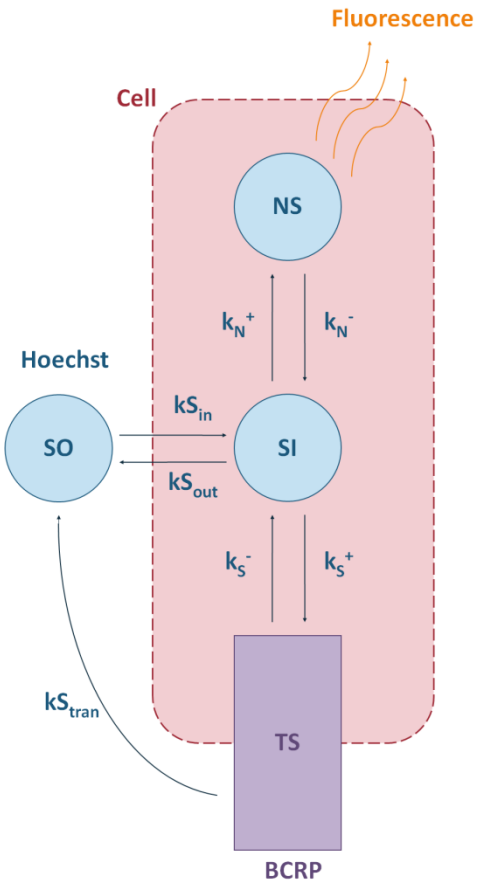

Figure 3.3: Reduced model representation (with no inhibitor)

The corresponding set of non-linear ODE characterising the reduced model with no inhibitor was derived using classical mass-balance principles and is given by:

$$\frac{dSO}{dt} = -kS_{in}SO + kS_{out}SI + kS_{tran}TS \tag{3.23}$$

$$\frac{dSI}{dt} = kS_{in}SO - kS_{out}SI - k_S^+ SI\left(T_0 - TS\right) + k_S^- TS - k_N^+ SI^m\left(N_0 - NS\right) + k_N^- NS \tag{3.24}$$

$$\frac{dTS}{dt} = k_S^+ SI\left(T_0 - TS\right) - \left(k_S^- + kS_{tran}\right)TS \tag{3.25}$$

$$\frac{dNS}{dt} = k_N^+ SI^m\left(N_0 - NS\right) - k_N^- NS \tag{3.26}$$

$$y = Fluorescence\,in\,RFU = NS \tag{3.27}$$

With initial conditions:

$$SO(0) = D_S\,, \tag{3.28}$$

$$SI(0) = TS(0) = NS(0) = 0\,. \tag{3.29}$$

The units for the states (*SO*, *SI*, *TS*, and *NS*) are in RFU and D_S is considered as unknown. It was assumed that any kinetic parameters estimated for this sub-model would then also be applicable for use in the full model with inhibitor present as the rate constants concerned should not be affected by its presence.

3.3 Steady State Analysis

From the data, it can be observed that the fluorescence does not reach steady state values in the time frame of the experiments (see *Figure* 3.2). Albeit perhaps for the compound concentration of 10 µmol; the plot suggests that the compound bound is approaching a steady state value. Although the purpose of the modelling is to investigate the relevant transient behaviour, a steady state analysis was performed since it could potentially be used at a later stage to validate the model. It identifies the levels at which each compartment quantity eventually settles and can be a useful method to obtain fundamental information on the system, the basic relationships between the compartments and for initial guesses for parameter estimation for subsequent fitting (i.e. saturation levels). Steady state analysis is performed by setting all the derivatives in the system equations to zero and solving the resulting algebraic equations for each system variable. Due to the complex non-linear nature of the equations, this was performed using symbolic mathematical packages capable

of solving simultaneous equations, namely Mathematica and Maple, which both yielded the same solutions.

3.3.1 Reduced Model

The steady state analysis solution for the reduced model of the form (3.23) - (3.27) is shown below.

$$SO = \frac{(kS_{out}(k_S^- + k_S^+ SI + kS_{tran}) + k_S^+ T_0 kS_{tran})SI}{kS_{in}(k_S^+ SI + k_S^- + kS_{tran})} \tag{3.30}$$

$$SI = SI \tag{3.31}$$

$$TS = \frac{k_S^+ T_0 SI}{k_S^+ SI + k_S^- + kS_{tran}} \tag{3.32}$$

$$NS = \frac{N_0 k_N^+ SI^m}{k_N^- + k_N^+ SI^m} \tag{3.33}$$

Equation (3.31) indicates that the equations under-determine the system and there is effectively one degree of freedom (DOF). For a given value of (*SI*), the other three compartment concentrations can be computed. This is because the steady state solution (3.30) - (3.33) is obtained by equating the four system equations (3.23) - (3.26) to zero and solving for the states, i.e. *SO*, *SI*, *TS*, and *NS*. The redundancy occurs because the reduced model of the form (3.23) - (3.27) is a closed system, that is to say the sum of the amount of drug in each compartment is equal to the initial dose of Hoechst. This is shown mathematically by adding *Equations* (3.23) - (3.27):

$$\frac{dSI}{dt} + \frac{dSO}{dt} + \frac{dTS}{dt} + \frac{dNS}{dt} = 0 \tag{3.34}$$

Integrating (3.34) and solving for the initial conditions yields:

$$SI + SO + TS + NS = D_S \,. \tag{3.35}$$

Equation (3.35) effectively constrains *SI*, i.e.

$$SI = D_S - SO - TS - NS \tag{3.36}$$

Substituting the steady state solutions for *SO*, *TS*, and *NS*, that is *Equations* (3.30), (3.32), and (3.33) respectively, into *Equation* (3.36) and re-arranging yields:

$$\frac{k_N^+ k_S^+ kS_{out} T_0 SI^{m+2} + a_1 SI^{m+1} + b_1 SI^m - k_N^- k_S^+ kS_{out} SI^2 + d_1 SI + e_1}{k_N^+ k_S^+ kS_{in} SI^{m+1} + k_N^+ kS_{in}(k_S^- + kS_{tran}) SI^m + k_N^- k_S^+ kS_{in} SI + k_N^- kS_{in}(k_S^- + kS_{tran})} = 0 \tag{3.37}$$

where

$$a_1 = k_N^+ k_S^+ kS_{in}(D_S - N_0) - k_N^+ k_S^+ (kS_{in} + kS_{tran}) T_0 - k_N^+ kS_{out}(k_S^- + kS_{tran}) \tag{3.38}$$

$$b_1 = k_N^+ k_S^- kS_{in}(D_S - N_0) + k_N^+ kS_{in} kS_{tran}(D_S - N_0) \tag{3.39}$$

$$d_1 = k_N^- k_S^+ kS_{in}(D_S - T_0) - k_N^- kS_{out}(k_S^- + kS_{tran}) - k_N^- k_S^+ kS_{tran} T_0 \tag{3.40}$$

$$e_1 = k_N^- kS_{in}(k_S^- + kS_{tran}) D_S \tag{3.41}$$

Solving *Equation* (3.37) for *SI* yields the steady states for *SI*. Although it is suspected that there is only one real possible solution in the feasible range for *SI*, i.e.

$$0 \le SI \le D_S \,, \tag{3.42}$$

it has not yet been possible to demonstrate this mathematically, as the undetermined number and complexity of the solutions make algebraic manipulation intractable.

3.3.2 Full Model

The steady state analysis solution for the full model of the form (3.11) - (3.18) is shown below.

$$SO = \frac{(k_S^+ kS_{out} SI + k_S^+ kS_{tran}(T_0 - TI) + k_S^- kS_{out} + kS_{out} kS_{tran})SI}{(k_S^+ SI + k_S^- + kS_{tran})kS_{in}} \tag{3.43}$$

$$SI = SI \tag{3.44}$$

$$IO = \frac{(+k_I^- kI_{out}(k_S^- + kI_{tran} + kS_{tran})(k_I^- + kI_{tran})k_S^+ kI_{out} SI + kI_{out} kI_{tran} kS_{tran})TI}{k_I^+ kI_{in}(k_S^- + kS_{tran})(T_0 - TI)}$$

$$+ \frac{kI_{tran}}{kI_{in}} TI \tag{3.45}$$

$$II = \frac{(k_I^- + kI_{tran})(k_S^+ + k_S^- + kS_{tran})TI}{k_I^+(k_S^- + kS_{tran})(T_0 - TI)} \tag{3.46}$$

$$TS = \frac{k_S^+ SI(T_0 - TI)}{k_S^+ SI + k_S^- + kS_{tran}} \tag{3.47}$$

$$TI = TI \tag{3.48}$$

$$NS = \frac{N_0 k_N^+ SI^m}{k_N^- + k_N^+ SI^m} \tag{3.49}$$

Similarly, *Equations* (3.44) and (3.48) indicate that the equations under-determine the system and there are effectively two DOFs. For given values of *SI* and *TS*, the other five compartment concentrations can be computed. As before, this is because the steady state solution (3.43) - (3.49) is obtained by equating the seven system *Equations* (3.11) - (3.17) to zero and solving for the states, i.e. *SO*, *SI*, *IO*, *II*, *TS*, *TI*,

and *NS*. The redundancies also occur because the full model of the form (3.11) - (3.18) is a closed system, that is to say the sum of the amount of drug and the sum of the amount of inhibitor in each compartment is equal to the initial doses of drug and inhibitor respectively. This is shown mathematically by adding the substrate *Equations* (3.11), (3.12), (3.15), and (3.17):

$$\frac{dSI}{dt}+\frac{dSO}{dt}+\frac{dTS}{dt}+\frac{dNS}{dt}=0\,, \tag{3.50}$$

and by adding the inhibitor *Equations* (3.13), (3.14), and (3.16):

$$\frac{dII}{dt}+\frac{dIO}{dt}+\frac{dTI}{dt}=0\,. \tag{3.51}$$

Integrating (3.50) and solving for the initial conditions yields:

$$SI+SO+TS+NS=D_S\,. \tag{3.52}$$

Integrating (3.51) and solving for the initial conditions yields:

$$II+IO+TI=D_I\,. \tag{3.53}$$

where D_I is the total amount of inhibitor present at the start of the experiment, i.e.

$$D_I=D_{II}+D_{IO}\,. \tag{3.54}$$

Substituting the steady state solutions for *SO*, *TS*, and *NS*, that is *Equations* (3.43), (3.47), and (3.49) respectively, into *Equation* (3.52) and re-arranging yields:

$$\frac{-k_N^+k_S^+kS_{out}SI^{m+2}+a_2SI^{m+1}+b_2SI^m-k_N^-k_S^+kS_{out}SI^2+c_2SI+d_2}{k_N^+k_S^+kS_{in}SI^{m+1}+k_N^+kS_{in}(k_S^-+kS_{tran})SI^m+k_N^-k_S^+kS_{in}SI+k_N^-kS_{in}(k_S^-+kS_{tran})}=0 \tag{3.55}$$

where

$$a_2 = -k_N^+ \left[k_S^+ kS_{in}(N_0 - D_S) + kS_{out}(k_S^- + kS_{tran}) + \right.$$

$$\left. k_S^+ (kS_{in} + kS_{tran})(T_0 - TI) \right] \tag{3.56}$$

$$b_2 = -k_N^+ kS_{in}(k_S^- + kS_{tran})(N_0 - D_s) \tag{3.57}$$

$$c_2 = -k_N^- \left[k_S^+ (kS_{in} + kS_{tran})(T_0 - TI) + kS_{out}(k_S^- + kS_{tran}) - k_S^+ kS_{in} D_S \right] \tag{3.58}$$

$$d_2 = k_N^- kS_{in}(k_S^- + kS_{tran}) D_S \tag{3.59}$$

Substituting the steady state solutions for *IO* and *I*, that is *Equations* (3.45) and (3.46) respectively, into *Equation* (3.53) and re-arranging yields:

$$\frac{a_3 TI^2 + b_3 SI\, TI + c_3 TI + d_3}{k_I^+ kI_{in}(k_S^- + kS_{tran})(T_0 - TI)} = 0 \tag{3.60}$$

where

$$a_3 = k_I^+ kI_{tran}(k_S^- + kS_{tran}) \tag{3.61}$$

$$b_3 = -k_S^+ (k_I^- + kI_{tran})(kI_{in} + kI_{out}) \tag{3.62}$$

$$c_3 = -(k_S^- + kS_{tran}) \left[(k_I^- + kI_{tran})(kI_{in} + kI_{out}) + k_I^+ kI_{tran} T_0 + k_I^+ kI_{in} D_I \right] \tag{3.63}$$

$$d_3 = k_I^+ kI_{in}(k_S^- + kS_{tran}) D_I T_0 \tag{3.64}$$

Simultaneously solving *Equations* (3.55) and (3.60) for *SI* and *TI* yields the steady solutions for *SI* and *TI*. As for the reduced model of the form (3.23) - (3.27); although it is suspected that there is only one real possible solution in the feasible ranges for *SI* and *TI*, i.e.

$$0 \le SI \le D_S \text{ and } 0 \le TI \le D_I, \tag{3.65}$$

respectively, it has not yet been possible to demonstrate this mathematically. Again, the undetermined number and complexity of the solutions make algebraic manipulation intractable.

The output of main interest, as might be expected, is the observation *NS*, which is the same function for the reduced model of form (3.23) - (3.27) and the full model of form (3.11) - (3.18) (*Equations* (3.33) and (3.49)). The steady state analysis shows that the ultimate level of binding to the DNA is a function of the total number of binding sites N_0, the intracellular quantity of compound *SI* and the substrate to DNA binding affinity, i.e. the binding association and dissociation rate constants, k_N^- and k_N^+. Although this is a fairly intuitive result, it describes the exact relationship and will be useful at a later stage for parameter estimation and model validation.

3.4 Structural Identifiability and Indistinguishability Analyses

Structural identifiability analysis has been performed on both of the Hoechst 33342 pharmacokinetic models developed; the reduced model of the form (3.23) - (3.27) and the full model of the form (3.11) - (3.18), using all five of the methods described in the literature review (a similarity transformation approach for uncontrolled systems - STAUS, differential algebra approach using characteristic sets - DAACS, algebraic input/output relationship approach - Ai/oRA, non-differential input/output observable normal form approach - NDi/oONF, and Taylor series expansion) in order to ascertain whether the unknown system parameters can be identified

uniquely or otherwise for the observation available and to ascertain the relative applicability of each approach.

3.4.1 Taylor Series Approach

This general method, introduced in Pohjanpalo 1978, is described in *Section* 2.3.2.6. For the reduced model of the form (3.23) - (3.27), the vector of unknown parameter is given by:

$$\boldsymbol{p} = \left[kS_{in}, kS_{out}, k_N^+, k_N^-, k_S^+, k_S^-, kS_{tran}, D, N_0, T_0 \right], \tag{3.66}$$

the alternate parameter vector,

$$\tilde{\boldsymbol{p}} = \left[\tilde{kS}_{in}, \tilde{kS}_{out}, \tilde{k}_N^+, \tilde{k}_N^-, \tilde{k}_S^+, \tilde{k}_S^-, \tilde{kS}_{tran}, \tilde{D}, \tilde{N}_0, \tilde{T}_0 \right], \tag{3.67}$$

the state vector,

$$\boldsymbol{q}(t, \boldsymbol{p}) = \left[SO, SI, TS, NS \right]^{\mathrm{T}}, \tag{3.68}$$

the initial condition vector,

$$\boldsymbol{q}_0(\boldsymbol{p}) = \left[D, 0, 0, 0 \right]^{\mathrm{T}}, \tag{3.69}$$

and the observation vector,

$$\boldsymbol{y}(t, \boldsymbol{p}) = \left[0, 0, 0, NS \right]^{\mathrm{T}}. \tag{3.70}$$

There is no input function as the initial dose of drug D is included in the initial condition vector $\boldsymbol{q}_0(\boldsymbol{p})$. For the full model of form (3.11) - (3.18), the vector of unknown parameter is given by:

$$\boldsymbol{p} = \left[kS_{in}, kS_{out}, kI_{in}, kI_{out}, k_N^+, k_N^-, k_S^+, k_S^-, k_I^+, k_I^-, kS_{tran}, kI_{tran}, D_S, D_{IO}, D_{II}, N_0, T_0 \right],$$

(3.71)

the alternate parameter vector,

$$\tilde{\boldsymbol{p}} = \left[\tilde{kS}_{in}, \tilde{kS}_{out}, \tilde{kI}_{in}, \tilde{kI}_{out}, \tilde{k}_N^+, \tilde{k}_N^-, \tilde{k}_S^+, \tilde{k}_S^-, \tilde{k}_I^+, \tilde{k}_I^-, \tilde{kS}_{tran}, \tilde{kI}_{tran}, \tilde{D}_S, \tilde{D}_{IO}, \tilde{D}_{II}, \tilde{N}_0, \tilde{T}_0 \right],$$

(3.72)

the state vector,

$$\boldsymbol{q}(t, \boldsymbol{p}) = \left[SO, SI, IO, II, TS, TI, NS \right]^{\mathrm{T}}, \tag{3.73}$$

the initial condition vector,

$$\boldsymbol{q}_0(\boldsymbol{p}) = \left[D_S, 0, D_{IO}, D_{II}, 0, 0, 0 \right]^{\mathrm{T}}, \tag{3.74}$$

and the observation vector,

$$\boldsymbol{y}(t, \boldsymbol{p}) = \left[0, 0, 0, NS \right]^{\mathrm{T}}. \tag{3.75}$$

Again, there is no input function as the initial doses of drug, D_S, and inhibitor, D_{IO} and D_{II}, are included in the initial condition vector $\boldsymbol{q}_0(\boldsymbol{p})$. Unfortunately, due to the structural complexity of the system (i.e. the non-linear terms, in particular the powers) this method did not converge to any solutions for either the reduced model of the form (3.23) - (3.27) or the full model of the form (3.11) - (3.18) in both Mathematica or Maple.

3.4.2 Similarity Transformation Approach for Uncontrolled Systems (STAUS)

The first four Lie derivatives (μ_{01}, μ_{02}, μ_{03}, and μ_{04}) as defined in *Section 2.3.2.1* are computed for the model of the form (3.23) - (3.27). The Jacobian matrix with respect to $\boldsymbol{q} = \left[SO, SI, TS, NS\right]^{\mathrm{T}}$, evaluated at $\boldsymbol{q}_0 = \left[D, 0, 0, 0\right]^{\mathrm{T}}$, of the resultant function $\boldsymbol{H} = \left[\mu_{01}, \mu_{02}, \mu_{03}, \mu_{04}\right]^{T}$ has full rank for appropriate row vectors φ_1 , φ_2, φ_3, and φ_4, which for $m = 1$ are given by the following:

$$\varphi_1 = \left[0\ ,0\ ,0\ ,k\right] \tag{3.76}$$

$$\varphi_2 = \left[0\ ,k\,k_N^{+}\,N_0\ ,0\ ,k\,k_N^{-}\right] \tag{3.77}$$

$$\varphi_3 = \left[k\,k_N^{+}\,N_0\,kS_{in}\ ,-k\,k_N^{+}\ N_0 kS_{out} - k\,k_N^{+2}\,N_0^{\,2} - k\,k_N^{-}\,k_N^{+}\ N_0\ ,k\,k_N^{+}\ N_0 k_N^{-}\ ,\right.$$
$$\left. k\,k_N^{-}\,k_N^{+}\ N_0 - k\,k_N^{+}\,kS_{in}\,D + k\,k_N^{-2}\right] \tag{3.78}$$

$$\varphi_4 = \left[-k\,k_N^{+}\,N_0\,kS_{in}^{\,2} - k\,k_N^{+2}\,N_0^{\,2}\,kS_{in} - k\,k_N^{+}\,N_0\,k_S^{+}\,T_0\,kS_{in} - k\,k_N^{+}\,N_0\,kS_{out}\,kS_{in}\right.$$
$$-k\,k_N^{-}\,k_N^{+}\ N_0\,kS_{in}, k\,k_N^{-2}\,k_N^{+}\ N_0 + k\,k_N^{+}\ N_0 kS_{out}^{\ 2} + 2k\,k_N^{+2}\,N_0^{\,2}\,kS_{out}$$
$$+2k\,k_N^{-}\,k_N^{+\,2}\,N_0^{\,2} + k\,k_N^{+3}\,N_0^{\,3} + k\,k_N^{-}\,k_N^{+}\ N_0\,k_S^{+}\,T_0 + k\,k_N^{+}\,N_0\,k_S^{-}\,k_S^{+}\,T_0$$
$$+2k\,k_N^{+}\,N_0\,kS_{out}\,k_S^{+}\,T_0 + k\,k_N^{+}\,N_0\,kS_{out}\,kS_{in} + k\,k_N^{+}\,N_0\,k_S^{+2}\,T_0^{\,2} + 2k\,k_N^{+2}\,N_0^{\,2}k_S^{+}\,T_0$$
$$+k\,k_N^{-}\,k_N^{+}\ N_0\,kS_{out} - 3k\,k_N^{+2}\,N_0\,kS_{in}\,D\ ,-k\,k_N^{+2}\,N_0^{\,2}\,k_S^{-} - k\,k_N^{+}\,N_0 k_S^{-2}$$
$$-k\,k_N^{+}\,N_0\,k_S^{-}\,k_S^{+}\,T_0 + k\,k_N^{+}\,N_0\,kS_{in}\,kS_{tran} + k\,k_N^{+}\,N_0\,k_S^{+}\,kS_{in}\,D\ ,-2k\,k_N^{-2}k_N^{+}\,N_0$$
$$\left.-k\,k_N^{-}\,k_N^{+\,2}\,N_0^{\,2} - k\,k_N^{-3} + k\,k_N^{+}\,kS_{in}^{\,2}\,D - k\,k_N^{-}\,k_N^{+}\,N_0\,k_S^{+}T_0 - k\,k_N^{-}\,k_N^{+}\,N_0\,kS_{out}\right.$$

$$+2k\,k_N^{+2}\,N_0 kS_{in}\,D + k\,k_N^{+}\,kS_{out}\,kS_{in}\,D + 3k_N^{-}\,k_N^{+}\,kS_{in}\,D + k_N^{+}\,k_S^{+}T_0\,kS_{in}\,D\Big] \quad (3.79)$$

The corresponding Jacobian matrix for the full model of the form (3.11) - (3.18) also has full rank (Appendix A). Analysis of the resulting equations is shown in Appendix A and demonstrates that both the reduced model of the form (3.23) - (3.27) and the full model of the form (3.11) - (3.18) are structurally globally identifiable (SGI).

3.4.3 Differential Algebra Approach

This approach generated the input/output relationship $g(y,\ldots,y^{(n-1)}, \boldsymbol{p})$ for the reduced model of the form (3.23) - (3.27) (see Appendix B). Solving

$$g(y,\ldots,y^{(n-1)}, \boldsymbol{p}) = g(y,\ldots,y^{(n-1)}, \tilde{\boldsymbol{p}}) \quad (3.80)$$

for $\boldsymbol{p}$ yields four solutions:

$$\boldsymbol{s}_1 = \Big\{kS_{in} = k_S^{-}, kS_{out} = kS_{out}, k_N^{+} = k_N^{+}, k_N^{-} = k_N^{-}, k_S^{+} = 0,$$

$$k_S^{-} = k_S^{-}, kS_{tran} = kS_{tran}, D = D, N_0 = 0, T_0 = \tilde{T}_0\Big\}, \quad (3.81)$$

$$\boldsymbol{s}_2 = \Big\{kS_{in} = kS_{in}, kS_{out} = kS_{out}, k_N^{+} = 0, k_N^{-} = k_N^{-}, k_S^{+} = 0,$$

$$k_S^{-} = k_S^{-}, kS_{tran} = kS_{tran}, D = D, N_0 = N_0, T_0 = T_0\Big\}, \quad (3.82)$$

$$\boldsymbol{s}_3 = \Big\{kS_{in} = kS_{in}, kS_{out} = kS_{out}, k_N^{+} = k_N^{+}, k_N^{-} = k_N^{-}, k_S^{+} = 0,$$

$$k_S^{-} = kS_{in}, kS_{tran} = kS_{tran}, D = D, N_0 = N_0, T_0 = T_0\Big\}, \quad (3.83)$$

$$\boldsymbol{s}_4 = \Big\{kS_{in} = \tilde{k}S_{in}, kS_{out} = \tilde{k}S_{out}, k_N^{+} = \tilde{k}_N^{+}, k_N^{-} = \tilde{k}_N^{-}, k_S^{+} = \tilde{k}_S^{+},$$

$$k_S^- = \tilde{k}_S^-, kS_{tran} = \tilde{k}S_{tran}, D = \tilde{D}, N_0 = \tilde{N}_0, T_0 = \tilde{T}_0 \Big\}. \quad (3.84)$$

However the first three solutions are not suitable as some parameters are equal to zero; for $\boldsymbol{s}_1$: $k_S^+ = 0$ and $N_0 = 0$, for $\boldsymbol{s}_2$: $k_N^+ = 0$ and $k_S^+ = 0$, and for $\boldsymbol{s}_3$: $k_S^+ = 0$. All the parameters must be generically non-zero by definition, i.e.

$$\boldsymbol{p}_i > 0 \ \ \forall i, \quad (3.85)$$

and therefore the only solution for *Equation* (3.80) is $\boldsymbol{s}_4$, i.e. $\boldsymbol{p} = \tilde{\boldsymbol{p}}$ and consequently the reduced model of the form (3.23) - (3.27) is structurally globally identifiable.

The differential algebra approach has not yet successfully been applied to the full model of form (3.11) - (3.18) since it has not yet been possible to generate the input output relationship $g(y, \ldots, y^{(n-1)}, \boldsymbol{p})$ due to computational difficulties.

3.4.4 Algebraic Input/Output Relationship Approach (Ai/oRA) and Non-differential Input/Output Observable Normal Form Approach (NDi/oONF)

These two approaches yielded exactly the same results for the reduced model of the form (3.23) - (3.27) as for the differential algebra approach; producing precisely the same input/output relationship (see Appendix C and D respectively), confirming the model is structurally globally identifiable. Both the Ai/oRA and the NDi/oONF approaches have not yet successfully been applied to the full model of the form (3.11) - (3.18). It has not yet been possible to generate the input output relationship due to computational difficulties.

3.4.5 Summary

The results of the structural identifiability analyses are summarised in *Table* 3.3. These analyses demonstrate that under appropriate conditions all models derived are uniquely identifiable for the experiments/observations available. This permits subsequent numerical parameter estimation to be performed with greater confidence.

Table 3.3: Summary of the structural identifiability of both models considered using all five approaches (SGI: structurally globally identifiable; DNC: does not converge)

Approach	Reduced model of the form (3.23) - (3.27)	Full model of the form (3.11) - (3.18)
2.3.2.1 STAUS	SGI	SGI
2.3.2.3 DAACS	SGI	DNC
2.3.2.4 Ai/oRA	SGI	DNC
2.3.2.5 NDi/oONF	SGI	DNC
2.3.2.6 Taylor	DNC	DNC

3.5 Data Analysis

3.5.1 Software

Considering the number of parameters to be estimated and the non-linear nature of the system equations, it was necessary to use an appropriate and numerically robust kinetic modelling software package to perform the parameter estimation. The commercial software package FACSIMILE (MCPA Software, UK) was used since it provides a powerful means of solving ODE (using a backward-difference predictor-corrector method) encountered in biomedical engineering systems modelling, in

particular the kinetics of physical and chemical systems. FACSIMILE utilises the VA05 routine from the Harwell Subroutine Library, which is a hybrid method amalgamating three optimisation methods; namely the Newton-Raphson, steepest descent and Levenber-Marquardt. This computer-modelling tool can easily cope with the robust numerical solution given by the system equations. A significant advantage of FACSIMILE is the ability to handle stiff systems, which exhibit widely varying time constants. Fixed time step numerical integrators cannot cope with stiff systems, as a combination of small and large time steps are required to estimate all the different rate constants accurately whereas the robust numerical integrator within FACSIMILE varies the time step accordingly. More importantly, the package also contains a powerful parameter-fitting option, whereby specified parameters can be adjusted to obtain the best fit to observed data whilst solving the ODE of the model simultaneously. The main limitation of the FACSIMILE software is that it uses local optimisation methods, and as a result it is sensitive to the initial guesses and may be entrapped in local minima. It is therefore important to use numerous wide ranging different combinations of initial guesses.

3.5.2 Parameter Estimation

During the optimisation process of the model parameter estimation described above, FACSIMILE measures the statistical goodness of the fit. This is achieved by calculating:

- The difference between the model and the experimental data, using a weighted residual sum of squares (RSS), i.e. the sum of the squares of the error at each time point. This provides an overall measure of how close the fit

is to the experimental data. This is minimised making the optimisation a least squares problem.

- The confidence levels of the estimated parameter values. This is a statistical measure of how well the model and the data define the parameter.

FACSIMILE outputs a combined weighted RSS value, which is the sum of the error at each individual time point for all the time series together and weighted by the range of each time series, given by:

$$RSS = \sum_{i=1}^{w} \sum_{j=1}^{z} \left(\frac{y_{ij} - \hat{y}_{ij}}{\sigma_i} \right)^2 \tag{3.86}$$

where i denotes the data curve and j the time point, y_{ij} is the i^{th} observed value at the j^{th} sampling time; $\hat{y}_{ij}$ is the corresponding calculated value; and $\sigma_i = e \cdot r_i$ is an estimate for the standard error of the curve i, in which $e = 0.01$ is the default value and the estimated overall data accuracy, and r_i the range of the curve i. Weighting each time series RSS by its range allows to simultaneously fit data that have different magnitudes more accurately. This means that the relative error for the data at lower initial concentrations of Hoechst 33342 contributes to the overall RSS as much as the relative error for high concentrations. FACSIMILE also weighs each data set by e, and thus negatively weighs the residuals by this amount, hence the RSS is effectively multiplied by a factor of 10^4.

The confidence level of the estimated parameter value is a statistical measure of how well the model and the data define the parameter. It is given as the standard deviation of the natural logarithms (SDLN) of the estimated parameters; FACSIMILE works in terms of natural logarithms of the parameters in order to ensure they are strictly

positive. The SDLN values are estimated using the variance-covariance matrix of the total number of parameters and the number of well-determined parameters and can be considered as a percentage error. The variance-covariance matrix also provides information about the estimated correlation between the parameters.

During the fitting procedure, FACSIMILE performs a statistical analysis to detect parameters that are not well determined (NWD) by the data, that is to say the data does not determine a parameter value within tight enough bounds. The values for these parameters are then fixed to the last value used in the statistical analysis before continuing with the parameter fitting, and treated as unknown in subsequent statistical tests.

3.6 Results

To obtain parameter estimates for the full system the data with Hoechst 33342 alone were initially fitted to the reduced model of the form (3.23) - (3.27). These were then used as initial estimates to fit the full system. The assumption is that the kinetic parameters are the same for Hoechst 33342 across the experiments - the only observed changes are due to the interaction with the inhibitor. The reduced model of the form (3.23) - (3.27) comprises the components of the full model of the form (3.11) - (3.18) that deal with Hoechst 33342 kinetics. Given these assumptions, and the fact the full model is identifiable, it is sensible to use the simplified model estimates as initial estimates for the full model of the form (3.11) - (3.18).

3.6.1 Reduced Model of the Form (3.23) - (3.27)

During the numerous preliminary fits undertaken, analysing the initial graphs showed that for both 0.5 μM and 10 μM initial substrate concentration, the fits consistently underestimated the data. Considering that each time series is a different experiment it was reasonable to assume that there could be some variance in the total number of binding sites on the nucleus, N_0. A higher number of binding sites would allow the time series to reach higher values and give a better visual fit. Instead of using one parameter value for N_0 common to all twelve time series, five individual parameters were set, one for each initial substrate data set. Similarly this approach was followed for the total number of binding sites on the BCRP transporter, T_0, to allow for variance and flexibility within the fitting process across the different experiments. As the structural identifiability analysis described in *Section 3.4* was performed assuming one experiment at one concentration, taking different N_0 and T_0 values across experiments while sharing the other parameters will not be to the detriment of the structural identifiability analysis results. A population approach has been considered and the data was fitted using Monolix and NONMEM, however neither software package was able to describe the data accurately for all the different initial conditions. *Table* 3.4 provides the parameter estimates for the best fit obtained for the twelve data sets used where no inhibitor is present.

Table 3.4: Well-determined parameters for reduced model of the form (3.23) - (3.27) with no inhibitor present

Parameters	**Value**	**SDLN**	**Parameters**	**Value**	**SDLN**
kS_{in}	2.45 x 10^{-7} s^{-1}	42.7 %	T_{03}	6.83 x 10^{5} RFU	8.6 %
kS_{out}	3.23 s^{-1}	6.5 %	T_{04}	2.27 x 10^{5} RFU	6.3 %
k_N^+	6.68 x 10^{-4} $RFU^{-m}s^{-1}$	39.3 %	T_{05}	4.41 x 10^{6} RFU	5.8 %
k_N^-	4.43 x 10^{-2} s^{-1}	42.5 %	N_{01}	2.49 x 10^{4} RFU	29.6 %
k_S^+	1.30 x 10^{-5} $RFU^{-1}s^{-1}$	7.3 %	N_{02}	3.11 x 10^{3} RFU	12.6 %
k_S^-	1.05 x 10^{-3} s^{-1}	10.9 %	N_{03}	9.91 x 10^{2} RFU	3.5 %
kS_{tran}	1.26 x 10^{-4} s^{-1}	51.5 %	N_{04}	1.33 x 10^{3} RFU	3.2 %
m	4.35	7.8 %	N_{05}	1.84 x 10^{3} RFU	2.1 %
T_{01}	2.91 x 10^{5} RFU	7.2 %	D	1.55 x 10^{7} RFU	36.3 %
T_{02}	4.48 x 10^{5} RFU	9.4 %	RSS	7.44	-

Figure 3.4 illustrates the best fit associated with *Table* 3.4, obtained for the twelve data sets used where no inhibitor is present.

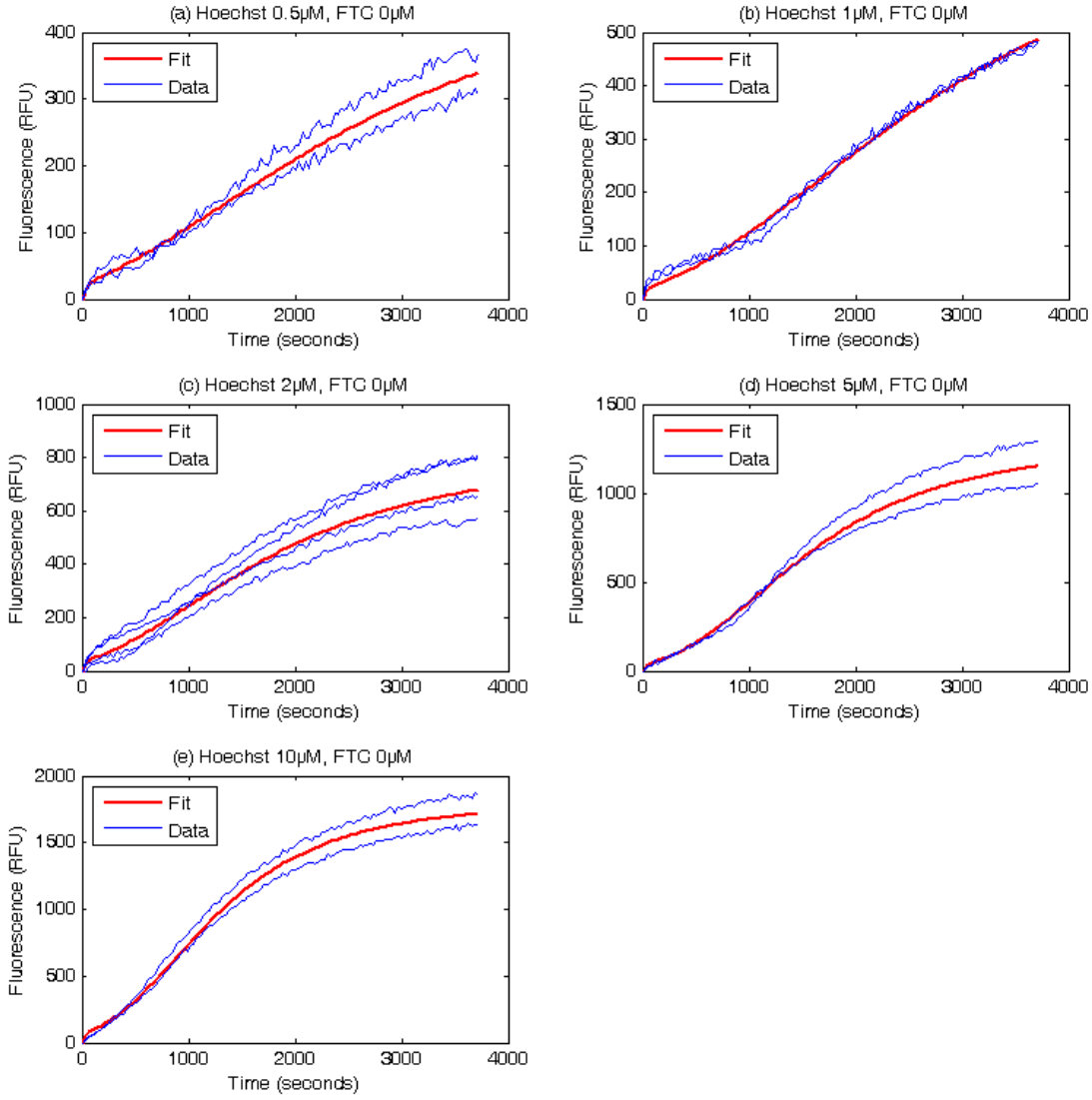

Figure 3.4: FACSIMILE fits for the reduced model
of the form (3.23) - (3.27) without inhibitor

Figure 3.4 is split into five separate charts (a-e), one for each initial substrate concentration.

3.6.2 Full Model of the Form (3.11) - (3.18)

It did not prove possible to obtain a complete set of well determined parameters within FACSIMILE for the full model. Although the model of the form (3.11) -

(3.18) is structurally identifiable (given perfect noise-free data), it was not numerically identifiable with respect to the data used, and as a result a number of parameters were highlighted as not well determined (NWD) within the software package FACSIMILE. In order to obtain good estimates for all the parameters, the well determined parameters with the lowest SDLN values were fixed. These were the 16 independent values of N_0 and T_0, the order of the nucleus binding reaction - m, the extracellular substrate quantity - D_S, the initial intracellular inhibitor quantity - D_{II}, and the initial extracellular inhibitor quantity - D_{IO}. It is assumed that fixing these parameters is justifiable as they were well determined by the data and had low SDLN values. It is suspected that the 16 independent values of N_0 and T_0 effectively over parameterised the system. Fixing these parameters essentially adds extra constraints to reduce the number of DOF, and enabled FACSIMILE to produce well determined estimates for the remaining parameters. *Table* 3.5 provides the parameter estimates for best fits obtained for the full model using all 32 data sets where inhibitor is present.

Table 3.5: Well determined parameters for full model of the form (3.11) - (3.18) with inhibitor present

Parameters	Value	SDLN	Parameters	Value	SDLN
kS_{in}	4.69 x 10^{-7} s^{-1}	3.5%	T_{05}	5.22 x 10^{5} RFU	fixed
kS_{out}	4.43 x 10^{-2} s^{-1}	157%	T_{06}	1.34 x 10^{6} RFU	fixed
kI_{in}	2.48 x 10^{-4} s^{-1}	27.6%	T_{07}	2.91 x 10^{6} RFU	fixed
kI_{out}	1.36 x 10^{-3} s^{-1}	71.2%	T_{08}	2.06 x 10^{6} RFU	fixed
k_N^+	1.75 x 10^{-4} $RFU^{-m}s^{-1}$	137%	N_{01}	1.55 x 10^{3} RFU	fixed
k_N^-	7.92 x 10^{-4} s^{-1}	59.2%	N_{02}	3.71 x 10^{3} RFU	fixed
k_S^+	2.36 x 10^{-6} $RFU^{-1}s^{-1}$	136%	N_{03}	4.79 x 10^{3} RFU	fixed
k_S^-	1.81 x 10^{-3} s^{-1}	46.6%	N_{04}	8.97 x 10^{3} RFU	fixed
k_I^+	5.27 x 10^{-9} s^{-1}	53.8%	N_{05}	6.16 x 10^{3} RFU	fixed
k_I^-	3.15 x 10^{-4} s^{-1}	138%	N_{06}	6.75 x 10^{3} RFU	fixed
kS_{tran}	2.56 x 10^{-4} s^{-1}	79.8%	N_{07}	7.25 x 10^{3} RFU	fixed
kI_{tran}	2.04 x 10^{-4} s^{-1}	168%	N_{08}	5.70 x 10^{3} RFU	fixed
T_{01}	6.55 x 10^{5} RFU	fixed	m	1	fixed
T_{02}	1.43 x 10^{6} RFU	fixed	D_S	3.20 x 10^{6} RFU	fixed
T_{03}	7.53 x 10^{5} RFU	fixed	D_{II}	5.75 x 10^{4} RFU	fixed
T_{04}	7.57 x 10^{5} RFU	fixed	D_{IO}	4.71 x 10^{3} RFU	fixed
RSS	48.627	-	-	-	-

The fixed parameter values are included in *Table* 3.5 and do not have SDLN values as they were not allowed to vary during the parameter fitting performed by FACSIMILE. The remaining SDLN values (ranging from 3.5% to 168%) are higher than for the reduced model of the form (3.23) - (3.27), see *Table* 3.4 (ranging from 2.1 - 51.5%). A perhaps counter intuitive result as there are more time series for the full model of the form (3.11) - (3.18) (32 time series compared to 12) and therefore the data should determine the parameters more accurately, resulting in lower SLDN

values. However the full model of the form (3.11) - (3.18) has many more parameters to estimate (32 compared to 19), which increases the numbers of DOF and the SDLN values.

In *Table* 3.5, the estimated values for the total number of binding sites on the nucleus, N_0 and the total number of binding sites on BCRP, T_0, do not vary greatly across each experiment, ranging from 1.55 x 10^3 to 8.97 x 10^3 RFU and from 5.22 x 10^5 to 2.91 x 10^6 RFU respectively. These are of the same order of magnitude as for the reduced model of the form (3.23) - (3.27), where N_0 ranges from 9.91 x 10^2 to 2.49 x 10^4 RFU and T_0 ranges from 2.27 x 10^5 to 4.41 x 10^6 RFU (see *Table* 3.4).

Furthermore, comparing *Tables* 3.4 and 3.5 shows that some parameters, namely kS_{in}, k_N^+, k_S^-, and kS_{tran} are of the same order of magnitude in both models, however there are some discrepancies between the reduced model of the form (3.23) - (3.27) and full model of the form (3.11) - (3.18) for certain other parameters, namely kS_{out}, k_N^-, and k_S^+. It is suspected that these discrepancies may be due to the different order of the nucleus binding reaction - m, which affects the curvature of the fit (a higher value producing a more sigmoidal shaped curve). For the reduced model of the form (3.23) - (3.27), FACSIMILE converged towards a value of m = 4.35, producing the sigmoidal shape at the beginning of the times series, whereas for the full model of the form (3.11) - (3.18) a value of m = 1 provided a more complete set of well determined parameters. The higher RSS value for the full model of the form (3.11) - (3.18) relative to the reduced model of the form (3.23) - (3.27) is believed to be due to the higher number of DOF and larger number of data sets used.

Figure 3.5 illustrates the best fit associated with *Table* 3.5, obtained for the full model using 32 data sets where inhibitor is present.

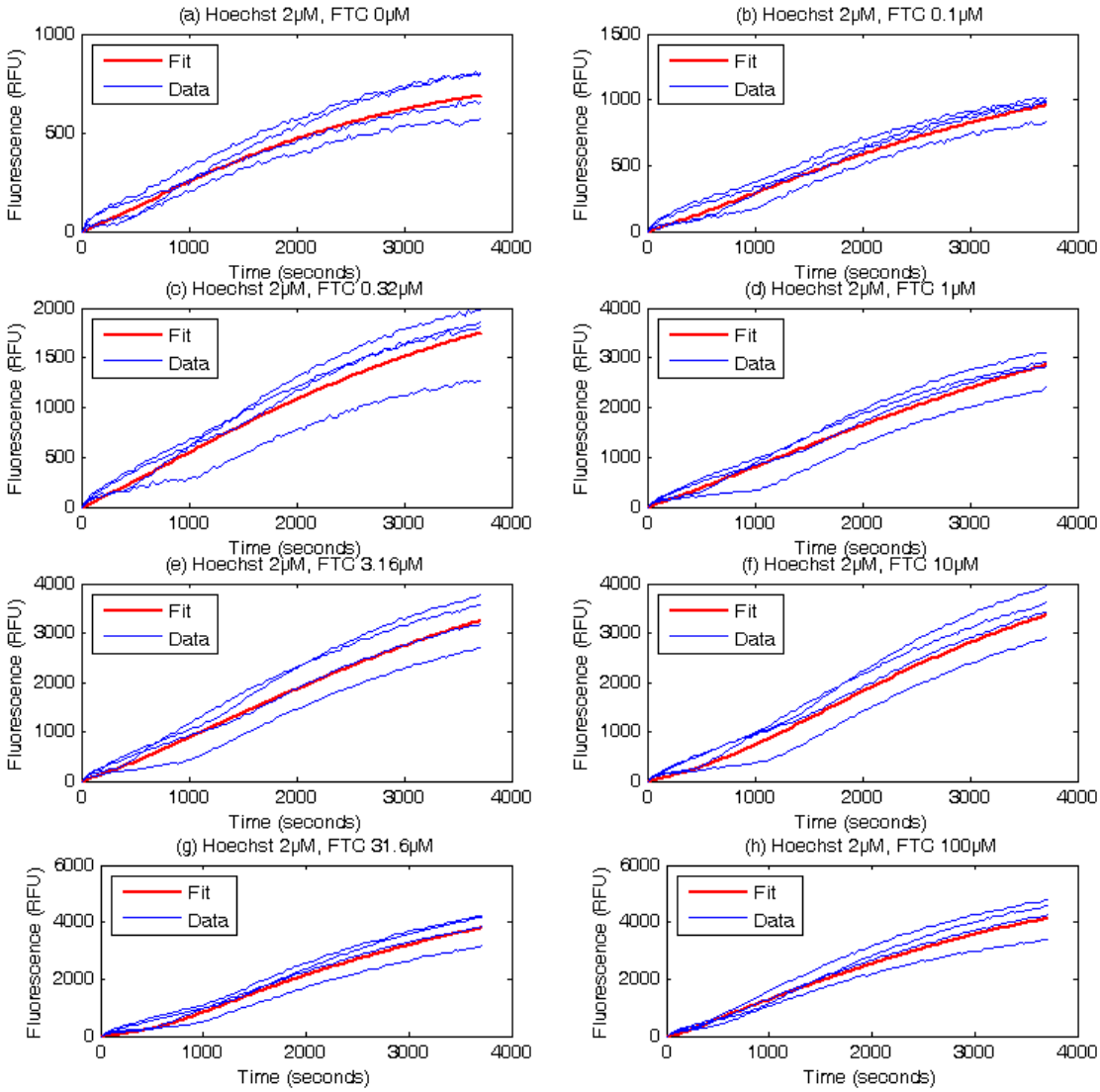

Figure 3.5: FACSIMILE fits for full model of the form (3.11) - (3.18) with inhibitor

Figure 3.5 is split into eight separate charts (a-h), one for each initial inhibitor concentration. It can be seen from each one that the initial step is less prominent (order of the nucleus binding reaction $m = 1$).

3.7 Discussion and Conclusions

The mathematical model derived adequately reproduces the observed time series. Though introduced into the model to improve the model fits, the estimated independent values for N_0 and T_0 across experiments do not differ greatly between experimental conditions, which suggests that the experimental conditions within each well of the multi-well plate are similar. Parameters were estimated with a reasonable level of confidence, which can be judged by the SDLN values produced by FACSIMILE for each parameter.

Given these estimates, the binding affinity of FTC for the BCRP transporter can be calculated to be:

$$k_D = \frac{k_I^+}{k_I^-} = 1.67 \times 10^{-5} \mu M \tag{3.87}$$

This is understandable given the effect small concentrations of FTC have on the observed fluorescence-time profiles.

The models fit their purpose, as they adequately describe the data observed and are derived on mechanistic principles based on knowledge of the processes considered. Additionally all the parameters and rate constants have been estimated to a reasonable degree of accuracy, characterising substrate binding to DNA with transportation of the substrate out of the cell numerically. It can be further seen that BCRP mediated cellular kinetics can be indirectly measured in this way. Structural identifiability analyses for the reduced model of the form (3.23) - (3.27) were performed successfully with four methods; a similarity transformation approach for uncontrolled systems (STAUS), differential algebra approach using characteristic

sets (DAACS), algebraic input/output relationship approach (Ai/oRA), non-differential input/output observable normal form approach (NDi/oONF). However only the STAUS approach was successfully applied to the full model of the form (3.11) - (3.18). The Taylor series expansion approach was also applied to both models but failed to produce any conclusive results (*Table* 3.3). The structural identifiability analyses show that all models derived are uniquely identifiable for the experiments/observations available, adding greater confidence to the numerical parameter estimation carried out.

By modelling the kinetics of the system the binding kinetics for FTC can be inferred. A more simplistic approach that used the change in the steady state fluorescence would only yield an extracellular concentration of FTC that would alter the observed fluorescence by a given amount and such information would be difficult to relate to *in vivo* data. The binding affinity can be compared to blood concentrations observed to assess the impact of BCRP on a drug's ability to penetrate cancer cells and this aspect is currently under investigation.

Further work is required to investigate the competitive binding between Hoechst 33342 and FTC, using other inhibitors, with a view to elucidate the small discrepancies between the two model's parameter estimates, and ultimately propose a more robust model for prediction of uptake at different dose levels. Such a model has the potential to be used to estimate the dosage levels required in order to achieve the levels of absorption desired once bound to DNA. A population approach was considered to account for the variability in the number of binding sites at the nucleus and the transporter availability across the different times series but the software packages used were unable to describe the data accurately for all the different initial conditions. The compartmental modelling approach used in this chapter is also being

applied to other processes and different transporter/inhibitor scenarios, such as the *in vivo* competitive binding of pharmaceuticals and bile acids in hepatic uptake (see Chapter 5).

3.8 References

Arndt-Jovin, D. J., & Jovin, T. M. (1977). Analysis and sorting of living cells according to deoxyribonucleic acid content. *Journal of Histochemistry & Cytochemistry*, 25(7), 585-589.

Aschner, M., Fitsanakis, V. A., dos Santos, A. P. M., Olivi, L., & Bressler, J. P. (2006). Blood-brain barrier and cell-cell interactions: methods for establishing in vitro models of the blood-brain barrier and transport measurements. *In Cell-Cell Interactions* (pp. 1-15). Humana Press.

Baker, M., & Parton, T. (2007). Kinetic determinants of hepatic clearance: plasma protein binding and hepatic uptake. *Xenobiotica*, 37(10-11), 1110-1134.

Doyle, L. A., Yang, W., Abruzzo, L. V., Krogmann, T., Gao, Y., Rishi, A. K., & Ross, D. D. (1998). A multidrug resistance transporter from human MCF-7 breast cancer cells. *Proceedings of the National Academy of Sciences*, 95(26), 15665-15670.

Facsimile (Version 4.0) Technical Reference. (1995), Laboratory, A.T.H., Didcot, Oxon, UK.

Fetsch, P. A., Abati, A., Litman, T., Morisaki, K., Honjo, Y., Mittal, K., & Bates, S. E. (2006). Localization of the ABCG2 mitoxantrone resistance-associated protein in normal tissues. *Cancer letters*, 235(1), 84-92.

Gottesman, M. M., Fojo, T., & Bates, S. E. (2002). Multidrug resistance in cancer: role of ATP-dependent transporters. *Nature Reviews Cancer*, 2(1), 48-58.

Grandjean, T. R., Chappell, M. J., Yates, J. T., Jones, K., Wood, G., & Coleman, T. (2011). Compartmental modelling of the pharmacokinetics of a breast cancer resistance protein. *Computer methods and programs in biomedicine*, 104(2), 81-92.

Huls, M., Brown, C. D. A., Windass, A. S., Sayer, R., van den Heuvel, J. J. M. W., Heemskerk, S., ... & Masereeuw, R. (2007). The breast cancer resistance protein transporter ABCG2 is expressed in the human kidney proximal tubule apical membrane. *Kidney international*, 73(2), 220-225.

Jacquez, J. A. (1996). *Compartmental analysis in biology and medicine*. Ann Arbor: University of Michigan Press.

Kim, M., Turnquist, H., Jackson, J., Sgagias, M., Yan, Y., Gong, M., & Cowan, K. (2002). The multidrug resistance transporter ABCG2 (breast cancer resistance protein 1) effluxes Hoechst 33342 and is overexpressed in hematopoietic stem cells. *Clinical Cancer Research*, 8(1), 22-28.

Lalande, M. E., Ling, V., & Miller, R. G. (1981). Hoechst 33342 dye uptake as a probe of membrane permeability changes in mammalian cells. *Proceedings of the National Academy of Sciences*, 78(1), 363-367.

Latt, S. A., & Stetten, G. (1976). Spectral studies on 33258 Hoechst and related bisbenzimidazole dyes useful for fluorescent detection of deoxyribonucleic acid synthesis. *Journal of Histochemistry & Cytochemistry*, 24(1), 24-33.

Maple (Version 13) Technical Reference. (2009), MapleSoft, Waterloo, ON, Canada.

Mathematica (Version 7.0) Technical Reference (2008), Wolfram Research, Champaign, Illinois.

Olive, P. L., Chaplin, D. J., & Durand, R. E. (1985). Pharmacokinetics, binding and distribution of Hoechst 33342 in spheroids and murine tumours. *British journal of cancer*, 52(5), 739.

Paine, S. W., Parker, A. J., Gardiner, P., Webborn, P. J., & Riley, R. J. (2008). Prediction of the pharmacokinetics of atorvastatin, cerivastatin, and indomethacin using kinetic models applied to isolated rat hepatocytes. *Drug Metabolism and Disposition*, 36(7), 1365-1374.

Rabindran, S. K., He, H., Singh, M., Brown, E., Collins, K. I., Annable, T., and Greenberger, L. M. (1998) Reversal of a novel multidrug resistance mechanism in human colon carcinoma cells by fumitremorgin C. *Cancer Res*. 58, 5850-5858

Rocchi, E., Khodjakov, A., Volk, E. L., Yang, C. H., Litman, T., Bates, S. E., & Schneider, E. (2000). The Product of the ABC Half-Transporter Gene ABCG2 (BCRP/MXR/ABCP) Is Expressed in the Plasma Membrane. *Biochemical and biophysical research communications*, 271(1), 42-46.

Scharenberg, C. W., Harkey, M. A., & Torok-Storb, B. (2002). The ABCG2 transporter is an efficient Hoechst 33342 efflux pump and is preferentially expressed by immature human hematopoietic progenitors. *Blood*, 99(2), 507-512.

Scheffer, G. L., Maliepaard, M., Pijnenborg, A. C., van Gastelen, M. A., de Jong, M. C., Schroeijers, A. B., & Scheper, R. J. (2000). Breast cancer resistance protein is localized at the plasma membrane in mitoxantrone-and topotecan-resistant cell lines. *Cancer research*, 60(10), 2589-2593.

Chapter 4

Organic Anion Transporting Polypeptide Pharmacokinetics

The liver plays a crucial role in drug metabolism and the clearance of endogenous substances and xenobiotics from blood to bile. These vital processes affect drug oral bioavailability (the amount of drug which reaches the target tissue) and drug efficacy, since drugs absorbed from the gut must pass through the liver in order to enter the systemic circulation. Hepatocytes are the cells in the main tissue of the liver responsible for drug metabolism and biliary excretion of drugs. Hepatic uptake is considered to consist of a non-saturable passive diffusion component (driven by the physicochemical properties of the drug investigated) and a saturable active transport component (Webborn *et al.* 2007; Watanabe *et al.* 2009). The latter process continues to be a central area of research in pharmacokinetics (Chandra & Brouwer, 2004; Shitara *et al.*, 2006) as transporter proteins are responsible for the vast majority of molecular movement in organisms.

In vitro isolated hepatocyte assays play a crucial role in the study of hepatic uptake of new chemical entities (Li *et al.* 1999; Soars *et al.*, 2007). Mathematical models can be developed to investigate the mechanisms present and quantify the kinetics of compounds (Paine *et al.* 2008). Rat hepatocytes can easily be isolated and since the cost of human hepatocytes remains preventative for widespread use, they are often used when developing new assays. The subsequent physiologically based models

provide a firm basis for the prediction of the liver's contribution to the pharmacokinetics of a given xenobiotic in man (Poirer *et al.* 2008; Watanabe *et al.* 2009).

It is well established that the Organic Anion Transporting Polypeptides (OATP) play a very important function in hepatic uptake (Jacquemin *et al.* 1994; Kullak-Ublick *et al.* 1994). Pitavastatin is a drug used to treat hypercholesterolaemia, which shows active uptake into hepatocytes, mediated mainly by OATP1B1 (Shimada *et al.* 2003; Hirano *et al.* 2004). The aim of this chapter is to investigate the non-linear kinetics of *in vitro* hepatic uptake of the OATP substrate, Pitavastatin, and quantify the mechanisms present, both structurally and numerically in three species (rat, dog and human). Mechanistic models have only been applied to artificial, hamster, and rat cells previously (Poirier *et al.* 2008, Menochet *et al.* 2012).

Hepatic uptake assays are normally split into two samples which are carried out in water baths at different temperatures: 4°C and 37°C. The latter is the commonly accepted average core body temperature in healthy humans. Hepatocytes are cryopreserved at sub-zero temperatures and the protocol is to place them in a refrigerator at 4°C for 24hrs before the experiment to warm up the fragile cells gradually. The 4°C control sample is performed in parallel because it is experimentally convenient to keep the hepatocytes at this temperature in a water bath with ice and it matches the refrigerator's normal working temperature. The current widely accepted view is that the rate of passive diffusion of Pitavastatin into the cell is the same at both 4°C and 37°C, but that the active transporter action only occurs at 37°C (Shimada *et al.* 2003). Data are normally collected at both 4°C and 37°C, and the 4°C data are used to estimate passive diffusion whilst the 37°C data are used to estimate the active transporter affinity, i.e. the transporter mediated uptake is the

uptake measured at 37°C minus the uptake measured at 4°C (known as the conventional two step approach). However a mechanistic two compartment model proposed by Poirier *et al.* 2008 suggests that diffusion is highly temperature dependent in Chinese hamster ovary control cells and artificial membranes (parallel artificial membrane permeability assay). Menochet *et al.* 2012 extend the model further, adding an extra parameter to account for non-specific cellular binding and find diffusion differs in freshly isolated rat hepatocytes. It is suspected that the current assumption of Shimada *et al.* (2003) is not valid and data at 4°C and 37°C were collected at AstraZeneca by Alex Lench and Charles O'Donnell in order to investigate its validity. Fitting 4°C and 37°C data simultaneously with the same diffusion rates gave very poor fits and therefore fits were carried out for 4°C and 37°C data individually to test the hypothesis. The main advantages compared to the Poirier *et al.* 2008 and Menochet *et al.* 2012 findings is that this is performed for more species (rat, dog and human compared to rat alone) and measures (residual sum of squares and individual parameter estimation accuracy) are given to compare which models describe the uptake more accurately.

In this chapter, six models are described and the structural identifiability and indistinguishability of all the models are investigated. The rate kinetics for the two best mechanistic models are compared between rat, dog and human cells to investigate if cross species scaling is appropriate.

4.1 Mathematical Models

As described previously, Pitavastatin is a substrate of OATP, which actively mediates the transport of the drug across the hepatocyte membrane. Diffusion also takes place at the cell membrane, where the drug flows in and out of the cell according to the concentration gradient. These two mechanisms can be represented by the compartmental model shown in *Figure* 4.1, where each compartment represents a different component of the hepatocyte cell.

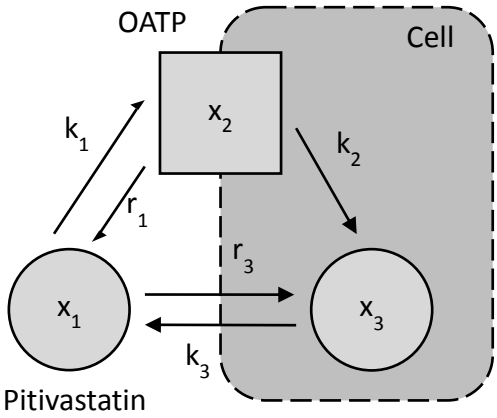

Figure 4.1: Conceptual model representation

A known concentration of Pitavastatin (converted to quantity for the modelling since volumes are known) can be added to the medium in which the hepatocytes sit at the beginning of the experiment, x_1. The substrate actively binds to OATP, x_2, via association and dissociation rate constants k_1 and r_1, respectively, and is mediated into the cell, x_3, by rate constant k_2. Extracellular Pitavastatin, x_1, also flows into and out of the cell, x_3, by diffusion with rate constants k_3 and r_3 respectively.

The three compartments used and the inter-comparmental rate transfers are summarised in *Table* 4.1. The units for the rate constants are in s^{-1} and $\mu mol^{-1}s^{-1}$, and the compartments are in absolute quantities of µmol.

Table 4.1: Description of the inter-compartment rate transfers and compartments

Inter-compartment rate transfers (s^{-1})		Compartments (µmol)	
k_1	OATP association ($\mu mol^{-1}s^{-1}$)	x_1	Pitavastatin extracellular quantity
r_1	OATP dissociation		
k_2	OATP cellular influx	x_2	Pitavastatin bound to OATP
k_3	Cellular efflux (diffusion)	x_3	Pitavastatin intracellular quantity
r_3	Cellular influx (diffusion)		

4.1.1 System Equations

The system of ordinary differential equations (ODE) describing the models is derived using classical mass-balance principles as per Jacquez 1996, see *Section 3.1.1* for more details. The corresponding set of non-linear ODEs characterising the proposed model is therefore given by the following:

$$\frac{dx_1}{dt} = k_3 x_3 - r_3 x_1 - k_1 x_1 (T_0 - x_2) + r_1 x_2 \tag{4.1}$$

$$\frac{dx_2}{dt} = k_1 x_1 (T_0 - x_2) - (k_2 + r_1) x_2 \tag{4.2}$$

$$\frac{dx_3}{dt} = r_3 x_1 - k_3 x_3 + k_2 x_2 \tag{4.3}$$

where T_0 is the total number of transporter binding sites on OATP. The unknown parameter set, $\boldsymbol{p}$, is given by:

$$\boldsymbol{p} = \{k_1, r_1, k_2, k_3, r_3, T_0\} \tag{4.4}$$

The initial conditions are given by:

$$x_1(0) = D \tag{4.5}$$

$$x_2(0) = 0 \tag{4.6}$$

$$x_3(0) = 0\,, \tag{4.7}$$

where D is the known initial dose in µmol (1 million cells). The initial concentration of the medium in which the hepatocytes sit at the beginning of the experiment is known and given in µmol/L. The initial volume is 1 mL and 1 million cells are used thus the initial concentration is multiplied by a factor of 10^{-3} to convert it from µmol/L to µmol (1 million cells); x_1, x_2, x_3 therefore denote quantities in µmol (1 million cells).

Finally there is the observation of the system which is a measurement of total Pitavastatin in the cell and therefore given by:

$$y = k(x_2 + x_3) \tag{4.8}$$

where k is the observation gain, i.e. the observation is the sum of the quantity of Pitavastatin in compartments x_2 and x_3. The observed concentration is given in nmol/L (0.1 million cells - 100 µL is taken from 1 mL) and the measured volume is 900 µL (800 µL of buffer is added). The observation is therefore multiplied by 9 x 10^{-6} to convert from nmol/L (0.1 million cells) to µmol (1 million cells). As the units for the initial dose D and the observation are equivalent, the observation gain k is effectively unitary, i.e. $k = 1$.

It is possible to simplify the model of the form (4.1) - (4.3), by noting that the system is closed and the total amount of Pitavastastin in all three compartments must remain

constant. This is expressed mathematically by adding *Equations* (4.1), (4.2), and (4.3) giving

$$\dot{x}_1 + \dot{x}_2 + \dot{x}_3 = 0\,. \tag{4.9}$$

Integrating (4.9) with respect to time and solving for the initial condition yields

$$x_1 + x_2 + x_3 = D\,. \tag{4.10}$$

Re-arranging (4.10) gives

$$x_1 = D - x_2 - x_3 \tag{4.11}$$

and substituting (4.11) into the model of the form (4.1) - (4.3) reduces it to a system of two ODEs;

$$\dot{x}_2 = k_1(D - x_2 - x_3)(T_0 - x_2) - (r_1 + k_2)x_2 \tag{4.12}$$

$$\dot{x}_3 = r_3(D - x_2 - x_3) - k_3 x_3 + k_2 x_2 \tag{4.13}$$

with initial conditions

$$x_2(0) = 0, x_3(0) = 0 \tag{4.14}$$

and observation

$$y = k(x_2 + x_3)\,. \tag{4.15}$$

Similarly x_2 can be eliminated by re-arranging (4.10) to

$$x_2 = D - x_1 - x_3\,, \tag{4.16}$$

or alternatively, x_3 can be eliminated by re-arranging (4.10) to give

$$x_3 = D - x_2 - x_3. \tag{4.17}$$

The resulting system equations and corresponding initial conditions and observation are shown in *Table* 4.2.

Table 4.2: Alternative system equations for the model of the form (4.1) - (4.3)

System equations	**Initial Conditions**	**Observation**
Eliminating x_2: $\dot{x}_1 = k_3 x_3 - r_3 x_1 - k_1 x_1 (T_0 - D + x_1 + x_3) + r_1 x_2$ (4.18) $\dot{x}_3 = r_3 x_1 - k_3 x_3 + k_2 (D - x_1 - x_3)$ (4.19)	$x_1(0) = D$ (4.20) $x_3(0) = 0$ (4.21)	$y = k(D - x_1)$ (4.22)
Eliminating x_3: $\dot{x}_1 = k_3 (D - x_1 - x_2) - r_3 x_1 - k_1 x_1 (T_0 - x_2) + r_1 x_2$ (4.23) $\dot{x}_2 = k_1 x_1 (T_0 - x_2) - (r_1 + k_2) x_2$ (4.24)	$x_1(0) = D$ (4.25) $x_2(0) = 0$ (4.26)	$y = k(D - x_1)$ (4.27)

Although both the alternative system equations shown in *Table* 4.2 ultimately have the same model structure as the model of the form (4.1) - (4.3), it is interesting to perform the structural identifiability analyses for all three versions as they may produce varied success and will help assess the robustness of the methods applied.

4.1.2 Pseudo Steady State Assumption

It is possible to reduce the above models using a common approximation used in the chemical/biological pharmacokinetic systems literature (Jaquez 1996 and Murray 2003). The necessary assumption is that the binding to the transporter occurs very rapidly on the time scale of the rate of appearance of intracellular compound

(Jacquez 1996). Taking the proposed model of the form (4.1) - (4.3), this is equivalent to assuming that the OATP association and dissociation rate constants, k_1 and r_1 are known to be considerably faster than the other rates, namely the flow into the cell, k_2 and the diffusion into the cell, k_3 and r_3, i.e. there is rapid equilibration of OATP. If this assumption is true then instantaneously after the experiment has begun, the amount of substrate bound to transporter (x_2) is effectively constant, the rate of change of OATP (4.2) can be set to zero and the right hand side of (4.2) can be re-arranged to give:

$$x_2 = \frac{T_0 x_1}{K_M + x_1}, \tag{4.28}$$

where

$$K_M = \frac{r_1 + k_2}{k_1} \tag{4.29}$$

is the relevant Michaelis-Menten constant in μmol. Substituting (4.28) back into the original system equations, (4.1) and (4.3) become

$$\frac{dx_1}{dt} = k_3 x_3 - r_3 x_1 - \frac{V_M x_1}{K_M + x_1} \tag{4.30}$$

$$\frac{dx_3}{dt} = r_3 x_1 - k_3 x_3 + \frac{V_M x_1}{K_M + x_1} \tag{4.31}$$

respectively, where

$$V_M = k_2 T_0 \tag{4.32}$$

is the maximum velocity of the reaction in $\mu mols^{-1}$. The unknown parameter set, $\boldsymbol{p}$, is now given by:

$$\boldsymbol{p} = \{V_M, K_M, k_3, r_3\} \ . \tag{4.33}$$

The initial conditions are now

$$x_1(0) = D \tag{4.34}$$

$$x_3(0) = 0 \, . \tag{4.35}$$

and the observation (4.8) is now given by

$$y = kx_3 \, . \tag{4.36}$$

It is possible to simplify the model of the form (4.30) - (4.31), by noting that adding (4.30) and (4.31) equals zero, as below

$$\dot{x}_1 + \dot{x}_3 = 0 \, . \tag{4.37}$$

Integrating (4.37) with respect to time and solving for the initial condition yields

$$x_1 + x_3 = D \, . \tag{4.38}$$

Re-arranging (4.38) gives

$$x_1 = D - x_3 \tag{4.39}$$

and substituting (4.39) into the model of form (4.30) - (4.31) reduces it to one ODE. Alternatively x_3 can be eliminated by re-arranging (4.38) as

$$x_3 = D - x_1 \, . \tag{4.40}$$

Both variations are shown in *Table* 4.3.

Table 4.3: Alternative system equations for the model of the form (4.30) - (4.31)

System equation	**Initial Condition**	**Observation**
Eliminating x_1: $\dot{x}_3 = r_3(D - x_3) - k_3 x_3 + \frac{V_M (D - x_3)}{K_M + D - x_3}$ (4.41)	$x_3(0) = 0$ (4.42)	$y = k x_3$ (4.43)
Eliminating x_3: $\dot{x}_1 = r_3 x_1 - k_3 (D - x_1) + \frac{V_M x_1}{K_M + x_1}$ (4.44)	$x_1(0) = D$ (4.45)	$y = k\left(D - x_1\right)$ (4.46)

Again, both the alternative system equations shown in *Table* 4.3 ultimately have the same model structure as the model of the form (4.30) - (4.31), it is interesting to perform the structural identifiability analyses for all three versions as they may produce varied success and will help assess the robustness of the methods applied.

4.1.3 Non-Specific Binding

Another candidate model developed allows for non-specific binding (Obrink *et al.* 1977) of Pitavastatin at the cell wall. This is where the medium in which the cells sit in at the beginning of the experiment is not homogenous and a concentration gradient occurs at the hepatic cell wall. This is described by adding a fourth compartment (x_4) to represent a concentration present at the cell wall, as shown in *Figure* 4.2.

The corresponding set of non-linear ODEs characterising the proposed model obtained by mass balance are given by:

$$\dot{x}_1 = k_4 x_4 - r_4 x_1 - k_1 x_1 (T_0 - x_2) + r_1 x_2 \quad (4.47)$$

$$\dot{x}_2 = k_1 x_1 (T_0 - x_2) - (r_1 + k_2) x_2 \tag{4.48}$$

$$\dot{x}_3 = r_3 x_4 - k_3 x_3 + k_2 x_2 \tag{4.49}$$

$$\dot{x}_4 = r_4 x_1 - (k_4 + r_3) x_4 + k_3 x_3 \tag{4.50}$$

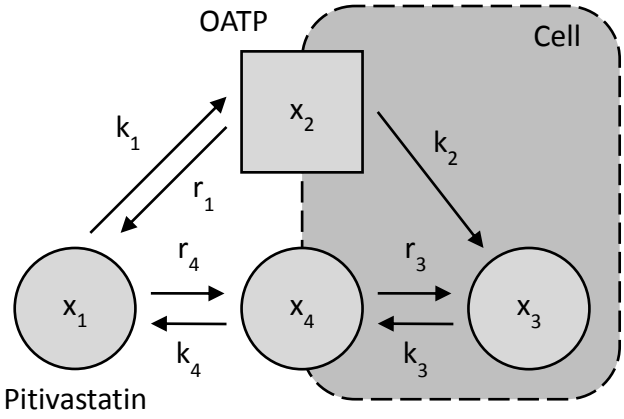

Figure 4.2: Non-specific binding model representation

with initial conditions

$$x_1(0) = D, x_2(0) = 0, x_3(0) = 0, x_4(0) = 0 \tag{4.51}$$

and observation

$$y = k\left(x_2 + x_3 + x_4\right). \tag{4.52}$$

Here the unknown parameter set, $\boldsymbol{p}$, is given by

$$\boldsymbol{p} = \left\{k_1, r_1, k_2, k_3, r_3, k_4, r_4, T_0\right\} \ . \tag{4.53}$$

Again it is possible to simplify the model of the form (4.47) - (4.50), by noting that adding (4.47), (4.48), (4.49), and (4.50) gives

$$\dot{x}_1 + \dot{x}_2 + \dot{x}_3 + \dot{x}_4 = 0\,. \tag{4.54}$$

Integrating (4.54) with respect to time and solving for the initial condition yields

$$x_1 + x_2 + x_3 + x_4 = D\,. \tag{4.55}$$

Table 4.4: Alternative system equations for the model of the form (4.47) - (4.50)

System equations	**Initial Conditions**	**Observation**
Eliminating x_1:		
$\dot{x}_2 = k_1(D - x_2 - x_3 - x_4)(T_0 - x_2) - (r_1 + k_2)x_2$ (4.56)	$x_2(0) = 0$ (4.59)	
$\dot{x}_3 = r_3 x_4 - k_3 x_3 + k_2 x_2$ (4.57)	$x_3(0) = 0$ (4.60)	$y = k\left(x_2 + x_3 + x_4\right)$
$\dot{x}_4 = r_4(D - x_2 - x_3 - x_4) - (k_4 + r_3)x_4 + k_3 x_3$ (4.58)	$x_4(0) = 0$ (4.61)	(4.62)
Eliminating x_2:		
$\dot{x}_1 = k_4 x_4 - r_4 x_1 - k_1 x_1(T_0 - D + x_1 + x_3 + x_4) + r_1(D - x_1 - x_3 - x_4)$ (4.63)	$x_1(0) = D$ (4.66)	
$\dot{x}_3 = r_3 x_4 - k_3 x_3 + k_2(D - x_1 - x_3 - x_4)$ (4.64)	$x_3(0) = 0$ (4.67)	$y = k\left(D - x_1\right)$ (4.69)
$\dot{x}_4 = r_4 x_1 - (k_4 + r_3)x_4 + k_3 x_3$ (4.65)	$x_4(0) = 0$ (4.68)	
Eliminating x_3:		
$\dot{x}_1 = k_4 x_4 - r_4 x_1 - k_1 x_1(T_0 - x_2) + r_1 x_2$ (4.70)	$x_1(0) = D$ (4.73)	
$\dot{x}_2 = k_1 x_1(T_0 - x_2) - (r_1 + k_2)x_2$ (4.71)	$x_2(0) = 0$ (4.74)	$y = k\left(D - x_1\right)$ (4.76)
$\dot{x}_4 = r_4 x_1 - (k_4 + r_3)x_4 + k_3(D - x_1 - x_2 - x_4)$ (4.72)	$x_4(0) = 0$ (4.75)	
Eliminating x_4:		
$\dot{x}_1 = k_4(D - x_1 - x_2 - x_3) - r_4 x_1 - k_1 x_1(T_0 - x_2) + r_1 x_2$ (4.77)	$x_1(0) = D$ (4.80)	
$\dot{x}_2 = k_1 x_1(T_0 - x_2) - (r_1 + k_2)x_2$ (4.78)	$x_2(0) = 0$ (4.81)	$y = k\left(D - x_1\right)$ (4.83)
$\dot{x}_3 = r_3(D - x_1 - x_2 - x_3) - k_3 x_3 + k_2 x_2$ (4.79)	$x_3(0) = 0$ (4.82)	

Re-arranging (4.55) and substituting into the model of the form (4.47) - (4.50) reduces it to three ODEs. The four alternative structures eliminating x_1, x_2, x_3, and x_4 respectively are show in *Table* 4.4.

As previously, all four alternative system equations shown in *Table* 4.4 ultimately have the same model structure as the model of the form (4.47) - (4.50), however it is desired to perform the structural identifiability analyses for all five versions as they may produce varied success and will help assess the robustness of the methods applied.

The same pseudo steady state assumption as in *Section 0*, can also be made to obtain another representation of this model of the form

$$\dot{x}_1 = k_4 x_4 - r_4 x_1 - \frac{V_M x_1}{K_M + x_1} \tag{4.84}$$

$$\dot{x}_3 = r_3 x_4 - k_3 x_3 + \frac{V_M x_1}{K_M + x_1} \tag{4.85}$$

$$\dot{x}_4 = r_4 x_1 - (k_4 + r_3) x_4 + k_3 x_3 . \tag{4.86}$$

with initial conditions

$$x_1(0) = D_1, x_3(0) = 0, x_4(0) = 0 \tag{4.87}$$

and observation

$$y = k\left(x_3 + x_4\right). \tag{4.88}$$

The unknown parameter set, $\boldsymbol{p}$, is now given by

$$\boldsymbol{p} = \left\{V_M, K_M, k_3, r_3, k_4, r_4\right\} \ . \tag{4.89}$$

It is possible to simplify the model of the form (4.84) - (4.86), by noting that adding (4.84), (4.85), and (4.86) gives

$$\dot{x}_1 + \dot{x}_3 + \dot{x}_4 = 0 \tag{4.90}$$

Integrating (4.54) with respect to time on both sides yields

$$x_1 + x_3 + x_4 = D\,. \tag{4.91}$$

Re-arranging (4.91) and substituting into the model of the form (4.84) - (4.86) reduces it to two ODEs. The three variations, eliminating x_1, x_3, and x_4 respectively are shown in *Table* 4.5.

Table 4.5: Alternative system equations for the model of the form (4.84) - (4.86)

System equations	**Initial Condition**	**Observation**
Eliminating x_1: $\dot{x}_3 = r_3 x_4 - k_3 x_3 + \frac{V_M (D - x_3 - x_4)}{K_M + D - x_3 - x_4}$ (4.92) $\dot{x}_4 = r_4 (D - x_3 - x_4) - (k_4 + r_3) x_4 + k_3 x_3$ (4.93)	$x_3(0) = 0$ (4.94) $x_4(0) = 0$ (4.95)	$y = k\left(x_3 + x_4\right)$ (4.96)
Eliminating x_3: $\dot{x}_1 = k_4 x_4 - r_4 x_1 - \frac{V_M x_1}{K_M + x_1}$ (4.97) $\dot{x}_4 = r_4 x_1 - (k_4 + r_3) x_4 + k_3 (D - x_1 - x_4)$ (4.98)	$x_1(0) = D$ (4.99) $x_4(0) = 0$ (4.100)	$y = k\left(D - x_1\right)$ (4.101)
Eliminating x_4: $\dot{x}_1 = k_4 (D - x_1 - x_3) - r_4 x_1 - \frac{V_M x_1}{K_M + x_1}$ (4.102) $\dot{x}_3 = r_3 (D - x_1 - x_3) - k_3 x_3 + \frac{V_M x_1}{K_M + x_1}$ (4.103)	$x_1(0) = D$ (4.104) $x_3(0) = 0$ (4.105)	$y = k\left(D - x_1\right)$ (4.106)

As for the other models, all three alternative system equations shown in *Table* 4.5 ultimately have the same model structure as the model of the form (4.84) - (4.86), however it is desired to perform the structural identifiability analyses for all four versions as they may produce varied success and will help investigate the robustness of the methods applied.

4.1.4 Drug Metabolism Models

Although it is suspected that there is minimal *in vitro* metabolism (Fujino *et al.* 1999) the final candidate models developed also account for the drug metabolising within the cell. This involves adding an elimination term, k_4, to the third compartment, as shown in *Figure* 4.3.

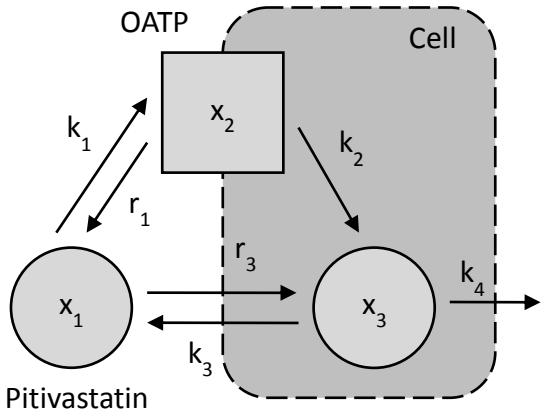

Figure 4.3: Metabolite model representation

The corresponding set of nonlinear ODEs characterising the proposed model obtained by mass balance are given by:

$$\dot{x}_1 = k_3 x_3 - r_3 x_1 - k_1 x_1 (T_0 - x_2) + r_1 x_2 \tag{4.107}$$

$$\dot{x}_2 = k_1 x_1 (T_0 - x_2) - (r_1 + k_2) x_2 \tag{4.108}$$

$$\dot{x}_3 = r_3 x_1 - (k_3 + k_4)x_3 + k_2 x_2 \tag{4.109}$$

with the initial conditions and observation are now given by

$$x_1(0) = D, x_2(0) = 0, x_3(0) = 0 \tag{4.110}$$

and observation

$$y = k(x_2 + x_3)\,. \tag{4.111}$$

The unknown parameter set, ***p***, is given by

$$\boldsymbol{p} = \{k_1, r_1, k_2, k_3, r_3, k_4, T_0\}\ . \tag{4.112}$$

The same pseudo steady state assumption as in *Section 0*, can also be made to obtain another representation of this model of the form

$$\dot{x}_1 = k_3 x_3 - r_3 x_1 - \frac{V_M x_1}{K_M + x_1} \tag{4.113}$$

$$\dot{x}_3 = r_3 x_1 - (k_3 + k_4)x_3 + \frac{V_M x_1}{K_M + x_1} \tag{4.114}$$

where the initial conditions are given by

$$x_1(0) = D, x_3(0) = 0\,, \tag{4.115}$$

and the observation is now given by

$$y = kx_3\,. \tag{4.116}$$

The unknown parameter set, ***p***, is given by

$$\boldsymbol{p} = \{V_M, K_M, k_3, r_3, k_4, r_4\}\ . \tag{4.117}$$

4.1.5 Passive Diffusion Model for the 4°C Data

In order to fit the 4°C data individually, the OATP rate constants $\{k_1, r_1, k_2\}$ are set to zero in the three compartment model of the form (4.1) - (4.3), as it is assumed that there is no transporter action at this temperature, only passive diffusion. The corresponding set of linear ODEs characterising the 4°C model is therefore given by the following:

$$\frac{dx_1}{dt} = k_3 x_3 - r_3 x_1 \tag{4.118}$$

$$\frac{dx_3}{dt} = r_3 x_1 - k_3 x_3 \tag{4.119}$$

with initial conditions

$$x_1(0) = D \tag{4.120}$$

$$x_3(0) = 0 \tag{4.121}$$

and observation:

$$y = k x_3 \tag{4.122}$$

4.2 Structural Identifiability and Indistinguishability Analyses

4.2.1 Taylor Series Expansion

To analyse the 4°C model of the form (4.118) - (4.119) using the Taylor series expansion, the observation $\boldsymbol{y}(t, \boldsymbol{p})$ from (4.122) is differentiated twice with respect to time:

$$y^{(1)} = \frac{dy}{dt} = k(r_3 x_1 - k_3 x_3)\,, \tag{4.123}$$

$$y^{(2)} = \frac{d^2 y}{dt^2} = k(k_3^{\,2} x_3 - k_3 r_3 x_1 + r_3 k_3 x_3 - r_3^{\,2} x_1)\,. \tag{4.124}$$

Evaluating *Equations* (4.123) at (4.124) at $t = 0$ yields

$$y^{(1)}(0, \boldsymbol{p}) = k r_3 D \tag{4.125}$$

and

$$y^{(2)}(0, \boldsymbol{p}) = -k r_3 (k_3 + r_3) D \tag{4.126}$$

The Taylor series coefficients for $\boldsymbol{y}(t, \tilde{\boldsymbol{p}})$ are therefore given by

$$y^{(1)}(0, \tilde{\boldsymbol{p}}) = k \tilde{r}_3 D\,, \tag{4.127}$$

and

$$y^{(2)}(0, \tilde{\boldsymbol{p}}) = -k \tilde{r}_3 (\tilde{k}_3 + \tilde{r}_3) D\,. \tag{4.128}$$

Equating the Taylor series coefficients and solving for the unknown parameter vector ***p*** yields one solution

$$\boldsymbol{s} = \{k_3 = \tilde{k}_3, r_3 = \tilde{r}_3\}, \tag{4.129}$$

demonstrating that the 4°C model of the form (4.118) - (4.119) is structurally globally identifiable (SGI).

The Taylor series expansion method was also successfully applied to the model of the form (4.41): differentiating the observation *y* from (4.43) with respect to time and using $k = 1$ (as shown in *Section 4.1.1*) yields

$$y^{(1)} = \frac{dy}{dt} = r_3(D - x_3) - k_3 x_3 + \frac{V_M(D - x_3)}{K_M + D - x_3} \tag{4.130}$$

which can be re-arranged as

$$y^{(1)} = \frac{a_4 x_3^2 + b_4 x_3 + c_4}{K_M + D - x_3} \tag{4.131}$$

where

$$a_4 = k_3 + r_3 \tag{4.132}$$

$$b_4 = -V_M - r_3 D - (k_3 + r_3)(K_M + D) \tag{4.133}$$

$$c_4 = V_M D + r_3 K_M D + r_3 D^2 \tag{4.134}$$

The derivatives of *y* up to the fourth order are then calculated as follows:

$$y^{(2)} = \frac{d^2 y}{dt^2} = \frac{(2a_4 x_3 + b_4 + y^{(1)})y^{(1)}}{K_M + D - x_3} \tag{4.135}$$

$$y^{(3)} = \frac{d^3 y}{dt^3} = \frac{2a_4 y^{(1)2} + (2a_4 x_3 + b_4 + 3y^{(1)})y^{(2)}}{K_M + D - x_3} \tag{4.136}$$

$$y^{(4)} = \frac{d^4 y}{dt^4} = \frac{3y^{(2)2} + 6a_4 y^{(1)} y^{(2)} + (2a_4 x_3 + b_4 + 4y^{(1)})y^{(3)}}{K_M + D - x_3} \tag{4.137}$$

Evaluating the derivatives at $t = 0$ gives

$$y^{(1)}(0) = \phi_1 = \frac{c_4}{K_M + D} \tag{4.138}$$

$$y^{(2)}(0) = \phi_2 = \frac{b_4\phi_1 + \phi_1^2}{K_M + D} \tag{4.139}$$

$$y^{(3)}(0) = \phi_3 = \frac{2a_4\phi_1^2 + b_4\phi_2 + 3\phi_1\phi_2}{K_M + D} \tag{4.140}$$

$$y^{(4)}(0) = \phi_4 = \frac{6a_4\phi_1\phi_2 + b_4\phi_3 + 3\phi_2^2 + 4\phi_1\phi_3}{K_M + D}. \tag{4.141}$$

Assuming that the initial dose D is known, solving (4.138) - (4.141) for all four parameters (K_M, V_M, k_3 and r_3) yields the unique solutions

$$K_M = \frac{3\phi_1^2(\phi_1\phi_3 - \phi_2^2)}{3\phi_2^3 - 4\phi_1\phi_2\phi_3 + \phi_1^2\phi_4} - D \tag{4.142}$$

$$V_M = \frac{27\phi_1^3\left(\phi_1\phi_3 - \phi_2^2\right)^4}{2\left(3\phi_2^3 - 4\phi_1\phi_2\phi_3 + \phi_1^2\phi_4\right)^2\left(3\phi_2^3 D - 4\phi_1\phi_2\phi_3 D + \phi_1^2\phi_4 D + 3\phi_1^2\phi_2^2 - 3\phi_1^3\phi_3\right)} \tag{4.143}$$

$$k_3 = \frac{2\phi_1 d\left(\phi_1\left(6\phi_2^3 + \phi_1^2\phi_4 - 7\phi_1\phi_2\phi_3\right) + \phi_2 D\left(\phi_1\phi_4 - \phi_2\phi_3\right)\right) + 3D^2\left(\phi_2^4 - \phi_1^2\phi_3^2\right) + 6\phi_1^4\left(\phi_2^2 - \phi_1\phi_3\right)}{\phi_1 D\left(3\phi_2^3 D - 4\phi_1\phi_2\phi_3 D + \phi_1^2\phi_4 D + 3\phi_1^2\phi_2^2 - 3\phi_1\phi_3^3\right)} \tag{4.144}$$

$$r_3 = \frac{\phi_1\left(12\phi_1^{\,2}\phi_2^{\,3}\phi_4 D - 16\phi_1^{\,3}\phi_2\phi_3\phi_4 D - 75\phi_1\phi_2^{\,4}\phi_3 D - 42\phi_1^{\,3}\phi_2^{\,3}\phi_3 + 59\phi_1^{\,2}\phi_2^{\,2}\phi_3^{\,2} D\right)}{2D\left(3\phi_2^{\,3} - 4\phi_1\phi_2\phi_3 + \phi_1^{\,2}\phi_4\right)\left(3\phi_2^{\,3} D - 4\phi_1\phi_2\phi_3 D + 3\phi_1^{\,2}\phi_2^{\,2} - 3\phi_1^{\,3}\phi_3 + \phi_1^{\,2}\phi_4 D\right)}$$
$$+\frac{\phi_1\left(24\phi_1^{\,4}\phi_2\phi_3^{\,2} + 6\phi_1^{\,4}\phi_2^{\,2}\phi_4 + 18\phi_1^{\,2}\phi_2^{\,5} - 6\phi_1^{\,5}\phi_3\phi_4 + 2\phi_1^{\,4}\phi_4^{\,2} D + 27\phi_2^{\,6} D - 9\phi_1^{\,3}\phi_3^{\,3} D\right)}{2D\left(3\phi_2^{\,3} - 4\phi_1\phi_2\phi_3 + \phi_1^{\,2}\phi_4\right)\left(3\phi_2^{\,3} D - 4\phi_1\phi_2\phi_3 D + 3\phi_1^{\,2}\phi_2^{\,2} - 3\phi_1^{\,3}\phi_3 + \phi_1^{\,2}\phi_4 d\right)} \quad (4.145)$$

The compartmental model of the form (4.41) is therefore structurally globally identifiable (SGI), as Φ_1, Φ_2, Φ_3, Φ_4, and D are measurable/known. Unfortunately, due to the structural complexity of the system, this approach did not converge to any solutions for the three compartment model of the form (4.1) - (4.3) due to computational limitations. Although it is possible to compute the first six derivatives of the observation; the resulting functions are too large and too complex for symbolic packages to manipulate.

The Taylor series expansion method was also successfully applied to the models of the form (4.30) - (4.31) and of the form (4.44), demonstrating that they are SGI. The Taylor series expansion approach was also applied to all the remaining models to ascertain structural identifiability. However this method did not converge for any of the other models proposed. The approach is intractable if it is not possible to obtain sufficient Taylor series coefficients or if they prove too complex in structure to yield solutions for the unknown parameters using symbolic tools such as Maple 2010 or Mathematica 9 (Windows XP Pro 2002 SP3, Intel Quad CPU 1.98GHz, 2.99GB of RAM).

4.2.2 Observability Rank Criterion

Given that $k = 1$, the first two Lie derivatives defined in *Section 2.3.2.1* of the model of the form (4.12) - (4.13) are given by:

$$\mu_1 = x_2 + x_3, \quad (4.146)$$

$$\mu_2 = k_1(D - x_2 - x_3)(T_0 - x_2) + r_3(D - x_2 - x_3) - k_3 x_3 - r_1 x_2 . \quad (4.147)$$

The Jacobian Matrix with respect to $\boldsymbol{x} = (x_2, x_3)^T$, evaluated at $\boldsymbol{x}_0 = (0,0)^T$, of the resultant function $\boldsymbol{H} = (\mu_1, \mu_2)^T$ is therefore given by:

$$J = \begin{bmatrix} 1 & 1 \\ -k_1 D - k_1 T_0 - r_1 - r_3 & -k_1 T_0 - k_3 - r_3 \end{bmatrix}, \quad (4.148)$$

which has full rank and therefore the model of the form (4.12) - (4.13) satisfies the Observability Rank Criterion (ORC). Similarly all the remaining candidate models derived can be shown to satisfy the ORC, allowing the four techniques (the similarity transformation approach for uncontrolled systems - STAUS, the algebra approach using characteristic sets - DAACS, the algebraic input/output relationship approach - Ai/oRA, and the non-differential input/output observable normal form approach - NDi/oONF) to be applied to all the models described.

4.2.3 Similarity Transformation Approach for Uncontrolled Systems (STAUS)

For the model of the form (4.41), given that $k = 1$ the first Lie derivative, defined in *Section 2.3.2.1* is

$$\mu_1 = x_3 , \quad (4.149)$$

which yields the following resultant function

$$\boldsymbol{H} = \mu_1 , \quad (4.150)$$

and therefore the smooth map λ calculated using (2.16) is given by

$$\boldsymbol{H}_{\boldsymbol{p}}\left(\boldsymbol{\lambda}(\boldsymbol{x})\right) = \lambda_3 = x_3 . \tag{4.151}$$

Substituting (4.151) into the left hand side of (2.18) yields

$$\boldsymbol{f}\left(\boldsymbol{\lambda}(\boldsymbol{x}(t, \tilde{\boldsymbol{p}})), \boldsymbol{p}\right) = k_3\lambda_3 - r_3(D - \lambda_3) - \frac{V_M(D - \lambda_3)}{K_M + D - \lambda_3} \tag{4.152}$$

Differentiating (4.151) with respect to x_3 yields

$$\frac{\partial \boldsymbol{\lambda}}{\partial \boldsymbol{x}}(\boldsymbol{x}(t, \tilde{\boldsymbol{p}})) = 1 . \tag{4.153}$$

Finally the system coordinate functions using a parameter vector $\tilde{\boldsymbol{p}}$ is

$$\boldsymbol{f}\left(\boldsymbol{x}(t, \tilde{\boldsymbol{p}}), \tilde{\boldsymbol{p}}\right) = \tilde{k}_3 x_3 - \tilde{r}_3\left(D - x_3\right) - \frac{\tilde{V}_M\left(D - x_3\right)}{\tilde{K}_M + D - x_3} . \tag{4.154}$$

Equating the monomials in x_3 of (4.152) and (4.154) yields the following four equations:

$$\begin{aligned} &\tilde{r}_3\left(\tilde{K}_M D^2 + K_M D^2 + K_M \tilde{K}_M D + D^3\right) + K_M \tilde{V}_M D + \tilde{V}_M D^2 \\ &\quad = r_3\left(\tilde{K}_M D^2 + K_M D^2 + K_M \tilde{K}_M D + D^3\right) + \tilde{K}_M V_M D + V_M D^2 \end{aligned} \tag{4.155}$$

$$\begin{aligned} &k_3 K_M \tilde{K}_M + k_3 K_M D + k_3 \tilde{K}_M D + k_3 D^2 + 2r_3 K_M D + r_3 K_M \tilde{K}_M + 2r_3 \tilde{K}_M D + 3r_3 D^2 + \tilde{K}_M V_M + 2V_M D \\ &= \tilde{k}_3 K_M \tilde{K}_M + \tilde{k}_3 K_M D + \tilde{k}_3 \tilde{K}_M D + \tilde{k}_3 D^2 + 2\tilde{r}_3 \tilde{K}_M D + \tilde{r}_3 K_M \tilde{K}_M + 2\tilde{r}_3 K_M D + 3\tilde{r}_3 D^2 + K_M \tilde{V}_M + 2\tilde{V}_M D \end{aligned} \tag{4.156}$$

$$\begin{aligned} &3\tilde{r}_3 D + r_3 K_M + \tilde{k}_3 \tilde{K}_M + 2\tilde{k}_3 D + \tilde{r}_3 \tilde{K}_M + \tilde{k}_3 K_M + \tilde{V}_M \\ &\quad = 2k_3 D + k_3 K_M + r_3 \tilde{K}_M + 3r_3 D + V_M + r_3 K_M + k_3 \tilde{K}_M \end{aligned} \tag{4.157}$$

$$k_3 + r_3 = \tilde{k}_3 + \tilde{r}_3 \tag{4.158}$$

Solving (4.155) - (4.158) simultaneously yields $k_3 = \tilde{k}_3$, $r_3 = \tilde{r}_3$, $K_M = \tilde{K}_M$, $V_M = \tilde{V}_M$, i.e. $\boldsymbol{p} = \tilde{\boldsymbol{p}}$ and the system is therefore SGI. The STAUS approach was also applied to the other models and the results are summarised in *Table* 4.6.

4.2.4 Differential Algebra Approach Using Characteristics Sets (DAACS)

As described in *Section 2.3.2.3*, the DAACS approach is implemented using the Rosenfeld-Gröbner algorithm in Maple 2010. The code is shown in Appendix E. For the two compartment model of the form (4.12) - (4.13), the Rosenfeld-Gröbner algorithm produces the following input/output map:

$$\theta_1(y, \boldsymbol{p}) = a_5 + b_5\mu_1 + c_5\mu_1^2 + k_1^2\mu_1^2\mu_2 + d_5\mu_1\mu_2 + e_5\mu_2 + k_1^2(k_3 + r_3)\mu_1^3 + k_1\mu_2^2 + f_5\mu_3 - k_1\mu_1\mu_3 \quad (4.159)$$

where

$$a_5 = \left(k_3 - r_1 - k_1 D\right)\left(k_1 k_2 T_0 + k_1 k_3 T_0 + k_1 r_3 D + k_2 r_3 + r_1 r_3\right) D \quad (4.160)$$

$$\begin{aligned} b_5 = {} & -k_1 k_2 k_3 T_0 + 2k_1^2 k_2 T_0 D + 2k_1^2 k_3 T_0 D + k_1 k_2 k_3 D + k_1 k_2 r_1 T_0 + k_1 k_3 r_1 T_0 + 2k_1 k_3 r_1 D \\ & + 2k_1 k_2 r_1 D - 2k_1 k_3 r_3 D + 4k_1 r_1 r_3 D - k_3 r_1 r_3 - k_2 k_3 r_3 + 3k_1^2 r_3 D^2 - k_1 k_3^2 T_0 + k_2 k_3 r_1 \\ & - k_1 k_3^2 D - k_3^2 r_1 + k_1^2 k_3 D^2 + k_3 r_1^2 - k_2 k_3^2 + k_2 r_1 r_3 + r_1^2 r_3 \end{aligned} \quad (4.161)$$

$$c_5 = k_1\left(k_1 k_2 T_0 + 2k_1 k_3 D + k_1 k_3 T_0 + 3k_1 r_3 D + k_2 k_3 - 2k_3 r_1 + k_2 r_3 - k_3 r_3 - k_3^2 + 2r_1 r_3\right) \quad (4.162)$$

$$d_5 = k_1\left(k_3 k_1 r_1 - 2k_1 D - k_2\right) \quad (4.163)$$

$$e_5 = k_1 k_2 D - k_1 k_3 T_0 + k_1 r_1 T_0 + 2k_1 r_1 D + k_1^2 D^2 - k_2 k_3 + k_2 r_1 - k_3^2 - k_3 r_3 + r_1^2 + r_1 r_3 \quad (4.164)$$

$$f_5 = r_1 - k_3 + k_1 D \quad (4.165)$$

Equating the monomials $\{\mu_1, \mu_2, \mu_3\}$ in $\theta_1(y, \boldsymbol{p}) = \theta_1(y, \tilde{\boldsymbol{p}})$ for the vector of unknown parameters, $\boldsymbol{p} = \{k_1, k_2, k_3, r_1, r_3, T_0\}$ yields one unique solution,

$$\boldsymbol{s} = \{k_1 = \tilde{k}_1, k_2 = \tilde{k}_2, k_3 = \tilde{k}_3, r_1 = \tilde{r}_1, r_3 = \tilde{r}_3, T_0 = \tilde{T}_0\}, \tag{4.166}$$

i.e. $\boldsymbol{p} = \tilde{\boldsymbol{p}}$, and thus the two compartment model of the form (4.12) - (4.13) is therefore also SGI. The differential algebra approach using characteristic sets was also applied to the other models and these results are summarised in *Table* 4.6.

4.2.5 Algebraic Input/Output Relationship Approach (Ai/oRA)

For the model of the form (4.44), given that $k = 1$ the first two Lie derivatives are given as

$$\mu_1 = D - x_1, \tag{4.167}$$

$$\mu_2 = \frac{V_M x_1}{K_M + x_1} - k_3(D - x_1) + r_3 x_1. \tag{4.168}$$

As described in *Section 2.3.2.4*, the Ai/oRA approach is implemented by using the Lie derivatives (4.167) and (4.168) into the Univariate Polynomial or Groebner Bases algorithms in Maple 2010. The code is shown in Appendix F. Both algorithms produce the same input/output map

$$\theta_2(y, \boldsymbol{p}) = \mu_1\mu_2 - (K_M + D)\mu_2 - (K_M r_3 + r_3 D + V_M)D$$

$$+(k_3 D + k_3 K_M + K_M r_3 + V_M + 2r_3 D)\mu_1 - (k_3 + r_3)\mu_1^2. \tag{4.169}$$

A second input/output map is generated by substituting $\boldsymbol{p}$ for $\tilde{\boldsymbol{p}}$ in the original input/output relationship (4.169),

$$\theta_2(y,\tilde{\boldsymbol{p}}) = \mu_1\mu_2 - (\tilde{K}_M + D)\mu_2 - (\tilde{K}_M\tilde{r}_3 + \tilde{r}_3 D + \tilde{V}_M)D$$

$$+(\tilde{k}_3 D + \tilde{k}_3\tilde{K}_M + \tilde{K}_M\tilde{r}_3 + \tilde{V}_M + 2\tilde{r}_3 D)\mu_1 - (\tilde{k}_3 + \tilde{r}_3)\mu_1^2 . \qquad (4.170)$$

Equating the monomials of $\{\mu_1, \mu_2\}$ in $\theta_2(y,\boldsymbol{p}) = \theta_2(y,\tilde{\boldsymbol{p}})$ yields the following four equations

$$K_M = \tilde{K}_M \qquad (4.171)$$

$$k_3 + r = \tilde{k}_3 + \tilde{r} \qquad (4.172)$$

$$K_M r_3 + r_3 D + V_M = \tilde{K}_M\tilde{r}_3 + \tilde{r}_3 D + \tilde{V}_M \qquad (4.173)$$

$$k_3 D + k_3 K_M + K_M r_3 + V_M + 2r_3 D = \tilde{k}_3 D + \tilde{k}_3\tilde{K}_M + \tilde{K}_M\tilde{r}_3 + \tilde{V}_M + 2\tilde{r}_3 D \qquad (4.174)$$

Solving *Equations* (4.171) - (4.174) simultaneously for the vector of unknown parameters, $\boldsymbol{p} = \{K_M, V_M, k_3, r_3\}$ yields one unique solution

$$\boldsymbol{s} = \{k_3 = \tilde{k}_3,\ r_3 = \tilde{r}_3,\ K_M = \tilde{K}_M,\ V_M = \tilde{V}_M\}, \qquad (4.175)$$

i.e. $\boldsymbol{p} = \tilde{\boldsymbol{p}}$, and therefore the model of the form (4.44) is structurally globally identifiable. The algebraic input/output relationship approach was also applied to the other models, the results are summarised in *Table* 4.6.

4.2.6 Non-Differential Input/Output Observable Normal Form Approach (NDi/oONF)

As previously stated, for the model of the form (4.44), given that $k=1$ the first Lie derivative is given as (4.167), which can be re-arranged to give

$$x_1 = D - \mu_1 \tag{4.176}$$

Substituting (4.176) into the second Lie derivative (4.168) yields the same input/output map $\theta_2(y, \boldsymbol{p})$ as for the Ai/oRA. The NDi/oONF approach was also applied to the other models and the results are summarised in *Table* 4.6.

4.2.7 Summary

The results for the similarity transformation approach for uncontrolled systems (STAUS), the algebra approach using characteristic sets (DAACS), the algebraic input/output relationship approach (Ai/oRA), and the non-differential input/output observable normal form approach (NDi/oONF) are summarised in *Table* 4.6.

Table 4.6: Summary of the structural identifiability of all six candidate models considered using all four approaches (SGI: structurally globally identifiable; SLI*: structurally locally identifiable with two solutions; DNC: does not converge)

	Basic						
	Original				**Pseudo Steady State Assumption**		
Approach	(4.1) - (4.3)	(4.12) - (4.13)	(4.18) - (4.19)	(4.23) - (4.24)	(4.30) - (4.31)	(4.41)	(4.44)
2.3.2.1 STAUS	*SGI*	*SGI*	*SGI*	*SGI*	DNC	*SGI*	*SGI*
2.3.2.3 DAACS	*SGI*	*SGI*	*SGI*	*SGI*	*SGI*	*SGI*	*SGI*
2.3.2.4 Ai/oRA	*SGI*	*SGI*	*SGI*	*SGI*	*SGI*	*SGI*	*SGI*
2.3.2.5 NDi/oONF	*SGI*	*SGI*	*SGI*	*SGI*	DNC	*SGI*	*SGI*

	Non specific binding				
	Original				
Approach	(4.47) - (4.50)	(4.56) - (4.58)	(4.63) - (4.65)	(4.70) - (4.72)	(4.77) - (4.79)
2.3.2.1 STAUS	DNC	*SLI**	*SLI**	*SLI**	*SLI**
2.3.2.3 DAACS	DNC	*SLI**	DNC	*SLI**	*SLI**
2.3.2.4 Ai/oRA	DNC	*SLI**	*SLI**	*SLI**	*SLI**
2.3.2.5 NDi/oONF	DNC	*SLI**	*SLI**	*SLI**	*SLI**

	Non specific Binding				**Metabolite**	
	Pseudo Steady State Assumption				**Original**	**Pseudo**
Approach	(4.84) - (4.86)	(4.92) - (4.93)	(4.97) - (4.98)	(4.102) - (4.103)	(4.107) - (4.109)	(4.113) - (4.114)
2.3.2.1 STAUS	DNC	*SGI*	*SGI*	*SGI*	DNC	DNC
2.3.2.3 DAACS	*SGI*	*SGI*	*SGI*	*SGI*	DNC	SGI
2.3.2.4 Ai/oRA	*SGI*	*SGI*	*SGI*	*SGI*	DNC	SGI
2.3.2.5 NDi/oONF	DNC	*SGI*	*SGI*	*SGI*	DNC	DNC

The models of the form (4.1) - (4.3), (4.12) - (4.13), (4.18) - (4.19), and (4.23) - (4.24) can all be shown to be SGI via all four techniques. The DAACS produces the same input/output map θ_1 for the four models. It is important to include *Equation* (4.10) in the DAACS for the model of the form (4.1) - (4.3), or the Rosenfeld-Gröbner algorithm is unable to produce the input/output map θ_1. The algebraic input/output relationship approach (Ai/oRA) produces the same map θ_1 for the models of the form (4.12) - (4.13), (4.18) - (4.19), and (4.23) - (4.24), confirming that they are structurally equivalent, however it produces a different input/output map θ_{1a} for the model of the form (4.1) - (4.3). The Ai/oRA map θ_{1a} is of higher order (in terms of the first three Lie derivative of the observation) than the DAACS map θ_1 (in terms of the first two Lie derivative of the observation). It is not possible to input *Equation* (4.10) into the Univariate Polynomial or Groebner Bases Maple algorithms and therefore they cannot reduce the system accordingly and produce an input/output map of the same order as the Rosenfeld-Gröbner algorithm. The maps θ_1 and θ_{1a} can be shown to be structurally equivalent and the Ai/oRA confirms that the models of the form (4.1) - (4.3), (4.12) - (4.13), (4.18) - (4.19), and (4.23) - (4.24) are structurally equivalent. It is therefore important to reduce the system to its minimal form when applying the DAACS and Ai/oRA.

The pseudo steady state models of the form (4.30) - (4.31), (4.41), and (4.44) can all be shown to be SGI via the differential algebra approach using characteristic sets (DAACS) and the algebraic input/output relationship approach (Ai/oRA). Again DAACS produces the same input/output map θ_2 for the three models and confirms that the models of the form (4.30) - (4.31), (4.41), and (4.44) are structurally equivalent. Ai/oRA produces the same input/output map as DAACS for the models

of the form (4.41) and of the form (4.44); however it produces a higher order input/output map θ_{2b} for the model of the form (4.30) - (4.31). In this instance the DAACS is able to produce an input/output map for the model of the form (4.30) - (4.31) without including *Equation* (4.38) and it is the same as the input/output map produced by Ai/oRA θ_{2b}. Again θ_2 and θ_{2b} can be shown to be structurally equivalent. The similarity transformation approach for uncontrolled systems (STAUS) and the non-differential input/output observable normal form approach (NDi/oONF) both confirm that the models of the form (4.41) and (4.44) are SGI, however they fail to produce conclusive results for the model of the form (4.30) - (4.31), highlighting the importance of reducing the system to its minimal form when applying the STAUS and NDi/oONF.

The non-specific binding models of the form (4.56) - (4.58), (4.63) - (4.65), (4.70) - (4.72), and (4.77) - (4.79) can all be shown to be structurally locally identifiable (SLI) using STAUS, Ai/oRA, and NDi/oONF. The latter two approaches produce exactly the same input/output map θ_3 for all four models, confirming that the models of the form (4.56) - (4.58), (4.63) - (4.65), (4.70) - (4.72), and (4.77) - (4.79) are structurally equivalent. The three approaches (STAUS, Ai/oRA, and NDi/oONF) demonstrate that there are two solutions vectors, namely:

$$\boldsymbol{s}_1 = \left\{\tilde{k}_1 = k_1, \tilde{r}_1 = r_1, \tilde{k}_2 = k_2, \tilde{k}_3 = k_3, \tilde{r}_3 = r_3, \tilde{k}_4 = k_4, \tilde{r}_4 = r_4, \tilde{T}_0 = T_0\right\}, \tag{4.177}$$

$$\boldsymbol{s}_2 = \left\{\tilde{k}_1 = k_1, \tilde{r}_1 = r_1 + k_2 - \tilde{k}_2, \tilde{k}_2 = k_3 + k_4 + r_3, \tilde{k}_3 = \frac{k_3 k_4}{\tilde{k}_4}, \tilde{r}_3 = \frac{r_4(k_3 + r_3)}{\tilde{r}_4} - \tilde{k}_3,\right.$$

$$\left.\tilde{k}_4 = k_2 - \frac{r_4(k_3 + r_3)}{\tilde{r}_4}, \tilde{r}_4 = r_4 + k_2 - \tilde{k}_2, \tilde{T}_0 = T_0\right\}, \tag{4.178}$$

which imply that there are two solutions for most of the unknown parameters, however k_1 and T_0 are globally identifiable. The DAACS approach confirms this result for the models of the form (4.56) - (4.58), (4.70) - (4.72), and (4.77) - (4.79), but it does not produce an input/output map for the model of the form (4.63) - (4.65) even though all four models have been shown to be structurally equivalent, indicating that this approach may be less robust than the Ai/oRA and NDi/oONF in obtaining input/output maps. Although it is suspected that the model of the form (4.47) - (4.50) has the same structure, none of the approaches produced conclusive results. The complexity, in particular the non-linear terms and the fact that the observation is a sum of compartments, means that solutions prove intractable. It is suspected that there is not enough memory available for Maple 2010 to perform the required symbolic calculations. This result demonstrates the importance of reducing the system to its minimal form when performing structural identifiability analyses. For example the algebraic input/output relationship approach (Ai/oRA) requires as many *Lie derivatives* as there are states, hence reducing the models by one or more states significantly simplifies the computation.

The non-specific binding models of the form (4.84) - (4.86), (4.92) - (4.93), (4.97) - (4.98), and (4.102) - (4.103), which include the pseudo steady state assumption, can be shown to be SGI using DAACS and Ai/oRA. As before the DAACS yields the same input/output maps θ_4 for all four models, confirming that they are structurally equivalent. The Ai/oRA produces the same map as DAACS θ_4 for the models of the form (4.92) - (4.93), (4.97) - (4.98), and (4.102) - (4.103), again generating a higher input/output map θ_{4b} for the model of the form (4.84) - (4.86), which can be shown to be structurally equivalent using *Equation* (4.91). The STAUS and NDi/oONF

confirm that the models of the form (4.92) - (4.93), (4.97) - (4.98), and (4.102) - (4.103) are SGI but do not produce conclusive results for the model of the form (4.84) - (4.86) even though it is structurally equivalent. The smooth map λ can be calculated when applying the STAUS approach, however it contains square roots and as a result is transcendental and therefore it is not possible to equate monomials and obtain results. Similarly for the NDi/oONF, solving the Lie derivatives simultaneously for all the states includes square roots, again highlighting the importance of reducing the system to its minimal form when applying the STAUS and NDi/oONF.

None of the approaches could provide conclusive results for the model of the form (4.107) - (4.109), as Maple 2010 is unable to perform the required symbolic manipulations. On the other hand the DAACS and Ai/oRA demonstrate that the model of the form (4.113) - (4.114) is SGI, with both methods producing identical input/output maps θ_5 .

The algebraic input/output relationship approach (Ai/oRA) proves to be the most successful on the hepatic uptake models derived, producing conclusive results for all but two of the candidate models, closely followed by the differential algebra approach using characteristic sets (DAACS), which produced conclusive results for one fewer model. In the models investigated the Ai/oRA approach was more efficient in obtaining input/output maps, however the DAACS approach did offer the possibility of entering extra algebraic equations and constraints such as (4.10). The similarity transformation approach for uncontrolled systems (STAUS) and the non-differential input/output observable normal form approach (NDi/oONF) do not provide any conclusive results for five of the candidate models derived. It is difficult

to conclude which approach is superior as different model structures may produce different results.

All of the analyses above were also duplicated in Mathematica 9 which yielded the same results as Maple 2010.

4.2.8 Structural Indistinguishability

The Taylor series expansion method was successfully applied to the models of the form (4.30) - (4.31), (4.41), and (4.44), confirming that they are structurally indistinguishable. The Taylor series expansion method was also applied pair-wise to all the remaining models, but did not produce conclusive results. As with structural identifiability; the approach is intractable if it is not possible to obtain sufficient Taylor series coefficients or if the Taylor series coefficient prove too complex in structure to yield solutions for the unknown parameters using symbolic tools.

The following input/output maps were generated in *Sections* 4.2.3 - 4.2.6:

θ_1 - models of the form (4.1) - (4.3), (4.12) - (4.13), (4.18) - (4.19), and (4.23) - (4.24)

θ_2 - models of the form (4.30) - (4.31), (4.41), and (4.44)

θ_3 - models of the form (4.56) - (4.58), (4.63) - (4.65), (4.70) - (4.72), and (4.77) - (4.79)

θ_4 - models of the form (4.84) - (4.86), (4.92) - (4.93), (4.97) - (4.98), and (4.102) - (4.103)

θ_5 - model of the form (4.113) - (4.114)

Equating the monomials of the Lie derivatives $\{\mu_1, \mu_2, \mu_3\}$ in $\theta_1(\boldsymbol{p}) = \theta_2(\tilde{\boldsymbol{p}})$, then solving for $\boldsymbol{p}$ yields no feasible solutions and the two models are therefore structurally distinguishable. Similarly, it is possible to show pair-wise that each of the five input/output maps are structurally distinguishable.

4.3 Steady State Analysis

Although the purpose of the modelling is to investigate the relevant transient behaviour, a steady state analysis was performed so that it can potentially be used at a later stage to assist in validating the models. It identifies the levels at which each compartmental quantity eventually settles and can be a useful method to obtain fundamental information about the system, the basic relationships between the compartments and for initial guesses for parameter estimation for subsequent fitting (i.e. saturation levels). Steady state analysis is performed by setting all the derivatives in the system equations to zero and solving the resulting algebraic equations for each system variable. Due to the complex non-linear nature of the equations, this was performed using a symbolic mathematical package capable of solving polynomial equations, namely Maple 2010.

4.3.1 Three Compartment Model

The steady state solution for the three compartment model of the form (4.1) - (4.3) is shown in (4.179) - (4.181) below:

$$\hat{x}_1 = \frac{2k_1k_3D - \Delta \mp \sqrt{\Delta^2 - 4k_1^{\,2}k_3T_0D\left(k_2 + k_3\right)}}{2k_1\left(k_3 + r_3\right)} \tag{4.179}$$

$$\hat{x}_2 = \frac{\Delta \pm \sqrt{\Delta^2 - 4k_1^{\,2}k_3T_0D\left(k_2 + k_3\right)}}{2k_1\left(k_2 + k_3\right)} \tag{4.180}$$

$$\hat{x}_3 = \frac{2k_1r_3D\left(k_2 + k_3\right) + \left(k_2 - r_3\right)\left(\Delta \pm \sqrt{\Delta^2 - 4k_1^{\,2}k_3T_0D\left(k_2 + k_3\right)}\right)}{2k_1\left(k_2 + k_3\right)\left(k_3 + r_3\right)} \tag{4.181}$$

where

$$\Delta = k_3r_1 + k_2k_3 + r_1r_3 + k_1k_3T_0 + k_2r_3 + k_1k_2T_0 + k_1k_3D\,. \tag{4.182}$$

Equations (4.179) - (4.181) show that there are two possible steady state solutions for the given model. It can be readily shown that (4.180) is always positive for both solutions. The term inside the square root, Δ^2 - 4 $k_1^{\,2}$ k_3 T_0 D (k_2 + k_3), can be re-arranged as

$$k_1^{\,2}(k_2T_0 + k_3T_0 - k_3D)^2 + (k_3 + r_3)(r_1 + k_2)(k_2k_3 + 2k_1k_2T_0 + k_2r_3 + k_3r_1 + 2k_1k_3T_0 + 2k_1k_3D + r_1r_3) \tag{4.183}$$

which is always positive (since k_1, k_2, k_3, r_1, r_3, T_0, and D are all positive by definition). This implies that

$$\Delta^2 > 4k_1^{\,2}k_3T_0D\left(k_2 + k_3\right) \tag{4.184}$$

and therefore

$$\Delta > \sqrt{\Delta^2 - 4k_1^{\,2}k_3T_0D\left(k_2 + k_3\right)}\,. \tag{4.185}$$

To determine the stability of the steady states the system is linearised by considering the relevant Jacobian matrix J. This is given by:

$$J = \begin{bmatrix} -k_1(T_0 - x_2) - r_3 & r_1 + k_1x_1 & k_3 \\ k_1(T_0 - x_2) & -k_2 - r_1 - k_1x_1 & 0 \\ r_3 & -k_2 & -k_3 \end{bmatrix} \tag{4.186}$$

The eigenvalues of the Jacobian matrix *J* are given as solutions of the following cubic equation:

$$\lambda^3 + b_5\lambda^2 + c_5\lambda = 0 \tag{4.187}$$

where

$$b_5 = k_1x_1 + k_1(T_0 - x_2) + k_2 + k_3 + r_1 + r_3, \tag{4.188}$$

$$c_5 = k_1k_2(T_0 - x_2) + k_1k_3x_1 + k_1k_3(T_0 - x_2) + k_1r_3x_1 + k_2k_3 + k_2r_3 + k_3r_1 + r_1r_3 \tag{4.189}$$

The Jacobian matrix (4.186) does not have full rank and therefore one of the eigenvalues is $\lambda = 0$. This occurs because the model of the form (4.1) - (4.3) underdetermines the system, as shown by *Equation* (4.9), and the model can be reduced to two states. The remaining eigenvalues of the Jacobian matrix *J* are given as solutions of the following quadratic equation:

$$\lambda^2 + b_5\lambda + c_5 = 0 \tag{4.190}$$

Both coefficients in the quadratic equation, b_5 and c_5, are non-negative since all the terms are also non-negative. By definition $0 \leq x_2 \leq T_0$, as T_0 is the total number of transporter binding sites on OATP (i.e. compartment x_2) hence the $(T_0 - x_2) \geq 0$. Solutions to (4.190) are given by

$$\lambda_1 = \frac{-b_5 - \sqrt{b_5^2 - 4c_5}}{2}\ ,\ \lambda_2 = \frac{-b_5 + \sqrt{b_5^2 - 4c_5}}{2}\ . \tag{4.191}$$

It can be shown that both solutions are negative using Descartes' rule of signs (Anderson *et al.* 1998), since there are no sign changes in (4.190) and λ_1 is always negative. In order for λ_2 to be negative, b_5 must be greater that the root, i.e.

$$b_5 > \sqrt{b_5^2 - 4c_5} \tag{4.192}$$

which in turn implies that $b_5^2 > 4c_5$ and the term inside the square root is always positive. Therefore both solutions of (4.190) are real and negative, hence both steady states are stable (Murray 2003).

Similar analyses for the models of the form (4.12) - (4.13), (4.18) - (4.19), and (4.23) - (4.24) yield the same solutions.

4.3.2 Two Compartment Model

The steady state solution for the two compartment model of the form (4.30) - (4.31) is shown in (4.193) - (4.194) below:

$$\hat{x}_1 = \frac{-b_6 \pm \sqrt{b_6^2 - 4a_6c_6}}{2a_6} \tag{4.193}$$

$$\hat{x}_3 = \frac{\alpha \pm \sqrt{b_6^2 - 4a_6c_6}}{2a_6} \tag{4.194}$$

where

$$a_6 = k_3 + r_3 \tag{4.195}$$

$$b_6 = k_3K_M - k_3D + r_3K_M + V_M \tag{4.196}$$

$$c_6 = -k_3K_MD \tag{4.197}$$

$$\alpha = k_3(K_M + D) + r_3(K_M + 2D) + V_M \tag{4.198}$$

Again, (4.193) - (4.194) indicate that the two compartment model of the form (4.30) - (4.31) has two possible steady states. However the steady states for x_1 are the solutions to the following quadratic

$$a_6\lambda^2 + b_6\lambda + c_6 = 0. \tag{4.199}$$

It can be shown that only one solution is positive using Descartes' rule of signs, since there is one sign change in (4.199) regardless of the sign of b_2 (since K_M, V_M, k_3, r_3, and D are all positive by definition). Since $b_6^2 - 4a_6c_6$ is always positive, as a_6 is positive and c_6 is negative, the solutions to (4.199) are

$$\lambda_1 = \frac{-b_6 - \sqrt{b_6^2 - 4a_6c_6}}{2a_6} < \lambda_2 = \frac{-b_6 + \sqrt{b_6^2 - 4a_6c_6}}{2a_6}. \tag{4.200}$$

As x_1 must always be positive, there is only one valid steady state for the model of the form (4.30) - (4.31), i.e.

$$\hat{x}_1 = \frac{-b_6 + \sqrt{b_6^2 - 4a_6c_6}}{2a_6}, \tag{4.201}$$

$$\hat{x}_3 = \frac{\alpha + \sqrt{b_6^2 - 4a_6c_6}}{2a_6}. \tag{4.202}$$

To determine the stability of the steady states the system is linearised by considering the relevant Jacobian matrix J. This is given by:

$$J = \begin{bmatrix} -\dfrac{V_M}{K_M + x_1} + \dfrac{V_M x_1}{(K_M + x_1)^2} - r_3 & k_3 \\ \dfrac{V_M}{K_M + x_1} - \dfrac{V_M x_1}{(K_M + x_1)^2} + r_3 & -k_3 \end{bmatrix} \tag{4.203}$$

The eigenvalues of the Jacobian matrix J are given as:

$$\lambda_1 = 0 \tag{4.204}$$

$$\lambda_2 = -\frac{V_M K_M + r_3 K_M^{\ 2} + 2r_3 K_M x_1 + r_3 x_1^{\ 2} + k_3 K_M^{\ 2} + 2k_3 K_M x_1 + k_3 x_1^{\ 2}}{(K_M + x_1)^2} \tag{4.205}$$

Once again, the Jacobian matrix (4.203) does not have full rank and therefore one of the eigenvalues is $\lambda_1 = 0$. This is because the model of the form (4.30) - (4.31) underdetermines the system, as shown by *Equation* (4.37), and the model can be reduced to a single state. The remaining Eigenvalue, λ_2, of the Jacobian matrix J is always negative and therefore the steady state is stable (Murray 2003).

Similar analyses for the models of the form (4.41) and (4.44) yield the same results. The output of main interest is the observation x_3. Both steady states (4.181) and (4.194) describe the exact relationships for x_3 and will be useful at a later stage for parameter estimation and model validation.

4.4 Experimental Data

Date were collected at AstraZeneca's R&D facility at Alderley Edge by Alex Lench and Charles O'Donnell according to the following protocol.

4.4.1 Preparation of Rat and Dog Hepatocytes

Isolation of rat and dog hepatocytes was performed essentially using the two-step collagenase perfusion method of Seglen (1976). Briefly for both Beagle dog (weight range 12 - 18 kg) and Hans Wistar rat (weight 200 - 300 g), a portion of liver was excised that contained suitable vasculature to allow cannulation. The liver was cannulated and liver perfusion medium (Invitrogen, Paisley, UK) was perfused via a

suitable vein until the liver cleared to an even tan colour (usually 7 - 8 min at a perfusion rate of 30 ml/min). Liver digestion medium (Invitrogen) was then perfused until the liver displayed evidence of extensive dissociation (usually a further 6 - 8 min at a perfusion rate of 30 ml/min). The liver was dissected from the rat, and cells were gently teased out of the liver capsule into a beaker containing ice-cold hepatocyte suspension buffer (2.34 g of sodium HEPES, 0.4 g of D-fructose, 2.0 g of bovine serum albumin (BSA)), 1-litre powder equivalent of Dulbecco's modified Eagle's medium (Sigma, Gillingham, UK) diluted in 1 litre of water and adjusted to pH 7.4 with 1 M HCl. The cell suspension was passed through a 250 μm mesh into a precooled tube and centrifuged at 50 *g* for 2 min at 4°C. The supernatant was decanted, the cell pellet was resuspended in suspension buffer (without BSA), and the centrifugation step was repeated. The resulting pellet of cells was resuspended in 10 ml of suspension buffer (without BSA), and an estimation of hepatocyte yield and viability was obtained using the trypan blue exclusion method. Only preparations with a viability of >80% were used.

4.4.2 Thawing of Cryopreserved Human Hepatocytes

Commercial cryopreserved human hepatocytes were purchased from Life Technologies Corporation. (Baltimore, MD). Aliquots (20 ml) of hepatocyte suspension buffer (with no added albumin) were prewarmed to 37°C. Cryopreserved cells were removed from liquid N_2 and immediately immersed in a water bath that had been preheated to 37°C. The vials were shaken gently until the contents were completely free of ice crystals (approximately 90 - 120 s) and were then emptied into the prewarmed hepatocyte suspension buffer. The cells were centrifuged at 40 *g* for 5 min at 19°C, the supernatant was removed by aspiration, and the resultant pellet was

suspended in hepatocyte suspension buffer. The concentration and viability of the hepatocytes were determined using trypan blue exclusion, and the cells were resuspended at a concentration of 2 million cells/ml.

4.4.3 Determination of CL_{int} for the Appearance of Pitavastatin into Hepatocytes

CL_{int} values for drug appearance into hepatocytes were determined using a method adapted from the centrifugal filtration technique of Petzinger & Fuckel 1992. A vial containing rat hepatocytes at a concentration of 2 million viable cells/ml was preincubated for 5 min in a waterbath at 37°C along with a vial containing 500 µl of Pitavastatin (final concentration 50 - 300µM) in suspension buffer. Reactions were initiated with the addition of 500 µl of hepatocyte suspension to the Pitavastatin buffer mix. Aliquots (100 µl) were removed at 10 s, 30 s, 50 s and 70 s and immediately centrifuged at 7000 *g* for 30 s through 150 µl of oil (density of 1.015 g/ml), layered on over 15 µl 3% caesium chloride, using a MiniSpin centrifuge (Eppendorf, Cambridge, UK). During this process the hepatocytes pass through the oil into the caesium chloride solution. After an overnight incubation at -80ºC, the caesium chloride layer (containing the separated cells) was then cut into a 96 well plate to which 300 µl of acetonitrile was added before being shaken for two hours after which 600µl water was added. The plate was then centrifuged for 10 mins at 4500 rpm and the supernatant analysed by LC/MS/MS (Liquid Chromatography tandem Mass Spectrometry - described in Section 4.4.4 below). Each experiment was carried out in triplicate and the mean rate was calculated. Incubations were preincubated for 10 mins, carried out on ice or in a water bath for the 4°C and 37°C

data respectively. A fifth time point of zero kmol/10^6 cells at time zero is assumed as no uptake should have taken place before the experiment has begun.

4.4.4 LC/MS/MS

Pitivastatin levels in the samples were assessed using LC/MS/MS. Liquid chromatography was performed using a Thermo MS pump plus (Thermo Fisher Scientific, San Jose, California, USA), the mobile phase consisted of water containing 0.1% formic acid (v/v) and the organic phase consisted of methanol containing 0.1% formic acid (v/v). Chromatographic separation was achieved with the following gradient; t = 0 min % organic = 5, t = 3 min % organic = 95, t = 4 min % organic = 95, t = 4.1 min % organic = 5 and a Synergi Max RP (Phenomenex, Macclesfield, UK) column. Electrospray ionisation on a TSQ Quantum Vantage (Thermo Fisher Scientific, San Jose, California, USA) in single reaction monitoring mode using a transition of 422.178>274.173, 46 V collision energy and the tube lens voltage at 236V.

4.4.5 Data Analysis

The commercial software package FACSIMILE (MCPA Software, UK) was used to perform the parameter estimation. FACSIMILE was selected over other packages such Matlab because it provides more robust statistical information about the fitting and is able to cope with stiffer systems. The software selection and parameter estimation procedure is detailed in *Section* 3.5.1. As described therein, FACSIMILE produces two measurements for the statistical goodness of the fit, namely a weighted residual sum of squares (RSS) and confidence levels for each estimated parameters entitled standard deviation of the natural logarithms (SDLN).

4.5 Results

4.5.1 4°C Diffusion Rates

The 4°C diffusion rates are estimated using the model of the form (4.118) - (4.119), which accounts for passive diffusion only (no active OATP uptake). The rat, dog, and human time series and fits are plotted in *Figures* 4.4 - 4.6 respectively.

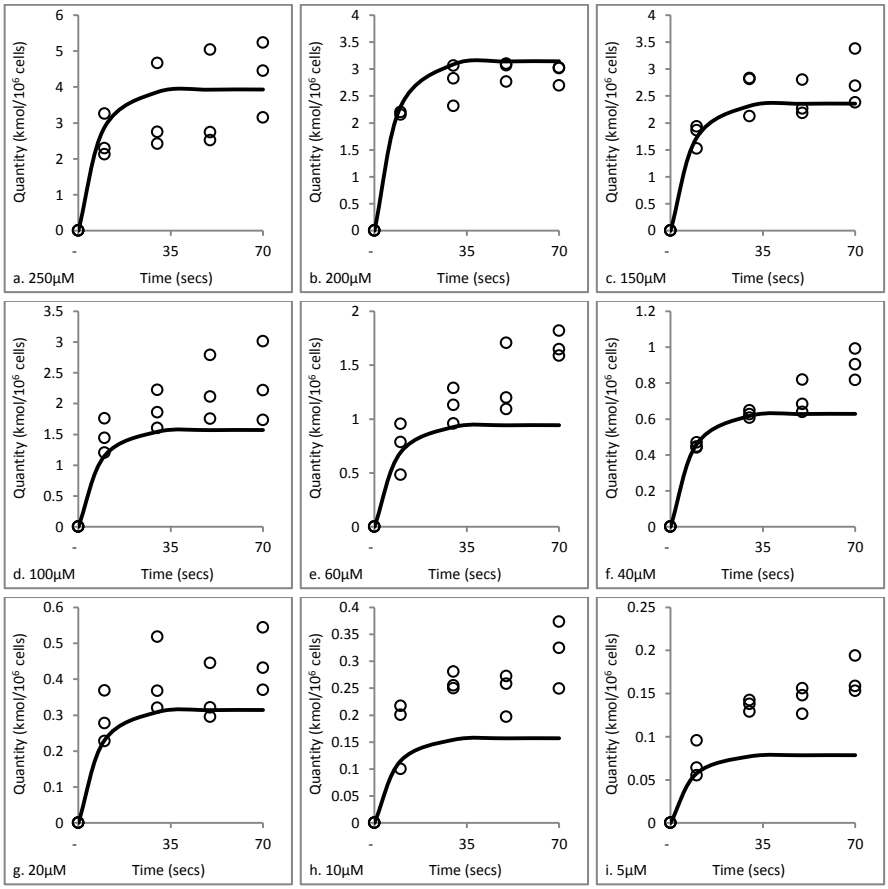

Figure 4.4: FACSIMILE fits of 4°C rat data at different initial concentrations (5 - 250 µM). Legend: solid trace - fit, data - circles.

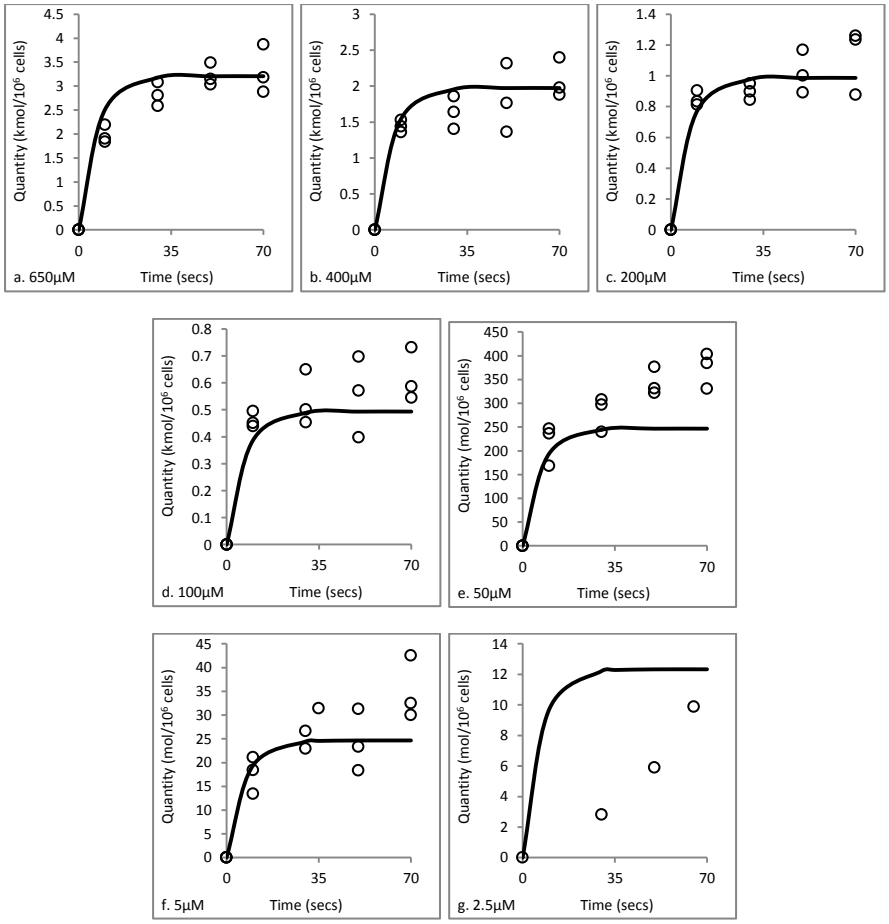

Figure 4.5: FACSIMILE fits of 4°C dog data at different initial concentrations (2.5 - 650 µM). Legend: solid trace - fit, data - circles.

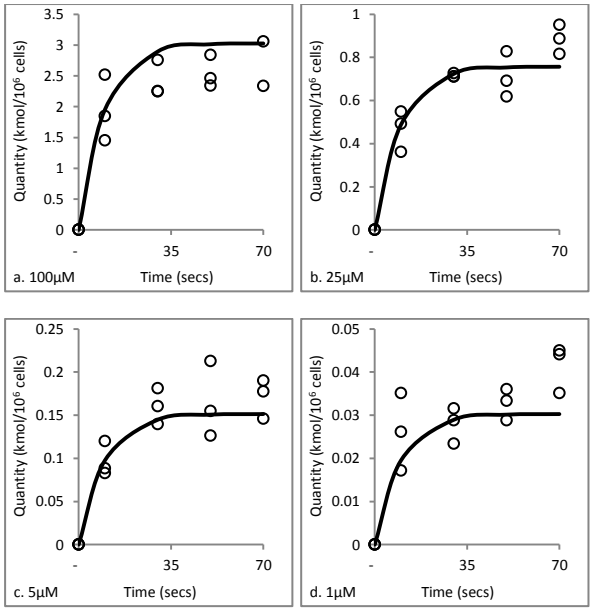

Figure 4.6: FACSIMILE fits of 4°C human data at different initial concentrations (1 - 100 µM). Legend: solid trace - fit, data - circles.

Table 4.7 below summarises the diffusions rates for all three species for the 4°C data fits.

Table 4.7: 4°C diffusion rates

	Rat		Dog		Human	
Parameters	**Value**	**SDLN**	**Value**	**SDLN**	**Value**	**SDLN**
k_3	1.31×10^{-1} s^{-1}	0.163	1.53×10^{-1} s^{-1}	0.135	1.01×10^{-1} s^{-1}	0.146
r_3	2.09×10^{-3} s^{-1}	0.152	7.57×10^{-4} s^{-1}	0.125	3.15×10^{-3} s^{-1}	0.130
RSS	433,280	-	184,820	-	11,901	-

4.5.2 Two Compartment Model of the form (4.30) - (4.31)

Table 4.8 below summarises the rate constants for all three species for the 37°C data fits using the 4°C diffusion rates obtained in *Section 4.5.1*. The two compartment model of the form (4.30) - (4.31), which combines passive diffusion and active OATP transport, is used for the fitting.

Table 4.8: 37°C parameters using 4°C diffusion rates

	Rat		Dog		Human	
Parameters	**Value**	**SDLN**	**Value**	**SDLN**	**Value**	**SDLN**
V_M [$\mu mols^{-1}$]	7.97×10^{-4}	0.116	2.93×10^{-1}	0.190	2.34×10^{-4}	0.227
K_M [µmol]	1.15×10^{-1}	0.188	7.48×10^{-4}	0.140	3.33×10^{-2}	0.288
k_3 [s^{-1}]	1.31×10^{-1}	Fixed	1.53×10^{-1}	Fixed	1.01×10^{-1}	Fixed
r_3 [s^{-1}]	2.09×10^{-3}	Fixed	7.57×10^{-4}	Fixed	3.15×10^{-3}	Fixed
RSS	190,430	-	205,580	-	39,513	-

Table 4.9 below summarises the rate constants for all three species for the 37°C data fits when diffusion rates are allowed to vary. Again, the two compartment model of the form (4.30) - (4.31) is used for the fitting.

Table 4.9: 37°C parameters

	Rat		**Dog**		**Human**	
Parameters	**Value**	**SDLN**	**Value**	**SDLN**	**Value**	**SDLN**
V_M [µmols^{-1}]	4.58 x 10^{-5}	0.173	1.55 x 10^{-5}	0.152	5.90 x 10^{-6}	0.227
K_M [µmol]	4.98 x 10^{-3}	0.472	1.88 x 10^{-2}	0.178	1.39 x 10^{-3}	0.399
k_3 [s^{-1}]	4.51 x 10^{-2}	0.089	2.66 x 10^{-2}	0.077	1.93 x 10^{-2}	0.158
r_3 [s^{-1}]	1.78 x 10^{-3}	0.073	4.89 x 10^{-4}	0.047	1.86 x 10^{-3}	0.080
RSS	106,100	-	40,520	-	12,717	-

The time series and fits for both scenarios are plotted in *Figures* 4.7 - 4.9.

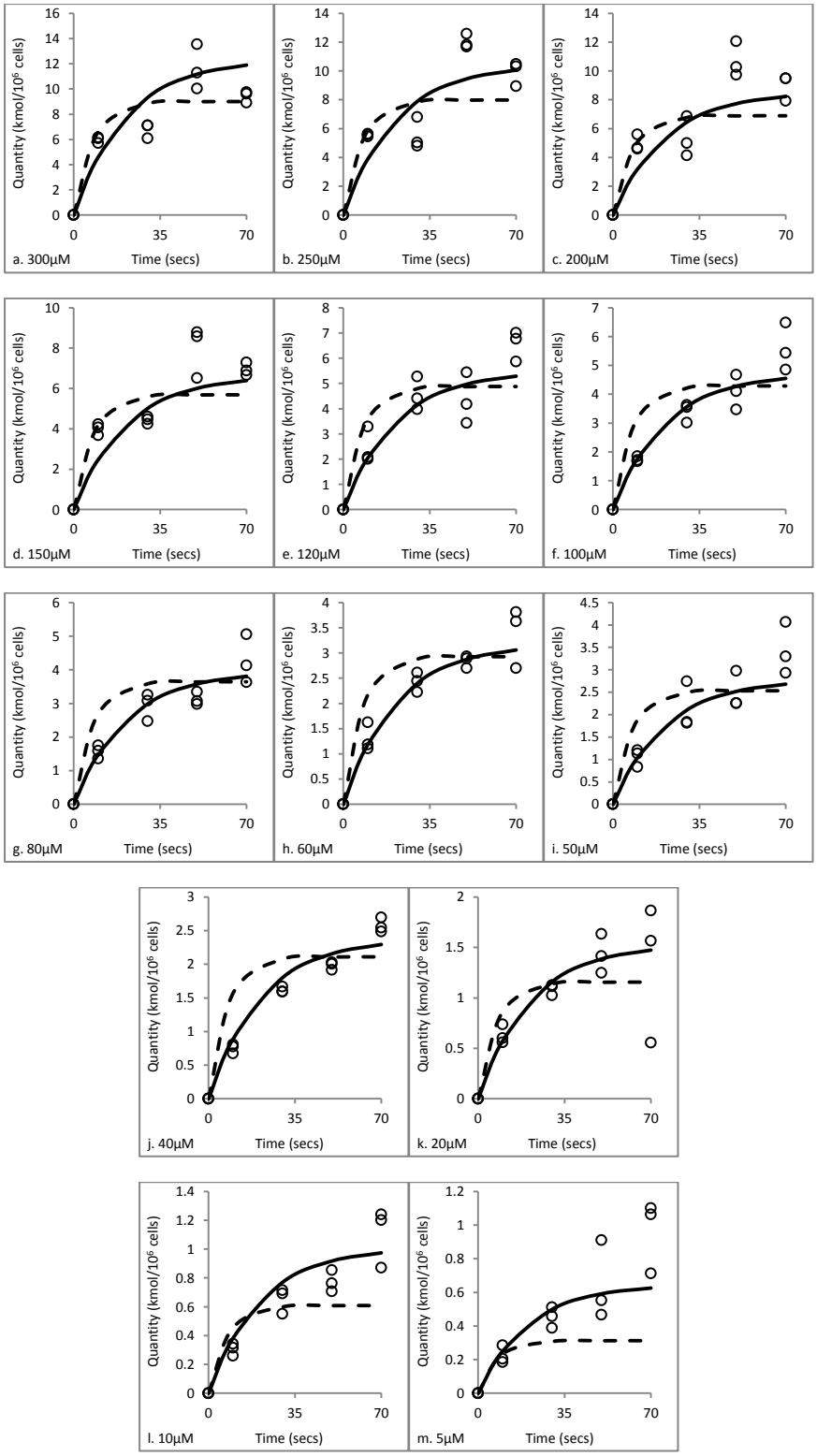

Figure 4.7: FACSIMILE fits of 37°C rat data at different initial concentrations (5 - 300 µM). The solid trace shows the fit using two compartment model of the form (4.30) - (4.31), the dashed trace using the diffusion rate from 4°C data, and the data are the circles.

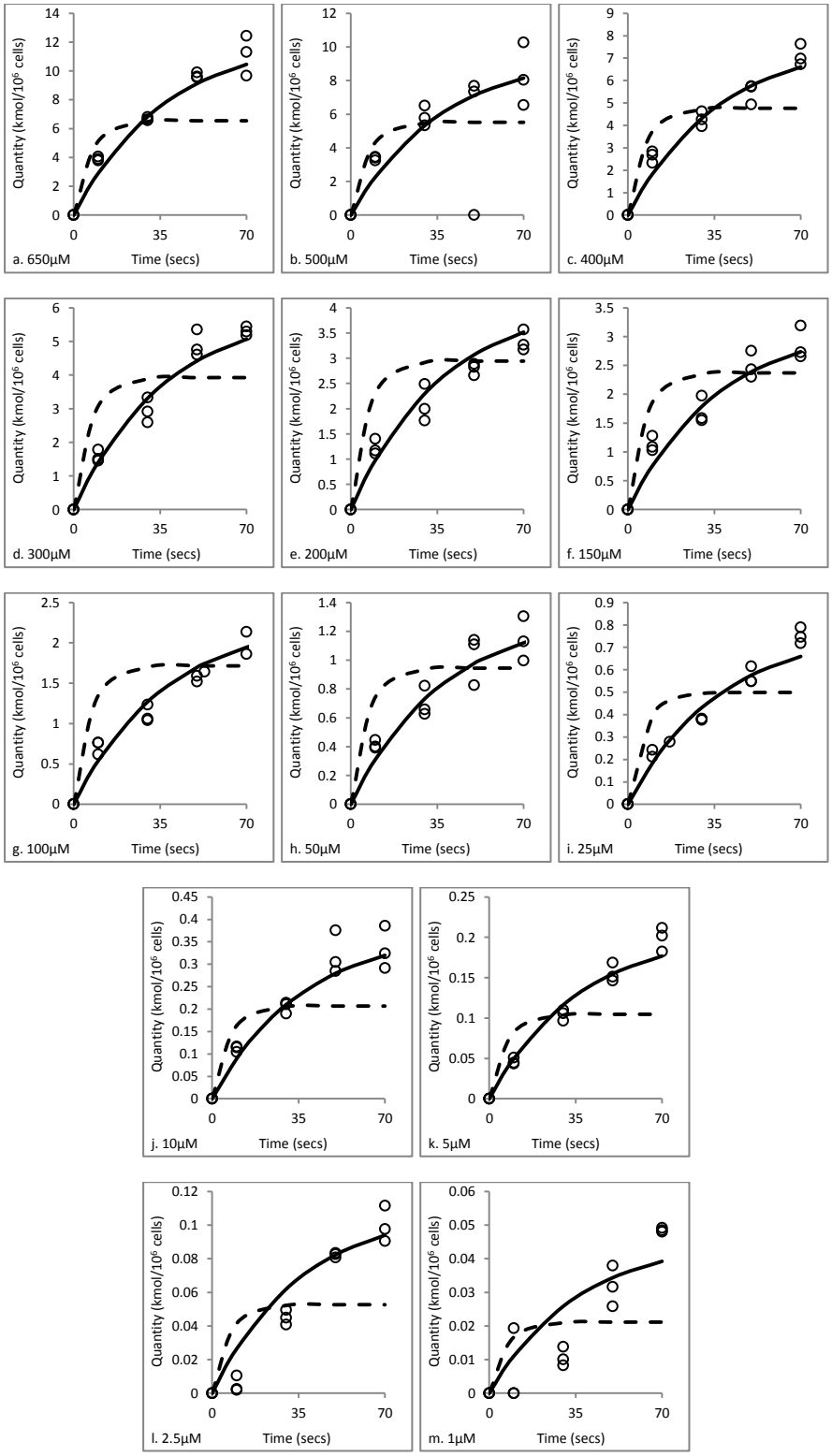

Figure 4.8: FACSIMILE fits of 37°C dog data at different initial concentrations (1 - 650 µM). The solid trace shows the fit using two compartment model of the form (4.30) - (4.31), the dashed trace using the diffusion rate from 4°C data, and the data are the circles.

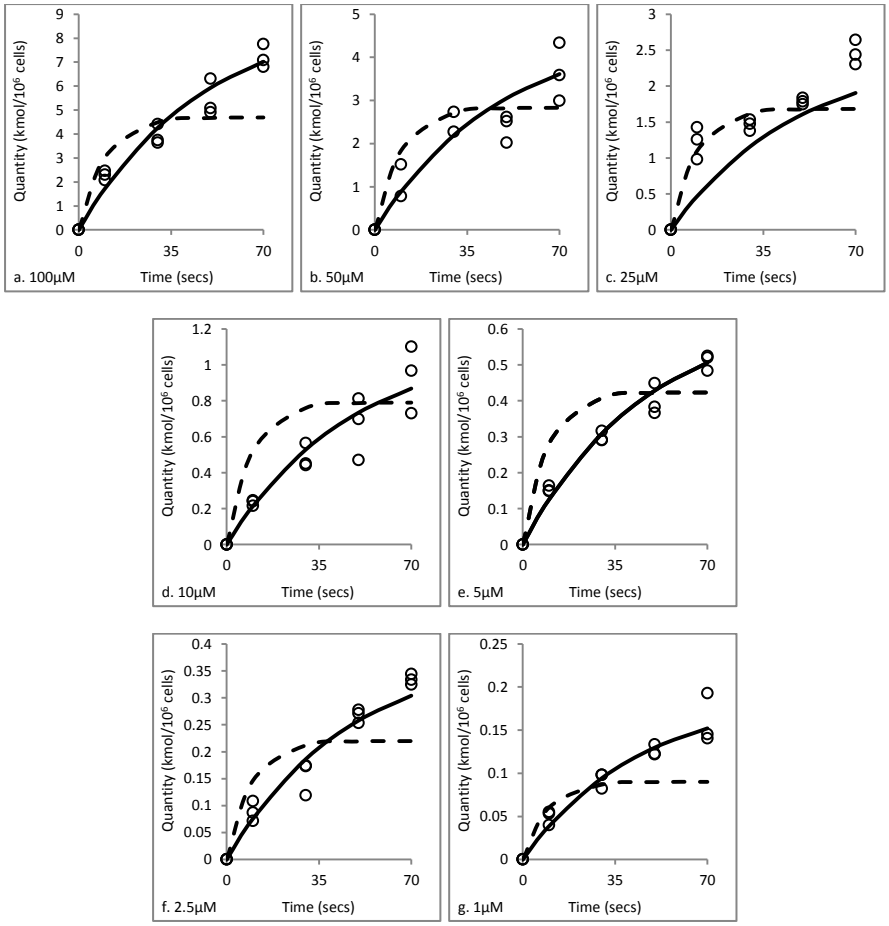

Figure 4.9: FACSIMILE fits of 37°C human data at different initial concentrations (1 - 100 µM). The solid trace shows the fit using two compartment model of the form (4.30) - (4.31), the dashed trace using the diffusion rate from 4°C data, and the data are the circles.

4.5.3 Three Compartment Model of the form (4.1) - (4.3)

Table 4.10 below summarises the rate constants for all three species for the 37°C data fits using the 4°C diffusion rates obtained in *Section* 4.5.1. The three compartment model of the form (4.1) - (4.3), which includes passive diffusion and active OATP uptake using a pseudo steady state assumption, is used for the fitting.

Table 4.10: 37°C parameters with 4°C diffusion rates
using three compartment model of the form (4.1) - (4.3)

	Rat		Dog		Human	
Parameters	**Value**	**SDLN**	**Value**	**SDLN**	**Value**	**SDLN**
k_1 [s^{-1}]	1.90×10^{-7}	0.123	6.95×10^{-8}	0.105	2.83×10^{-3}	0.288
k_2 [s^{-1}]	5.72×10^{-5}	NWD	5.33×10^{-8}	NWD	9.88×10^{1}	NWD
k_3 [s^{-1}]	1.31×10^{-1}	Fixed	1.53×10^{-1}	Fixed	1.01×10^{-1}	Fixed
r_1 [s^{-1}]	3.73×10^{-3}	1.04	4.49×10^{-7}	NWD	4.71×10^{-2}	NWD
r_3 [s^{-1}]	2.09×10^{-3}	Fixed	7.57×10^{-4}	Fixed	3.15×10^{-3}	Fixed
T_0 [µmol]	5.69×10^{-3}	0.103	4.80×10^{-3}	0.080	2.46×10^{-6}	0.228
RSS	127,510	-	89,198	-	39,494	-

Table 4.11 below summarises the rate constants for all three species for the 37°C data fits when diffusion rates are allowed to vary. Again, the three compartment model of the form (4.1) - (4.3) is used for the fitting.

Table 4.11: 37°C parameters using three compartment
model of the form (4.1) - (4.3)

	Rat		Dog		Human	
Parameters	**Value**	**SDLN**	**Value**	**SDLN**	**Value**	**SDLN**
k_1 [s^{-1}]	2.86×10^{-7}	0.231	1.31×10^{-6}	0.125	1.24×10^{-4}	0.510
k_2 [s^{-1}]	1.03×10^{-5}	NWD	5.34×10^{-8}	NWD	7.17×10^{-2}	0.850
k_3 [s^{-1}]	3.53×10^{-1}	0.125	2.54×10^{-2}	0.088	1.49×10^{-2}	0.273
r_1 [s^{-1}]	2.86×10^{-3}	NWD	4.41×10^{-7}	NWD	1.05×10^{-1}	NWD
r_3 [s^{-1}]	1.50×10^{-3}	0.088	4.83×10^{-4}	0.051	1.67×10^{-3}	0.108
T_0 [µmol]	8.07×10^{-3}	0.110	3.17×10^{-4}	0.100	5.56×10^{-5}	0.598
RSS	101,600	-	32,095	-	12,340	-

The time series and fits for both scenarios are plotted in *Figures* 4.10 - 4.12.

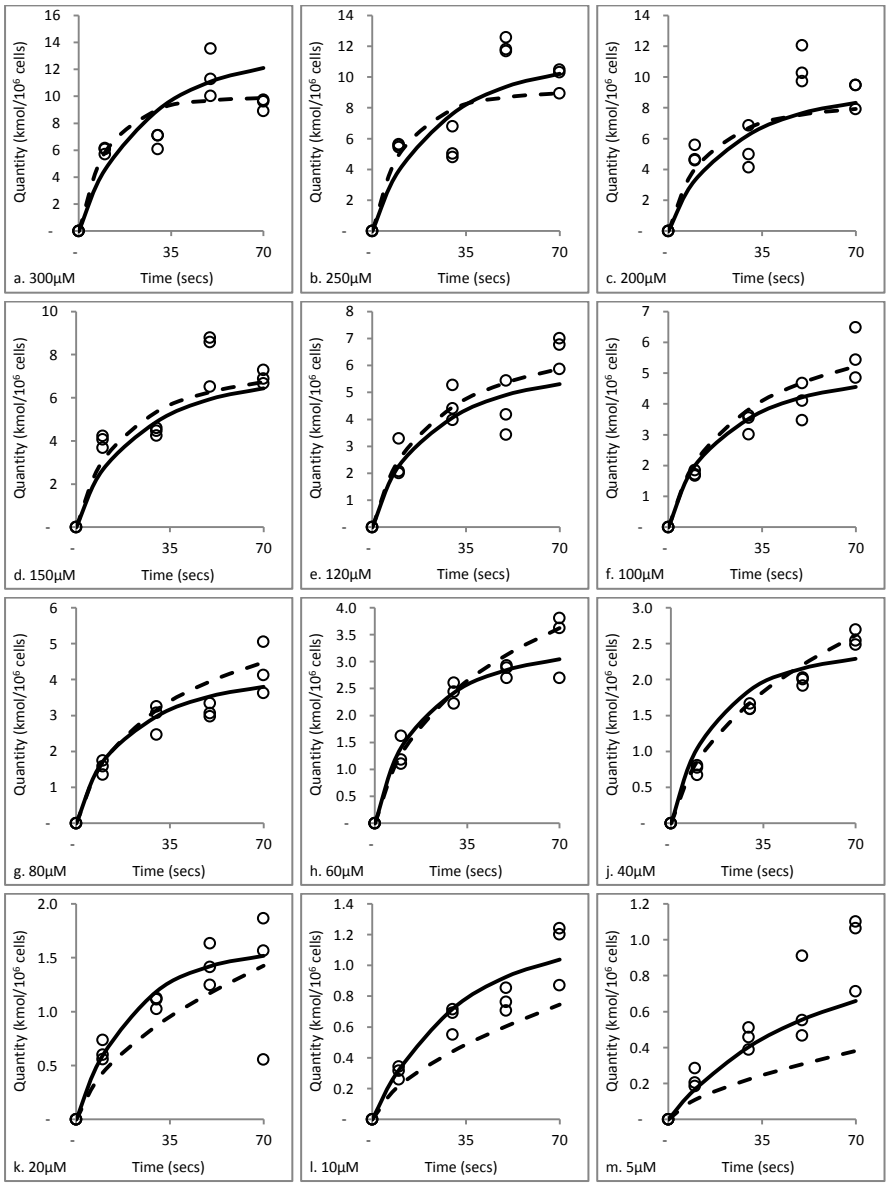

Figure 4.10: FACSIMILE fits of 37°C rat data at different initial concentrations (5 - 300 μM). The solid trace shows the fit using two compartment model of the form (4.1) - (4.3), the dashed trace using the diffusion rate from 4°C data, and the data are the circles.

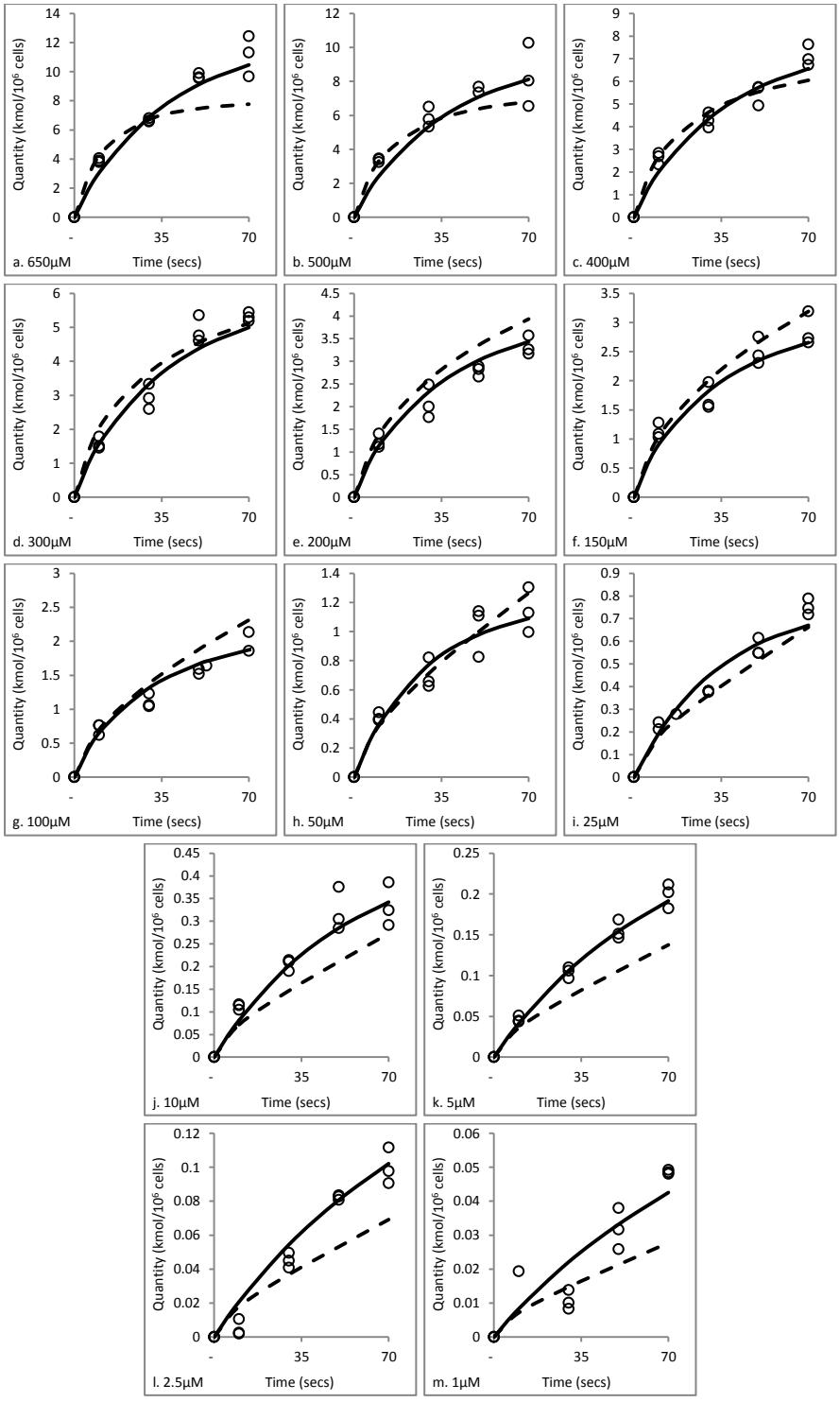

Figure 4.11: FACSIMILE fits of 37°C dog data at different initial concentrations (1 - 650 µM). The solid trace shows the fit using two compartment model of the form (4.1) - (4.3), the dashed trace using the diffusion rate from 4°C data, and the data are the circles.

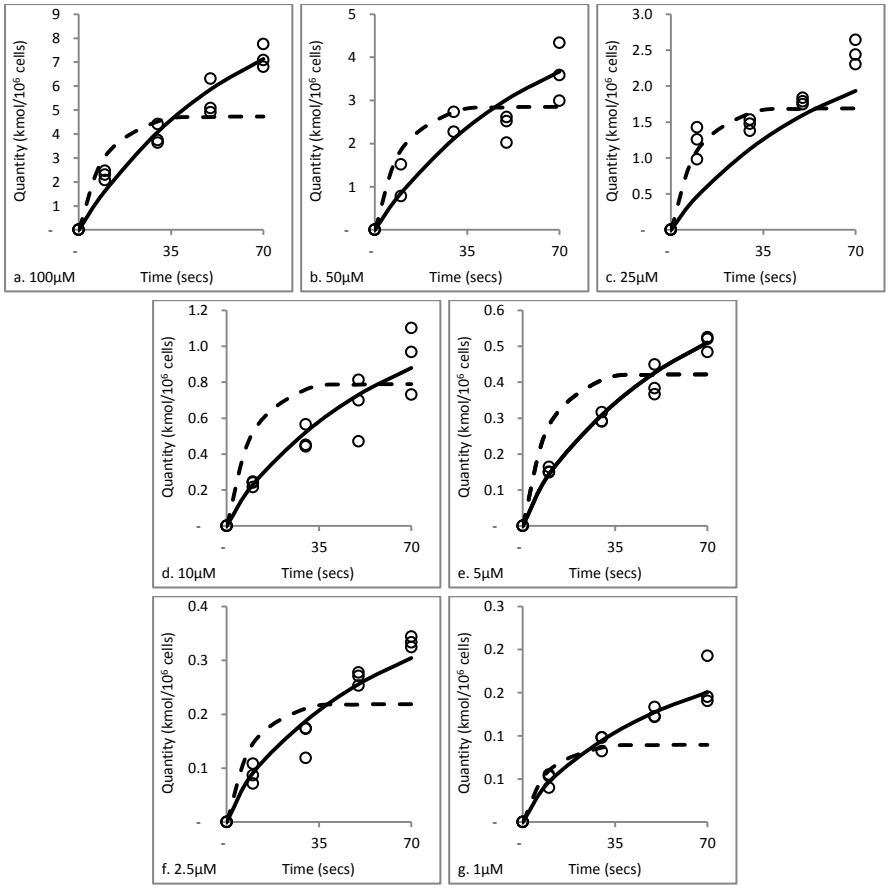

Figure 4.12: FACSIMILE fits of 37°C human data at different initial concentrations (1 - 100 µM). The solid trace shows the fit using two compartment model of the form (4.1) - (4.3), the dashed trace using the diffusion rate from 4°C data, and the data are the circles.

4.5.4 Other Models

The available data were also fitted using the models of the form (4.84) - (4.86) and (4.113) - (4.114). Although the fits described the data accurately both visually and in terms of the RSS values, FACSIMILE was unable to obtain good SDLN values (<1) for both of those models. The data does not determine the parameters values within tight enough bounds, suggesting that the models do not represent the mechanisms present. It is suspected that the model of the form (4.84) - (4.86) is over-parameterised for the data available. The model of the form (4.56) - (4.58) was not

used for parameter estimation as it was shown to be locally identifiable. Similarly for the model of the form (4.107) - (4.109), which could not be shown to be SGI.

4.6 Discussion

4.6.1 4°C diffusion Rates

The plots in *Figures* 4.4 - 4.6 show that the model of the form (4.118) - (4.119) visually fits the data adequately for all three species. The model does appear to underestimate the rat data somewhat at low concentrations, in particular for 5 µM and 10 µM initial concentrations (see *Figures* 4.4h and 4.4i). The model does also overestimate the dog data at 2.5 µM initial concentration (see *Figure* 4.5g), however for this concentration only one time series is available and it does not follow the same pattern as the remaining data. The values of cellular influx, k_3, and cellular efflux, r_3, from *Table* 4.7 are of similar orders of magnitude across the three species and the SDLN values are relatively low for all the rate parameters estimated (0.125 - 0.163). The model suitably describes the diffusion process.

4.6.2 Two Compartment Model of the form (4.30) - (4.31)

Visually it can be seen from *Figures* 4.7 - 4.9 that the fits where the diffusion rates are allowed to vary (solid traces) are better across all three species, especially for the lower concentrations. Comparing the values in *Tables* 4.8 and 4.9, we can see the RSS values for those fits are much improved (Rat: 190,430 compared with 106,100. Dog: 205,580 compared with 40,520. Human: 39,513 compared with 12,717). However the model using the 4°C diffusion rates obtained in *Section* 4.5.1 is restricted, whereas the other model is unrestricted. The restricted model is ‘nested’

within the unrestricted one. That is, the restricted model has two degrees of freedom P_R (K_M and V_M), and the unrestricted model has four degrees of freedom, P_U (K_M, V_M, k_3 and r_3). For any values of parameters in the restricted model, the same regression curve can be obtained by an appropriate choice of parameters for the unrestricted model. The model with more parameters is generally able to fit the data at least as well as the model with fewer parameters. Thus, typically, the unrestricted model will give a better fit and hence a lower RSS value than the restricted model. A statistical *F* test was used to determine whether the unrestricted model gives a significantly better fit to the data. If there are *N* data points available to estimate the parameters of both models, then we can calculate the *F* statistic using:

$$F = \frac{\left(\frac{RSS_R - RSS_U}{P_U - P_R} \right)}{\left(\frac{RSS_U}{N - P_U} \right)} \tag{4.206}$$

where RSS_R is the RSS value for the restricted model and RSS_U, the RSS value for the unrestricted model. Under the null hypothesis that the unrestricted model does not provide a significantly better fit than the restricted model, *F* will have an *F*-distribution, with (P_U - P_R, N - P_U) degrees of freedom. The null hypothesis is rejected if the *F* value calculated from the data is greater than the critical value of the *F*-distribution (F_{crit}) for the false-rejection probability of 0.01. The *F* values for the three species are displayed in *Table* 4.12. In all three cases, the F_{crit} value is much smaller than the *F* value calculated from the data. The null hypothesis is therefore rejected; thus the unrestricted model does provide a significantly better fit to the data than the restricted model.

Table 4.12: 37°C parameters

	Rat		Dog		Human	
	Restricted	Unrestricted	Restricted	Unrestricted	Restricted	Unrestricted
RSS	190,430	106,100	205,580	40,520	39,513	12,717
DOF *(P)*	4	6	4	6	4	6
N	195		194		103	
F	75.1		383		102	
F crit (0.01)	4.72		4.72		4.83	

From *Table* 4.9 we can see the values of cellular influx, k_3, and cellular efflux, r_3, are of similar orders of magnitude across all three species. In this case the SDLN values for the diffusion parameters are lower than those for the 4°C fits in *Section* 4.5.1. The cellular influx, k_3, is approximately four times smaller than cellular efflux, r_3, which combined are in a similar ratio as per the 4°C fits.

4.6.3 Three Compartment Model of the form (4.1) - (4.3)

Visually it can be seen from *Figures* 4.10 - 4.12 that the fits where the diffusion rates are allowed to vary (solid traces) are better across all three species, especially in the lower concentrations. Comparing *Tables* 4.10 and 4.11, we can see the RSS values for those fits are improved (Rat: 127,510 compared with 101,600. Dog: 89,198 compared with 32,095. Human: 39,494 compared with 12,340). However, as described in *Section* 4.6.2, the model using the 4°C diffusion rates obtained in *Section* 4.5.1 is restricted, whereas the other model is unrestricted. An *F* test is performed again to show that the improvement in the RSS value is statistically significant (*Table* 4.13).

From *Table* 4.11 we can see the values of cellular influx, k_3, and cellular efflux, r_3, are of similar orders of magnitude across all three species and the SDLN values are low, but this time not hugely different to the values obtained in *Section* 4.5.1. We note that for the fits using the three compartment model of the form (4.1) - (4.3), the parameters k_2 and r_1 have a tendency to be not well determined (NWD).

The fits from the three compartment model of the form (4.1) - (4.3) are also compared with those obtained from the two compartment model of the form (4.30) - (4.31). In this instance the two compartment model is nested within the three compartment model, the latter has two more degrees of freedom and the lower RSS value, as shown in *Table* 4.13 below:

Table 4.13: 37°C parameters

	Rat		**Dog**		**Human**	
Compartments	**2**	**3**	**2**	**3**	**2**	**3**
RSS	106,100	101,600	40,520	32,095	12,717	12,340
DOF *(P)*	4	6	4	6	4	6
N	195		194		103	
F	4.19		24.7		1.48	
F crit (0.01)	4.72		4.72		4.83	

This time the F_{crit} value is higher for the rat and human data, suggesting that the two compartment model fits the data better, whereas for the dog the converse is true.

4.6.4 Sensitivity Analysis

In order to use the mathematical models as predictive tools, it is necessary to obtain a measure of the sensitivity of each parameter, that is to say how much does an individual small change of each rate constant affect the system's response. Although mathematical models are used in all areas of society and technology, stringent standards of proof are demanded from model-based numbers. Quantitative sensitivity analysis is generally agreed to be one such standard (Satelli *et al.* 2008). Sensitivity analysis is used to investigate the robustness of the model predictions and identify the parameters that contribute most to the output variability. Direct differential methods are used to numerically solve each sensitivity coefficient at each time point. Taking a mathematical model of the form (2.11) - (2.13), the system equations (2.11) are differentiated with respect to each of the parameters to obtain:

$$\frac{d}{dt}\frac{\partial \mathbf{x}}{\partial p_j} = J(t)\frac{\partial \mathbf{x}}{\partial p_j} + \frac{\partial \mathbf{f}(t)}{\partial p_j} \tag{4.207}$$

where $J(t)$ is a Jacobian matrix, defined as:

$$J(t) = \begin{bmatrix} \frac{\partial f_1}{\partial x_1} & \cdots & \frac{\partial f_1}{\partial x_n} \\ \vdots & \ddots & \vdots \\ \frac{\partial f_n}{\partial x_1} & \cdots & \frac{\partial f_n}{\partial x_n} \end{bmatrix} \tag{4.208}$$

For the three compartment model of the form (4.1) - (4.3) the corresponding sensitivity differential equations for x_3 are given by:

$$S_{11} = \frac{d}{dt}\frac{\partial x_1}{\partial k_1} = -\left(k_1\left(T_0 - x_2\right) + r_3\right)\frac{\partial x_1}{\partial k_1} + \left(r_1 + k_1 x_1\right)\frac{\partial x_2}{\partial k_1} + k_3\frac{\partial x_3}{\partial k_1} - x_1\left(T_0 - x_2\right) \tag{4.209}$$

$$S_{12} = \frac{d}{dt}\frac{\partial x_2}{\partial k_1} = k_1\left(T_0 - x_2\right)\frac{\partial x_1}{\partial k_1} - \left(r_1 + k_2 + k_1 x_1\right)\frac{\partial x_2}{\partial k_1} + x_1\left(T_0 - x_2\right) \tag{4.210}$$

$$S_{13} = \frac{d}{dt}\frac{\partial x_3}{\partial k_1} = r_3\frac{\partial x_1}{\partial k_1} + k_2\frac{\partial x_2}{\partial k_1} - k_3\frac{\partial x_3}{\partial k_1} \tag{4.211}$$

$$S_{21} = \frac{d}{dt}\frac{\partial x_1}{\partial k_2} = -\left(k_1\left(T_0 - x_2\right) + r_3\right)\frac{\partial x_1}{\partial k_2} + \left(r_1 + k_1 x_1\right)\frac{\partial x_2}{\partial k_2} + k_3\frac{\partial x_3}{\partial k_2} \tag{4.212}$$

$$S_{22} = \frac{d}{dt}\frac{\partial x_2}{\partial k_2} = k_1\left(T_0 - x_2\right)\frac{\partial x_1}{\partial k_2} - \left(r_1 + k_2 + k_1 x_1\right)\frac{\partial x_2}{\partial k_2} - x_2 \tag{4.213}$$

$$S_{23} = \frac{d}{dt}\frac{\partial x_3}{\partial k_2} = r_3\frac{\partial x_1}{\partial k_2} + k_2\frac{\partial x_2}{\partial k_2} - k_3\frac{\partial x_3}{\partial k_2} + x_2 \tag{4.214}$$

$$S_{31} = \frac{d}{dt}\frac{\partial x_1}{\partial k_3} = -\left(k_1\left(T_0 - x_2\right) + r_3\right)\frac{\partial x_1}{\partial k_3} + \left(r_1 + k_1 x_1\right)\frac{\partial x_2}{\partial k_3} + k_3\frac{\partial x_3}{\partial k_3} + x_3 \tag{4.215}$$

$$S_{32} = \frac{d}{dt}\frac{\partial x_2}{\partial k_3} = k_1\left(T_0 - x_2\right)\frac{\partial x_1}{\partial k_3} - \left(r_1 + k_2 + k_1 x_1\right)\frac{\partial x_2}{\partial k_3} \tag{4.216}$$

$$S_{33} = \frac{d}{dt}\frac{\partial x_3}{\partial k_3} = r_3\frac{\partial x_1}{\partial k_3} + k_2\frac{\partial x_2}{\partial k_3} - k_3\frac{\partial x_3}{\partial k_3} - x_3 \tag{4.217}$$

$$S_{41} = \frac{d}{dt}\frac{\partial x_1}{\partial r_1} = -\left(k_1\left(T_0 - x_2\right) + r_3\right)\frac{\partial x_1}{\partial r_1} + \left(r_1 + k_1 x_1\right)\frac{\partial x_2}{\partial r_1} + k_3\frac{\partial x_3}{\partial r_1} + x_2 \tag{4.218}$$

$$S_{42} = \frac{d}{dt}\frac{\partial x_2}{\partial r_1} = k_1\left(T_0 - x_2\right)\frac{\partial x_1}{\partial r_1} - \left(r_1 + k_2 + k_1 x_1\right)\frac{\partial x_2}{\partial r_1} - x_2 \tag{4.219}$$

$$S_{43} = \frac{d}{dt}\frac{\partial x_3}{\partial r_1} = r_3\frac{\partial x_1}{\partial r_1} + k_2\frac{\partial x_2}{\partial r_1} - k_3\frac{\partial x_3}{\partial r_1} \tag{4.220}$$

$$S_{51} = \frac{d}{dt}\frac{\partial x_1}{\partial r_3} = -\left(k_1\left(T_0 - x_2\right) + r_3\right)\frac{\partial x_1}{\partial r_3} + \left(r_1 + k_1 x_1\right)\frac{\partial x_2}{\partial r_3} + k_3\frac{\partial x_3}{\partial r_3} - x_1 \tag{4.221}$$

$$S_{52} = \frac{d}{dt}\frac{\partial x_2}{\partial r_3} = k_1\left(T_0 - x_2\right)\frac{\partial x_1}{\partial r_3} - \left(r_1 + k_2 + k_1 x_1\right)\frac{\partial x_2}{\partial r_3} \tag{4.222}$$

$$S_{53} = \frac{d}{dt}\frac{\partial x_3}{\partial r_3} = r_3\frac{\partial x_1}{\partial r_3} + k_2\frac{\partial x_2}{\partial r_3} - k_3\frac{\partial x_3}{\partial r_3} + x_1 \tag{4.223}$$

$$S_{61} = \frac{d}{dt}\frac{\partial x_1}{\partial T_0} = -\left(k_1\left(T_0 - x_2\right) + r_3\right)\frac{\partial x_1}{\partial T_0} + \left(r_1 + k_1 x_1\right)\frac{\partial x_2}{\partial T_0} + k_3\frac{\partial x_3}{\partial T_0} - k_1 x_1 \tag{4.224}$$

$$S_{62} = \frac{d}{dt}\frac{\partial x_2}{\partial T_0} = k_1\left(T_0 - x_2\right)\frac{\partial x_1}{\partial T_0} - \left(r_1 + k_2 + k_1 x_1\right)\frac{\partial x_2}{\partial T_0} + k_1 x_1 \tag{4.225}$$

$$S_{63} = \frac{d}{dt}\frac{\partial x_3}{\partial T_0} = r_3\frac{\partial x_1}{\partial T_0} + k_2\frac{\partial x_2}{\partial T_0} - k_3\frac{\partial x_3}{\partial T_0} \tag{4.226}$$

The sensitivity differential equations for the two compartment model of the form (4.30) - (4.31) are given by:

$$S_{71} = \frac{d}{dt}\frac{\partial x_1}{\partial k_3} = \left(\frac{V_M x_1}{\left(K_M + x_1\right)^2} - \frac{V_M}{K_M + x_1} - r_3\right)\frac{\partial x_1}{\partial k_3} + k_3\frac{\partial x_3}{\partial k_3} + x_3 \tag{4.227}$$

$$S_{73} = \frac{d}{dt}\frac{\partial x_3}{\partial k_3} = \left(\frac{V_M}{K_M + x_1} - \frac{V_M x_1}{\left(K_M + x_1\right)^2} + r_3\right)\frac{\partial x_1}{\partial k_3} - k_3\frac{\partial x_3}{\partial k_3} - x_3 \tag{4.228}$$

$$S_{81} = \frac{d}{dt}\frac{\partial x_1}{\partial r_3} = \left(\frac{V_M x_1}{\left(K_M + x_1\right)^2} - \frac{V_M}{K_M + x_1} - r_3\right)\frac{\partial x_1}{\partial r_3} + k_3\frac{\partial x_3}{\partial r_3} - x_1 \tag{4.229}$$

$$S_{83} = \frac{d}{dt}\frac{\partial x_3}{\partial r_3} = \left(\frac{V_M}{K_M + x_1} - \frac{V_M x_1}{\left(K_M + x_1\right)^2} + r_3\right)\frac{\partial x_1}{\partial r_3} - k_3\frac{\partial x_3}{\partial r_3} + x_1 \tag{4.230}$$

$$S_{91} = \frac{d}{dt}\frac{\partial x_1}{\partial K_M} = \left(\frac{V_M x_1}{\left(K_M + x_1\right)^2} - \frac{V_M}{K_M + x_1} - r_3\right)\frac{\partial x_1}{\partial K_M} + k_3\frac{\partial x_3}{\partial K_M} + \frac{V_M x_1}{\left(K_M + x_1\right)^2} \tag{4.231}$$

$$S_{93} = \frac{d}{dt}\frac{\partial x_3}{\partial K_M} = \left(\frac{V_M}{K_M + x_1} - \frac{V_M x_1}{\left(K_M + x_1\right)^2} + r_3\right)\frac{\partial x_1}{\partial K_M} - k_3\frac{\partial x_3}{\partial K_M} - \frac{V_M x_1}{\left(K_M + x_1\right)^2} \tag{4.232}$$

$$S_{101} = \frac{d}{dt}\frac{\partial x_1}{\partial V_M} = \left(\frac{V_M x_1}{\left(K_M + x_1\right)^2} - \frac{V_M}{K_M + x_1} - r_3 \right) \frac{\partial x_1}{\partial V_M} + k_3 \frac{\partial x_3}{\partial V_M} - \frac{x_1}{K_M + x_1} \tag{4.233}$$

$$S_{103} = \frac{d}{dt}\frac{\partial x_3}{\partial V_M} = \left(\frac{V_M}{K_M + x_1} - \frac{V_M x_1}{\left(K_M + x_1\right)^2} + r_3 \right) \frac{\partial x_1}{\partial V_M} - k_3 \frac{\partial x_3}{\partial V_M} + \frac{x_1}{K_M + x_1} \tag{4.234}$$

FACSIMILE is used to numerically solve each sensitivity coefficient at each time point. The code is shown in Appendix G. The sensitivity coefficients are normalised by dividing each sensitivity coefficient by the square root of the sum of all the squares of the individual sensitivity coefficients. The normalised sensitivity coefficients are therefore dimensionless. *Figures* 4.13 - 4.18 show sensitivity plots for both the model of the form (4.1) - (4.3) and the two compartment model of the form (4.30) - (4.31) for all three hepatocytes (rat, dog and human).

Almost all the sensitivity coefficients increase in magnitude over time, with the exception of $S_{13} = \frac{d}{dt}\frac{\partial x_3}{\partial k_1}$ for the rat and dog hepatocyte using the three compartment model of the form (4.1) - (4.3) (see *Figures* 4.13a and 4.15a). In both those instances, the magnitude of the sensitivity increases to a peak then attenuates. The time of the peak depends on the initial concentration of Pitavastatin; the higher the initial concentration, the earlier the peak occurs. In both cases, for the lowest concentrations (5 µM for rat, 1 µM for dog) the sensitivity plots suggest that it has not yet reached its maximum magnitude after 70 seconds.

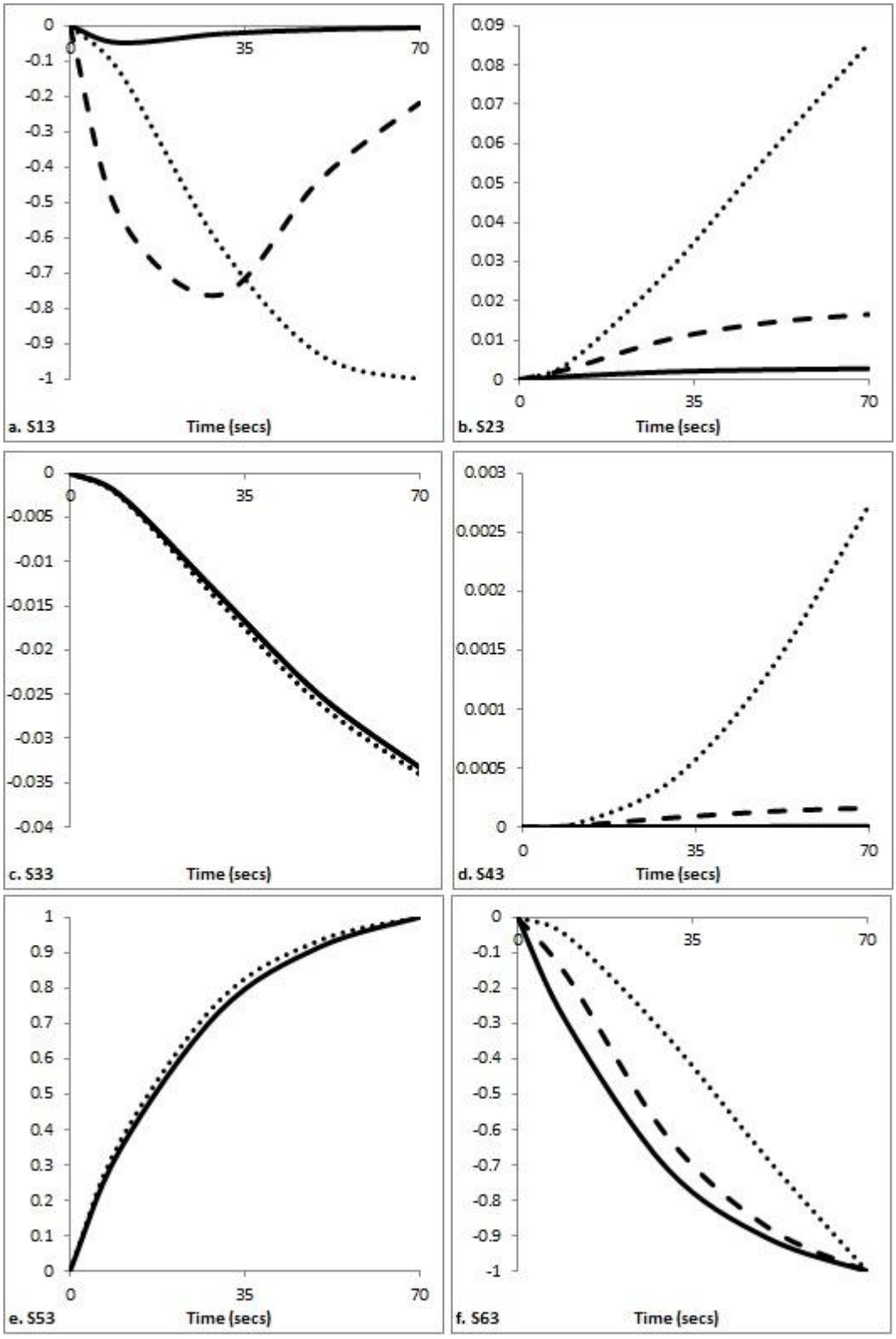

Figure 4.13: Rat hepatocyte normalised sensitivity coefficient plots for each parameter using three compartment model of the form (4.1) - (4.3). The three traces represent different initial concentrations: solid trace shows 300 µM, dashes trace shows 50 µM, dotted trace shows 5 µM.

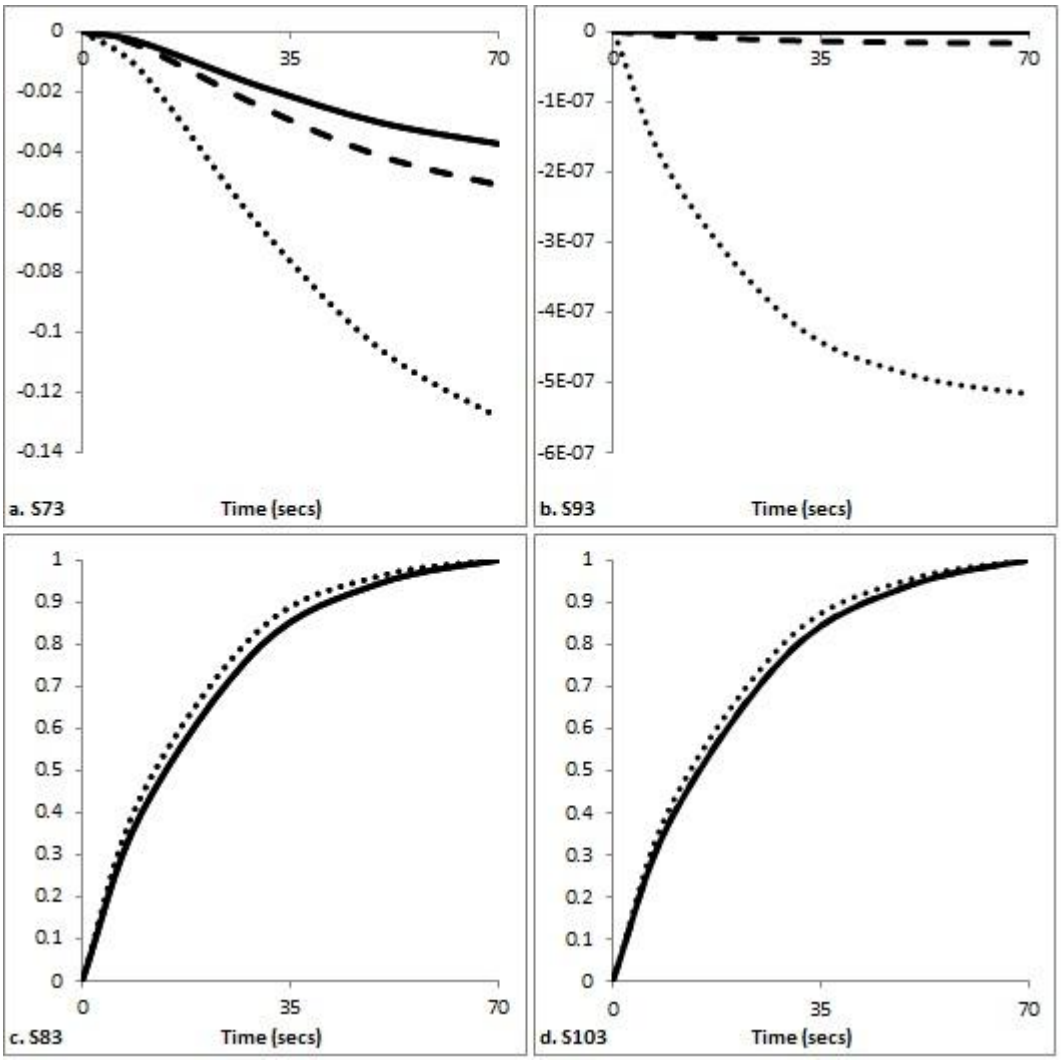

Figure 4.14: Rat hepatocyte normalised sensitivity coefficient plots for each parameter using two compartment model of the form (4.30) - (4.31). The three traces represent different initial concentrations: solid trace shows 300 µM, dashes trace shows 50 µM, dotted trace shows 5 µM.

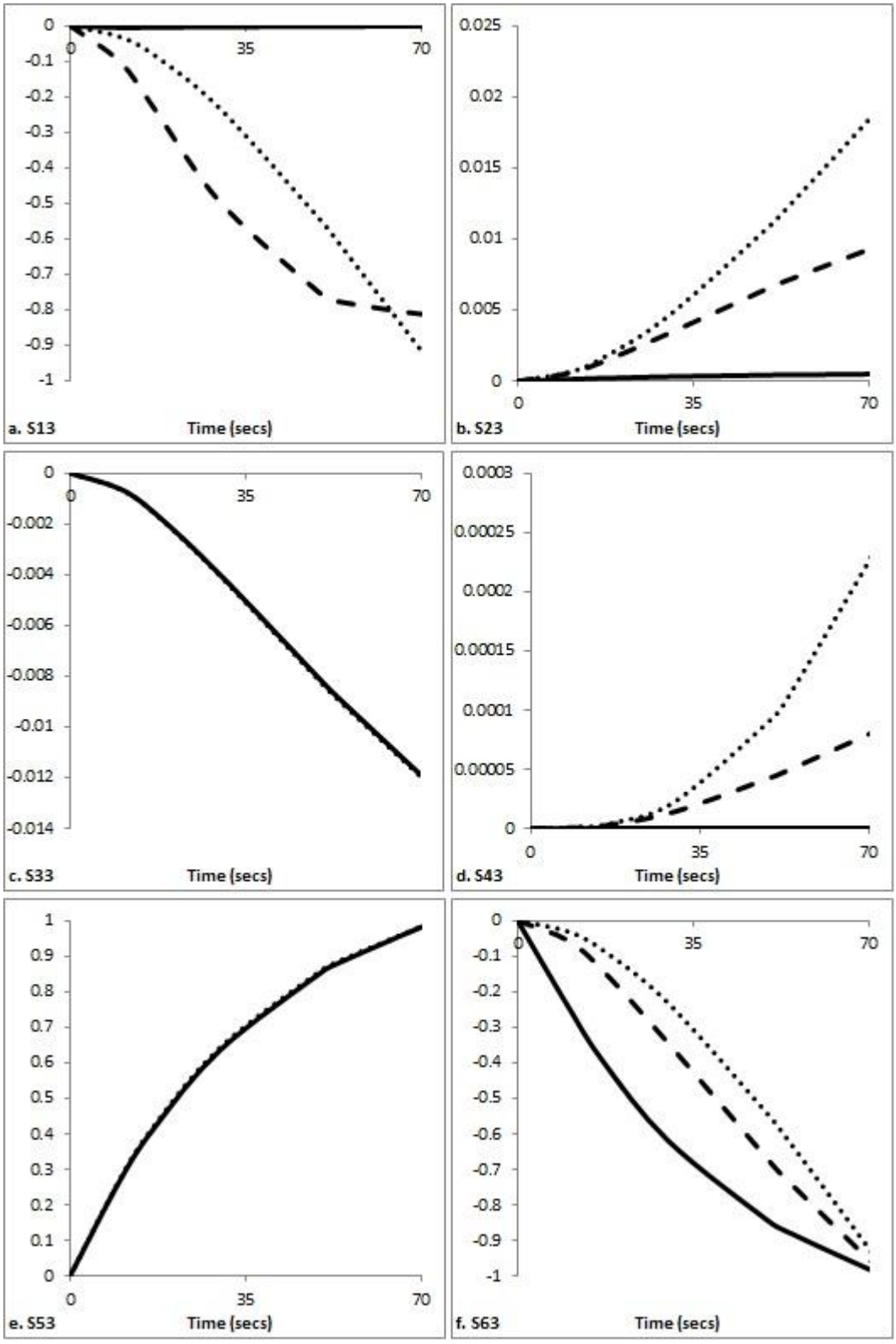

Figure 4.15: Dog hepatocyte normalised sensitivity coefficient plots for each parameter using three compartment model of the form (4.1) - (4.3). The three traces represent different initial concentrations: solid trace shows 650 µM, dashes trace shows 25 µM, dotted trace shows 1 µM.

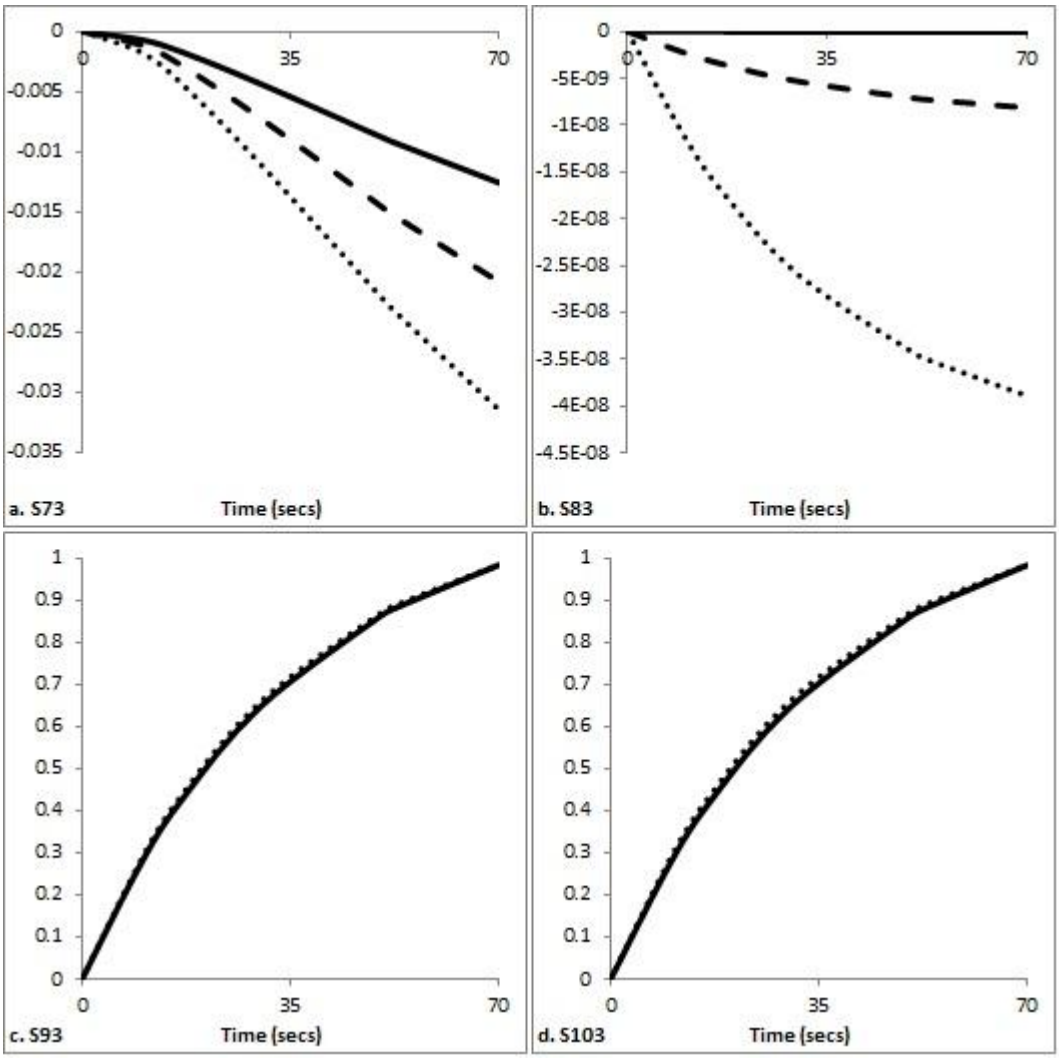

Figure 4.16: Dog hepatocyte normalised sensitivity coefficient plots for each parameter using two compartment model of the form (4.30) - (4.31). The three traces represent different initial concentrations: solid trace shows 650 µM, dashes trace shows 25 µM, dotted trace shows 1 µM.

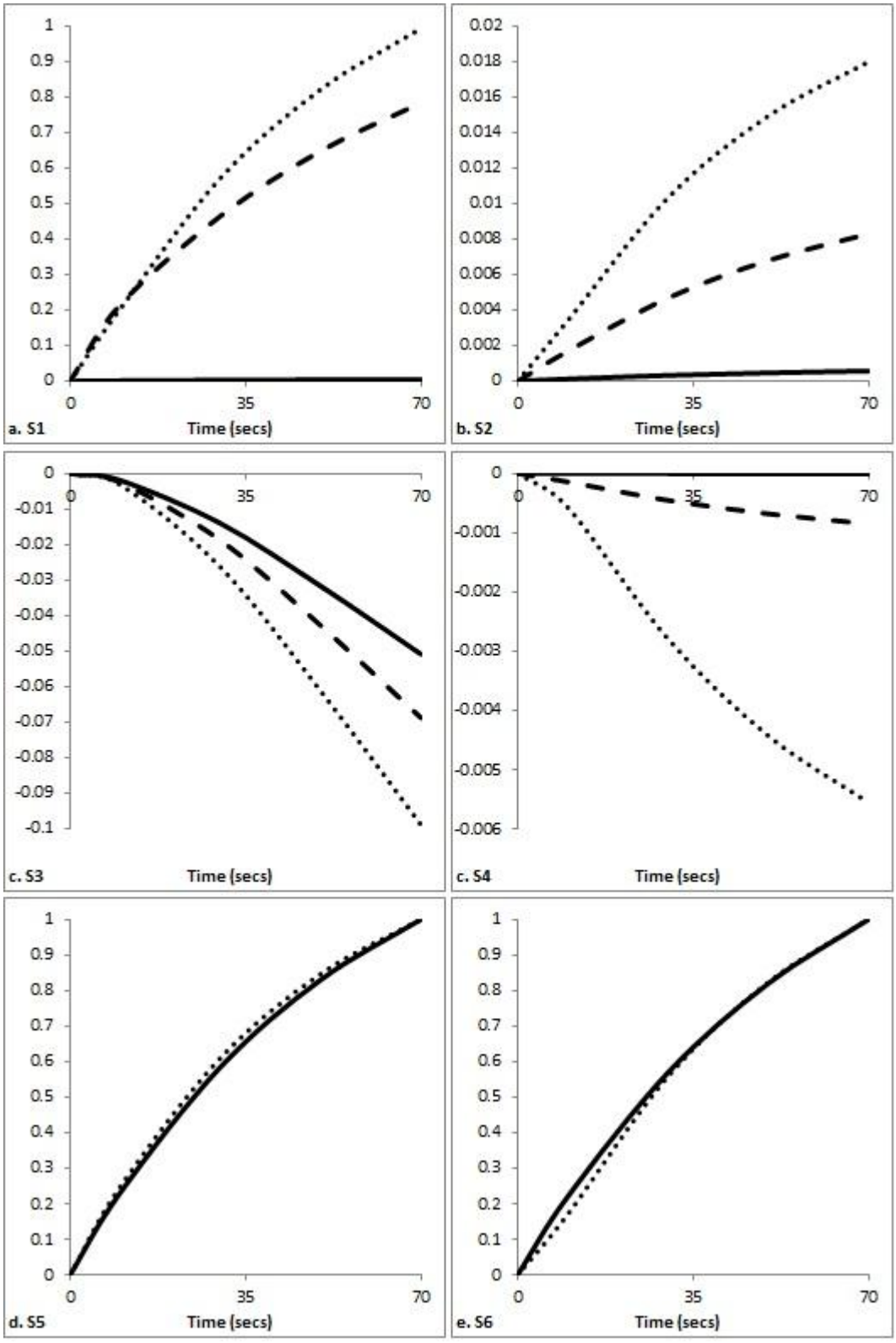

Figure 4.17: Human hepatocyte normalised sensitivity coefficient plots for each parameter using three compartment model of the form (4.1) - (4.3). The three traces represent different initial concentrations: solid trace shows 100 µM, dashes trace shows 5 µM, dotted trace shows 1 µM.

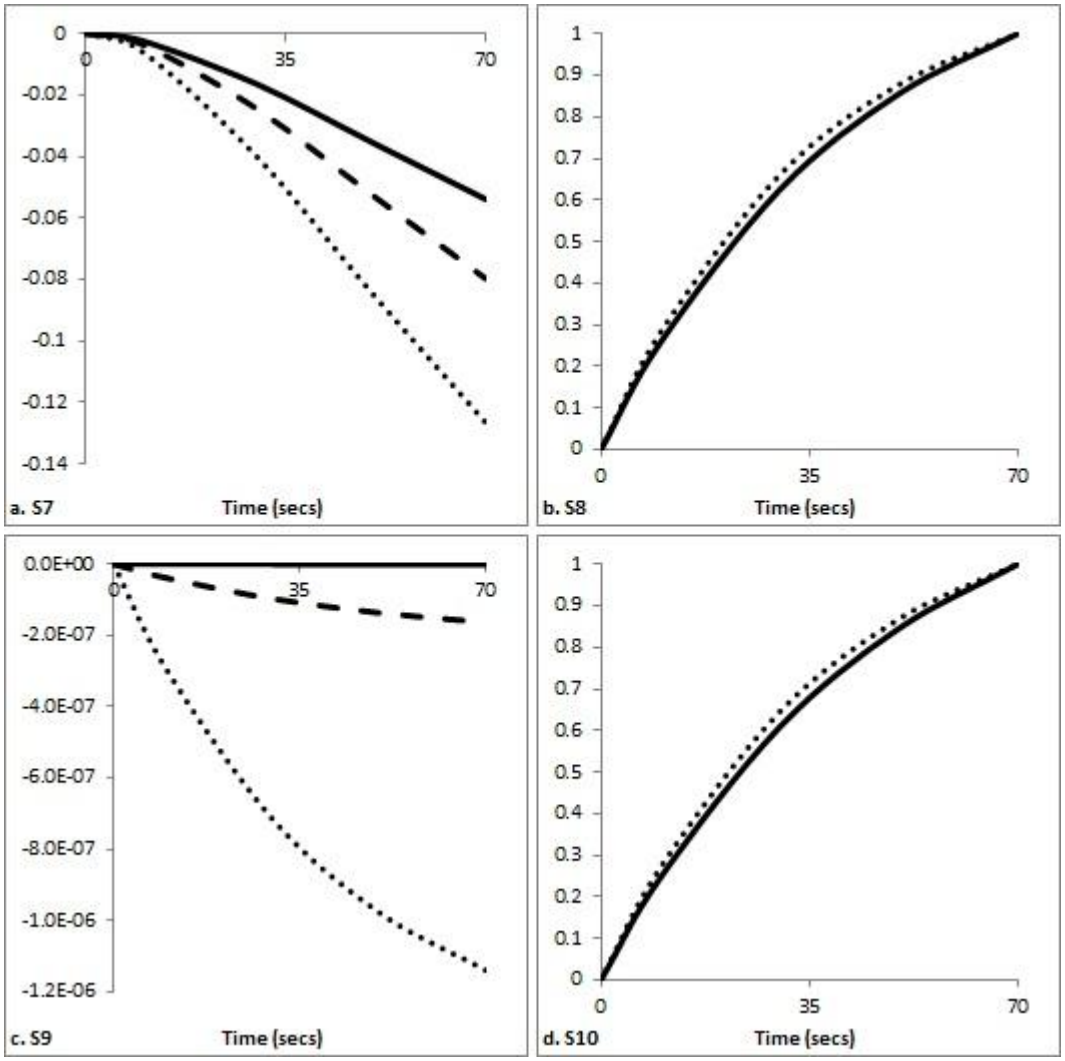

Figure 4.18: Human hepatocyte normalised sensitivity coefficient plots for each parameter using two compartment model of the form (4.30) - (4.31). The three traces represent different initial concentrations: solid trace shows 100 µM, dashes trace shows 5 µM, dotted trace shows 1 µM.

The magnitude of the peak also depends on the initial concentration of Pitavastatin; the higher the initial concentration, the smaller the magnitude of the peak. The sensitivity coefficients for the rat (*Figures* 4.13 and 4.14) are very similar to the sensitivity coefficients for the dog (*Figures* 4.15 and 4.16), following comparable trajectories and having comparable magnitudes. The sensitivity coefficients for the human are also alike except for $S_{13} = \frac{d}{dt}\frac{\partial x_3}{\partial k_1}$, $S_{43} = \frac{d}{dt}\frac{\partial x_3}{\partial r_1}$, and $S_{63} = \frac{d}{dt}\frac{\partial x_3}{\partial T_0}$ which have

similar magnitudes to the rat and dog sensitivity coefficients, but are of opposite sign.

From *Figures* 4.13, 4.15, and 4.17, it is possible to identify k_1, r_3 and T_0 as the most sensitive parameters for the three compartment model of the form (4.1) - (4.3) for all three hepatocytes, as these have the largest magnitudes. The rate constant r_1 is the least sensitive parameter for this candidate model. In *Figures* 4.13 and 4.15 it can be seen that k_3 and r_3 have similar sensitivity across the different concentration ranges for the rat and dog hepatocytes, whereas the other four rate parameters (k_1, k_2, r_3 and T_0) show different sensitivity trajectories depending on the initial conditions. For k_1, k_2 and r_3 the sensitivities decrease the higher the initial concentration while the plot for T_0 shows the opposite correlation. For k_1, the sensitivity decreases so much that it is not one of the most sensitive parameters at high initial concentration. In comparison, for the human hepatocytes (*Figure* 4.17), it is T_0 and r_3 that have almost identical sensitivity across the different concentration ranges (compared to k_3 and r_3 for the rat and the dog hepatocytes). This time, for all four remaining parameters (k_1, k_2, r_3 and T_0) the sensitivity decreases at higher concentrations. Again for k_1, the sensitivity decreases so much that it is not one of the most sensitive parameters at high initial concentration.

For the two compartment model of the form (4.30) - (4.31), *Figures* 4.14, 4.16 and 4.18 show that the sensitivities are very similar for all three hepatocytes (rat, dog and human). In this case r_3 and V_M are the most sensitive (compared with k_1, r_3 and T_0 for the three compartment model of the form (4.1) - (4.3)) and K_M is the least sensitive (compared to r_1). V_M and r_3 have almost the same sensitivity across the different concentration ranges, whereas the other two rate parameters show different sensitivity trajectories. The sensitivities for the rate constants k_3 and K_M decrease

with higher initial concentrations of Pitavastatin, however the range between the trajectories is much smaller than for the three compartment model of the form (4.1) - (4.3), therefore the sensitivity analysis shows that the two compartment model of the form (4.30) - (4.31) is more robust to different initial concentrations of Pitavastatin. Finally it is interesting to note that r_3 is almost identical in terms of sensitivity for both models across all three hepatocytes.

4.6.5 Previous modelling

Three models have been identified in the literature previously; Paine *et al.* 2008 put forward a linear three compartment model, whilst Poirier *et al*, 2008 proposed a non-linear mechanistic two compartment model, which Menochet *et al.* 2012 extended by adding an extra parameter to account for non-specific cellular binding. The main limitations of the model proposed by Paine *et al.* 2008 are that it is linear and no structural identifiability analysis was performed. An analysis of this model by the author of this thesis suggests that it is in fact unidentifiable and any numerical estimates obtained can therefore not be considered with confidence. In contrast, although no structural identifiability analysis was performed by Poirier *et al.*, 2008, an analysis by the author of this thesis suggests it is SGI. Its main limitations are that it does not account for non-specific binding of Pitavastatin and that numerical integration was performed using the Runge-Kutta method, which cannot cope easily with highly stiff systems. The stiffness of the numerical solution of a particular system may be estimated from the ratio of the largest rate constant over the smaller constant. Using this notion of stiffness, the corresponding stiffness ratios for the models developed in this chapter are given in *Table* 4.14.

Table 4.14: Stiffness ratios

Models	Rat	Dog	Human
4°C passive diffusion model of the form (4.118) - (4.119)	10^2	10^3	10^2
model of the form (4.30) - (4.31) using 4°C passive diffusion rates	10^8	10^9	10^7
model of the form (4.30) - (4.31)	10^6	10^8	10^6
model of the form (4.1) - (4.3) using 4°C passive diffusion rates	10^{10}	10^{11}	10^4
model of the form (4.1) - (4.3)	10^{10}	10^{10}	10^5

Table 4.14 shows that the numerical solutions for the rat, dog, and human data are highly stiff apart from the 4°C passive diffusion model of the form (4.118) - (4.119). The Runge-Kutta method would not be able to cope with these systems. Menochet *et al.*, 2012 is the most comprehensive non-linear mechanistic model, although it is implemented with the algorithms present in Matlab, which may also struggle with highly stiff systems. FACSIMILE's algorithms and fitting procedure are able to handle highly stiff systems; the confidence in the parameter estimate values it produces is therefore increased.

4.6.6 Conclusions

The disposition of the established OATP substrate Pitavastatin has been evaluated in suspended rat, dog and human hepatocytes using two non-linear pharmacokinetic models. In this chapter, a physiological three compartment model of the form (4.1) - (4.3) is derived to describe Pitavastatin uptake mechanistically, which is reduced to a two compartment model of the form (4.30) - (4.31) using a pseudo steady state assumption. The reduced model of the form (4.30) - (4.31) is similar to the Menochet *et al.*, 2012 model, which is compared with the two step method for some plated rat

hepatocyte. Similarly, Poirier *et al.*, 2008 compares their fits obtained from the mechanistic model to the two step approach and suggest that diffusion is highly temperature dependent in Chinese hamster ovary control cells and artificial membranes (parallel artificial membrane permeability assay). Neither studies offer a measure for the goodness of fit of their results and it is therefore impossible to establish whether their respective models are an improvement on the two step approach. Here simultaneous fits of numerous concentrations of 4°C and 37°C data are directly compared with 37°C only data for three species (rat, dog and human), offering not only an advantage in terms of the number of species evaluated, but also allowing for statistical comparison as to which fits describe the data more accurately.

This analysis demonstrates that both models proposed characterise the data more accurately than the conventional two step approach for all three species (rat, dog and human), and that the estimated passive diffusion rates from 37°C data are significantly different to those estimated from 4°C data. This suggests that the current widely accepted view, that the rate of diffusion of Pitavastatin into the cell is the same at both 4°C and 37°C, but that the transporter action only occurs at 37°C (Shimada *et al.*, 2003), is inaccurate. It follows that 37°C data should be fitted independently and it is therefore unnecessary to collect 4°C data altogether, potentially cutting down the number of experiments performed, reducing costs and supporting the 3Rs (reduce, replace, refine).

Both models are shown to be structurally identifiable and distinguishable. However during the parameter estimation it was found that the three compartment model of the form (4.1) - (4.3) is not numerically identifiable as k_2 and r_1 are not well determined (NWD). The two compartment model of the form (4.30) - (4.31) tends to fit the data better for the rat and human hepatocytes. Neither the SDLN or

confidence levels are improved and there is no significant rise in the RSS, whereas the three compartment model of the form (4.1) - (4.3) fits the dog hepatocytes more accurately. This suggests that the pseudo steady state assumption is not valid for the dog data, that is the OATP association and dissociation rate constants, k_1 and r_1, are not significantly faster than the other rates, namely the flow into the cell, k_2 and the diffusion into and out of the cell, k_3 and r_3 respectively. Different transporter expression in dog compared to rat and human hepatocytes may explain why a different model fits the dog data more precisely.

Steady state analysis on both models revealed that the two compartment model of the form (4.30) - (4.31) is more robust to different initial concentrations of Pitavastatin than the three compartment model of the form (4.1) - (4.3) across all species. The most sensitive parameters are r_3 and K_M for the two compartment model of the form (4.30) - (4.31). The most sensitive parameters for the three compartment model of the form (4.1) - (4.3) depend on the initial concentration of Pitavastatin: k_1, r_3, and T_0 are the most sensitive at low initial concentrations and only r_3 and T_0 are the most sensitive at the higher initial concentrations across all species.

Once fully validated the models have the potential to perform robust, predictive simulations to ascertain optimal levels of uptake of Pitavastatin in rat, dog, and human.

4.7 References

Anderson, B., Jackson, J., & Sitharam, M. (1998). Descartes' rule of signs revisited. *The American mathematical monthly*, *105*(5), 447-451.

Chandra, P., Brouwer, K. L. (2004). The complexities of hepatic drug transport: current knowledge and emerging concepts. *Pharm Res 21*:719-735.

Fujino, H., Yamada, I., Kojima, J., Hirano, M., Matsumoto, H., and Yoneda, M. (1999). Studies on the metabolic fate of NK-104, a new inhibitor HMG-CoA reductase (5): in vitro metabolism and plasma protein binding in animals and human. *Xenobiotics and Metabolic Disposition*. 1999; 14: 415-424.

Hassen, A. M., Lam, D., Chiba, M., Tan, E., Geng, W., Sandy, K. S. (1996). Uptake of sulfate conjugates by isolated rat hepatocytes. *Drug Metabolism and Disposition*; 24: 792-798.

Hirano, M., Maeda, K., Shitara, Y., Sugiyama, Y. (2004). Contribution of OATP2 (OATP1B1) and OATP8 (OATP1B3) to the hepatic uptake of of pitavastatin in humans. *The Journal of Pharmacology and Experimental Therapeutics.* 311: 139-146.

Jacquemin, E., Hagenbuch, B., Stieger, B., Wolkoff, A. W., Meier, P. J. (1994). Expression cloning of a rat liver Na^+-independent organic anion transporter. *Proc Natl Acad Sci USA 91: 133-13*

Jacquez, J. A. (1996). *Compartmental analysis in biology and medicine.* Ann Arbor, MI : BioMedware.

Kullak-Ublick, G. A., Hagenbuch, B., Stieger, B., Wolkoff, A. W., Meier, P. J. (1994). Functional characterization of the basolateral rat liver organic anion transporting polypeptide. *Hepatology 20: 411-416.*

Li, A. P., Lu, C., Brent, J. A., Pham, C., Fackett, A., Ruegg, C. E., Silber, P. M. (1999). Cryopreserved human hepatocytes: characterization of drug-metabolizing activities and applications in higher throughput screening assays for hepatotoxicity, metabolic stability, and drug-drug interaction potential. *Chem Biol Interact 121*:17-35.

Ménochet K, Kenworthy K, Houston JB, Galetin A (2012) Simultaneous assessment of uptake and metabolism in rat hepatocytes: a comprehensive mechanistic model. *J Pharmacol Exp Ther*. 341 (1):2-15

Obrink, B., Waemegaard, B., Pertoft, H. (1977). Specific binding of rat liver plasma membranes by rat liver cells. Biochem. & Biophysic. *Research Coms*, vol77, 665-670

Paine, S. W., Parker, A. J., Gardiner, P., Webborn, P. J., Riley, R. J. (2008). Prediction of thepharmacokinetics of atorvastatin, cerivastatin, and indomethacin using kinetic models applied to isolated rat hepatocytes. *Drug Metab Dispos 36*:1365-1374.

Poirier, A., Lave, T., Portmann, R., Brun, M. E., Senner, F., Kansy, M., Grimm, H. P., Funk, C. (2008). Design, data analysis, and simulation of in vitro drug transport kinetic experiments using a mechanistic in vitro model. *Drug Metab Dispos 36*:2434-2444.

Pohjanpalo, H. (1978). System identifiability based on the power series expansion of the solution. *Math. Biosci.* 60:89-108, 1978.

Shimada, S., Fujino, H., Morikawa, T., Moriyasu, M., Jojima, J. (2003). Uptake mechanism of pitavastatin, a new inhibitior of HMG-CoA reductase, in rat hepatocytes. *Drug Metabolism and Pharmacokinetics*. 18 (4): 245-251.

Shitara, Y., Horie, T., Sugiyama, Y. (2006). Transporters as a determinant of drug clearance and tissue distribution. *Eur J Pharm Sci 27*:425-446.

Soars, M. G., Grime, K., Sproston, J. L., Webborn, P. J. H., Riley, R. J. (2007). Use of hepatocytes to assess the contribution of hepatic uptake to clearance in vivo. *Drug Metab Dispos 35:*859-865.

Watanabe, T., Kusuhara, H., Maeda, K., Shitara, Y., Sugiyama, Y. (2009). Physiologically based pharmacokinetic modeling to predict transporter-mediated clearance and distribution of pravastatin in humans. *J Pharmacol Exp Ther 328*:652-662.

Webborn, P. J., Parker, A. J., Denton, R. L., Riley, R. J. (2007). In vitro-in vivo extrapolation of hepatic clearance involving active uptake: theoretical and experimental aspects. *Xenobiotica 37*:1090-1109.

Chapter 5

Transporter Mediated Drug-Drug Interactions

Following on from the *in vitro* data modelling presented in the two previous chapters, the impact of transporter mediated drug-drug interactions *in vivo* is considered. One experimentally convenient method is to look at the effects on the blood levels of endogenous substances after dosing a drug. Bile acids are actively removed from the hepatic portal circulation into the liver by Organic Anion Transport Polypeptides (OATPs) amongst other transporters (Hagenbuch & Gui 2008). Pharmaceuticals that are substrates of OATPs compete for the limited number of binding sites on the transporter, impeding bile acid uptake. This results in increased bile acid concentrations in the systemic blood stream, which are undesirable as bile acids are surfactants and their subsequent detergent-like properties have been shown to be cytotoxic (Rust *et al.* 2000, Higuchi & Gores 2003). Prolonged exposure to elevated bile acid levels have also been reported to cause spontaneous liver tumour growth in mice (Kim *et al.* 2007, Yang *et al.* 2007). In addition, bile acid homeostasis is a vital hepatic function since bile acids are responsible for regulating liver regeneration (Huang *et al.* 2006) and energy expenditure (Watanabe *et al.* 2006). Disruption to relatively stable bile acid concentrations may cause cholestasis, diarrhoea, and poor lipid absorption (Krone 1970, Van Deest *et al.* 1968, Hofmann 2002, Westergaard 2007).

Bile acids play a crucial role in dietary fat digestion, catabolising lipids for absorption. Like all detergents, bile salt molecules aggregate to form micelles once their concentration exceeds a critical value (Hofmann & Borgström 1964). These bile salt solutions dissolve fatty acids and monoglycerides, enabling the assimilation of lipids. In humans, primary bile acids, namely cholic acid and chenodeoxycholic acid, are synthesised from cholesterol metabolisation in the liver and secreted into the gall bladder for storage. During digestion, cholecystokinim is secreted from the duodenum in response to food intake (Shaffer 2000). This hormone causes the gall bladder to contract and release bile acids into the lumen of the intestine, where a proportion are dehydroxylated into secondary bile acids by intestinal bacteria. Removing a hydroxyl group modifies cholic acid and chenodeoxycholic acid to form deoxycholic acid and lithocholic, respectively (Stellwag & Hylemon 1979). The enterohepatic circulation of bile acids is represented in *Figure* 5.1.

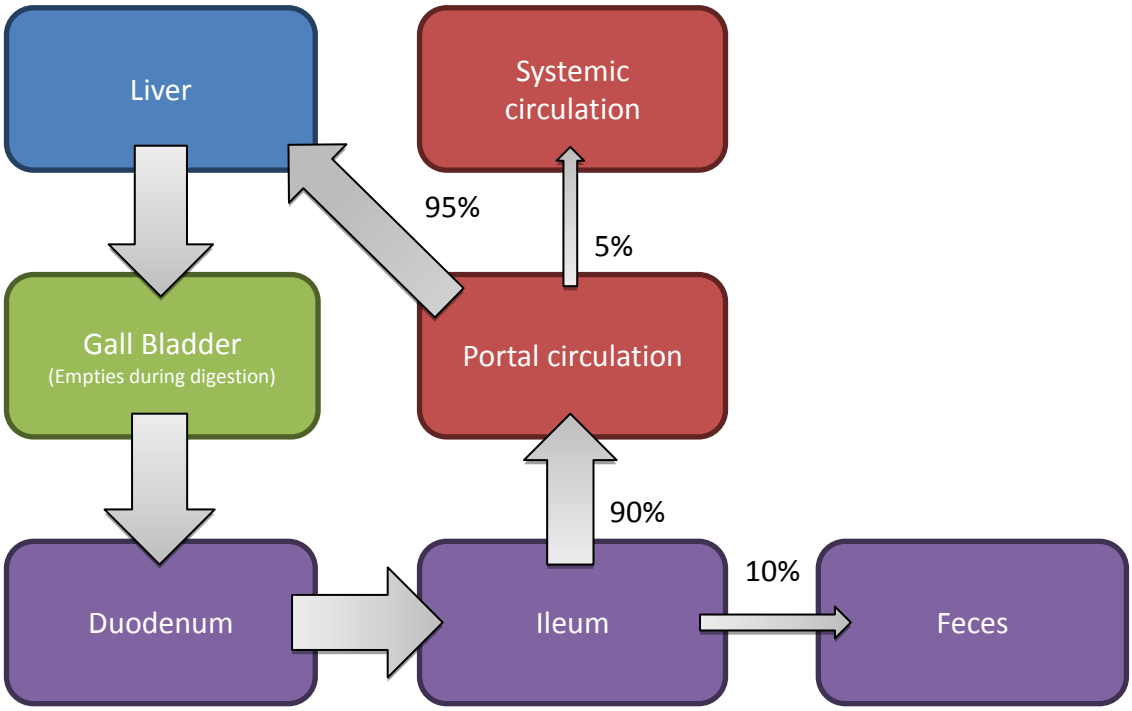

Figure 5.1: Circulation of bile acids in man

Bile acid enterohepatic circulation is a process whereby bile acids are reabsorbed into the circulation and returned to the liver where they can be re-secreted (Hofmann 1999). Most bile salts are reabsorbed into the hepatic portal circulation by active and passive transport. A very small percentage reaches the systemic circulation, as hepatocytes actively extract bile acids from the portal vein. The liver may conjugate them with an amino acid, namely glycine or taurine, before secreting them again. *Figure* 5.2 summarises the eight conjugated bile acids, which depend on the amino acid and primary or secondary acid used. Bile acids are synthesised daily to replenish the proportion excreted in feaces.

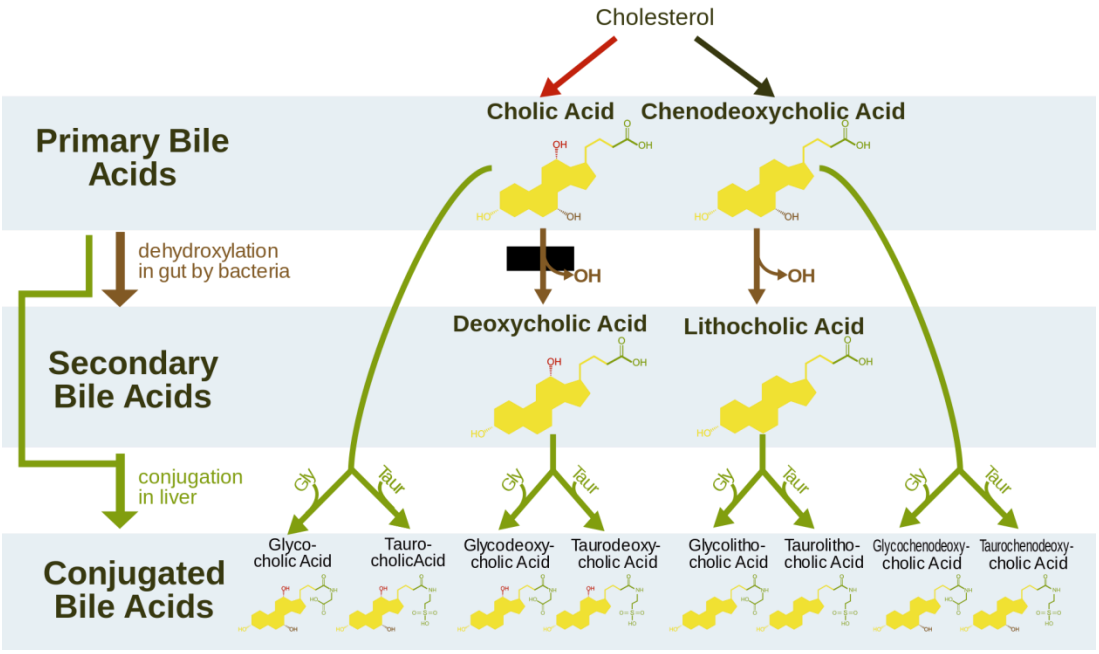

Figure 5.2: Bile acid synthesis in human from the two primary bile acids.

The rat digestive system is similar to that of a human but it has two major differences. The first is that rats do not have gallbladders; not all mammals have gallbladders and rats do not generally eat large amounts of fatty food, thereby make a bile storage organ useless. The second difference is that rats have an enlarged

intestine, namely the cecum, for fermenting grains and seeds (DeSesso & Jacobson 2001).

Rats were dosed with a compound (Cyclosporin A) considered to interact with OATPs (Endres *et al.* 2006); drug and bile acid blood levels were measured over time at AstraZeneca. In this chapter it was investigated whether the resulting data could be explained by a mechanistic model and which parameters could be uniquely identified, in order to support model based inference. Two candidate models are proposed, a seven compartment and a five compartment model. Both models are founded on the competitive binding mechanism of the BCRP transporter developed in Chapters 3, which accurately described Hoechst 33342 uptake *in vitro*, accounting for inhibitor action. Although both BCRP and OATP assist the movement of molecules by active transport, they have different mechanisms; BRCP utilises chemical energy (adenosine triphosphate - ATP) for primary active transport and OATP takes advantage of the potential energy stored in electrochemical gradients for secondary active transport (see Chapter 2 for more detail). Whilst the mechanisms are different, the BRCP model is utilised as a starting point. The five compartment model includes a pseudo steady state assumption, which was found to describe the OATP hepatic uptake mechanism in both rat and human more accurately than its counterpart (see Chapter 4).

The structural identifiability of both models is explored using all the methods described in Chapter 2, namely the Taylor series expansion, the similarity transformation approach for uncontrolled systems (including the sufficient condition for unidentifiability), the differential algebra approach using characteristic sets - DAACS, the algebraic input/output relationship approach - Ai/oRA, and the non-differential input/output observable normal form approach - NDi/oONF. Although it

is not essential to demonstrate the structural identifiability of models with more than one method, it is desired to investigate the applicability of each approach.

Steady state analyses are also performed on both models and the stability of the solutions is investigated by evaluating the relevant Jacobian matrix. Preliminary fits of *in vivo* experimental data are presented and the ability of the model to describe the data is discussed.

5.1 Mathematical Model

As described earlier, Cyclosporin A (CsA) is administered orally and is subsequently absorbed into the systemic blood stream. CsA has been shown to be a substrate of OATP previously (Endres *et al.* 2006), which actively uptakes the drug into the liver. From the *in vitro* data modelling performed in Chapter 4, it is also suspected that diffusion takes place, where the drug flows in and out of the liver according to the concentration gradient. As rats do not possess gall bladders, bile acid is secreted directly from the liver to the intestine. Bile acids are re-absorbed into the liver by OATP. These mechanisms can be represented by the compartment model shown in *Figure* 5.3.

In *Figure* 5.3, the drug compartments (*G*, *DO*, *DI*, and *TD*) are coloured in green, whereas the bile compartments (*BO*, *TB*, and *BI*) are in red. A known dose of CsA is administered and is represented by an initial quantity in the gut compartment *G*. The compound is absorbed into the blood stream (*DO*) via the absorption rate k_a. The substrate actively binds to OATP, *TD*, via association and dissociation rate constants k_D^+ and k_D^-, respectively, and is mediated into the liver, *DI*, by rate constant k_{Dtran}. The compound also flows into the liver, *DI*, by passive diffusion with rate constants

k_{Din} and k_{Dout}. The compound is metabolised and eliminated from the liver via drug elimination rate k_{De}. Meanwhile a constant bile acid production, k_p, into the blood steam (*BO*) is assumed. Although bile acid synthesis is unlikely to be perfectly

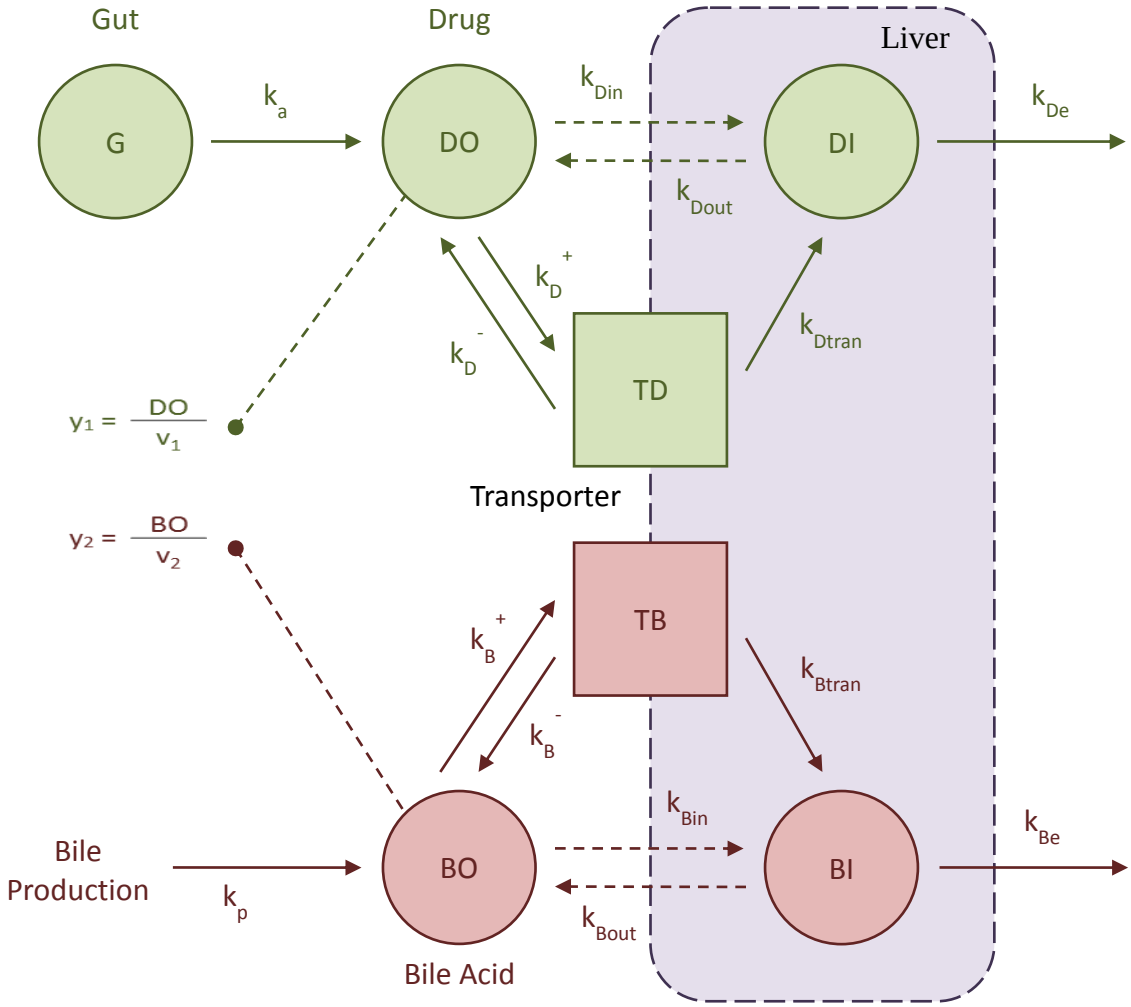

Figure 5.3: Rat bile acid model representation

constant, especially when concentration levels increase, this approximation is made in order to keep the model uncomplicated at this stage. The validity of this assumption is discussed later and a negative feedback loop is proposed as an alternative model structure. The bile acid actively binds to OATP (*TB*) via association and dissociation rate constants k_B^+ and k_B^-, respectively, and is mediated

into the liver, *BI*, by rate constant k_{Btran}. The bile acids also flow into the liver, *BI*, by passive diffusion with rate constants k_{Bin} and k_{Bout}. The bile acid may be conjugated and secreted out of the liver with drug elimination rate k_{Be}.

Although the level of OATP can conceptually be described by a single compartment, it is represented mathematically by two state variables (species) as there are two different complexes present; the substrate CsA and bile acids, which both compete for the same limited number of binding sites on the OATP transporter molecules.

The CsA blood concentration y_1 and bile acid blood concentration y_2 (see *Figure* 5.3) are measured directly from blood samples. Both observations are divided by the corresponding volume of distribution, v_1 and v_2 respectively, to convert the quantities for the model variables (μmol) to concentrations (μMol). The seven compartments used and the fourteen inter-compartmental rate transfers are summarised in *Table* 5.1.

Table 5.1: Description of the inter-compartmental rate transfer and compartments

Inter-compartmental rate transfers (units = h^{-1} unless otherwise stated)		**Compartments (units = µmol)**	
k_a	absorption rate from gut	*G*	Gut
k_{Din}	drug cellular influx		
k_{Dout}	drug cellular efflux	*DO*	Extracellular Drug (Blood)
k_{De}	drug elimination		
k_D^+	drug transporter binding	*DI*	Intracellular Drug
k_D^-	drug transporter dissociation		
k_{Dtran}	drug transporter flow	*TD*	Drug bound to Transporter
k_p	bile production (µmol h^{-1})		
k_{Bin}	bile acid cellular influx	*BO*	Extracellular Bile Acid (Blood)
k_{Bout}	bile acid cellular efflux		
k_{Be}	bile acid elimination	*BI*	Intracellular Bile Acid
k_B^+	bile acid transporter binding		
k_B^-	bile acid transporter dissociation	*TB*	Bile Acid bound to Transporter
k_{Btran}	bile acid transporter flow		

5.1.1 System Equations

The system of ordinary differential equations describing the models is derived using classical mass-balance principles as per Jacquez 1996, see *Section 3.1.1* for more details. The corresponding set of non-linear ordinary differential equations characterising the proposed model is therefore given by the following:

$$\frac{dG}{dt} = -k_a G \tag{5.1}$$

$$\frac{dDO}{dt} = k_a G - k_D^+ DO\left(T_0 - TD - TB\right) + k_D^- TD + k_{Dout} DI - k_{Din} DO \tag{5.2}$$

$$\frac{dTD}{dt} = k_D^+ DO\left(T_0 - TD - TB\right) - \left(k_{Dtran} + k_D^-\right) TD \tag{5.3}$$

$$\frac{dDI}{dt} = k_{Din} DO - \left(k_{Dout} + k_{De}\right) DI + k_{Dtran} TD \tag{5.4}$$

$$\frac{dBO}{dt} = k_p - k_B^+ BO\left(T_0 - TD - TB\right) + k_B^- TB + k_{Bout} BI - k_{Bin} BO \tag{5.5}$$

$$\frac{dTB}{dt} = k_B^+ BO\left(T_0 - TD - TB\right) - \left(k_{Btran} + k_B^-\right) TB \tag{5.6}$$

$$\frac{dBI}{dt} = k_{Bin} BO - \left(k_{Bout} + k_{Be}\right) BI + k_{Btran} TB \tag{5.7}$$

where T_0 is the total number of transporter binding sites on OATP. The initial conditions are given by

$$G(0) = D \tag{5.8}$$

$$BI(0) = B_{in} \tag{5.9}$$

$$BO(0) = B_{out} \tag{5.10}$$

$$DO(0) = DI(0) = TD(0) = TB(0) = 0 \tag{5.11}$$

where D is the initial dose of CsA in μmol, B_{in} is the initial quantity of bile acid in the liver, and B_{out} is the initial quantity of bile acid in the blood stream. The CsA

blood concentration and bile acid blood concentration observations of the system, y_1 and y_2 respectively, are given by:

$$y_1 = \frac{DO}{v_1} \text{ and } y_2 = \frac{DI}{v_2} \tag{5.12}$$

where v_1 is the CsA apparent volume of distribution and v_2 is the bile acid apparent volume of distribution. The unknown parameter set, $\boldsymbol{p}$, is given by

$$\boldsymbol{p} = \left\{k_a, k_{Din}, k_{Dout}, k_{De}, k_D^+, k_D^-, k_{Dtran}, k_p, k_{Bin}, k_{Bout}, k_{Be}, k_B^+, k_B^-, k_{Btran}, B_{in}, B_{out}, v_1, v_2, T_0\right\} \tag{5.13}$$

5.1.2 Pseudo steady state assumption

As for the models developed in Chapter 4, it is possible to reduce the above model using a common approximation in the chemical/biological pharmacokinetic systems literature (Jaquez 1996 and Murray 2003). As previously described, the model with the pseudo steady state assumption described rat *in vitro* data more accurately and it is suspected that this will also be the case *in vivo*. The necessary assumption is that the binding to the transporter occurs very rapidly compared to the time scale of the rate of appearance of intracellular compound (Jacquez 1996). Taking the proposed model of the form (5.1) - (5.7), this is equivalent to assuming that the OATP association and dissociation rate constants; k_D^+ , k_D^- , k_B^+ , and k_B^-, are known to be considerably faster than the other rates, namely the flows into the cell, k_{Dtran} and k_{Btran}, and the diffusion into the cell, k_{Din} , k_{Dout} , k_{Bin}, and k_{Bout} , i.e. there is rapid equilibration of OATP. If this assumption is true then instantaneously after the experiment has begun, the amount of CsA and bile acids bound to transporter (*TD* and *TB*) is effectively constant, the rates of change of OATP (5.3) and (5.6) can be set to zero and the right hand side of (5.3) can be re-arranged to give:

$$TD = \frac{T_0 DO}{K_D + DO}, \tag{5.14}$$

where

$$K_D = \frac{k_D^- + k_{Dtran}}{k_D^+} \tag{5.15}$$

is the relevant Michaelis-Menten constant. Similarly the right hand side of (5.6) can be re-arranged to give

$$TB = \frac{T_0 BO}{K_B + BO}, \tag{5.16}$$

where

$$K_B = \frac{k_B^- + k_{Btran}}{k_B^+}. \tag{5.17}$$

Substituting (4.28) and (5.16) back into the original system equations (5.1) - (5.7) yields

$$\frac{dG}{dt} = -k_a G \tag{5.18}$$

$$\frac{dDO}{dt} = -k_a G - \frac{V_D K_{BA} DO}{K_D K_{BA} + K_{BA} DO + K_D BO} + k_{Dout} DI - k_{Din} DO \tag{5.19}$$

$$\frac{dDI}{dt} = \frac{V_D K_{BA} DO}{K_D K_{BA} + K_{BA} DO + K_D BO} - (k_{Dout} + k_{De}) DI + k_{Din} DO \tag{5.20}$$

$$\frac{dBO}{dt} = k_p - \frac{V_{BA} K_D BO}{K_D K_{BA} + K_{BA} DO + K_D BO} + k_{Bout} BI - k_{Bin} BO \tag{5.21}$$

$$\frac{dBI}{dt} = \frac{V_{BA} K_D BO}{K_D K_{BA} + K_{BA} DO + K_D BO} - (k_{Bout} + k_{Be}) BI + k_{Bin} BO \tag{5.22}$$

where

$$V_D = k_{Stran} T_0 \text{ and } V_{BA} = k_{Btran} T_0 \tag{5.23}$$

are the maximum velocities of the reactions for CsA and bile acid respectively. The unknown parameter set, ***p***, is now given by:

$$\boldsymbol{p} = \left\{ k_a, k_{Din}, k_{Dout}, k_{De}, K_D, V_D, k_p, k_{Bin}, k_{Bout}, k_{Be}, K_B, V_B, B_{in}, B_{out}, v_1, v_2 \right\} . \tag{5.24}$$

The initial conditions are now given by:

$$B(0) = D \tag{5.25}$$

$$BI(0) = B_{in} \tag{5.26}$$

$$BO(0) = B_{out} \tag{5.27}$$

$$DO(0) = DI(0) = 0 \tag{5.28}$$

and the observations (4.8) remain unchanged. The five compartments used and the twelve inter-compartmental rate transfers are summarised in *Table* 5.2.

Table 5.2: Description of the inter-compartmental rate transfer and compartments

Inter-compartmental rate transfers (units = h^{-1} unless otherwise state)		**Compartments (units = µmol)**	
k_a	absorption rate from gut	*G*	Gut
k_{Din}	drug cellular influx		
k_{Dout}	drug cellular efflux	*DO*	Extracellular Drug (Blood)
k_{De}	drug elimination		
V_D	drug max velocity (µmol h^{-1})	*DI*	Intracellular Drug
K_D	drug Michaelis Mentem constant (µmol)		
k_p	bile production (µmol h^{-1})	*BO*	Extracellular Bile Acid (Blood)
k_{Bin}	bile acid cellular influx		
k_{Bout}	bile acid cellular efflux	*BI*	Intracellular Bile Acid
k_{Be}	bile acid elimination		
V_{BA}	bile acid max velocity (µmol h^{-1})		
K_{BA}	bile acid Michaelis Mentem constant (µmol)		

5.2 Structural Identifiability Analyses

5.2.1 Taylor Series Expansion

Due to the structural complexity of the systems, this approach did not converge to any solutions for the seven compartment model of the form (5.1) - (5.7) or the five compartment model of the form (5.18) - (5.22). It is not possible to compute enough Taylor series expansion coefficients to converge to any solutions due to computational limitations.

5.2.2 Observability rank criterion

Lie derivatives, defined in *Section 2.3.2.1,* were calculated for both observations (4.8) of the five compartment model of the form (5.18) - (5.22). The first three Lie derivatives of y_1 are μ_{11}, μ_{12}, and μ_{13}, whilst the first three Lie derivatives of y_2 are μ_{21}, μ_{22}, and μ_{23}. The Jacobian matrix of these Lie derivatives with respect to $\boldsymbol{x} = (G, DO, DI, BO, BI)^T$, evaluated at $\boldsymbol{x}_0 = \left(D, 0, 0, B_{out}, B_{in}\right)^T$, of the resultant function $\boldsymbol{H} = \left(\mu_{11}, \mu_{12}, \mu_{13}, \mu_{21}, \mu_{22}\right)^T$ has full rank (see Appendix H) and therefore the five compartment model of the form (5.18) - (5.22) satisfies the observability rank criterion (ORC).

For the seven compartment model of the form (5.1) - (5.7), eight Lie derivatives are computed; the first four Lie derivatives of y_1 are μ_{31}, μ_{32}, μ_{33}, and μ_{34}, whilst the first four Lie derivatives of y_2 are μ_{41}, μ_{42}, μ_{43}, and μ_{44}. As above, the Jacobian matrix with respect to $\boldsymbol{x} = (G, DO, TD, DI, BO, TB, BI)^T$, evaluated at $\boldsymbol{x}_0 = \left(D, 0, 0, 0, B_{out}, 0, B_{in}\right)^T$, of the resultant function $\boldsymbol{H} = \left(\mu_{31}, \mu_{32}, \mu_{33}, \mu_{34}, \mu_{41}, \mu_{42}, \mu_{43}\right)^T$ has full rank (see Appendix I) and therefore the seven compartment model of the form (5.1) - (5.7) also satisfies the ORC. The five techniques (the similarity transformation approach for uncontrolled systems - STAUS, the sufficient condition for unidentifiability, the differential algebra approach using characteristic sets - DAACS, the algebraic input/output relationship approach - Ai/oRA, and the non-differential input/output observable normal form approach - NDi/oONF) may therefore be applied to both models described. However the DAACS, Ai/oRA, and NDi/oONF approaches are not suitable in determining the structurally identifiability of the system as some of the initial conditions are unknown, namely B_{in} and B_{out}. Although all three of the methods are unable to check for unknown initial conditions, they are still

implemented as they can produce input/output maps and provide important information about the system identifiablity; the input/output maps describe the exact structure of the system and may be to used to determine the identifiability of the unknown parameters excluding the initial conditions. It is also desired to investigate how each approach copes with the two candidate models to evaluate the applicability of each method.

5.2.3 Similarity Transformation Approach for Uncontrolled Systems (STAUS)

For the five compartment model of the form (5.18) - (5.22), it is possible to compute a smooth map λ from (2.16) using $\boldsymbol{H} = (\mu_{11}, \mu_{12}, \mu_{13}, \mu_{21}, \mu_{22})^T$ and the alternate parameter vector

$$\tilde{\boldsymbol{p}} = \left\{ \tilde{k}_a, \tilde{k}_{Din}, \tilde{k}_{Dout}, \tilde{k}_{De}, \tilde{k}_D^+, \tilde{k}_D^-, \tilde{k}_{Dtran}, \tilde{k}_p, \tilde{k}_{Bin}, \tilde{k}_{Bout}, \tilde{k}_{Be}, \tilde{k}_B^+, \tilde{k}_B^-, \tilde{k}_{Btran}, \tilde{v}_1, \tilde{v}_2, \tilde{T}_0 \right\}. \qquad (5.29)$$

Equating the monomials of the states $\{G, DO, DI, BO, BI\}$ in *Equation* (2.18) generates 807 equations, which Maple is unable to solve simultaneously for the unknown parameter vector. The 807 equations were therefore split into groups and each group was solved simultaneously. The solutions were subsequently combined and solved in conjunction with *Equation* (2.17) to yield one unique solution:

$$\boldsymbol{s}_1 = \left\{ k_a = \tilde{k}_a, k_{Din} = \tilde{k}_{Din}, k_{Dout} = \tilde{k}_{Dout}, k_{De} = \tilde{k}_{De}, K_D = \tilde{K}_D, V_D = \tilde{V}_D, k_p = \frac{B_{in}\tilde{k}_p}{\tilde{B}_{in}}, k_{Bin} = \tilde{k}_{Bin}, k_{Bout} = \tilde{k}_{Bout}, \right.$$

$$\left. k_{Be} = \tilde{k}_{Be}, K_{BA} = \frac{B_{in}\tilde{K}_{BA}}{\tilde{B}_{in}}, V_{BA} = \frac{B_{in}\tilde{V}_{BA}}{\tilde{B}_{in}}, B_{in} = B_{in}, B_{out} = \frac{B_{in}\tilde{B}_{out}}{\tilde{B}_{in}}, v_1 = \tilde{v}_1, v_2 = \frac{B_{in}\tilde{v}_2}{\tilde{B}_{in}} \right\}, \quad (5.30)$$

demonstrating that the five compartment model of the form (5.18) - (5.22) is structurally unidentifiable as although ten parameters, namely k_a, k_{Din}, k_{Dout}, k_{De}, K_D, V_D, k_{Bin}, k_{Bout}, k_{Be}, and v_1 are uniquely identifiable, the remaining six parameters, namely k_p, K_{BA}, V_{BA}, B_{in}, B_{out}, and v_2 are unidentifiable.

The model or observations therefore need to be modified accordingly in order to have a structurally identifiable system. It can be shown that if any of the six unidentifiable parameters are known then the model is structurally globally identifiable by re-arranging the six equations for the unknown parameters from (5.30) as follows:

$$\frac{K_{BA}}{\tilde{K}_{BA}} = \frac{B_{in}}{\tilde{B}_{in}} = \frac{k_p}{\tilde{k}_p} = \frac{V_{BA}}{\tilde{V}_{BA}} = \frac{B_{out}}{\tilde{B}_{out}} = \frac{v_2}{\tilde{v}_2}. \tag{5.31}$$

Therefore if one of the six parameters can be estimated from a different experiment or obtained from using values in the literature then the resulting model would be structurally globally identifiable.

It is also possible to demonstrate that if the two apparent volumes of distribution are equal ($v_1 = v_2$), but unknown, then the model is structurally globally identifiable. Using this assumption allows the model to be used for parameter estimation.

Unfortunately it is not possible to generate a smooth map for the seven compartment model of the form (5.1) - (5.7) as the resulting equations prove computationally intractable.

5.2.4 A Sufficient Condition for Unidentifiability

As described in *Section 2.3.2.2*, a straightforward consequence of the similarity transformation approach gives rise to a sufficient condition for unidentifiability (Evans *et al.* 2005). This test for unidentifiability confirms that the six parameters k_p, K_{BA}, V_{BA}, B_{in}, B_{out}, and v_2 are unidentifiable for the five compartment model of the form (5.18) - (5.22). If the apparent volumes of distribution are equal ($v_1 = v_2$) then the five compartment model of the form (5.18) - (5.22) passes the test.

The seven compartment model of the form (5.1) - (5.7) passes the sufficient condition for unidentifiability with two distinct unknown apparent volumes of distribution.

5.2.5 Differential Algebra Approach Using Characteristics Sets (DAACS)

As described in *Section 2.3.2.3*, this approach is implemented using the Rosenfeld-Gröbner algorithm in Maple 2010. Unfortunately the Rosenfeld-Gröbner algorithm failed to produce an input/output map for either model. Analysis of the five compartment model of the form (5.18) - (5.22) with the alternative structure, i.e. equal apparent volumes of distribution ($v_1 = v_2$), was also attempted, but Maple was again unable to produce an input/output map.

5.2.6 Algebraic Input/Output Relationship Approach (Ai/oRA)

As described in *Section 2.3.2.4*, this approach is implemented by using the Lie derivatives as inputs into the Univariate Polynomial or Groebner Bases algorithms in Maple 2010. As for the DAACS approach, both algorithms failed to produce

input/output maps for either models. It is suspected that there is not enough memory available for Maple 2010 to perform the required symbolic calculations. Different Lie derivative combinations were also attempted, i.e. for the five compartment model of the form (5.18) - (5.22):

$$(\mu_{11}, \mu_{12}, \mu_{13}, \mu_{14}, \mu_{21}, \mu_{22})^T \tag{5.32}$$

$$(\mu_{11}, \mu_{12}, \mu_{21}, \mu_{22}, \mu_{23}, \mu_{24})^T \tag{5.33}$$

where μ_{14} and μ_{24} are the fourth Lie derivatives of y_1 and y_2 respectively. These combinations also satisfy the ORC. However neither algorithm was able to generate an input/output map for either model. Similarly for the five compartment model of the form (5.18) - (5.22) with the alternative structure, i.e. equal apparent volumes of distribution ($v_1 = v_2$).

5.2.7 Non-differential Input/Output Observable Normal Form Approach (NDi/oONF)

For the five compartment model of the form (5.18) - (5.22), it is possible to solve the five Lie derivatives μ_{11}, μ_{12}, μ_{13}, μ_{21}, and μ_{22}, simultaneously and obtain equations for the five states (G, DO, DI, BO, BI) strictly in terms of those Lie derivatives, i.e.

$$G = \psi_1(\mu_{11}), \tag{5.34}$$

$$DO = \psi_1(\mu_{11}, \mu_{12}, \mu_{13}), \tag{5.35}$$

$$DI = \psi_1(\mu_{11}, \mu_{12}, \mu_{13}), \tag{5.36}$$

$$BO = \psi_1(\mu_{21}), \tag{5.37}$$

$$BI = \psi_1(\mu_{21}, \mu_{22}). \tag{5.38}$$

Equations (5.34) - (5.38) are substituted into a higher Lie derivative, namely μ_{23}, to obtain an input/output map θ_{10}. A second input/output map $\tilde{\theta}_{10}$ is generated by substituting for $\boldsymbol{p}$ by $\tilde{\boldsymbol{p}} = \{\tilde{k}_a, \tilde{k}_{Din}, \tilde{k}_{Dout}, \tilde{k}_{De}, \tilde{K}_D, \tilde{V}_D, \tilde{k}_p, \tilde{k}_{Bin}, \tilde{k}_{Bout}, \tilde{k}_{Be}, \tilde{K}_B, \tilde{V}_B, \tilde{B}_{in}, \tilde{B}_{out}, \tilde{v}_1, \tilde{v}_2\}$ in the original input/output relationship θ_{10}. Equating the monomials of μ_{11}, μ_{12}, μ_{13}, μ_{21}, μ_{22}, and μ_{23} in $\theta_{10} = \tilde{\theta}_{10}$ yields 22 equations; solving them simultaneously for the unknown parameter vector $\boldsymbol{p}$ yields one unique solution

$$\boldsymbol{s}_1 = \left\{ K_{BA} = \frac{v_2 \tilde{K}_{BA}}{\tilde{v}_2}, K_D = \frac{\tilde{v}_2 \sqrt{v_2 \tilde{v}_2}\, \tilde{K}_D}{v_2^2}, V_{BA} = \frac{v_2 \tilde{V}_{BA}}{\tilde{v}_2}, V_D = V_D, k_{Din} = k_{Din}, k_{Dout} = k_{Dout}, k_{De} = k_{De}, \right.$$

$$\left. k_{Bin} = \tilde{k}_{Bin}, k_{Bout} = \tilde{k}_{Bout}, k_{Be} = \tilde{k}_{Be}, k_a = k_a, k_p = \frac{v_2 \tilde{k}_p}{\tilde{v}_2}, v_1 = \frac{\tilde{v}_1 \tilde{v}_2 \sqrt{v_2 \tilde{v}_2}}{v_2^2}, v_2 = v_2 \right\}. \tag{5.39}$$

It is interesting to note that given known initial conditions, three parameters, namely k_{Bin}, k_{Bout}, and k_{Be} are uniquely identifiable, the remaining eleven parameters, namely K_{BA}, K_D, V_{BA}, V_D, k_p, k_{Din}, k_{Dout}, k_{De}, k_a, v_1, and v_2 are unidentifiable. However the input/output map θ_{10} does not contain V_D, k_{Din}, k_{Dout}, k_{De} and k_a. It is possible to generate another input/output map θ_{11} by substituting *Equations* (5.34) - (5.38) into the fourth Lie derivative of y_1 (μ_{14}). A second input/output map $\tilde{\theta}_{11}$ is generated by substituting $\boldsymbol{p}$ for $\tilde{\boldsymbol{p}}$ in the original input/output relationship θ_{11}. Equating the monomials of μ_{11}, μ_{12}, μ_{13}, μ_{14}, μ_{21}, and μ_{22} in $\theta_{11} = \tilde{\theta}_{11}$ yields 78 equations, which Maple is unable to solve simultaneously for the unknown parameter vector. The 78 equations were therefore split into groups and each group was solved

simultaneously. The solutions were subsequently combined to yield one unique solution:

$$\boldsymbol{s}_2 = \left\{ K_{BA} = \frac{\tilde{v}_1 \tilde{K}_{BA}}{v_1}, K_D = \frac{v_1 \tilde{K}_D}{\tilde{v}_1}, V_{BA} = \frac{\tilde{v}_1 \tilde{V}_{BA}}{v_1}, V_D = \frac{v_1 \tilde{V}_D}{\tilde{v}_1}, k_{Din} = \tilde{k}_{Din}, k_{Dout} = \tilde{k}_{Dout}, k_{De} = \tilde{k}_{De}, \right.$$

$$\left. k_{Bin} = \tilde{k}_{Bin}, k_{Bout} = \tilde{k}_{Bout}, k_{Be} = \tilde{k}_{Be}, k_a = \tilde{k}_a, k_p = \frac{\tilde{k}_p \tilde{v}_1}{v_1}, v_1 = v_1, v_2 = \frac{\tilde{v}_1 \tilde{v}_2}{v_1} \right\} \quad (5.40)$$

This solution shows that, given known initial conditions, seven parameters, namely k_{Din}, k_{Dout}, k_{De}, k_{Bin}, k_{Bout}, k_a, and k_{Be} are uniquely identifiable, the remaining seven parameters, namely K_{BA}, K_D, V_{BA}, V_D, k_p, v_1, and v_2 are unidentifiable. However solving $\boldsymbol{s}_1$ from (5.39) and $\boldsymbol{s}_2$ from (5.40) simultaneously yields one unique solution:

$$\boldsymbol{s}_3 = \left\{ K_{BA} = \tilde{K}_{BA}, K_D = \tilde{K}_D, V_{BA} = \tilde{V}_{BA}, V_D = \tilde{V}_D, k_{Din} = \tilde{k}_{Din}, k_{Dout} = \tilde{k}_{Dout}, k_{De} = \tilde{k}_{De}, \right.$$

$$\left. k_{Bin} = \tilde{k}_{Bin}, k_{Bout} = \tilde{k}_{Bout}, k_{Be} = \tilde{k}_{Be}, k_a = \tilde{k}_a, k_p = \tilde{k}_p, v_1 = \tilde{v}_1, v_2 = \tilde{v}_2 \right\} \quad (5.41)$$

This confirms that the five compartment model of the form (5.18) - (5.22) is therefore structurally globally identifiable given known initial conditions (as demonstrated previously by the STAUS approach).

Unfortunately it is not possible to solve the seven Lie derivatives μ_{31}, μ_{32}, μ_{33}, μ_{34}, μ_{41}, μ_{42}, and μ_{43}, simultaneously and obtain equations for the seven states $(G, DO, TD, DI, BO, TB, BI)$ strictly in terms of those Lie derivatives.

5.2.8 Summary

The results of the structural identifiability analyses for both models are summarised in *Table* 5.3.

Table 5.3: Summary of the structural identifiability of both candidate models using all five approaches. The results for the DAACS, Ai/oRA, and NDi/oONF approaches are in brackets as they assume known initial conditions (SGI: structurally globally identifiable; DNC: does not converge; SU: structurally unidentifiable)

Approach	**Model of the form (5.1) - (5.7)**	**Model of the form (5.18) - (5.22)**	
		$v_1 \neq v_2$	$v_1 = v_2$
2.4.2.1 STAUS	DNC	SU	SGI
2.4.2.3 DAACS	(DNC)	(DNC)	(DNC)
2.4.2.4 Ai/oRA	(DNC)	(DNC)	(DNC)
2.4.2.5 NDi/oONF	(DNC)	(SGI)	(SGI)
2.4.2.6 Taylor	DNC	DNC	DNC

It has not been possible to demonstrate whether the seven compartment model of the form (5.1) - (5.7) is structurally identifiable or otherwise as none of the approaches implemented produced any conclusive results. On the other hand it is possible to demonstrate that the five compartment model of the form (5.18) - (5.22) is structurally unidentifiable using the STAUS approach. However, this method demonstrates that if the apparent volumes of distribution are equal ($v_1 = v_2$) and unknown then the model is structurally globally identifiable. Apparent volumes of distribution are a pharmacological theoretical volume that represents the total amount of blood plasma an administered compound would have to occupy if it were uniformly distributed. Although it is suspected that bile and CsA have different apparent volumes of distribution as they have significantly different molecule size; the assumption is made as a first approximation in order to be able to perform parameter estimation.

For the models developed in this chapter, the STAUS approach is the most useful, as it is the only method that produces conclusive results. It is interesting to note that the NDi/oONF approach is the only method able to generate an input/output map for the five compartment model of the form (5.18) - (5.22), however this is insufficient to demonstrate structural identifiability as this approach does not appropriately account for unknown initial conditions.

5.3 Steady State Analysis

Although the purpose of the modelling is to investigate the relevant transient behaviour, a steady state analysis was performed so that it can potentially be used at a later stage to assist in validating the models. It identifies the levels at which each compartmental quantity eventually settles and can be a useful method to obtain fundamental information on the system, the basic relationships between the compartments and for initial guesses for parameter estimation for subsequent fitting (i.e. saturation levels). Steady state analysis is performed by setting all the derivatives in the system equations to zero and solving the resulting algebraic equations for each system variable. Due to the complex non-linear nature of the equations, this was performed using a symbolic mathematical package capable of solving polynomial equations, namely Maple 2010.

As it was not possible to demonstrate whether the seven compartment model of the form (5.1) - (5.7) is structurally identifiable, this model was not taken forward for parameter estimation and consequently, the steady state analysis is not included.

5.3.1 Five compartment model of the form (5.18) - (5.22)

The steady state solutions for the five compartment model of the form (5.18) - (5.22) are shown in (5.42) - (5.44) below:

$$\boldsymbol{s}_1 = \left\{ G = 0, DO = 0, DI = 0, BO = \frac{-b_7 + \sqrt{b_7^2 - 4a_7c_7}}{2a_7}, BI = \frac{k_p}{k_{Be}} \right\} \tag{5.42}$$

$$\boldsymbol{s}_2 = \left\{ G = 0, DO = 0, DI = 0, BO = \frac{-b_7 - \sqrt{b_7^2 - 4a_7c_7}}{2a_7}, BI = \frac{k_p}{k_{Be}} \right\} \tag{5.43}$$

$$\boldsymbol{s}_3 = \left\{ G = 0, DO = -\frac{V_D + k_{Din}K_D}{k_{Din}} - \frac{k_pV_DK_{BA}(k_{Bout} + k_{Be})}{k_{Be}(k_{Bin}V_DK_{BA} - k_{Din}K_DV_{BA})}, DI = 0, \right.$$

$$\left. BO = \frac{k_pV_DK_D(k_{Bout} + k_{Be})}{k_{Be}(k_{Bin}V_DK_{BA} - k_{Din}K_DV_{BA})}, BI = \frac{k_p}{k_{Be}} \right\} \tag{5.44}$$

where

$$a_7 = k_{Be}k_{Bin}, \tag{5.45}$$

$$b_7 = -k_p(k_{Bout} + k_{Be}) + k_{Be}(K_{BA} + V_{BA}), \tag{5.46}$$

$$c_7 = -k_pK_{BA}(k_{Bout} + k_{Be}). \tag{5.47}$$

However $\boldsymbol{s}_3$ is not a valid solution as DO is negative and all the states must be positive by definition. From (5.44), in order for BO to be positive then $k_{Bin}V_DK_{BA} > k_{Din}K_DV_{BA}$, since all the parameters are strictly positive by definition, which therefore implies that DO is negative. It is also possible to show that $\boldsymbol{s}_2$ is not a valid solution either. In (5.42) and (5.43), the solutions for BO are the roots of the following quadratic equation

$$a_7 BO^2 + b_7 BO + c_7 = 0. \tag{5.48}$$

Regardless of the sign of b_7, there is only one sign change in (5.48) as a_7 is positive and c_7 is negative (since k_{Be}, k_{Bin}, k_p, K_{BA}, and k_{Bout} are all positive by definition). It can therefore be shown that only one solution is positive using Descartes' rule of signs and since

$$\frac{-b_7 + \sqrt{b_7^2 - 4a_7c_7}}{2a_7} > \frac{-b_7 - \sqrt{b_7^2 - 4a_7c_7}}{2a_7} \tag{5.49}$$

the only valid solution is therefore s_1.

To determine the stability of the steady state the system is linearised by considering the relevant Jacobian matrix ***J***. This is given by:

$$\boldsymbol{J} = \begin{bmatrix} a_{11} & k_{Dout} & \alpha_1^2 K_D V_D K_{BA} DO & 0 & k_a \\ a_{21} & -k_{Dout} - k_{De} & -\alpha_1^2 K_D V_D K_{BA} DO & 0 & 0 \\ \alpha_1^2 K_D V_{BA} K_{BA} DO & 0 & a_{33} & k_{Bout} & 0 \\ -\alpha_1^2 K_D V_{BA} K_{BA} DO & 0 & a_{43} & -k_{Bout} - k_{Be} & 0 \\ 0 & 0 & 0 & 0 & -k_a \end{bmatrix} \tag{5.50}$$

where

$$a_{11} = -\alpha_1^2 K_{BA} K_D V_D (K_{BA} + DO) - k_{Din}, \tag{5.51}$$

$$a_{21} = \alpha_1^2 K_{BA} K_D V_D (K_{BA} + DO) + k_{Din}, \tag{5.52}$$

$$a_{33} = -\alpha_1^2 K_{BA} K_D V_{BA} (K_D + DO) - k_{Bin}, \tag{5.53}$$

$$a_{43} = \alpha_1^2 K_{BA} K_D V_{BA} (K_D + DO) + k_{Bin}, \tag{5.54}$$

$$\alpha_1 = \frac{1}{K_D K_{BA} + K_{BA} DO + K_D BI}. \tag{5.55}$$

Unfortunately Maple is unable to compute the eigenvalues of the corresponding Jacobian matrix *J* for the linearised model of (5.18) - (5.22) symbolically as quintic equations are not solvable in symbolic form (Abel-Ruffini theorem). However, as the steady states for the three drug compartments G, DO, and DI are all zero, it is possible to reduce the five compartment model of the form (5.18) - (5.22) to two compartments by setting G, DO, and DI equal to zero. The corresponding system of equations therefore become

$$\frac{dBO}{dt} = k_p - \frac{V_{BA} BO}{K_{BA} + BO} + k_{Bout} BI - k_{Bin} BO \tag{5.56}$$

$$\frac{dBI}{dt} = \frac{V_{BA} BO}{K_{BA} + BO} - (k_{Bout} + k_{Be}) BI + k_{Bin} BO \tag{5.57}$$

Setting *Equations* (5.56) and (5.57) equal to zero and solving for *BO* and *BI* yields two solutions:

$$\boldsymbol{s}_4 = \left\{ BO = \frac{-b_7 + \sqrt{b_7^2 - 4a_7 c_7}}{2a_7}, BI = \frac{k_p}{k_{Be}} \right\} \tag{5.58}$$

$$\boldsymbol{s}_5 = \left\{ BO = \frac{-b_7 - \sqrt{b_7^2 - 4a_7 c_7}}{2a_7}, BI = \frac{k_p}{k_{Be}} \right\} \tag{5.59}$$

As expected, the two solutions are exactly the same as the solutions for BO and BI in $\boldsymbol{s}_1$ and $\boldsymbol{s}_2$. As shown above, $\boldsymbol{s}_2$ is not a valid solution ($\boldsymbol{s}_1$ is the only valid solution) and therefore nor is $\boldsymbol{s}_5$. It is now possible to determine the stability of the steady state

$\boldsymbol{s}_4$; the system of the form (5.56) - (5.57) is linearised by considering the relevant Jacobian matrix $\boldsymbol{J}_2$ given by:

$$\boldsymbol{J}_2 = \begin{bmatrix} -\alpha_2 & k_{Bout} \\ \alpha_2 & -k_{Bout} - k_{Be} \end{bmatrix} \tag{5.60}$$

where

$$\alpha_2 = \frac{V_{BA} K_{BA}}{(K_{BA} + BO)^2} + k_{Bin} \tag{5.61}$$

The eigenvalues of the Jacobian matrix $\boldsymbol{J}_2$ are given as roots of the following quadratic equation

$$\lambda^2 + b_8 \lambda + c_8 = 0 \tag{5.62}$$

where

$$b_8 = \alpha_2 + k_{Bout} + k_{Be} \tag{5.63}$$

$$c_8 = \alpha_2 k_{Be} \tag{5.64}$$

The parameters k_{Bout}, k_{Be}, V_{BA}, K_{BA}, k_{Bin}, and K_{BA} are all positive by definition, and therefore α_2, b_8, and c_8 are also positive. Consequently there are no sign changes in (5.62) and it can be shown that both roots of *Equation* (5.62) have the same sign using Descartes' rule of signs. The roots of *Equation* (5.62) are given as

$$\lambda_{1,2} = \frac{-b_8 \pm \sqrt{b_8^2 - 4c_8}}{2} \tag{5.65}$$

Substituting *Equations* (5.63) and (5.64) into (5.65) yields

$$\lambda_1 = \frac{-\alpha_2 - k_{Bout} - k_{Be} + \sqrt{(\alpha_2 - k_{Be})^2 + k_{Bout}(k_{Bout} + 2\alpha_2 + 2k_{Be})}}{2}, \quad (5.66)$$

$$\lambda_2 = \frac{-\alpha_2 - k_{Bout} - k_{Be} - \sqrt{(\alpha_2 - k_{Be})^2 + k_{Bout}(k_{Bout} + 2\alpha_2 + 2k_{Be})}}{2}. \quad (5.67)$$

Since k_{Bout}, α_2, and k_{Be} are positive, the term inside the square root of *Equation* (5.66) and (5.67) is positive and therefore both roots λ_1 and λ_2 are real. Since it can be shown that both roots λ_1 and λ_2 have the same sign using Descartes' rule of signs and given that λ_2 is negative (α_2, k_{Bout}, k_{Be}, and the square root are positive), both roots λ_1 and λ_2 must therefore be real and negative. Consequently the solutions $\boldsymbol{s}_4$ and $\boldsymbol{s}_5$ are stable. It can therefore be inferred that the steady state solution $\boldsymbol{s}_1$ is also stable for $G = DO = DI = 0$.

5.4 Experimental Data

Data were collected at AstraZeneca's R&D facility at Alderley Edge by Dr. Simone Stahl. Four groups of three male rats (Strain: AlpkHsdBrlHan:WIST) were administered with Cyclosporine A, Neoral™ Oral Solution. The first group was used as control and the other three groups were given different repeat oral doses, namely 15, 30, and 40 mg/kg over 14 days. The doses were administered daily (14 doses) and the dose volume was 8 ml/kg and the vehicle was aqueous 5% (w/v) glucdextroseose. Doses are converted into µmol/kg using CsA's molecular mass of 1202.61 g/mol. Measurements of CsA blood concentration and plasma bile acid (microM) were collect at five different times points (0, 2, 6, 12, and 24h) on three separate days (day 1, 4, and 11). The 0 h measurements were taken pre dose whereas

the 24h measurements were taken post dose. Only the measurements for the first day are used in the fitting as the model does not account for repeat dosing.

5.4.1 Data Analysis

The commercial software package FACSIMILE (MCPA Software, UK) was used to perform the parameter estimation. The software selection and parameter estimation procedure is detailed in *Section* 3.5.1. As described therein, FACSIMILE produces two measurements for the statistical goodness of the fit, namely a weighted residual sum of squares (RSS) and confidence levels for each estimated parameters entitled standard deviation of the natural logarithms (SDLN). As per the fitting in Chapter 3 and 4, numerous wide ranging different combinations of initial guesses were implemented in order to attempt to find a global minimum for the optimisation.

5.5 Results

The unknown rate constants are estimated using the five compartment model of the form (5.18) - (5.22) with equal apparent volumes of distribution ($v_1 = v_2$). The time series and simultaneous fits are plotted in *Figure* 5.4, where the CsA time series and fits are shown on the left hand side (*Figures* 5.4b, 5.4d, and 5.4f) and the corresponding bile acid data and fits are shown on the right hand side (*Figures* 5.4c, 5.4e, and 5.4g). There is no CsA plot for the control time series with 0 μM initial conditions, as the blood concentrations were not measured because there is no drug present.

Table 5.4 below summarises the corresponding rate constants for the fits.

Table 5.4: Parameter estimates (NWD - not well determined)

Parameters	Value	SDLN	Parameters	Value	SDLN
k_a	1.89 x 10^{-1} h^{-1}	0.504	kB_{out}	1.73 h^{-1}	NWD
kD_{in}	3.60 h^{-1}	0.400	kB_e	1.49 x 10^{1} h^{-1}	NWD
kD_{out}	8.25 x 10^{-2} h^{-1}	0.512	V_{BA}	1.30 x 10^{3} µmol h^{-1}	0.893
V_D	4.32 x 10^{-3} µmol h^{-1}	NWD	K_{BA}	1.23 µmol	NWD
K_D	1.94 x 10^{-2} µmol	0.842	B_{out}	4.19 µmol	NWD
kD_e	7.78 x 10^{-3} h^{-1}	NWD	B_{in}	4.79 x 10^{-1} µmol	NWD
k_p	9.45 x 10^{2} µmol h^{-1}	0.880	v_1	2.68 x 10^{-1} L	0.182
kB_{in}	3.26 x 10^{1} h^{-1}	0.843	RSS	83,151	-

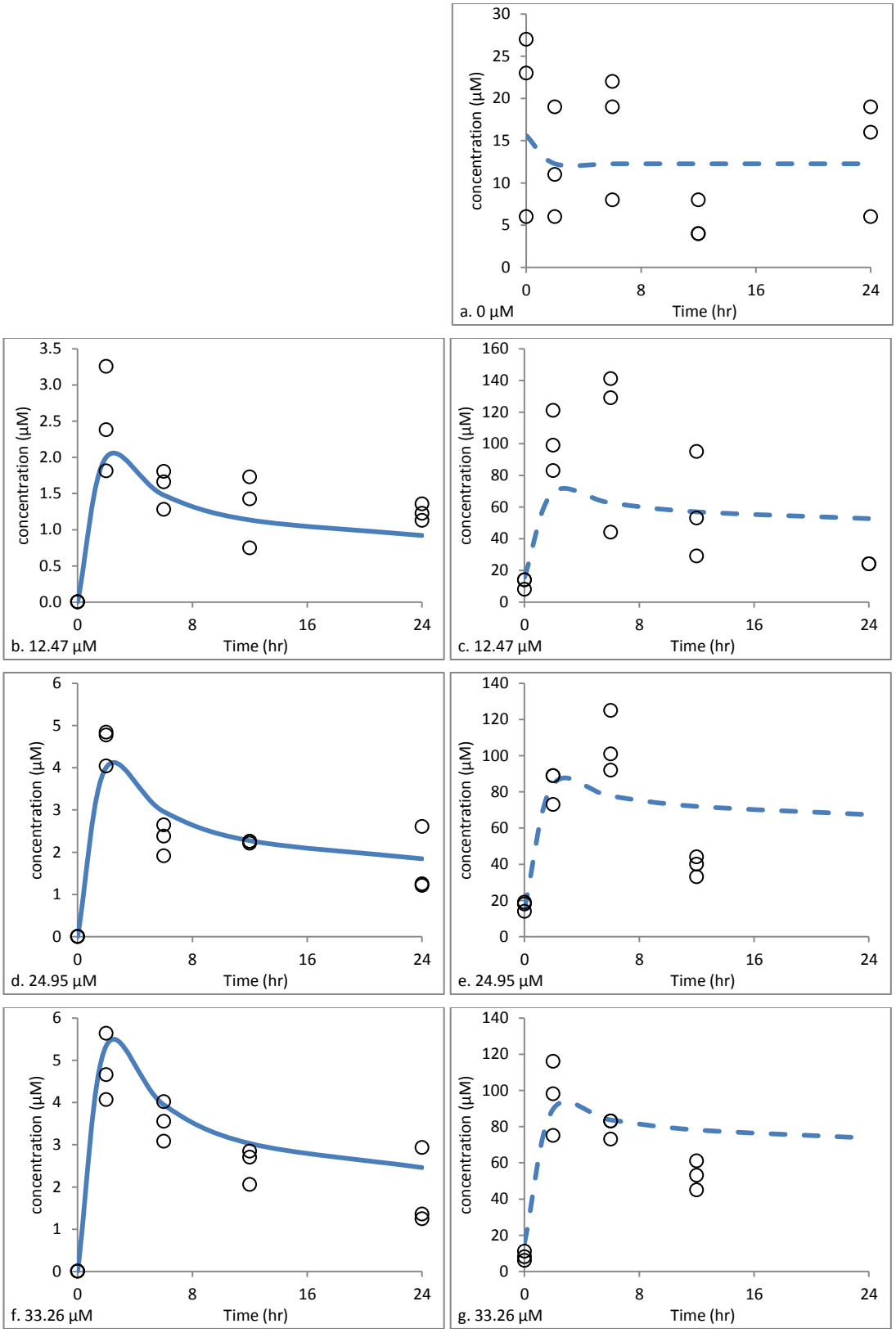

Figure 5.4: FACSIMILE fits of rat data at
different initial concentrations (0-33.26µM).
Legend: solid trace - CsA fit, dashed trace - bile fit, data - circles.

5.6 Discussion

The plots in *Figure* 5.4 show that the five compartment model of the form (5.18) - (5.22) visually fits the CsA data adequately for all three different initial concentration (*Figure* 5.4b, *Figure* 5.4d, and *Figure* 5.4f). The maximum CsA concentration occurs at two hours for all three initial concentrations as the compound is absorbed relatively rapidly and is subsequently eliminated from the blood stream at a slower rate. The peak CsA concentration increase non-linearly with increased initial doses of CsA. The average CsA concentration at two hours is 2.48 µM for the 12.47 µM initial CsA concentration (*Figure* 5.4b), 4.55 µM for the 24.95 µM initial CsA concentration (*Figure* 5.4d), and 4.79 µM for the 33.26 µM initial CsA concentration (*Figure* 5.4f). This highlights the non-linear nature of the uptake and the relatively small increase in peak CsA concentrations of 0.24 µM (4.79 - 4.55 µM) for the 8.31 µM (33.26 - 24.95 µM) increase in initial concentration between the two highest initial concentrations suggests that the uptake is close to saturation at those values.

Conversely, the bile acid concentration fits are not as good. The fits peak at two hours, whereas the data appear to peak at six hours for the 12.47 µM and 24.95 µM initial concentrations (*Figure* 5.4*c* and Figure 5.4e). For the 33.26 µM initial concentration (*Figure* 5.4g), the data and the fit both peak at two hours, however the fit appears to overestimate the data for the later time point, which is also noticeable in the other plots. This is not a surprising result as there is only one bile acid concentration time point at 24 hours for the three plots with CsA (*Figure* 5.4c, *Figure* 5.4e, and *Figure* 5.4g). In comparison, most of the other measurement times have three data points for each measurement time and initial concentration of CsA.

In total, there are 33 bile acid concentration measurements for the first 12 hours and only one post 12 hours. Considering that FACSIMILE minimises the total residual sum of squares (RSS) for all the data points, this uneven measurement distribution has the effect of heavily weighting the first 12 hours. It is therefore necessary to repeat the experiments and obtain more bile acid measurements later on in the experiment in order to be able to fit the data more accurately across the 24 hours.

The fit for the lowest initial concentration of CsA, i.e. 12.47 µM (*Figure* 5.4g), grossly underestimates the data for the first two non-zero time points (2h and 6h). However it is important to note that the peak bile acid concentration is higher for the 12.47 µM initial concentration (*Figure* 5.4g) than the other two initial concentrations (*Figure* 5.4e and *Figure* 5.4g). This is an unexpected result as it is understood that higher concentrations of CsA should correlate to higher bile acid concentrations. Furthermore, the range between the three subjects is inconsistent and particularly large at 6 hours in *Figure* 5.4g; 97 µM range compared to a mean measurement of 105 µM. It is suspected that the eating patterns of the rats affected the bile acid concentration measurements, as the animals have access to food throughout the assay and their food intake and times were not monitored. The quantity and timing of when the test subjects feed is likely to affect their bile acid concentrations.

The control plot with no CsA present (*Figure* 5.4a) shows how the base bile acid concentrations fluctuate throughout 24 hours. Again the range (23 µM) is very large compared to the mean concentration for all three animals (13 µM) and the intra subject variability is suspected to arise from the different feeding patterns of the animals. It is therefore recommended to repeat the experiments with a fixed feeding protocol to ascertain whether this is one of the factors responsible for the variability in the bile acid measurements. It is suspected that bile acids levels do vary

significantly between subjects; however any reduction in the range would be advantageous for fitting the data more accurately. Although it is a very small discrepancy, it is also interesting to note from the control plot with no CsA present (*Figure* 5.4a), that the initial bile acid concentration at 0 hours is slightly higher than the remaining steady state level. Nonetheless, the fit for the control plot with no CsA present (*Figure* 5.4a) visually describes the bile acid data adequately, that is to say apart from the small artefact at the beginning the fit is at steady state and close to the mean concentration of 13 μM. The slightly larger value at time zero occurs because the initial quantity of bile acid in the blood stream, B_{out}, is a variable that FACSIMILE is estimating across all the time series (including when there is CsA present).

In

Table 5.4, four of the six parameters associated with CsA kinetics (k_a, k_{Din}, k_{Dout}, k_{De}, K_D, and V_D) are well determined, whereas only three out of the eight bile acids parameters (k_p, k_{Bin}, k_{Bout}, k_{Be}, K_{BA}, V_{BA}, B_{in}, and B_{out}) are well determined. All the CsA parameters' SDLN values (0.400 - 0.842) are also lower than the bile acid parameters (0.843 - 0.893), reflecting the plots in *Figure* 5.4, which show that the five compartment model of the form (5.18) - (5.22) describes the CsA kinetics much better than the bile acids kinetics. Overall, seven out of the fifteen parameters estimated, i.e. almost half, are not well determined (NWD) by the data available. From the remaining eight, only two, namely k_{Din} and v_1, have SDLN values below 0.5. As a whole, the five compartment model of the form (5.18) - (5.22) describes the *in vivo* CsA binding kinetics precisely but does not capture the bile acid kinetics very well, which is not wholly unexpected given the relatively small number of data

points available. Although model improvements are suggested below, the main reason for the latter is the poor quality of the data. The feeding protocol for the experiments needs to be controlled and more frequent data should be collected. In particular for the later time point of 24 hours; one data point is not sufficient to model the competitive kinetics accurately. Another issue is the repeatability of the bile acid concentration measurements; with a range of almost 100μM for some bile acids measurements, it would as a consequence prove problematic to fit to the data accurately.

5.6.1 Suggested model improvements

As described previously, bile acids are surfactants and their subsequent detergent-like properties have been shown to be cytotoxic. As a result their concentrations are tightly regulated by feedback control mechanisms that activate when their concentration is too high. The liver and the intestines contain FXR, a nuclear hormone receptor with the gene name NR1H4. Bile acids function as a signalling molecule for FXR and its activation in the liver inhibits the synthesis of bile acids. Activation of FXR by bile salts during digestion in the intestine promotes transcription and synthesis of FGF19, which subsequently inhibits bile acid production in the liver (Kim et al. 2007). Consequently bile acid synthesis is not constant if their concentration is too elevated. A feedback mechanism to replicate bile acid synthesis inhibition may improve the model accuracy.

Another proposed alteration is to use different apparent volumes of distribution for CsA and the bile acid. One volume value was used for both in order to make the five compartment model of the form (5.18) - (5.22) structurally globally identifiable (see *Section* 5.2.3). However it may prove advantageous to use values from the literature

for the volumes, as the five compartment model of the form (5.18) - (5.22) has been demonstrated by both the STAUS and NDi/oONF approaches to be structurally globally identifiable for known initial conditions. An improvement is the fitting is expected as it is suspected the apparent volumes of distribution are different. An additional advantage of this modification would be reducing the total number of unknown parameters as the volumes would now be known. This could also be achieved via a model reparametrisation, which in turn reduces the total number of degrees of freedom (DoF) and may assist FACSIMILE to improve the fits, both in term of the RSS and SDLN values, as shown in Chapter 3.

5.7 Conclusions

The *in vivo* disposition of the established OATP substrate Cyclosporin A (CsA) has been evaluated in rat using a non-linear pharmacokinetic model. The mechanistic model describes the competitive binding that occurs between CsA and bile acids in the liver and combines the characteristics from two *in vitro* data models developed in previous chapters. The *in vitro* binding kinetics of Pitavastatin to OATP were investigated in three species, (rat, dog, and man) in *Chapter* 4. A mechanistic model was found to describe experimental data accurately and its mechanisms are incorporated in the *in vivo* data model described in this chapter. Similarly, the *in vitro* competitive binding kinetics of Hoeschst 33342 and a potent inhibitor Fumitremorgin C (FTC) to breast cancer resistance protein (BCRP) were investigated in *Chapter* 3. Although BCRP and OATP are different transporters which utilise different processes to translocate substances across cell membranes, the competitive binding for the limited number of binding sites on the transporters is

believed to be analogous and therefore this element of the model is incorporated in the *in vivo* data model described in this chapter.

The five compartment model of the form (5.18) - (5.22) with equal apparent volumes of distribution ($v_1 = v_2$) has been shown to be structurally identifiable using the similarity transformation approach for uncontrolled systems (STAUS) described in *Section* 2.3.2.1. With individual apparent volumes of distribution, the model is shown to be structurally unidentifiable. Other methods were also implemented in order to investigate their suitability for performing the analyses; however none were able to produce conclusive results. The NDi/oONF approach is the only method able to generate an input/output map for the five compartment model of the form (5.18) - (5.22), however this is insufficient to demonstrate structural identifiability as this approach does not account for unknown initial conditions. The structural identifiability analyses show that the five compartment model of the form (5.18) - (5.22) with equal apparent volumes of distribution is uniquely identifiable for the experiments/observations available, adding greater confidence to the numerical parameter estimation carried out.

The five compartment model of the form (5.18) - (5.22) is derived on mechanistic principles based on knowledge of the processes considered and describes the OATP binding kinetics of CsA accurately, endorsing the applicability and robustness of the model developed in Chapter 4 for both *in vitro* and *in vivo* applications. Additionally most of the parameters and rate constants have been estimated to a reasonable degree of accuracy, characterising substrate binding to OATP with transportation into hepatic cells numerically.

Unfortunately the model of the form (5.18) - (5.22) does not describe the bile acid concentration measurements very accurately. However there are significant issues with the quantity and quality of the bile acid data; better quality and more frequent data are required in order to develop the model further via incremental changes. It may be possible that inherent bile acid inter-subject variability is too large in order to model the mechanism precisely. Further work is therefore required to investigate the competitive binding between CsA and bile acids, using other compounds, to ascertain the suitability of the model and potentially propose a more robust model for the prediction of uptake at different dose levels.

5.8 References

DeSesso, J. M., & Jacobson, C. F. (2001). Anatomical and physiological parameters affecting gastrointestinal absorption in humans and rats. *Food and Chemical Toxicology*, *39*(3), 209-228.

Endres, C. J., Hsiao, P., Chung, F. S., & Unadkat, J. D. (2006). The role of transporters in drug interactions. *European journal of pharmaceutical sciences*, *27*(5), 501-517.

Hagenbuch, B., & Gui, C. (2008). Xenobiotic transporters of the human organic anion transporting polypeptides (OATP) family. *Xenobiotica*, *38*(7-8), 778-801.

Higuchi, H., & Gores, G. J. (2003). IV. Bile acids and death receptors. *American Journal of Physiology-Gastrointestinal and Liver Physiology*, *284*(5), G734-G738.

Hofmann, A. F., & Borgström, B. (1964). The intraluminal phase of fat digestion in man: the lipid content of the micellar and oil phases of intestinal content obtained during fat digestion and absorption. *Journal of Clinical Investigation*, *43*(2), 247.

Hofmann, A. F. (1999). The continuing importance of bile acids in liver and intestinal disease. *Archives of internal medicine*, *159*(22), 2647.

Hofmann, A. F., (2002). Cholestatic liver disease: pathophysiology and therapeutic options. *Liver*, *22*(s2), 14-19.

Huang, W., M, K., Zhang, J., Qatanani, M., Cuvillier, J., Liu, J., & Moore, D. D. (2006). Nuclear receptor-dependent bile acid signaling is required for normal liver regeneration. *Science*, *312*(5771), 233-236.

Kim, I., Morimura, K., Shah, Y., Yang, Q., Ward, J. M., & Gonzalez, F. J. (2007). Spontaneous hepatocarcinogenesis in farnesoid X receptor-null mice. *Carcinogenesis*, *28*(5), 940-946.

Kim, I., Ahn, S. H., Inagaki, T., Choi, M., Ito, S., Guo, G. L., & Gonzalez, F. J. (2007). Differential regulation of bile acid homeostasis by the farnesoid X receptor in liver and intestine. *Journal of lipid research*, *48*(12), 2664-2672.

Krone, C. L. (1970). Defective intraluminal lipid digestion following ileectomy. *Arizona medicine*, *27*(4), 99.

Rust, C., Karnitz, L. M., Paya, C. V., Moscat, J., Simari, R. D., & Gores, G. J. (2000). The bile acid taurochenodeoxycholate activates a phosphatidylinositol 3-kinase-dependent survival signaling cascade. *Journal of Biological Chemistry*, *275*(26), 20210-20216.

Shaffer, E. A. (2000). Review article: control of gall-bladder motor function. *Alimentary pharmacology & therapeutics*, *14*(s2), 2-8.

Stellwag, E. J., & Hylemon, P. B. (1979). 7alpha-Dehydroxylation of cholic acid and chenodeoxycholic acid by Clostridium leptum. *Journal of lipid research*, *20*(3), 325-333.

Van Deest, B. W., Fordtran, J. S., Morawski, S. G., & Wilson, J. D. (1968). Bile salt and micellar fat concentration in proximal small bowel contents of ileectomy patients. *Journal of Clinical Investigation*, *47*(6), 1314.

Watanabe, M., Houten, S. M., Mataki, C., Christoffolete, M. A., Kim, B. W., Sato, H., & Auwerx, J. (2006). Bile acids induce energy expenditure by promoting intracellular thyroid hormone activation. *Nature*, *439*(7075), 484-489.

Westergaard, H. (2007). Bile acid malabsorption. *Current treatment options in gastroenterology*, *10*(1), 28-33.

Yang, F., Huang, X., Yi, T., Yen, Y., Moore, D. D., & Huang, W. (2007). Spontaneous development of liver tumors in the absence of the bile acid receptor farnesoid X receptor. *Cancer research*, *67*(3), 863-867.

Chapter 6

Conclusions

Mathematical modelling using compartmental analysis of transporter kinetics has been investigated using existing knowledge of the biological processes considered. The motivation for this work was to describe breast cancer resistance protein (BCRP) cellular efflux and organic anion transporting polypeptide (OATP) hepatic uptake using physiologically based pharmacokinetic (PBPK) modelling to gain mechanistic insights into the complex and often non-linear physiological processes present. Furthermore, *in vitro* competitive binding to BCRP was investigated using a potent inhibitor, Fumitremorgin C (FTC). Similarly *in vivo* competitive binding to OATP between bile acid and an immunosuppressant drug, Cyclosporin A (CsA), was explored.

6.1 BCRP Models

The two mathematical models derived in Chapter 3 adequately reproduced the observed time series data provided by AstraZeneca. The parameter estimates across experimental values for total number of binding sites on the transporter and the nucleus did not differ greatly between experimental conditions, which suggested that the conditions within each well of the multi-well plate are similar.

The models fit their purpose, as they adequately describe the data observed and are derived on mechanistic principles based on knowledge of the biological processes considered. Additionally all the parameters and rate constants have been estimated to

a reasonable degree of accuracy, which can be judged by the SDLN values produced by FACSIMILE for each parameter characterising substrate binding to DNA with transportation of the substrate out of the cell numerically. Given these estimates, the binding affinity of FTC for the BCRP transporter was calculated to be $1.67 \times 10^{-5}\,\mu\mathrm{M}$. It can further be seen that BCRP mediated cellular kinetics can be indirectly measured in this way.

6.2 OATP Models

The *in vitro* disposition of OATP binding kinetics was characterised using two non-linear pharmacokinetic models, one for rat and human and another for dog. Previously modelling has not considered dog and human data. The models developed in this thesis offer significant advantages over the three mechanistic models published previously, namely Paine *et al.*, 2008; Poirier *et al.*, 2008; Menochet *et al.* 2012, which studied rat hepatocytes, Chinese hamster ovary control cells, and artificial membranes. One of the main limitations of the previous modelling is the data analysis, in particular the choice of numerical integrator for the parameter fitting; the models developed in Chapter 4 were found to be highly stiff (see *Table* 4.14) and the numerical integrators implemented in the previously published models (Runge-Kutta and algorithms present in Matlab) are likely to struggle with highly stiff systems and hence with parameter estimation. FACSIMILE's numerical integrator used for the modelling in this thesis is able to handle highly stiff systems and give greater confidence to the parameter estimates obtained. Furthermore, although these mechanistic model are suspected to be superior to the conventional two step approach, the authors do not offer a measure for the goodness of fit of their results and it is therefore impossible to establish

whether their respective models are an improvement. It is therefore the first time the underlying assumption supporting the conventional two step approach is comprehensively debunked using statistical testing.

In Chapter 4, fits of numerous concentration data profiles are directly compared to the conventional two step approach for three species (rat, dog and human), offering not only an advantage in terms of the number of species evaluated, but also allowing for statistical comparison as to which fits describe the data more accurately. This analysis demonstrates that both models proposed characterise the data more accurately than the conventional two step approach for all three species (rat, dog and human), and that the estimated passive diffusion rates from 37°C data are significantly different to those estimated from 4°C data. This suggests that the current widely accepted view, that the rate of diffusion of Pitavastatin into the cell is the same at both 4°C and 37°C, but that the transporter action only occurs at 37°C, is inaccurate. It follows that 37°C data should be fitted independently and it is therefore unnecessary to collect 4°C data altogether, potentially cutting down the number of experiments performed, reducing costs and supporting the 3Rs.

Steady state analysis on both models revealed that the model for rat and human hepatocytes is more robust to different initial concentrations of Pitavastatin than the three compartment model for the dog data. The most sensitive parameters are r_3 and K_M for the rat and human model, whereas the most sensitive parameters for the dog model depend on the initial concentration of Pitavastatin: k_1, r_3, and T_0 are the most sensitive at low initial concentrations and only r_3 and T_0 are the most sensitive at the higher initial concentrations.

The *in vivo* disposition of the established OATP substrate Cyclosporin A (CsA) was subsequently evaluated in rat. The mechanistic model developed describes the competitive binding that occurs between CsA and bile acids in the liver and combines the characteristics from the *in vitro* data models developed in Chapters 3 and 4, and characterises the OATP binding kinetics of CsA accurately, offering some validation to the applicability and robustness of the model developed in Chapter 4 for both *in vitro* and *in vivo* applications. Additionally most of the parameters and rate constants have been estimated to a reasonable degree of accuracy, characterising *in vivo* substrate binding to OATP with transportation into hepatic cells numerically. However the model developed does not describe the bile acid concentration measurements very precisely, mainly due to the poor quantity and quality of the bile acid data, thus further work with more data is required.

6.3 Passive Diffusion vs Active transport

As described in Chapter 2, it has only been recently proposed that carrier mediated cellular uptake is responsible for most of the membrane drug transport in biological systems. Up until this point it had generally been widely accepted that numerous medicinal molecules were transported across biological membranes via simple diffusion alone. This has been an area of contention; with completely different points of view expressed in the literature. Sugano *et al.* 2010 support the view that passive diffusion and carrier mediated cellular transport coexist in membrane drug transport, both having a vital role and their relative importance being dependent on the specific drug and conditions. By contrast, Kell *et al*. 2011 assert that drug transport through biological membranes is in fact almost exclusively carrier mediated. However all the models developed in this thesis include both passive diffusion and active transport,

as they were found to describe experimental data more accurately than each process on its own, in line with all of the latest evidence on drug transport (Di *et al.* 2012).

6.4 Structural Identifiability and Indistinguishability Analyses

Structural identifiability analyses were performed on all the models developed in this thesis using a variety of methods applicable to non-linear systems. The similarity transformation approach for uncontrolled systems (STAUS) proved the most useful for the models developed in Chapters 3 and 5, whereas the Algebraic Input/Output Relationship Approach (Ai/oRA) was the most successful in terms of obtaining conclusive results for the models developed in Chapter 4. These two methods consistently outperform the Differential Algebra Approach Using Characteristic Sets (DAACS) and Non-differential Input/Output Observable Normal Form Approach (NDi/oONF). The Taylor series expansion approach proves to be the least suitable in all cases. Other methods were also implemented, but failed to produce solutions. The direct test (Denis-Vidal & Joly-Blanchard 2000) is not applicable for most of the models described in this thesis as it requires measuring at least one compartment directly. DAISY (Bellu *et al.* 2007) is another differential algebra method software base tool, which is less efficient and generally unable to solve the algebraic equations generated. GenSSI (Chis *et al.* 2011) produces identifiability tableaus and reduces them sequentially but fails to solve the remaining equations in most cases.

The structural identifiability analyses show that all models used for parameter estimation are uniquely identifiable for the experiments/observations available, adding greater confidence to the numerical parameter estimation carried out.

6.5 Further work

Further work is required to investigate the competitive binding between Hoechst 33342 and FTC, using other inhibitors, with a view to elucidate the small discrepancies between the two models' parameter estimates. The intention here would be to produce simultaneous fits of different inhibitors across different initial concentrations whilst keeping the Hoechst kinetics common. The author also recommends investigating if the pseudo steady state assumption from *Section* 5.1.2 could be applied to the BCRP model. Incremental changes and improvements should ultimately propose a more robust model for prediction of uptake at different dose levels. Such a model has the potential to be used to estimate the dosage levels required in order to achieve the levels of absorption desired once bound to DNA.

More data are required in order to develop the *in vivo* OATP model further. It may be possible that inherent bile acid inter-subject variability is too large in order to model the mechanism precisely and mixed effects modelling should therefore be considered. Further work is required to investigate the competitive binding between CsA and bile acid, using other compounds, to ascertain the suitability of the model and potentially propose a more robust model for prediction of uptake at different dose levels.

6.6 References

Bellu, G., Saccomani, M. P., Audoly, S., D'Angio, L. (2007) DAISY: A new software tool to test global identifiability of biological and physiological systems, *Comput. Methods Programs Biomed.* Vol 88, 52-61

Chiş, O., Banga, J. R., & Balsa-Canto, E. (2011). GenSSI: a software toolbox for structural identifiability analysis of biological models. *Bioinformatics*, *27*(18), 2610-2611.

Denis-Vidal, L., Joly-Blanchard, G. (2000). An easy to check criterion for (un)identifiability of uncontrolled systems and its applications. IEEE Transactions on Automatic Control 45: 768-771.

Di, L., Artursson, P., Avdeef, A., Ecker, G. F., Faller, B., Fischer, H., & Sugano, K. (2012). Evidence-based approach to assess passive diffusion and carrier-mediated drug transport. *Drug discovery today*, *17*(15), 905-912.

Kell, D. B., Dobson, P. D., & Oliver, S. G. (2011). Pharmaceutical drug transport: the issues and the implications that it is essentially carrier-mediated only. *Drug discovery today*, *16*(15), 704-714.

Sugano, K., Kansy, M., Artursson, P., Avdeef, A., Bendels, S., Di, L., & Senner, F. (2010). Coexistence of passive and carrier-mediated processes in drug transport. *Nature reviews Drug discovery*, *9*(8), 597-614.

Appendix A

Maple code for demonstrating that the reduced model of the form (3.23) - (3.27) is structurally globally identifiable (SGI) using the STAUS approach.

```
restart
with(LinearAlgebra) :
eqn1 := -kSin·SO + kSout·SI + kStran·TS :
eqn2 := kSin·SO − kSout·SI − kSplus·SI·(T0 − TS) + kSminus·TS
      − kNplus·SI·(N0 − NS) + kNminus·NS :
eqn3 := kSplus·SI·(T0 − TS) − kSminus·TS − kStran·TS :
eqn4 := kNplus·SI·(N0 − NS) − kNminus·NS :
simplify(eqn1 + eqn2 + eqn3 + eqn4);
S := {SO = Ds − NS − SI − TS, } :
eq2 := subs(S, eqn2) :
eq3 := subs(S, eqn3) :
eq4 := subs(S, eqn4) :
```

$$0$$

```
F := Vector([eq2, eq3, eq4 ]) :
lieDer[0] := NS :
N := Dimension(F) :
vars := [SI, TS, NS] :
v := map( (a, b) → diff(b, a), vars, lieDer[0]) :
V[1] := Vector_row([seq(v[t], t = 1 .. N) ]) :

lieDer[1] := simplify(DotProduct(F, V[1], conjugate = false)) :
v := map( (a, b) → diff(b, a), vars, lieDer[1]) :
V[2] := Vector_row([seq(v[t], t = 1 .. N) ]) :

lieDer[2] := simplify(DotProduct(F, V[2], conjugate = false)) :
v := map( (a, b) → diff(b, a), vars, lieDer[2]) :
V[3] := Vector_row([seq(v[t], t = 1 .. N) ]) :

lieDer[3] := simplify(DotProduct(F, V[3], conjugate = false)) :
ORC := Matrix([seq([V[t]], t = 1 .. N) ]) :
ORC0 := subs({SI = 0, TS = 0, NS = 0}, ORC) :
Rank(ORC0)
```

$$3$$

```
Hp := Vector([seq(μ[i] = lieDer[i], i = 0 ..N) ]) :
S1 := {kSin = kbSin, kSout = kbSout, kStran = kbStran, kSplus
     = kbSplus, kSminus = kbSminus, kNplus = kbNplus, kNminus
     = kbNminus, N0 = N0b, T0 = T0b, Ds = Dbs} :

Hpb := subs(S1, Hp) :
Hpλ := subs([SI = λ1, TS = λ2, NS = λ3],Hp) :
temp := solve([Hpλ(1) − Hpb(1), Hpλ(2) − Hpb(2), Hpλ(3)
     − Hpb(3) ], [λ1, λ2, λ3]) :

lhs(temp[1][1]), lhs(temp[1][2]), lhs(temp[1][3])
```

$$\lambda_1, \lambda_2, \lambda_3$$

$\Lambda := Vector([rhs(temp[1][1]), rhs(temp[1][2]), rhs(temp[1][3])])$:

$\Lambda x0p := subs([SI = 0, TS = 0, NS = 0], \Lambda)$:

$sa := \{\Lambda x0p[1] = 0, \Lambda x0p[2] = 0, \Lambda x0p[3] = 0\}$:

$F\lambda := simplify(subs([SI = \Lambda_1, TS = \Lambda_2, NS = \Lambda_3], F))$:

$t1 := Vector([\mathrm{diff}(\Lambda_1, SI), \mathrm{diff}(\Lambda_2, SI), \mathrm{diff}(\Lambda_3, SI)])$:

$t2 := Vector([\mathrm{diff}(\Lambda_1, TS), \mathrm{diff}(\Lambda_2, TS), \mathrm{diff}(\Lambda_3, TS)])$:

$t3 := Vector([\mathrm{diff}(\Lambda_1, NS), \mathrm{diff}(\Lambda_2, NS), \mathrm{diff}(\Lambda_3, NS)])$:

$d\Lambda := Matrix([t1, t2, t3])$:

$Fb := subs(S1, F)$:

$d\Lambda Fb := simplify(d\Lambda Fb)$:

$t1 := simplify(d\Lambda Fb(1) - F\lambda(1))$:

$t2 := simplify(d\Lambda Fb(2) - F\lambda(2))$:

$t3 := simplify(d\Lambda Fb(3) - F\lambda(3))$:

$ta1 := collect(\mathrm{numer}(t1), vars, distributed)$:

$ta2 := collect(\mathrm{numer}(t2), vars, distributed)$:

$ta3 := collect(\mathrm{numer}(t3), vars, distributed)$:

$s1 := \{coeffs(ta1, vars)\}$:

$s2 := \{coeffs(ta2, vars)\}$:

$s3 := \{coeffs(ta3, vars)\}$:

$s := solve(\{op(sa), op(s1), op(s2), op(s3)\}, \{kSin, kSout, kStran, kSplus, kSminus, kNplus, kNminus, N0, T0, Ds\})[\,]$;

$Ds = Dbs, N0 = N0b, T0 = T0b, kNminus = kbNminus, kNplus = kbNplus, kSin = kbSin, kSminus = kbSminus, kSout = kbSout, kSplus = kbSplus, kStran = kbStran$

APPENDIX A

Maple code for demonstrating that the full model of the form (3.11) - (3.18) is structurally globally identifiable (SGI) using the STAUS approach.

```
restart
with(LinearAlgebra):
eqn1 := -kSin·SO + kSout·SI + kStran·TS:
eqn2 := kSin·SO - kSout·SI - kSplus·SI·(T0 - TS - TI) + kSminus
     ·TS - kNplus·SI·(N0 - NS) + kNminus·NS:
eqn3 := -kIin·IO + kIout·II + kItran·TI:
eqn4 := kIin·IO - kIout·II - kIplus·II·(T0 - TS - TI) + kIminus
     ·TI:
eqn5 := kSplus·SI·(T0 - TS - TI) - kSminus·TS - kStran·TS:
eqn6 := kIplus·II·(T0 - TS - TI) - kIminus·TI - kItran·TI:
eqn7 := kNplus·SI·(N0 - NS) - kNminus·NS:
simplify(eqn1 + eqn2 + eqn3 + eqn4 + eqn5 + eqn6 + eqn7);
S := {SO = Ds - NS - SI - TS, IO = Di - II - TI}:
eq2 := subs(S, eqn2):
eq4 := subs(S, eqn4):
eq5 := subs(S, eqn5):
eq6 := subs(S, eqn6):
eq7 := subs(S, eqn7):
```

0

```
F := Vector([eq2, eq4, eq5, eq6, eq7]):
lieDer[0] := NS:
N := Dimension(F):
vars := [SI, II, TS, TI, NS]:
v := map((a,b) -> diff(b,a), vars, lieDer[0]):
V[1] := Vector_row([seq(v[t], t = 1..N)]):

lieDer[1] := simplify(DotProduct(F, V[1], conjugate = false)):
v := map((a,b) -> diff(b,a), vars, lieDer[1]):
V[2] := Vector_row([seq(v[t], t = 1..N)]):

lieDer[2] := simplify(DotProduct(F, V[2], conjugate = false)):
v := map((a,b) -> diff(b,a), vars, lieDer[2]):
V[3] := Vector_row([seq(v[t], t = 1..N)]):

lieDer[3] := simplify(DotProduct(F, V[3], conjugate = false)):
v := map((a,b) -> diff(b,a), vars, lieDer[3]):
V[4] := Vector_row([seq(v[t], t = 1..N)]):

lieDer[4] := simplify(DotProduct(F, V[4], conjugate = false)):
v := map((a,b) -> diff(b,a), vars, lieDer[4]):
V[5] := Vector_row([seq(v[t], t = 1..N)]):

lieDer[5] := simplify(DotProduct(F, V[5], conjugate = false)):
ORC := Matrix([seq([V[t]], t = 1..N)]):
ORC0 := subs({SI = 0, II = Di - Dio, TS = 0, TI = 0, NS = 0}, ORC):
Rank(ORC0)
```

5

```
Hp := Vector([seq(μ[i] = lieDer[i], i = 0..N)]):
```

$$S1 := \{kSin = kbSin, kSout = kbSout, kStran = kbStran, kSplus = kbSplus, kSminus = kbSminus, kIin = kbIin, kIout = kbIout, kItran = kbItran, kIplus = kbIplus, kIminus = kbIminus, kNplus = kbNplus, kNminus = kbNminus, N0 = N0b, T0 = T0b, Ds = Dbs, Di = Dbi\} :$$

$$Hpb := subs(S1, Hp) :$$

$$Hp\lambda := subs\left(\left[SI = \lambda_1, II = \lambda_2, TS = \lambda_3, TI = \lambda_4, NS = \lambda_5\right], Hp\right) :$$

$$temp := solve\left([Hp\lambda(1) - Hpb(1), Hp\lambda(2) - Hpb(2), Hp\lambda(3) - Hpb(3), Hp\lambda(4) - Hpb(4), Hp\lambda(5) - Hpb(5)], \left[\lambda_1, \lambda_2, \lambda_3, \lambda_4, \lambda_5\right]\right) :$$

$$lhs(temp[1][1]), lhs(temp[1][2]), lhs(temp[1][3]), lhs(temp[1][4]), lhs(temp[1][5])$$

$$\lambda_1, \lambda_2, \lambda_3, \lambda_4, \lambda_5$$

$$\Lambda := Vector([rhs(temp[1][1]), rhs(temp[1][2]), rhs(temp[1][3]), rhs(temp[1][4]), rhs(temp[1][5])]) :$$

$$\Lambda x0p := subs([SI = 0, II = Dbii, TS = 0, TI = 0, NS = 0], \Lambda) :$$

$$sa := \{\Lambda x0p[1] = 0, \Lambda x0p[2] = Dii, \Lambda x0p[3] = 0, \Lambda x0p[4] = 0, \Lambda x0p[5] = 0\} :$$

$$F\lambda := simplify\left(subs\left(\left[SI = \Lambda_1, II = \Lambda_2, TS = \Lambda_3, TI = \Lambda_4, NS = \Lambda_5\right], F\right)\right) :$$

$$t1 := Vector\left(\left[\mathrm{diff}\left(\Lambda_1, \mathrm{SI}\right), \mathrm{diff}\left(\Lambda_2, SI\right), \mathrm{diff}\left(\Lambda_3, \mathrm{SI}\right), \mathrm{diff}\left(\Lambda_4, SI\right), \mathrm{diff}\left(\Lambda_5, \mathrm{SI}\right)\right]\right) :$$

$$t2 := Vector\left(\left[\mathrm{diff}\left(\Lambda_1, II\right), \mathrm{diff}\left(\Lambda_2, II\right), \mathrm{diff}\left(\Lambda_3, II\right), \mathrm{diff}\left(\Lambda_4, II\right), \mathrm{diff}\left(\Lambda_5, II\right)\right]\right) :$$

$$t3 := Vector\left(\left[\mathrm{diff}\left(\Lambda_1, TS\right), \mathrm{diff}\left(\Lambda_2, TS\right), \mathrm{diff}\left(\Lambda_3, \mathrm{TS}\right), \mathrm{diff}\left(\Lambda_4, TS\right), \mathrm{diff}\left(\Lambda_5, \mathrm{TS}\right)\right]\right) :$$

$$t4 := Vector\left(\left[\mathrm{diff}\left(\Lambda_1, \mathrm{TI}\right), \mathrm{diff}\left(\Lambda_2, TI\right), \mathrm{diff}\left(\Lambda_3, TI\right), \mathrm{diff}\left(\Lambda_4, TI\right), \mathrm{diff}\left(\Lambda_5, TI\right)\right]\right) :$$

$$t5 := Vector\left(\left[\mathrm{diff}\left(\Lambda_1, \mathrm{NS}\right), \mathrm{diff}\left(\Lambda_2, NS\right), \mathrm{diff}\left(\Lambda_3, \mathrm{NS}\right), \mathrm{diff}\left(\Lambda_4, NS\right), \mathrm{diff}\left(\Lambda_5, \mathrm{NS}\right)\right]\right) :$$

$$d\Lambda := Matrix([t1, t2, t3, t4, t5]) :$$

$$Fb := subs(S1, F) :$$

$$d\Lambda Fb := simplify(d\Lambda Fb) :$$

$$t1 := simplify(d\Lambda Fb(1) - F\lambda(1)) :$$

$$t2 := simplify(d\Lambda Fb(2) - F\lambda(2)) :$$

$$t3 := simplify(d\Lambda Fb(3) - F\lambda(3)) :$$

$$t4 := simplify(d\Lambda Fb(4) - F\lambda(4)) :$$

$$t5 := simplify(d\Lambda Fb(5) - F\lambda(5)) :$$

$$ta1 := collect(\mathrm{numer}(t1), \mathrm{vars}, distributed) :$$

$$ta2 := collect(\mathrm{numer}(t2), \mathrm{vars}, distributed) :$$

$ta3 := collect(\text{numer}(t3), \text{vars}, distributed)$:
$ta4 := collect(\text{numer}(t4), \text{vars}, distributed)$:
$ta5 := collect(\text{numer}(t5), \text{vars}, distributed)$:
$s1 := \{coeffs(ta1, vars)\}$:
$s2 := \{coeffs(ta2, vars)\}$:
$s3 := \{coeffs(ta3, vars)\}$:
$s4 := \{coeffs(ta4, vars)\}$:
$s5 := \{coeffs(ta5, vars)\}$:
$s := solve(\{op(sa), op(s1), op(s2), op(s3), op(s4), op(s5)\}, \{kSin, kSout, kStran, kSplus, kSminus, kIin, kIout, kItran, kIplus, kIminus, kNplus, kNminus, N0, T0, Ds, Di, Dii\})[\,]$;

$$Di = Dbi, Dii = Dbii, Ds = Dbs, N0 = N0b, T0 = T0b, kIin = kbIin, kIminus = kbIminus, kIout = kbIout, kIplus = kbIplus, kItran = kbItran, kNminus = kbNminus, kNplus = kbNplus, kSin = kbSin, kSminus = kbSminus, kSout = kbSout, kSplus = kbSplus, kStran = kbStran$$

Appendix B

Maple code for demonstrating that the reduced model of the form (3.23) - (3.27) is structurally globally identifiable (SGI) using the DAACS approach.

```
restart :
with(diffalg) :
F := field_extension(transcendental_elements = {kSin, kSout, kStran,
     kSplus, kSminus, kNplus, kNminus, N0, T0, Ds }) :

R := differential_ring(derivations = [t], ranking = [SO, SI, TS, NS, y],
     field_of_constants = F, notation = diff) :

eq1 := -diff(SO(t), t) -kSin·SO(t) + kSout·SI(t) + kStran·TS(t) :
eq2 := -diff(SI(t), t) + kSin·SO(t) - kSout·SI(t) - kSplus·SI(t)·(T0
     - TS(t)) + kSminus·TS(t) - kNplus·SI(t)·(N0 - NS(t))
     + kNminus·NS(t) :
eq3 := -diff(TS(t), t) + kSplus·SI(t)·(T0 - TS(t)) - kSminus·TS(t)
     - kStran·TS(t) :
eq4 := -diff(NS(t), t) + kNplus·SI(t)·(N0 - NS(t)) - kNminus
     ·NS(t) :
eq5 := -Ds + SO(t) + SI(t) + TS(t) + NS(t) :
eq6 := y(t) - NS(t) :

P := Rosenfeld_Groebner([eq1, eq2, eq3, eq4, eq5, eq6], R);
                                        [characterizable]
y3d := rewrite_rules(P)[ ][5] :
tempa := subs(diff(y(t), [t$3]) = y3, diff(y(t), [t$2]) = y2, diff(y(t),
     t) = y1, y(t) = y, y3d) :

S1 := {kSin = kbSin, kSout = kbSout, kStran = kbStran, kSplus
     = kbSplus, kSminus = kbSminus, kNplus = kbNplus, kNminus
     = kbNminus, N0 = N0b, T0 = T0b, Ds = Dbs} :

tempb := subs(S1, tempa) :
inout1 := numer(rhs(tempa - tempb)) :
inout2 := collect(inout1, {y, y1, y2}, distributed) :
sol := {coeffs(inout2, {y, y1, y2})} :
s := solve(sol, {kSin, kSout, kStran, kSplus, kSminus, kNplus, kNminus,
     N0, T0, Ds}) :

s[1][2], s[2][5], s[2][9]
                                        N0 = 0, kNplus = 0, kSplus = 0
s[4]
 {Ds = Dbs, N0 = N0b, T0 = T0b, kNminus = kbNminus, kNplus
     = kbNplus, kSin = kbSin, kSminus = kbSminus, kSout = kbSout,
     kSplus = kbSplus, kStran = kbStran}
```

Appendix C

Maple code for demonstrating that the reduced model of the form (3.23) - (3.27) is structurally globally identifiable (SGI) using the Ai/oRA approach.

```
restart
with(LinearAlgebra) : with(Groebner) :
eqn1 := -kSin·SO + kSout·SI + kStran·TS :
eqn2 := kSin·SO − kSout·SI − kSplus·SI·(T0 − TS) + kSminus·TS
      − kNplus·SI·(N0 − NS) + kNminus·NS :
eqn3 := kSplus·SI·(T0 − TS) − kSminus·TS − kStran·TS :
eqn4 := kNplus·SI·(N0 − NS) − kNminus·NS :
simplify(eqn1 + eqn2 + eqn3 + eqn4);
S := {SO = Ds − NS − SI − TS, } :
eq2 := subs(S, eqn2) :
eq3 := subs(S, eqn3) :
eq4 := subs(S, eqn4) :
```

0

```
F := Vector([eq2, eq3, eq4 ]) :
lieDer[0] := NS :
N := Dimension(F) :
vars := [SI, TS, NS] :
v := map( (a, b) → diff(b, a), vars, lieDer[0]) :
V[1] := Vector_row([seq(v[t], t = 1 .. N) ]) :

lieDer[1] := simplify(DotProduct(F, V[1], conjugate = false)) :
v := map( (a, b) → diff(b, a), vars, lieDer[1]) :
V[2] := Vector_row([seq(v[t], t = 1 .. N) ]) :

lieDer[2] := simplify(DotProduct(F, V[2], conjugate = false)) :
v := map( (a, b) → diff(b, a), vars, lieDer[2]) :
V[3] := Vector_row([seq(v[t], t = 1 .. N) ]) :

lieDer[3] := simplify(DotProduct(F, V[3], conjugate = false)) :
L := [seq(y[i] − lieDer[i], i = 0 ..N) ] :
vars2 := {op(vars), y[N]} :
out := UnivariatePolynomial(y[N], L, vars2) :
G := Basis(L, plex(op(vars2))) :
out2 := simplify(G[1]) :
simplify(out − out2);
```

0

```
yout := {seq(y[t], t = 0 .. N)} :
p1 := collect(out, yout,'distributed') : u1 := {coeffs(p1, yout,'t')} :
ub := eval(u1, [kSin = kbSin, kSout = kbSout, kStran = kbStran, kSplus
      = kbSplus, kSminus = kbSminus, kNplus = kbNplus, kNminus
      = kbNminus, N0 = N0b, T0 = T0b, Ds = Dbs]) :

eqns := convert(u1, list) - convert(ub, list) :
s := solve({seq(eqns[i], i = 1 ..30)}, {kSin, kSout, kStran, kSplus,
     kSminus, kNplus, kNminus, N0, T0, Ds });
```

$$\{Ds = Dbs, N0 = N0b, T0 = T0b, kNminus = kbNminus, kNplus = kbNplus, kSin = kbSin, kSminus = kbSminus, kSout = kbSout, kSplus = kbSplus, kStran = kbStran\}$$

Appendix D

Maple code for demonstrating that the reduced model of the form (3.23) - (3.27) is structurally globally identifiable (SGI) using the NDi/oONF approach.

```
restart
with(LinearAlgebra) :
eqn1 := -kSin·SO + kSout·SI + kStran·TS :
eqn2 := kSin·SO − kSout·SI − kSplus·SI·(T0 − TS) + kSminus·TS
      − kNplus·SI·(N0 − NS) + kNminus·NS :
eqn3 := kSplus·SI·(T0 − TS) − kSminus·TS − kStran·TS :
eqn4 := kNplus·SI·(N0 − NS) − kNminus·NS :
simplify(eqn1 + eqn2 + eqn3 + eqn4);
S := {SO = Ds − NS − SI − TS, } :
eq2 := subs(S, eqn2) :
eq3 := subs(S, eqn3) :
eq4 := subs(S, eqn4) :
```

$$0$$

```
F := Vector([eq2, eq3, eq4 ]) :
lieDer[0] := NS :
N := Dimension(F) :
vars := [SI, TS, NS] :
v := map( (a, b) → diff(b, a), vars, lieDer[0]) :
V[1] := Vector_row([seq(v[t], t = 1 .. N) ]) :

lieDer[1] := simplify(DotProduct(F, V[1], conjugate = false)) :
v := map( (a, b) → diff(b, a), vars, lieDer[1]) :
V[2] := Vector_row([seq(v[t], t = 1 .. N) ]) :

lieDer[2] := simplify(DotProduct(F, V[2], conjugate = false)) :
v := map( (a, b) → diff(b, a), vars, lieDer[2]) :
V[3] := Vector_row([seq(v[t], t = 1 .. N) ]) :

lieDer[3] := simplify(DotProduct(F, V[3], conjugate = false)) :
s := solve({seq(y[i] = lieDer[i], i = 0 ..2)}, vars) :  iomap := simplify(subs(s[ ], lieDer[3])) :
S1 := {kSin = kbSin, kSout = kbSout, kStran = kbStran, kSplus
      = kbSplus, kSminus = kbSminus, kNplus = kbNplus, kNminus
      = kbNminus, N0 = N0b, T0 = T0b, Ds = Dbs} :

altmap := subs(S1, iomap) :
ta := simplify(iomap − altmap) :
vars2 := {seq(y[i], i = 0 ..N)} :
tb := collect(numer(ta), vars2, distributed) :
tc := {coeffs(tb, vars2)} :

par := {kSin, kSout, kStran, kSplus, kSminus, kNplus, kNminus, N0, T0,
     Ds} :

s := solve(tc, par)[ ] :
s[1][2], s[2][9], s[3][9]
```

$$N0 = 0, kSplus = 0, kSplus = 0$$

```
s[4]
```

$$\{Ds = Dbs, N0 = N0b, T0 = T0b, kNminus = kbNminus, kNplus = kbNplus, kSin = kbSin, kSminus = kbSminus, kSout = kbSout, kSplus = kbSplus, kStran = kbStran\}$$

Appendix E

Maple code for demonstrating that the model of the form (4.30) - (4.31) is structurally globally identifiable (SGI) using the DAACS approach.

```
restart :
with(diffalg) :
F := field_extension(transcendental_elements = {k[3], r[3], V[M],
     K[M], d}) :

R := differential_ring(derivations = [t], ranking = [x[1], x[3], y],
     field_of_constants = F, notation = diff) :

eq1 := -diff(x[1](t), t)·(K_M + x_1(t)) − V_M·x_1(t) + k_3·x_3(t)·(K_M
     + x_1(t)) − r_3·x_1(t)·(K_M + x_1(t)) :
eq2 := -diff(x[3](t), t)·(K_M + x_1(t)) + V_M·x_1(t) − k_3·x_3(t)·(K_M
     + x_1(t)) + r_3·x_1(t)·(K_M + x_1(t)) :
eq3 := -y(t) + x[3](t) :
eq4 := -d + x[1](t) + x[3](t) :

P := Rosenfeld_Groebner([eq1, eq2, eq3, eq4], R);
                                        [characterizable]
y3 := rewrite_rules(P)[ ][ ] :
tempa := subs( diff(y(t), [t$2]) = y[2], diff(y(t), t) = y[1], y(t) = y[0],
     y3) :

S1 := { V[M] = Vb[M], K[M] = Kb[M], k[3] = kb[3], r[3] = rb[3]} :

tempb := subs(S1, tempa) :
inout1 := numer(rhs(tempa - tempb)) :
inout2 := collect(inout1, {y[0], y[1]}, distributed) :
sol := {coeffs(inout2, {y[0], y[1]})} :
s2 := solve(sol, { Vb[M], Kb[M], kb[3], rb[3]})[ ];
Kb_M = K_M, Vb_M = V_M, kb_3 = k_3, rb_3 = r_3
```

Appendix F

Maple code for demonstrating that the model of the form (4.84) - (4.86) is structurally globally identifiable (SGI) using the Ai/oAR approach.

```
restart
with(LinearAlgebra) : with(Groebner) :
x1dot := -V[M]·x[1]/(K[M] + x[1]) + k[4]·x[4] - r[4]·x[1] :
x3dot := V[M]·x[1]/(K[M] + x[1]) - k[3]·x[3] + r[3]·x[4] :
x4dot := r[4]·x[1] - k[4]·x[4] + k[3]·x[3] - r[3]·x[4] :
simplify(x1dot + x3dot + x4dot);
```

$$0$$

```
F := Vector([ x1dot, x3dot, x4dot]) :
lieDer[0] := x[3] + x[4] :
N := Dimension(F) :
L := [y[0] - H] :
vars := [x[1], x[3], x[4]] :
v := map( (a, b) → diff(b, a), vars, lieDer[0]) :
V[1] := Vector_row([seq(v[t], t = 1 .. N) ]) :

lieDer[1] := simplify(DotProduct(F, V[1], conjugate = false)) :
v := map( (a, b) → diff(b, a), vars, lieDer[1]) :
V[2] := Vector_row([seq(v[t], t = 1 .. N) ]) :

lieDer[2] := simplify(DotProduct(F, V[2], conjugate = false)) :
v := map( (a, b) → diff(b, a), vars, lieDer[2]) :
V[3] := Vector_row([seq(v[t], t = 1 .. N) ]) :

lieDer[3] := simplify(DotProduct(F, V[3], conjugate = false)) :
ORC := Matrix([seq([V[t]], t = 1 .. N) ]) :
ORC0 := subs( {x[1] = d, seq(x[t] = 0, t = 2 .. 4)}, ORC) :
Rank(ORC0)
```

$$3$$

```
L := [y[0] - lieDer[0], simplify( (y[1] - lieDer[1]) · (K_M + x_1) ),
      simplify( (y[2] - lieDer[2]) · (K_M + x_1)^3 ), simplify( (y[3]
      - lieDer[3]) · (K_M + x_1)^5 ) ] :

vars2 := [op(vars), y[N]] :
out := UnivariatePolynomial(y[N], L, vars2) :
G := Basis(L, plex(op(vars2))) :
out2 := simplify(G[1]) :
simplify(out - out2);
```

$$0$$

```
yout := {seq(y[t], t = 0 .. N)} :
p := collect(out, yout, 'distributed') : u := {coeffs(p, yout, 't')} :
```

```
ub := eval(u, [K[M] = Kb[M], V[M] = Vb[M], k[4] = kb[4], r[4]
      = rb[4], k[3] = kb[3], r[3] = rb[3]]) :

eqns := convert(u, list) - convert(ub, list) :
s := solve({seq(eqns[i], i = 1 ..30)}, {Kb[M], Vb[M], kb[4], rb[4],
     kb[3], rb[3]}) ;
```

$$\left\{Kb_M = K_M, Vb_M = V_M, kb_3 = k_3, kb_4 = k_4, rb_3 = r_3, rb_4 = r_4\right\}, \left\{Kb_M = -\frac{V_M\left(k_4 + k_3 + r_3\right)}{r_4\left(k_3 + r_3\right)}, Vb_M = -\frac{K_M r_4\left(k_3 + r_3\right)}{k_4 + k_3 + r_3}, kb_3 = k_3, kb_4 = k_4, rb_3 = r_3, rb_4 = r_4\right\}$$

Appendix G

FACSIMILE code for performing the sensitivity analysis.

```
*========================================================== ;
* 8 June 2011 University of Warwick;
* Thomas Grandjean PhD research - T.Grandjean@hotmail.com ;
*========================================================== ;

EXECUTE ;

OPEN 8  "H:\hepatocytes\calc.out";
OPEN 9  "H:\hepatocytes\residuals.out";
OPEN 10 "H:\hepatocytes\h297sa2p.out";
**;

PARAMETER
K1 2.86E-06
K2 1.00E-04
K3 3.53E-02
R1 2.86E-06
R3 1.50E-03
T0 8.07E+02;

VARIABLE
x1_01 x2_01 x3_01 y_01
x1k1_01 x1k2_01 x1k3_01 x1r1_01 x1r3_01 x1T0_01
x2k1_01 x2k2_01 x2k3_01 x2r1_01 x2r3_01 x2T0_01
x3k1_01 x3k2_01 x3k3_01 x3r1_01 x3r3_01 x3T0_01
…
x1k1_39 x1k2_39 x1k3_39 x1r1_39 x1r3_39 x1T0_39
x2k1_39 x2k2_39 x2k3_39 x2r1_39 x2r3_39 x2T0_39
x3k1_39 x3k2_39 x3k3_39 x3r1_39 x3r3_39 x3T0_39
;

INTEGER #COUNT ;

COMPILE INITIAL ;
x1_01 = 300000 ;
x2_01 = 0 ;
x3_01 = 0 ;
y_01  = 0 ;
…
x1_39 = 5000 ;
x2_39 = 0 ;
x3_39 = 0 ;
y_39  = 0 ;

**;

COMPILE EQUATIONS ;
'x1_01 = r1*x2_01 - k1*x1_01*(T0-x2_01) + k3*x3_01 - r3*x1_01
;
```

```
'x2_01 = k1*x1_01*(T0-x2_01) - (r1+k2)*x2_01 ;
'x3_01 = r3*x1_01 + k2*x2_01 - k3*x3_01 ;
'y_01  =  k1*x1_01*(T0-x2_01) - (r1+k2)*x2_01
 + r3*x1_01 + k2*x2_01 - k3*x3_01 ;
'x1k1_01 = (-k1*(T0-x2_01)-r3)*x1k1_01 + (r1+k1*x1_01)*x2k1_01
 + k3*x3k1_01 - x1_01*(T0-x2_01) ;
'x2k1_01 = k1*(T0-x2_01)*x1k1_01 - (r1+k2+k1*x1_01)*x2k1_01
 + x1_01*(T0-x2_01) ;
'x3k1_01 = r3*x1k1_01 + k2*x2k1_01 - k3*x3k1_01 ;
'x1k2_01 = (-k1*(T0-x2_01)-r3)*x1k2_01 + (r1+k1*x1_01)*x2k2_01
 + k3*x3k2_01 ;
'x2k2_01 = k1*(T0-x2_01)*x1k2_01 - (r1+k2+k1*x1_01)*x2k2_01 -
x2_01 ;
'x3k2_01 = r3*x1k2_01 + k2*x2k2_01 - k3*x3k2_01 + x2_01 ;
'x1k3_01 = (-k1*(T0-x2_01)-r3)*x1k3_01 + (r1+k1*x1_01)*x2k3_01
 + k3*x3k3_01 + x3_01 ;
'x2k3_01 = k1*(T0-x2_01)*x1k3_01 - (r1+k2+k1*x1_01)*x2k3_01 ;
'x3k3_01 = r3*x1k3_01 + k2*x2k3_01 - k3*x3k3_01 - x3_01 ;
'x1r1_01 = (-k1*(T0-x2_01)-r3)*x1r1_01 + (r1+k1*x1_01)*x2r1_01
 + k3*x3r1_01 + x2_01 ;
'x2r1_01 = k1*(T0-x2_01)*x1r1_01 - (r1+k2+k1*x1_01)*x2r1_01 -
x2_01 ;
'x3r1_01 = r3*x1r1_01 + k2*x2r1_01 - k3*x3r1_01 ;
'x1r3_01 = (-k1*(T0-x2_01)-r3)*x1r3_01 + (r1+k1*x1_01)*x2r3_01
 + k3*x3r3_01 - x1_01 ;
'x2r3_01 = k1*(T0-x2_01)*x1r3_01 - (r1+k2+k1*x1_01)*x2r3_01 ;
'x3r3_01 = r3*x1r3_01 + k2*x2r3_01 - k3*x3r3_01 + x1_01 ;
'x1T0_01 = (-k1*(T0-x2_01)-r3)*x1T0_01 + (r1+k1*x1_01)*x2T0_01
 + k3*x3T0_01 - k1*x1_01 ;
'x2T0_01 = k1*(T0-x2_01)*x1T0_01 - (r1+k2+k1*x1_01)*x2T0_01
 + k1*x1_01 ;
'x3T0_01 = r3*x1T0_01 + k2*x2T0_01 - k3*x3T0_01 ;
…
'x1_39 = r1*x2_39 - k1*x1_39*(T0-x2_39) + k3*x3_39 - r3*x1_39
;
'x2_39 = k1*x1_39*(T0-x2_39) - (r1+k2)*x2_39 ;
'x3_39 = r3*x1_39 + k2*x2_39 - k3*x3_39 ;
'y_39  =  k1*x1_39*(T0-x2_39) - (r1+k2)*x2_39
 + r3*x1_39 + k2*x2_39 - k3*x3_39 ;
'x1k1_39 = (-k1*(T0-x2_39)-r3)*x1k1_39 + (r1+k1*x1_39)*x2k1_39
 + k3*x3k1_39 - x1_39*(T0-x2_39) ;
'x2k1_39 = k1*(T0-x2_39)*x1k1_39 - (r1+k2+k1*x1_39)*x2k1_39
 + x1_39*(T0-x2_39) ;
'x3k1_39 = r3*x1k1_39 + k2*x2k1_39 - k3*x3k1_39 ;
'x1k2_39 = (-k1*(T0-x2_39)-r3)*x1k2_39 + (r1+k1*x1_39)*x2k2_39
 + k3*x3k2_39 ;
'x2k2_39 = k1*(T0-x2_39)*x1k2_39 - (r1+k2+k1*x1_39)*x2k2_39 -
x2_39 ;
'x3k2_39 = r3*x1k2_39 + k2*x2k2_39 - k3*x3k2_39 + x2_39 ;
'x1k3_39 = (-k1*(T0-x2_39)-r3)*x1k3_39 + (r1+k1*x1_39)*x2k3_39
 + k3*x3k3_39 + x3_39 ;
'x2k3_39 = k1*(T0-x2_39)*x1k3_39 - (r1+k2+k1*x1_39)*x2k3_39 ;
'x3k3_39 = r3*x1k3_39 + k2*x2k3_39 - k3*x3k3_39 - x3_39 ;
'x1r1_39 = (-k1*(T0-x2_39)-r3)*x1r1_39 + (r1+k1*x1_39)*x2r1_39
 + k3*x3r1_39 + x2_39 ;
'x2r1_39 = k1*(T0-x2_39)*x1r1_39 - (r1+k2+k1*x1_39)*x2r1_39 -
```

```
x2_39 ;
'x3r1_39 = r3*x1r1_39 + k2*x2r1_39 - k3*x3r1_39 ;
'x1r3_39 = (-k1*(T0-x2_39)-r3)*x1r3_39 + (r1+k1*x1_39)*x2r3_39
 + k3*x3r3_39 - x1_39 ;
'x2r3_39 = k1*(T0-x2_39)*x1r3_39 - (r1+k2+k1*x1_39)*x2r3_39 ;
'x3r3_39 = r3*x1r3_39 + k2*x2r3_39 - k3*x3r3_39 + x1_39 ;
'x1T0_39 = (-k1*(T0-x2_39)-r3)*x1T0_39 + (r1+k1*x1_39)*x2T0_39
 + k3*x3T0_39 - k1*x1_39 ;
'x2T0_39 = k1*(T0-x2_39)*x1T0_39 - (r1+k2+k1*x1_39)*x2T0_39
 + k1*x1_39 ;
'x3T0_39 = r3*x1T0_39 + k2*x2T0_39 - k3*x3T0_39 ;
**;

SETPSTREAM 1 8;
**;
SETPSTREAM 2 9;
**;

DATA ;
TIME y_01    y_02    y_03    y_04    y_05    y_06    y_07    y_08
y_09
 y_10    y_11    y_12    y_13    y_14    y_15    y_16    y_17    y_18
y_19
 y_20    y_21    y_22    y_23    y_24    y_25    y_26    y_27    y_28
y_29
 y_30    y_31    y_32    y_33    y_34    y_35    y_36    y_37    y_38
y_39 ;
RANGE  5596.2 7460.1 3864.6 6770.7 7785.9 6250.5 5597.1 5610.6
6459.3
 2656.8  4514.4  5098.5  4697.1  3714.3  3865.5  4805.1  3711.6
3006.9 2539.8
 3302.1  2273.4  2700     2439     1079.1  2099.7  2861.1  2164.5
1872.9 1678.5
 1918.8 1075.5 828    1305.9 885.6  610.2  898.2  527.4  816.3
859.5 ;
0 1E-36 1E-36 1E-36 1E-36 1E-36 1E-36 1E-36 1E-36 1E-36
 1E-36 1E-36 1E-36 1E-36 1E-36 1E-36 1E-36 1E-36 1E-36 1E-36
 1E-36 1E-36 1E-36 1E-36 1E-36 1E-36 1E-36 1E-36 1E-36 1E-36
 1E-36 1E-36 1E-36 1E-36 1E-36 1E-36 1E-36 1E-36 1E-36 1E-36 ;
10  5688  6083.1  6149.7  5635.8  5565.6  5434.2  4592.7  4646.7
5582.7
 4227.3  4067.1  3681  2073.6  3287.7  2004.3  1675.8  1716.3  1845
1580.4
 1744.2  1351.8  1106.1  1179  1618.2  824.4  1198.8  1125.9  670.5
803.7
 773.1 599.4 736.2 558.9 315.9 260.1 342.9 184.5 284.4 204.3 ;
30  6087.6  7092.9  7090.2  5028.3  4790.7  6800.4  4127.4  4979.7
6852.6
 4602.6  4458.6  4246.2  4406.4  5274.9  3970.8  3623.4  3014.1
3549.6 2463.3
 3252.6  3073.5  2605.5  2438.1  2218.5  1810.8  2738.7  1831.5
1589.4 1666.8
 1595.7  1125.9  1113.3  1025.1  692.1  550.8  714.6  458.1  388.8
511.2 ;
50  11284.2  13543.2  10014.3  11799  12576.6  11684.7  9724.5
10257.3 12042
```

```
 6510.6  8581.5  8779.5  3427.2  5432.4  4183.2  4670.1  3471.3
4101.3 3058.2
 3337.2 2970.9 2928.6 2884.5 2697.3 2250 2969.1 2252.7 1916.1
2001.6
 2027.7  1631.7  1412.1  1246.5  762.3  706.5  854.1  466.2  910.8
551.7 ;
70  9733.5  9605.7  8910  10308.6  10460.7  8931.6  9476.1  9463.5
7922.7
 6884.1 7292.7 6659.1 6770.7 7002 5869.8 6480.9 5427.9 4851.9
4120.2
 5046.3 3625.2 3806.1 3618 2692.8 2924.1 4059.9 3290.4 2543.4
2482.2
 2691.9 556.2 1564.2 1864.8 1201.5 870.3 1241.1 711.9 1100.7
1063.8 ;
**;

SETVARY K1 K2 K3 R1 R3 T0 ;

BEGIN;

COMPILE INSTANT ;
WRITE  1=10,  "TIME    y_01  x3k1_01  x3k2_01  x3k3_01  x3r1_01
x3r3_01 x3T0_01
 y_04 x3k1_04 x3k2_04 x3k3_04 x3r1_04 x3r3_04 x3T0_04
 y_07 x3k1_07 x3k2_07 x3k3_07 x3r1_07 x3r3_07 x3T0_07
 y_10 x3k1_10 x3k2_10 x3k3_10 x3r1_10 x3r3_10 x3T0_10
 y_13 x3k1_13 x3k2_13 x3k3_13 x3r1_13 x3r3_13 x3T0_13
 y_16 x3k1_16 x3k2_16 x3k3_16 x3r1_16 x3r3_16 x3T0_16
 y_19 x3k1_19 x3k2_19 x3k3_19 x3r1_19 x3r3_19 x3T0_19
 y_22 x3k1_22 x3k2_22 x3k3_22 x3r1_22 x3r3_22 x3T0_22
 y_25 x3k1_25 x3k2_25 x3k3_25 x3r1_25 x3r3_25 x3T0_25
 y_28 x3k1_28 x3k2_28 x3k3_28 x3r1_28 x3r3_28 x3T0_28
 y_31 x3k1_31 x3k2_31 x3k3_31 x3r1_31 x3r3_31 x3T0_31
 y_34 x3k1_34 x3k2_34 x3k3_34 x3r1_34 x3r3_34 x3T0_34
 y_37 x3k1_37 x3k2_37 x3k3_37 x3r1_37 x3r3_37 x3T0_37" % ;
#COUNT=0 ;
**;

COMPILE PRINT;
* Output routine called during the final phase;
#COUNT = #COUNT + 1 ;
DO 10 FOR #2=#COUNT-1 ;
WRITE 1=10,  ((E14,6))TIME,
y_01, x3k1_01, x3k2_01, x3k3_01, x3r1_01, x3r3_01, x3T0_01,
y_04, x3k1_04, x3k2_04, x3k3_04, x3r1_04, x3r3_04, x3T0_04,
y_07, x3k1_07, x3k2_07, x3k3_07, x3r1_07, x3r3_07, x3T0_07,
y_10, x3k1_10, x3k2_10, x3k3_10, x3r1_10, x3r3_10, x3T0_10,
y_13, x3k1_13, x3k2_13, x3k3_13, x3r1_13, x3r3_13, x3T0_13,
y_16, x3k1_16, x3k2_16, x3k3_16, x3r1_16, x3r3_16, x3T0_16,
y_19, x3k1_19, x3k2_19, x3k3_19, x3r1_19, x3r3_19, x3T0_19,
y_22, x3k1_22, x3k2_22, x3k3_22, x3r1_22, x3r3_22, x3T0_22,
y_25, x3k1_25, x3k2_25, x3k3_25, x3r1_25, x3r3_25, x3T0_25,
y_28, x3k1_28, x3k2_28, x3k3_28, x3r1_28, x3r3_28, x3T0_28,
y_31, x3k1_31, x3k2_31, x3k3_31, x3r1_31, x3r3_31, x3T0_31,
y_34, x3k1_34, x3k2_34, x3k3_34, x3r1_34, x3r3_34, x3T0_34,
y_37, x3k1_34, x3k2_37, x3k3_37, x3r1_37, x3r3_37, x3T0_37;
```

```
LABEL 10;
**;

SETNOFIT;
WHENEVER TIME = TOBS % CALL PRINT;
**;

BEGIN;
STOP;
```

Appendix H

Maple code for demonstrating that the five compartment model of the form (5.18) - (5.22) satisfies the ORC.

```
restart
with(LinearAlgebra) :
f1 := -ka G :
f2 := ka G - V_D K_BA DO / (K_D K_BA + DO K_BA + BO K_D) + kDout DI - kDin DO :

f3 := V_D K_BA DO / (K_D K_BA + DO K_BA + BO K_D) - (kDout + kDe) DI
      + kDin DO :
f4 := kp - V_BA K_D BO / (K_D K_BA + DO K_BA + BO K_D) + kBout BI - kBin BO :
f5 := V_BA K_D BO / (K_D K_BA + DO K_BA + BO K_D) - ( kBout + kBe) BI + kBin BO :
simplify(f1 + f2 + f3 + f4 + f5 );
```

$$-DI\,kDe + kp - BI\,kBe$$

```
F := Vector([f1, f2, f3, f4, f5]) :
lieDer[0] := DO / V1 :
N := Dimension(F) :
vars := [G, DO, DI, BO, BI] :
v := map( (a,b) -> diff(b,a), vars, lieDer[0]) :
V[1] := Vector_row([seq(v[t], t = 1 .. N) ]) :

lieDer[1] := simplify(DotProduct(F, V[1], conjugate = false)) :
v := map( (a,b) -> diff(b,a), vars, lieDer[1]) :
V[2] := Vector_row([seq(v[t], t = 1 .. N) ]) :

lieDer[2] := simplify(DotProduct(F, V[2], conjugate = false)) :
v := map( (a,b) -> diff(b,a), vars, lieDer[2]) :
V[3] := Vector_row([seq(v[t], t = 1 .. N) ]) :

lieDer[3] := BO / V2 :
v := map( (a,b) -> diff(b,a), vars, lieDer[3]) :
V[4] := Vector_row([seq(v[t], t = 1 .. N) ]) :

lieDer[4] := simplify(DotProduct(F, V[4], conjugate = false)) :
v := map( (a,b) -> diff(b,a), vars, lieDer[4]) :
V[5] := Vector_row([seq(v[t], t = 1 .. N) ]) :

lieDer[5] := simplify(DotProduct(F, V[5], conjugate = false)) :
ORC := Matrix([seq([V[t]], t = 1 .. N) ]) :
ORC0 := subs( {G = D, DO = 0, DI = 0, BO = Bout , BI = Bin}, ORC) :
Rank(ORC0);  5
```

Appendix I

Maple code for demonstrating that the seven compartment model of the form (5.1) - (5.7) satisfies the ORC.

```
restart
with(LinearAlgebra) :
f1 := -ka G :
f2 := ka G - kDplus DO (T0 - TD - TB) + kDminus TD + kDout DI
      - kDin DO :
f3 := kDplus DO (T0 - TD - TB) - (kDtran + kDminus) TD :
f4 := kDtran TD - (kDout + kDe) DI + kDin DO :
f5 := kp -kBplus BO (T0 - TD - TB) + kBminus TB + kBout BI
      - kBin BO :
f6 := kBplus BO (T0 - TD - TB) - (kBtran + kBminus) TB :
f7 := kBin BO - (kBout + kBe) BI + kBtran TB :
simplify(f1 + f2 + f3 + f4 + f5 + f6 + f7);
```

$$-DI\,kDe + kp - BI\,kBe$$

```
F := Vector([f1, f2, f3, f4, f5, f6, f7]) :
lieDer[0] := DO/V1 :
N := Dimension(F) :
vars := [G, DO, TD, DI, BO, TB, BI] :
v := map( (a,b) -> diff(b,a), vars, lieDer[0]) :
V[1] := Vector_row([seq(v[t], t=1..N)]) :

lieDer[1] := simplify(DotProduct(F, V[1], conjugate=false)) :
v := map( (a,b) -> diff(b,a), vars, lieDer[1]) :
V[2] := Vector_row([seq(v[t], t=1..N)]) :

lieDer[2] := simplify(DotProduct(F, V[2], conjugate=false)) :
v := map( (a,b) -> diff(b,a), vars, lieDer[2]) :
V[3] := Vector_row([seq(v[t], t=1..N)]) :

lieDer[3] := simplify(DotProduct(F, V[3], conjugate=false)) :
v := map( (a,b) -> diff(b,a), vars, lieDer[3]) :
V[4] := Vector_row([seq(v[t], t=1..N)]) :

lieDer[4] := BO/V2 :
v := map( (a,b) -> diff(b,a), vars, lieDer[4]) :
V[5] := Vector_row([seq(v[t], t=1..N)]) :

lieDer[5] := simplify(DotProduct(F, V[5], conjugate=false)) :
v := map( (a,b) -> diff(b,a), vars, lieDer[5]) :
V[6] := Vector_row([seq(v[t], t=1..N)]) :

lieDer[6] := simplify(DotProduct(F, V[6], conjugate=false)) :
v := map( (a,b) -> diff(b,a), vars, lieDer[6]) :
V[7] := Vector_row([seq(v[t], t=1..N)]) :

ORC := Matrix([seq([V[t]], t=1..N)]) :
```

```
ORC0 := subs({G = D, DO = 0, TD = 0, DI = 0, BO = Bout, TB = 0, BI
    = Bin}, ORC) :

Rank(ORC0);
```

7